INVESTIGATION OF COMBUSTION CHARACTERISTICS OF BIOMASS AND COAL MIXTURES IN A CIRCULATING FLUIDIZED BED COMBUSTOR

A THESIS SUBMITTED TO
THE GRADUATE SCHOOL OF NATURAL AND APPLIED SCIENCES
OF
MIDDLE EAST TECHNICAL UNIVERSITY

BY

MURAT VAROL

IN PARTIAL FULLFILLMENT OF THE REQUIREMENTS
FOR
THE DEGREE OF DOCTOR OF PHILOSOPHY
IN
ENVIRONMENTAL ENGINEERING

SEPTEMBER 2013

Approval of the thesis:

INVESTIGATION OF COMBUSTION CHARACTERISTICS OF BIOMASS AND COAL MIXTURES IN A CIRCULATING FLUIDIZED BED COMBUSTOR

submitted by **MURAT VAROL** in partial fulfillment of the requirements for the degree of **Doctor of Philosophy in Environmental Engineering Department, Middle East Technical University** by,

Prof. Dr. Canan Özgen _____
Dean, Graduate School of **Natural and Applied Sciences**

Prof. Dr. F. Dilek Sanin _____
Head of Department, **Environmental Engineering**

Prof. Dr. Aysel Atımtay _____
Supervisor, **Environmental Engineering Dept., METU**

Examining Committee Members:
Prof. Dr. F. Dilek Sanin _____
Environmental Engineering Dept., METU

Prof. Dr. Aysel Atımtay _____
Environmental Engineering Dept., METU

Prof. Dr. Hüsnü Atakül _____
Chemical Engineering Dept., ITU

Prof. Dr. Hayati Olgun _____
Solar Energy Institute, Ege University

Assist. Prof. Dr. Ahmet Yozgatlıgil _____
Mechanical Engineering Dept., METU

Date: 03.09.2013

I hereby declare that all information in this document has been obtained and presented in accordance with academic rules and ethical conduct. I also declare that, as required by these rules and conduct, I have fully cited and referenced all material and results that are not original to this work.

Name, Last name: Murat VAROL

Signature :

ABSTRACT

INVESTIGATION OF COMBUSTION CHARACTERISTICS OF BIOMASS AND COAL MIXTURES IN A CIRCULATING FLUIDIZED BED COMBUSTOR

VAROL, Murat
Ph.D., Department of Environmental Engineering
Supervisor: Prof. Dr. Aysel T. ATIMTAY

September 2013, 290 pages

In this study, combustion and co-combustion tests of Bursa/Orhaneli lignite with two biomass fuels (olive cake and woodchips) were carried out in a laboratory scale Circulating Fluidized Bed (CFB) combustor, 6 m high and 108 mm inside diameter, in order to investigate the effect of excess air ratio (λ), secondary air ratio (SAR) and location of secondary air injection along the combustor wall on the emissions. Optimum λ and SAR was determined for each test. The flue gas emissions were compared with limits in the EU and Turkish Regulation. A series of co-combustion tests of olive cake (50% by wt.) with Bursa/Orhaneli lignite (S_{total} < 2.7%) and with Denizli/Kale lignite (S_{total} > 3.6%) were also done to investigate the effect of sulfur content of fuel and coal+biomass interaction on the ash composition. Olive cake was chosen to represent high alkali content biomass (50% K_2O in ash). Samples taken from the bottom ash, fly ashes from cyclones and bag filter were subjected to XRF and XRD analyses. A Deposit Sampling Probe was used to simulate a heat exchanger surfaces in a boiler. The deposit accumulated on the probe and bottom ash samples were subjected to XRD and SEM-EDS analysis.

The results showed that increasing share of biomass in the fuel mixture shifted combustion characteristics from char combustion to volatile combustion. Addition of biomass increased CO emission, reduced char formation and NO emission. It was proved that sulfur in coal helped to prevent agglomeration, slagging and fouling in the combustor. Optimum excess air ratio increased with addition of biomass to fuel mixture.

Key Words: Combustion, Coal, Biomass, Co-combustion, Circulating fluidized bed, Emissions, Ash deposition, Slagging and fouling

ÖZ

BİYOKÜTLE-KÖMÜR KARIŞIMLARININ DOLAŞIMLI AKIŞKAN YATAKLI KAZANLARDA YANMA KARAKTERİSTİKLERİNİN İNCELENMESİ

VAROL, Murat
Doktora, Çevre Mühendisliği Bölümü
Tez Danışmanı: Prof. Dr. Aysel T. ATIMTAY

Eylül 2013, 290 sayfa

Bu çalışmada, hava fazlalık oranı (λ), ikincil hava oranı (SAR) ve ikincil havanın yakıcıya verildiği konumun baca gazı emisyonlarına etkisini incelemek ve her bir test için en uygun λ ve SAR değerlerini belirlenmek amacıyla Bursa/Orhaneli linyiti iki çeşit biyokütle ile yakılmıştır. Yakma için 6 m yüksekliği ve 108 mm iç çapı olan, laboratuvar ölçekli bir Dolaşımlı Akışkan Yatak (DAY) sistemi kullanılmıştır. Kömürü tek başına yakma ve kömürü biyokütle ile birlikte-yakma testleri yapılmıştır. Baca gazı emisyonları AB ve Türk Yönetmeliği'ndeki sınır değerler ile karşılaştırılmıştır. Yakıt içerisindeki kükürt içeriğinin ve kömür+biyokütle etkileşiminin kül kompozisyonu üzerindeki etkisini incelemek için prina+Bursa/Orhaneli linyiti (S_{toplam}<%2.7) ve prina+Denizli/Kale linyiti (S_{toplam}>%3.6) ile birlikte-yakma testleri de yapılmıştır. Prina, yüksek alkali oksit (külde %50 K_2O) içerdiği için seçilmiştir. Yanma sonunda dip külü, siklonlardan ve torbalı filtreden alınan uçucu kül numunelerinde XRF ve XRD analizleri yapılmıştır. Kazandaki ısı değiştirici yüzeylerini temsil etmesi için yakıcı içinde bir Depozit Örnekleme Sondası kullanılmıştır. Sonda üzerinde biriken depozit örneklerinde XRD ve SEM-EDS analizleri, yine dip kül örneklerinde SEM-EDS analizi yapılmıştır.

Elde edilen sonuçlar yakıt karışımındaki biyokütle oranının artması ile yakıt karışımının yanma karakteristiğinin genellikle kok yanmasından uçucu madde yanmasına doğru değiştiğini göstermiştir. Yakıttaki biyokütle oranının artmasıyla CO emisyonu artmış, kok oluşumu ve NO emisyonu azalmıştır. Kömürdeki kükürtün yakıcıdaki kül yumuşamasını ve aglomerasyonu, ısı değiştirici yüzeylerindeki birikimi azaltmaya/önlemeye yardımcı olduğu tesbit edilmiştir. Yakıt karışımına biyokütle eklenmesiyle optimum hava fazlalık oranı artmıştır.

Anahtar Sözcükler: Yanma, Kömür, Biyokütle, Birlikte-yanma, Dolaşımlı akışkan yatak, Emisyonlar, Kül birikimi, Curuf bağlaması ve tortu oluşumu

To my dear family and uncle Mecit Varol

ACKNOWLEDGMENTS

I would like to express my deepest gratitude to my supervisor Prof. Dr. Aysel Atimtay for her guidance, advice, criticism and encouragement and insight throughout this study. Her support in dealing with the difficult and rather complicated issues in this study was priceless.

I would like to thank my Ph.D. committee members and jury members, Prof. Dr. Dilek Sanin, Prof. Dr. Hüsnü Atakül, Prof. Dr. Hayati Olgun and Assist. Prof. Dr. Ahmet Yozgatlıgil for their suggestions and helpful comments for this study.

Funding from TUBITAK for the project (project no: TUBITAK-105G023) "Development of Circulating Fluidized Bed Technology for the Combustion of Biomass and Biomass/Coal Mixtures" is gratefully acknowledged in order to carry out this research.

This Ph.D. Thesis could not have been completed without the assistance of a number of people. I wish to express my appreciation to Prof. Dr. Hayati Olgun who was a researcher in TUBITAK-MRC during the conduct of this project. His efforts and suggestions throughout this study were invaluable. Also the technician at MRC, Erdal Gügük, is the person to mention here with great appreciation.

I want to express my thanks to the technical and scientific staff of the TUBITAK-MRC. They supported me in this work with their help and research activity. I am also grateful to the technical and scientific staff of METU-Central Laboratory for their support in XRD and SEM analyses.

I would like to thank my mother, Hükmiye Varol; my father, A. Fikri Varol; and my sister, Selen Varol for supporting and encouraging me at every step of this study. Their confidence in me is invaluable.

My deep gratitude is due to all my friends in the Department of Environmental Engineering, METU and to those who helped me over the last few years during this research project. Their support and encouragement is highly appreciated.

TABLE OF CONTENTS

ABSTRACT v
ÖZ vi
ACKNOWLEDGMENTS viii
TABLE OF CONTENTS ix
LIST OF TABLES xiv
LIST OF FIGURES xix
LIST OF ABBREVIATIONS xxix
CHAPTERS
1. INTRODUCTION 1
1.1. General 1
1.2. Aim of the Study 3
2. THEORETICAL BACKGROUND 5
2.1. Fluidized Bed Combustion Technology 5
2.1.1. Advantages of Fluidized Bed Combustion Technology 6
2.1.2. Types of Fluidized Bed Combustors 7
2.2. Combustion and Co-combustion of Biomass with Coal in Fluidized Bed Combustors 8
2.2.1. Major Air Pollutants in the Flue Gas of a Fluidized Bed Combustor 9
2.2.1.1. CO Emission 10
2.2.1.2. NO_x Emission 10
2.2.1.3. N_2O Emission 12
2.2.1.4. SO_2 Emission 13
2.2.2. Ash Related Operational Problems in Fluidized Bed Combustors 14
2.2.2.1. Ash Deposition Mechanisms 14
2.2.2.2. Agglomeration of Bed Material 15
2.2.2.3. Slagging, Fouling and Corrosion 18
2.3. Circulating Fluidized Bed Combustors 22
2.3.1. Circulating Fluidized Bed Combustors in Turkey 22
2.4. Emission Limits in EU and Turkey 24
3. LITERATURE SURVEY 27

3.1. Energy Review 27
3.1.1. World's Energy Outlook 27
3.1.2. Turkey's Energy Outlook 28
3.2. Coal Review 31
3.2.1. World's Coal Review 31
3.2.1.1. Coal Reserves 31
3.2.1.2. Total Coal Production 32
3.2.1.3. Total Coal Consumption 34
3.2.1.4. Lignite Reserves, Production and Consumption 34
3.2.1.5. World's CO_2 Emissions from Fuel Combustion 35
3.2.2. Turkey's Coal Review 37
3.2.2.1. Turkey's Greenhouse Gas Emissions 39
3.2.2.1.1. Turkey's CO_2 Emissions from Fuel Combustion 40
3.3. Biomass Review 41
3.3.1. World Biomass Potential 41
3.3.2. Turkey's Biomass Potential 41
3.3.2.1. Olive and Olive Cake Production 42
3.3.2.2. Forestry Biomass and Woodchips Potentials 44
3.4. Emission Characteristics of Combustion and Co-combustion of Coal and Biomass in Fluidized Bed Combustors 45
3.5. Ash-related Problems during Fluidized Bed Combustion 54
4. MATERIALS AND METHODS 59
4.1. Characteristics of Fuels and Limestone 59
4.1.1. Fuels Characterization 59
4.1.2. Limestone Characterization 63
4.2. A Laboratory-Scale Circulating Fluidized Bed Combustor 64
4.2.1. Fuel Feeding System 71
4.2.1.1. Calibration of the Fuel Feeding System 71
4.2.2. Design Details of Components of Combustor 71
4.2.2.1. Windbox 71
4.2.2.2. Distributor Plate 71
4.2.2.3. Module-101 72
4.2.2.4. Module-102 and Module-107 72

4.2.2.5. Module-103, Module-104, Module-105 and Module-106 72
4.2.2.6. Module-108 72
4.3. Operational Procedure 73
4.4. Experimental Matrix 74
4.5. Deposit Sampling Probe 81
4.6. Flue Gas Analyses 83
4.7. Ash Analyses 84
4.7.1. X-ray Fluorescence (XRF) 84
4.7.2. X-ray Diffraction (XRD) 85
4.7.3. Scanning Electron Microscopy 86
4.7.4. Ash Fusion Temperatures 86
5. RESULTS AND DISCUSSION 87
5.1. Assessment of Experiments for SET#1 87
5.1.1. Combustion of Bursa/Orhaneli Lignite (C1-1) 87
5.1.2. Co-Combustion of Bursa/Orhaneli Lignite with 10% (by wt.) Olive Cake (C1-B1-1) 92
5.1.3. Co-Combustion of Bursa/Orhaneli Lignite with 30% (by wt.) Olive Cake (C1-B1-2) 96
5.1.4. Co-Combustion of Bursa/Orhaneli Lignite with 50% (by wt.) Olive Cake (C1-B1-3) 100
5.1.5. Combustion of Olive Cake (B1-1) 104
5.1.6. Co-Combustion of Bursa/Orhaneli Lignite with 10% (by wt.) Woodchips (C1-B2-1) 109
5.1.7. Co-Combustion of Bursa/Orhaneli Lignite with 30% (by wt.) Woodchips (C1-B2-2) 113
5.1.8. Co-Combustion of Bursa/Orhaneli Lignite with 50% (by wt.) Woodchips (C1-B2-3) 116
5.1.9. Discussion on the Effect of Excess Air Ratio on Emissions in SET#1 119
5.2. Assessment of Experiments for SET#2 129
5.2.1. Co-Combustion of Bursa/Orhaneli Lignite with 30% (by wt.) Olive Cake (C1-B1-4) 129
5.2.2. Co-Combustion of Bursa/Orhaneli Lignite with 50% (by wt.) Olive Cake (C1-B1-5) 131

5.2.3. Co-Combustion of Bursa/Orhaneli Lignite with 30% (by wt.) Woodchips (C1-B2-4) 133
5.2.4. Co-Combustion of Bursa/Orhaneli Lignite with 50% (by wt.) Woodchips (C1-B2-5) 135
5.2.5. Discussion on the Effect of Secondary Air Ratio on Emissions in SET#2 137
5.3. Assessment of Experiments for SET#3 154
5.3.1. Combustion of Bursa/Orhaneli Lignite with Addition of Çan Limestone (Ca/S = 2.0) (C1-2) 154
5.3.2. Combustion of Bursa/Orhaneli Lignite with Addition of Çan Limestone (Ca/S = 2.5) (C1-3) 155
5.3.3. Combustion of Bursa/Orhaneli Lignite with Addition of Çan Limestone (Ca/S = 3.0) (C1-4) 155
5.3.4. Combustion of Denizli/Kale Lignite (C2-1) 155
5.3.5. Combustion of Denizli/Kale Lignite with Addition of Çan Limestone (Ca/S = 2.0) (C2-2) 156
5.3.6. Combustion of Denizli/Kale Lignite with Addition of Çan Limestone (Ca/S = 2.5) (C2-3) 156
5.3.7. Combustion of Denizli/Kale Lignite with Addition of Çan Limestone (Ca/S = 3.0) (C2-4) 156
5.3.8. Discussion on the Effect of Ca/S Ratio on SO_2 Emissions in SET#3 156
5.4. Assessment of Experiments for SET#4 158
5.4.1. Co-Combustion of Bursa/Orhaneli Lignite and Olive Cake (50% by wt.) – Long Term Test (C1-B1-6) 158
5.4.2. Co-Combustion of Bursa/Orhaneli Lignite and Olive Cake (50% by wt.) with Çan Limestone (Ca/S_{total} = 2.0) – Long Term Test (C1-B1-7) 164
5.4.3. Co-Combustion of Denizli/Kale Lignite and Olive Cake (50% by wt.) – Long Term Test (C2-B1-1) 169
5.4.4. Co-Combustion of Denizli/Kale Lignite and Olive Cake (50% by wt.) with Çan Limestone (Ca/S_{total} = 2.0) – Long Term Test (C2-B1-2) 173
5.4.5. Combustion of Olive Cake – Long Term Test (B1-2) 178
5.4.6. Comparison of Emissions in SET#4 with the Limits in Turkish Regulation 179
5.4.7. Combustion Efficiency (Carbon-based) 182
5.5. Assessment of Ash Analysis for Experiments in SET#4 185

5.5.1. Co-Combustion of Bursa/Orhaneli Lignite and Olive Cake (50% by wt.) (C1-B1-6) 186
5.5.1.1. SEM-EDS Analysis of Bottom Ash (C1-B1-6) 190
5.5.1.2. SEM-EDS Analysis of Deposit on the Deposit Sampling Probe (C1-B1-6) 194
5.5.2. Co-Combustion of Bursa/Orhaneli Lignite and Olive Cake (50% by wt.) with Çan Limestone (Ca/S_{total} = 2.0) (C1-B1-7) 203
5.5.2.1. SEM-EDS Analysis of Bottom Ash (C1-B1-7) 207
5.5.2.2. SEM-EDS Analysis of Deposit on the Deposit Sampling Probe (C1-B1-7) 211
5.5.3. Co-Combustion of Denizli/Kale Lignite and Olive Cake (50% by wt.) (C2-B1-1) 218
5.5.3.1. SEM-EDS Analysis of Bottom Ash (C2-B1-1) 221
5.5.3.2. SEM-EDS Analysis of Deposit on the Deposit Sampling Probe (C2-B1-1) 224
5.5.4. Co-Combustion of Denizli/Kale Lignite and Olive Cake (50% by wt.) with Çan Limestone (Ca/S_{total} = 2.0) (C2-B1-2) 230
5.5.4.1. SEM-EDS Analysis of Bottom Ash (C2-B1-2) 233
5.5.4.2. SEM-EDS Analysis of Deposit on the Deposit Sampling Probe (C2-B1-2) 238
5.5.5. Discussion on Ash Analyses in SET#4 246
5.5.5.1. Bed Agglomeration 246
5.5.5.2. Slagging and Fouling 249
5.5.5.3. Conclusive Remarks 250
6. CONCLUSIONS 253
7. RECOMMENDATIONS FOR FURTHER STUDIES 257
8. REFERENCES 259
APPENDICES
A. STANDARD PIPE SIZES FOR SELECTED PIPES 273
B. TECHNICAL DRAWINGS 275
C. CALIBRATION OF THE FUEL FEEDING SYSTEM 283
CURRICULUM VITAE 287

LIST OF TABLES

TABLES

Table 2.1 Fluidized bed power plants owned by the legal entities who have electricity production license in Turkey ("Üretim Lisansı Verilen Tüzel Kişiler (in Turkish)," 2013)..... 23

Table 2.2 CO, NO_x (measured as NO_2) and SO_x (measured as SO_2) emission limits for the combustion plants using solid fuels according to the EU Directive ("Directive 2001/08/EC of the European Parliament and of the Council of 23 October 2001 on the limitation of emission of certain pollutants into air from large combustion plants," 2001) and the Turkish Regulation ("Turkish Regulation for Industrial Air Pollution Control," 2009)..... 25

Table 3.1 Energy outlook of Turkey between 1985 and 2011 ("Energy Balances of Turkey," 2013)..... 31

Table 3.2 Major coal* producers, net exporters and net importers in 2011 (*IEA Key World Energy Statistics*, 2012)..... 32

Table 3.3 Major lignite producers in 2011 (*IEA Statistics Coal Information*, 2012)..... 35

Table 3.4 Turkey's GHG emissions by sectors and gases for the years 1990 and 2010 (*TurkStat National Greenhouse Gas Inventory Report 1990-2010*, 2012)..... 39

Table 3.5 CO_2 emissions (sectoral approach) from fuel combustion for the years 1990 and 2010 (million tonnes of CO_2) (*IEA Statistics CO_2 Emissions from Fuel Combustion*, 2012)..... 40

Table 3.6 Renewables indicators in 2010 (*IEA Statistics Renewables Information*, 2012)42

Table 3.7 World olive production between 2008 and 2011 and the average production for 10 years between 2002 and 2011 ("FAOSTAT Crop Productions," 2013)..... 43

Table 4.1 List of standards used in the analyses..... 60

Table 4.2 Proximate analysis and heating values of coals and biomasses..... 61

Table 4.3 Ultimate analysis of coals and biomasses..... 62

Table 4.4 Chlorine contents of fuel samples..... 63

Table 4.5 Reactivity index of different limestones..... 63

Table 4.6 Total porosity and BET surface area of Çan limestone..... 64

Table 4.7 Chemical composition of Çan limestone..... 64

Table 4.8 Goals; constant, variable and control parameters of the experimental sets..... 75

Table 4.9 List of experiments in SET#1 76
Table 4.10 List of experiments in SET#2 77
Table 4.11 List of experiments in SET#3 78
Table 4.12 List of experiments in SET#4 79
Table 4.13 Details of experiments in each set 80
Table 4.14 Measurement ranges of ABB-AO 2000 flue gas analyzer 83
Table 4.15 Measurement ranges of GASMET-DX 4000 flue gas analyzer 83
Table 4.16 Ash composition of fuel samples according to the XRF analysis 85
Table 4.17 Ash fusion temperatures of fuel used in SET#4 86
Table 5.1 Operational conditions for the combustion and co-combustion tests in SET#1 119
Table 5.2 Optimum excess air ratios, corresponding thermal power, superficial velocity and flue gas emissions for the combustion and co-combustion experiments in SET#1 120
Table 5.3 Flue gas emission limits according to the Turkish Regulation ("Turkish Regulation for Industrial Air Pollution Control," 2009) 120
Table 5.4 Comparison of flue gas emissions at the optimum excess air ratio for combustion experiments in SET#1 with the limits in the Turkish Regulation ("Turkish Regulation for Industrial Air Pollution Control," 2009) 128
Table 5.5 Secondary air ratios and corresponding CO, NO, and SO_2 emissions and T_{dp} for the co-combustion of Bursa/Orhaneli lignite with 30% olive cake (by wt.) (C1-B1-4) 138
Table 5.6 Secondary air ratios and corresponding CO, NO, and SO_2 emissions and T_{dp} for the co-combustion of Bursa/Orhaneli lignite with 50% olive cake (by wt.) (C1-B1-5) 142
Table 5.7 Secondary air ratios and corresponding CO, NO, and SO_2 emissions and T_{dp} for the co-combustion of Bursa/Orhaneli lignite with 30% woodchips (by wt.) (C1-B2-4) 146
Table 5.8 Secondary air ratios and corresponding CO, NO, and SO_2 emissions and T_{dp} for the co-combustion of Bursa/Orhaneli lignite with 50% woodchips (by wt.) (C1-B2-5) 151
Table 5.9 Proximate and ultimate analyses of fuels used in the co-combustion test (C1-B1-6) 159
Table 5.10 Operational Parameters for the co-combustion test (C1-B1-6) 160

Table 5.11 Flue gas emission limits for the co-combustion test (C1-B1-6) according to the Turkish Regulation ("Turkish Regulation for Industrial Air Pollution Control," 2009) 163
Table 5.12 Measurement duration, optimum excess air ratios, corresponding thermal power, superficial velocity and flue gas emissions for the co-combustion test (C1-B1-6) 163
Table 5.13 Proximate and ultimate analyses of fuels used in the co-combustion test (C1-B1-7) 165
Table 5.14 Operational Parameters for the co-combustion test (C1-B1-7) 165
Table 5.15 Flue gas emission limits for the co-combustion test (C1-B1-7) according to the Turkish Regulation ("Turkish Regulation for Industrial Air Pollution Control," 2009) 168
Table 5.16 Proximate and ultimate analyses of fuels used in the co-combustion test (C2-B1-1) 170
Table 5.17 Operational Parameters for the co-combustion test (C2-B1-1) 170
Table 5.18 Flue gas emission limits for the co-combustion test (C2-B1-1) according to the Turkish Regulation ("Turkish Regulation for Industrial Air Pollution Control," 2009) 173
Table 5.19 Proximate and ultimate analyses of fuels used in the co-combustion test (C2-B1-2) 174
Table 5.20 Operational Parameters for the co-combustion test (C2-B1-2) 175
Table 5.21 Flue gas emission limits for the co-combustion test (C2-B1-2) according to the Turkish Regulation ("Turkish Regulation for Industrial Air Pollution Control," 2009) 177
Table 5.22 Operational conditions for the co-combustion tests in SET#4 179
Table 5.23 Optimum excess air ratios, corresponding thermal power, superficial velocity and flue gas emissions for the co-combustion tests in SET#4 180
Table 5.24 Comparison of flue gas emissions at the optimum excess air ratio for the co-combustion tests in SET#4 with the limits in the Turkish Regulation ("Turkish Regulation for Industrial Air Pollution Control," 2009) 181
Table 5.25 Percentages of unburnt carbon in the ashes and ash discharge rates for co-combustion tests in SET#4 184

Table 5.26 Combustion losses and carbon-based combustion efficiencies for the co-combustion tests in SET#4 185
Table 5.27 List of experiments conducted in the scope of SET#4 186
Table 5.28 Range of operational parameters for the co-combustion test (C1-B1-6) 186
Table 5.29 XRF results of fuel ashes and ashes formed at the end of the co-combustion test (C1-B1-6) 187
Table 5.30 XRD (Rietveld method) results of fuel ashes and ashes formed at the end of the co-combustion test (C1-B1-6) 188
Table 5.31 XRD (RIR method) results of deposit collected from deposit sampling probe at the end of the co-combustion test (Analyses were done at METU-Central Laboratory) (C1-B1-6) 189
Table 5.32 Range of operational parameters for the co-combustion test (C1-B1-7) 203
Table 5.33 XRF results of fuel ashes and ashes formed at the end of the co-combustion test (C1-B1-7) 204
Table 5.34 XRD (Rietveld method) results of fuel ashes and ashes formed at the end of the co-combustion test (C1-B1-7) 205
Table 5.35 XRD (RIR method) results of deposit collected from deposit sampling probe at the end of the co-combustion test (Analyses were done at METU-Central Laboratory) (C1-B1-7) 206
Table 5.36 Range of operational parameters for the co-combustion test (C2-B1-1) 218
Table 5.37 XRF results of fuel ashes and ashes formed at the end of the co-combustion test (C2-B1-1) 219
Table 5.38 XRD (Rietveld method) results of fuel ashes and ashes formed at the end of the co-combustion test (C2-B1-1) 220
Table 5.39 XRD (RIR method) results of deposit collected from deposit sampling probe at the end of the co-combustion test (Analyses were done at METU-Central Laboratory) (C2-B1-1) 220
Table 5.40 Range of operational parameters for the co-combustion test (C2-B1-2) 230
Table 5.41 XRF results of fuel ashes and ashes formed at the end of the co-combustion test (C2-B1-2) 231
Table 5.42 XRD (Rietveld method) results of fuel ashes and ashes formed at the end of the co-combustion test (C2-B1-2) 232

Table 5.43 XRD (RIR method) results of deposit collected from deposit sampling probe at the end of the co-combustion test (Analyses were done at METU-Central Laboratory) (C2-B1-2) 233
Table A.1 Standard Pipe Sizes for Selected Pipes 273
Table B.1 Specifications of Windbox 275
Table B.2 Specifications of Moduel-101 276
Table B.3 Temperature Transmitters 278
Table B.4 Pressure Transmitters 280
Table B.5 Critical measurement points on the combustion system 280

LIST OF FIGURES

FIGURES

Figure 2.1 Different types of fuels used for FBC technology (Winter and Szentannai, 2010) 6

Figure 2.2 (a) Circulating fluidized bed combustor (b) Bubbling fluidized bed combustor (Khan, 2007) 8

Figure 2.3 Ash Fusion Temperatures (*ASTM Standard D1857 Standard Test Method for Fusibility of Coal and Coke Ash*, 2004) 21

Figure 3.1 World's TPES (Mtoe) from 1971 to 2010 (*IEA Key World Energy Statistics*, 2012) 27

Figure 3.2 Shares of world's TPES for the years 1973 and 2010 (*IEA Key World Energy Statistics*, 2012) 28

Figure 3.3 Turkey's TPES for the years 2003 and 2011 ("Energy Balances of Turkey," 2013) 29

Figure 3.4 Turkey's Total Energy Production between the years 2003 and 2011 ("Energy Balances of Turkey," 2013) 29

Figure 3.5 Total energy production, net imports and primary energy supply between 1985 and 2011 in Turkey ("Energy Balances of Turkey," 2013) 30

Figure 3.6 World coal production by region (Mt) (*IEA Key World Energy Statistics*, 2012). 33

Figure 3.7 Coal production in different regions of the world for the years 1973 and 2011 (*IEA Key World Energy Statistics*, 2012) 34

Figure 3.8 World CO_2 emissions from fuel combustion between 1971 and 2010 by fuel (Mt of CO_2) (*IEA Key World Energy Statistics*, 2012) 36

Figure 3.9 world CO_2 emissions for the years 1973 and 2010 (*IEA Key World Energy Statistics*, 2012) 36

Figure 3.10 Turkey's coal map by 2011 ("Coal, Country Profiles, Turkey," 2011) 38

Figure 3.11 World olive production by countries between 2002 and 2011 ("FAOSTAT Crop Productions," 2013) 44

Figure 4.1 Schematic diagram of the combustion system 65

Figure 4.2 Control screen of the combustion system 66

Figure 4.3 A photograph of the combustion system 67

Figure 4.4 Process and instrumentation diagram of the circulating fluidized bed combustion system (flue gas path)..... 69
Figure 4.5 Process and instrumentation diagram of circulating fluidized bed combustion system (water/air path)..... 70
Figure 4.6 The distributor plate used in the combustor..... 71
Figure 4.7 Air Cooled Deposit Sampling Probe with a Detachable Ring 82
Figure 5.1 Temperature profile along the combustor for the combustion of Bursa/Orhaneli lignite (C1-1) 88
Figure 5.2 Temperature profile along the return leg for the combustion of Bursa/Orhaneli lignite (C1-1)..... 89
Figure 5.3 Effect of excess air ratio on flue gas emissions for the combustion of Bursa/Orhaneli lignite (C1-1) 90
Figure 5.4 Emissions measured by Gas Analyzer-2 with respect to excess air ratio for the combustion of Bursa/Orhaneli lignite (C1-1) 92
Figure 5.5 Temperature profile along the combustor for the co-combustion of Bursa/Orhaneli lignite with 10% (by wt.) olive cake (C1-B1-1)..... 93
Figure 5.6 Temperature profile along the return leg for the co-combustion of Bursa/Orhaneli lignite with 10% (by wt.) olive cake (C1-B1-1)..... 94
Figure 5.7 Effect of excess air ratio on flue gas emissions for the co-combustion of Bursa/Orhaneli lignite with 10% (by wt.) olive cake (C1-B1-1); a-) original figure, b-) enlarged view..... 95
Figure 5.8 Temperature profile along the combustor for the co-combustion of Bursa/Orhaneli lignite with 30% (by wt.) olive cake (C1-B1-2)..... 97
Figure 5.9 Temperature profile along the return leg for the co-combustion of Bursa/Orhaneli lignite with 30% (by wt.) olive cake (C1-B1-2)..... 98
Figure 5.10 Effect of excess air ratio on flue gas emissions for the co-combustion of Bursa/Orhaneli lignite with 30% (by wt.) olive cake (C1-B1-2); a-) original figure, b-) enlarged view..... 99
Figure 5.11 Temperature profile along the combustor for the co-combustion of Bursa/Orhaneli lignite with 50% (by wt.) olive cake (C1-B1-3)..... 101
Figure 5.12 Temperature profile along the return leg for the co-combustion of Bursa/Orhaneli lignite with 50% (by wt.) olive cake (C1-B1-3)..... 102

Figure 5.13 Effect of excess air ratio on flue gas emissions for the co-combustion of Bursa/Orhaneli lignite with 50% (by wt.) olive cake (C1-B1-3); a-) original figure, b-) enlarged view..... 103
Figure 5.14 Temperature profile along the combustor for the combustion of olive cake (B1-1)..... 105
Figure 5.15 Temperature profile along the return leg for the combustion of olive cake (B1-1)..... 106
Figure 5.16 Effect of excess air ratio on flue gas emissions for the combustion of olive cake (B1-1) 107
Figure 5.17 Emissions measured by Gas Analyzer-2 with respect to excess air ratio for the combustion of olive cake (B1-1) 109
Figure 5.18 Temperature profile along the combustor for the co-combustion of Bursa/Orhaneli lignite with 10% (by wt.) woodchips (C1-B2-1)..... 110
Figure 5.19 Temperature profile along the return leg for the co-combustion of Bursa/Orhaneli lignite with 10% (by wt.) woodchips (C1-B2-1)..... 111
Figure 5.20 Effect of excess air ratio on flue gas emissions for the co-combustion of Bursa/Orhaneli lignite with 10% (by wt.) woodchips (C1-B2-1)..... 112
Figure 5.21 Temperature profile along the combustor for the co-combustion of Bursa/Orhaneli lignite with 30% (by wt.) woodchips (C1-B2-2)..... 113
Figure 5.22 Temperature profile along the return leg for the co-combustion of Bursa/Orhaneli lignite with 30% (by wt.) woodchips (C1-B2-2)..... 114
Figure 5.23 Effect of excess air ratio on flue gas emissions for the co-combustion of Bursa/Orhaneli lignite with 30% (by wt.) woodchips (C1-B2-2)..... 115
Figure 5.24 Temperature profile along the combustor for the co-combustion of Bursa/Orhaneli lignite with 50% (by wt.) woodchips (C1-B2-3)..... 116
Figure 5.25 Temperature profile along the return leg for the co-combustion of Bursa/Orhaneli lignite with 50% (by wt.) woodchips (C1-B2-3)..... 117
Figure 5.26 Effect of excess air ratio on flue gas emissions for the co-combustion of Bursa/Orhaneli lignite with 50% (by wt.) woodchips (C1-B2-3)..... 118
Figure 5.27 Effect of olive cake addition on CO emissions with respect to excess air ratio and comparison of emissions to the limits in the Turkish Regulation ("Turkish Regulation for Industrial Air Pollution Control," 2009) for co-combustion of

Bursa/Orhaneli lignite and olive cake fuel mixtures; a-) original figure, b-) enlarged view, c-) emission trendlines, d-) temperature profile at optimum λ... 121

Figure 5.28 Effect of olive cake addition on NO emissions with respect to excess air ratio and comparison of emissions to the limits in the Turkish Regulation ("Turkish Regulation for Industrial Air Pollution Control," 2009) for the co-combustion of Bursa/Orhaneli lignite and olive cake fuel mixtures..... 123

Figure 5.29 Effect of olive cake addition on SO_2 emissions with respect to excess air ratio and comparison of emissions to the limits in the Turkish Regulation ("Turkish Regulation for Industrial Air Pollution Control," 2009) for the co-combustion of Bursa/Orhaneli lignite and olive cake fuel mixtures..... 124

Figure 5.30 Effect of woodchips addition on CO emissions with respect to excess air ratio and comparison of emissions to the limits in the Turkish Regulation ("Turkish Regulation for Industrial Air Pollution Control," 2009) for co-combustion of Bursa/Orhaneli lignite and woodchips fuel mixtures; a-) original figure, b-) enlarged view, c-) emission trendlines, d-) temperature profile at optimum λ..... 125

Figure 5.31 Effect of woodchips addition on NO emissions with respect to excess air ratio and comparison of emissions to the limits in the Turkish Regulation ("Turkish Regulation for Industrial Air Pollution Control," 2009) for the co-combustion of Bursa/Orhaneli lignite and woodchips fuel mixtures..... 126

Figure 5.32 Effect of woodchips addition on SO_2 emissions with respect to excess air ratio and comparison of emissions to the limits in the Turkish Regulation ("Turkish Regulation for Industrial Air Pollution Control," 2009) for the co-combustion of Bursa/Orhaneli lignite and woodchips fuel mixtures..... 127

Figure 5.33 Effect of secondary air ratio and its location on temperature profile along the combustor for co-combustion of Bursa/Orhaneli lignite with 30% (by wt.) olive cake (C1-B1-4) 130

Figure 5.34 Effect of secondary air ratio and its location on temperature profile along the return leg for co-combustion of Bursa/Orhaneli lignite with 30% (by wt.) olive cake (C1-B1-4) 131

Figure 5.35 Effect of secondary air ratio and its location on temperature profile of combustor for co-combustion of Bursa/Orhaneli lignite with 50% (by wt.) olive cake (C1-B1-5) 132

Figure 5.36 Effect of secondary air ratio and its location on temperature profile of return leg for co-combustion of Bursa/Orhaneli lignite with 50% (by wt.) olive cake (C1-B1-5)..... 133

Figure 5.37 Effect of secondary air ratio and its location on temperature profile along the combustor for co-combustion of Bursa/Orhaneli lignite with 30% (by wt.) woodchips (C1-B2-4) 134

Figure 5.38 Effect of secondary air ratio and its location on temperature profile along the return leg for co-combustion of Bursa/Orhaneli lignite with 30% (by wt.) woodchips (C1-B2-4) 135

Figure 5.39 Effect of secondary air ratio and its location on temperature profile of combustor for co-combustion of Bursa/Orhaneli lignite with 50% (by wt.) woodchips (C1-B2-5) 136

Figure 5.40 Effect of secondary air ratio and its location on temperature profile of return leg for co-combustion of Bursa/Orhaneli lignite with 50% (by wt.) woodchips (C1-B2-5)..... 137

Figure 5.41 Effect of secondary air ratio and its location on CO emission and comparison of CO emission to emission limits for co-combustion of Bursa/Orhaneli lignite with 30% (by wt.) olive cake (C1-B1-4) 139

Figure 5.42 Effect of secondary air ratio and its location on NO emission and comparison of NO emission to emission limits for co-combustion of Bursa/Orhaneli lignite with 30% (by wt.) olive cake (C1-B1-1) 140

Figure 5.43 Effect of secondary air ratio and its location on SO_2 emission and comparison of SO_2 emission to emission limits for co-combustion of Bursa/Orhaneli lignite with 30% (by wt.) olive cake (C1-B1-4)..... 141

Figure 5.44 Effect of secondary air ratio and its location on CO emission and comparison of CO emission to emission limits for co-combustion of Bursa/Orhaneli lignite with 50% (by wt.) olive cake (C1-B1-5) 143

Figure 5.45 Effect of secondary air ratio and its location on NO emission and comparison of NO emission to emission limits for co-combustion of Bursa/Orhaneli lignite with 50% (by wt.) olive cake (C1-B1-5) 144

Figure 5.46 Effect of secondary air ratio and its location on SO_2 emission and comparison of SO_2 emission to emission limits for co-combustion of Bursa/Orhaneli lignite with 50% (by wt.) olive cake (C1-B1-5)..... 145

Figure 5.47 Effect of secondary air ratio and its location on CO emission and comparison of CO emission to emission limits for co-combustion of Bursa/Orhaneli lignite with 30% (by wt.) woodchips (C1-B2-4)..... 147

Figure 5.48 Effect of secondary air ratio on CO emission with respect to cyclone outlet temperature for co-combustion of Bursa/Orhaneli lignite with 30% (by wt.) woodchips (C1-B2-4)..... 148

Figure 5.49 Effect of secondary air ratio and its location on NO emission and comparison of NO emission to emission limits for co-combustion of Bursa/Orhaneli lignite with 30% (by wt.) woodchips (C1-B2-4)..... 149

Figure 5.50 Effect of secondary air ratio and its location on SO_2 emission and comparison of SO_2 emission to emission limits for co-combustion of Bursa/Orhaneli lignite with 30% (by wt.) woodchips (C1-B2-4)..... 150

Figure 5.51 Effect of secondary air ratio and its location on CO emission and comparison of CO emission to emission limits for co-combustion of Bursa/Orhaneli lignite with 50% (by wt.) woodchips (C1-B2-5)..... 152

Figure 5.52 Effect of secondary air ratio and its location on NO emission and comparison of NO emission to emission limits for co-combustion of Bursa/Orhaneli lignite with 50% (by wt.) woodchips (C1-B2-5)..... 153

Figure 5.53 Effect of secondary air ratio and its location on SO_2 emission and comparison of SO_2 emission to emission limits for co-combustion of Bursa/Orhaneli lignite with 50% (by wt.) woodchips (C1-B2-5)..... 154

Figure 5.54 Effect of Ca/S ratio on SO_2 emission for the combustion of Bursa/Orhaneli lignite in SET#3..... 157

Figure 5.55 Effect of Ca/S ratio on SO_2 emission for the combustion of Denizli/Kale lignite in SET#3..... 158

Figure 5.56 Temperature profile along the combustor for the co-combustion of Bursa/Orhaneli lignite and 50% olive cake (by wt.) - Long Term Test (C1-B1-6)161

Figure 5.57 Temperature profile along the return leg for the co-combustion of Bursa/Orhaneli lignite and 50% olive cake (by wt.) - Long Term Test (C1-B1-6)162

Figure 5.58 Effect of excess air ratio on flue gas emissions for the co-combustion of Bursa/Orhaneli lignite and 50% olive cake (by wt.) - Long Term Test (C1-B1-6)164

Figure 5.59 Temperature profile along the combustor for the co-combustion of Bursa/Orhaneli lignite and 50% olive cake (by wt.) with Çan Limestone (Ca/S_{total} = 2.0) - Long Term Test (C1-B1-7) 166
Figure 5.60 Temperature profile along the return leg for the co-combustion of Bursa/Orhaneli lignite and 50% olive cake (by wt.) with Çan Limestone (Ca/S_{total} = 2.0) - Long Term Test (C1-B1-7) 167
Figure 5.61 Effect of excess air ratio on flue gas emissions for the co-combustion of Bursa/Orhaneli lignite and 50% olive cake (by wt.) with Çan Limestone (Ca/S_{total} = 2.0) - Long Term Test (C1-B1-7) 169
Figure 5.62 Temperature profile along the combustor for the co-combustion of Denizli/Kale lignite and 50% olive cake (by wt.) - Long Term Test (C2-B1-1) 171
Figure 5.63 Temperature profile along the return leg for the co-combustion of Denizli/Kale lignite and 50% olive cake (by wt.) - Long Term Test (C2-B1-1) 172
Figure 5.64 Effect of excess air ratio on flue gas emissions for the co-combustion of Denizli/Kale lignite and 50% olive cake (by wt.) - Long Term Test (C2-B1-1) 173
Figure 5.65 Temperature profile along the combustor for the co-combustion of Denizli/Kale lignite and 50% olive cake (by wt.) with Çan Limestone (Ca/S_{total} = 2.0) - Long Term Test (C2-B1-2) 176
Figure 5.66 Temperature profile along the return leg for the co-combustion of Denizli/Kale lignite and 50% olive cake (by wt.) with Çan Limestone (Ca/S_{total} = 2.0) - Long Term Test (C2-B1-2) 177
Figure 5.67 Effect of excess air ratio on flue gas emissions for the co-combustion of Denizli/Kale lignite and 50% olive cake (by wt.) with Çan Limestone (Ca/S_{total} = 2.0) - Long Term Test (C2-B1-1) 178
Figure 5.68 General view of sample taken from the bottom ash (C1-B1-6) 190
Figure 5.69 SEM micrograph and SEM-EDS result of point A on the particle shown as "1" in Figure 5.68 191
Figure 5.70 SEM micrograph and SEM-EDS result of point A on the particle shown as "2" in Figure 5.68 191
Figure 5.71 Enlarged view of the region shown as "3" in Figure 5.68 192
Figure 5.72 Enlarged view of the particle in Figure 5.71 and SEM-EDS results of points A and B on the particle 193

Figure 5.73 SEM micrograph and SEM-EDS results of points A and B on the particle shown as "4" in Figure 5.68 194
Figure 5.74 Images of the deposit sampling probe a) top view b) right-side view c) bottom view d) left-side view (C1-B1-6) 195
Figure 5.75 General view of sample taken from deposit sampling probe (C1-B1-6) 196
Figure 5.76 Enlarged view of particle shown as "1" in Figure 5.75 197
Figure 5.77 Enlarged view of the surface of the particle shown as "1" in Figure 5.76 and SEM-EDS results of points A and B 198
Figure 5.78 Enlarged view of the particle shown as "2" in Figure 5.75 199
Figure 5.79 Enlarged view of the area shown as "1" in Figure 5.78 and SEM-EDS results of points A and B 200
Figure 5.80 Enlarged view of particle shown as "3" in Figure 5.75 201
Figure 5.81 Enlarged view of the area shown as "1" in Figure 5.80 and SEM-EDS results of points A, B, C, and D 202
Figure 5.82 General view of sample taken from bottom ash (C1-B1-7) 207
Figure 5.83 Enlarged view of the region shown as "1" in Figure 5.82 208
Figure 5.84 SEM micrograph and SEM-EDS results of points A and B on the particle shown as "1" in Figure 5.83 209
Figure 5.85 Enlarged view of the region shown as "2" in Figure 5.82 210
Figure 5.86 SEM micrograph and SEM-EDS results of points A and B on the particle shown as "1" in Figure 5.85 211
Figure 5.87 Image of the deposit sampling probe a) top b) right-side c) bottom d) left-side (C1-B1-7) 212
Figure 5.88 General view of sample taken from deposit sampling probe (C1-B1-7) 213
Figure 5.89 Enlarged view of region shown as "1" in Figure 5.88 214
Figure 5.90 SEM micrograph and SEM-EDS results of points A, B and C on the particle shown as "1" in Figure 5.89 215
Figure 5.91 Enlarged view of region shown as "2" in Figure 5.89 216
Figure 5.92 SEM micrograph and SEM-EDS results of four points (A, B, C and D) on the particle shown as "1" in Figure 5.91 217
Figure 5.93 General view of sample taken from bottom ash (C2-B1-1) 221
Figure 5.94 Enlarged view of the particle shown as "1" in Figure 5.93 222

Figure 5.95 SEM micrograph and SEM-EDS results of points A, B and C on the particle shown as "1" in Figure 5.94 223
Figure 5.96 Enlarged view of the particle shown as "2" in Figure 5.93 and SEM-EDS results of points A and B 224
Figure 5.97 Image of the deposit sampling probe a) top b) right-side c) bottom d) left-side (C2-B1-1) 225
Figure 5.98 General view of sample taken from deposit sampling probe (C2-B1-1) 226
Figure 5.99 Enlarged view of region shown as "1" in Figure 5.98 226
Figure 5.100 SEM micrograph and SEM-EDS results of points A and B on the particle shown as "1" in Figure 5.99 227
Figure 5.101 Enlarged view of the region shown as "2" in Figure 5.98 and SEM-EDS results of points A, B and C 228
Figure 5.102 Enlarged view of the region shown as "3" in Figure 5.98 and SEM-EDS results of points A, B, C, D, E and F 229
Figure 5.103 General view of sample taken from bottom ash (C2-B1-2) 233
Figure 5.104 Enlarged view of the region shown as "1" in Figure 5.103 and SEM-EDS results of points A, B and C 234
Figure 5.105 Enlarged view of the particle shown as "2" in Figure 5.103 and SEM-EDS results of points A and B 235
Figure 5.106 Another view of sample taken from bottom ash (C2-B1-2) 236
Figure 5.107 Enlarged view of the region shown as "1" in Figure 5.106 and SEM-EDS results of points A, B, C and D 237
Figure 5.108 Image of the deposit sampling probe a) top b) right-side c) bottom d) left-side (C2-B1-2) 238
Figure 5.109 General view of sample taken from deposit sampling probe (C2-B1-2) .. 239
Figure 5.110 Enlarged view of the particle shown as "1" in Figure 5.109 and SEM-EDS results of points A and B 240
Figure 5.111 Enlarged view of the region shown as "1" in Figure 5.110 and SEM-EDS results of points A, B and C 241
Figure 5.112 Enlarged view of the particle shown as "2" in Figure 5.109 and SEM-EDS results of points A, B and C 242
Figure 5.113 Enlarged view of the particle shown as "3" in Figure 5.109 and SEM-EDS results of points A, B and C 243

Figure 5.114 Another view of sample taken from deposit sampling probe (C2-B1-2).. 244
Figure 5.115 Enlarged view of the region shown as "1" in Figure 5.114 and SEM-EDS results of points A, B, C, D, E and F 245
Figure B.1 Technical drawings of Windbox 275
Figure B.2 Technical drawings of Module-101 276
Figure B.3 Technical drawings of Module-102 and Module-107 277
Figure B.4 Technical drawings of Module-103, Module-104, Module-105 and Module-106 277
Figure B.5 Technical drawings of Module-108 278
Figure C.1 Feeding rate calibration curve of M-01 for Olive Cake 284
Figure C.2 Feeding rate calibration curve of M-01 for Woodchips 284
Figure C.3 Feeding rate calibration curve of M-02 for Bursa/Orhaneli lignite..... 285
Figure C.4 Feeding rate calibration curve of M-02 for Denizli/Kale lignite 285

LIST OF ABBREVIATIONS

GHG	Greenhouse gases
LULUCF	Land Use, Land Use Change and Forestry
TPES	Total Primary Energy Supply
Mt	Million tonnes (1 tonne * 10^6)
Gt	Giga tonnes (1 tonne * 10^9)
ktoe	kilotonnes of oil equivalent
Mtoe	Million tonnes of oil equivalent
MW_e	Megawatt (electric)
MW_{th}	Megawatt (thermal)
GW_{th}	Gigawatt (thermal)
GJ	Gigajoule (10^9 joules)
PJ	Petajoule (10^{15} joules)
EJ	Exojoule (10^{18} joules)
ASTM	the American Society for Testing and Measurement
BGR	German Federal Institute for Geosciences and Natural Resources
EU	European Union
EÜAŞ	Turkish Electricity Generation Company
FAO	Food and Agriculture Organization of the United Nations
IPCC	Intergovernmental Panel on Climate Change
IEA	International Energy Agency
IEKP	German Government's Integrated Energy and Climate Programme
METU	Middle East Technical University
MRC-CI	Marmara Research Center-Chemistry Institute
MRC-EI	Marmara Research Center-Energy Institute
MRC-MI	Marmara Research Center-Material Institute
OECD	Organization for Economic and Co-operation Development (Includes countries Australia, Austria, Belgium, Canada, Chile, the Czech Republic, Denmark, Estonia, Finland, France, Germany, Greece, Hungary, Iceland, Ireland, Israel, Italy, Japan, Korea, Luxembourg, Mexico, the Netherlands, New Zealand, Norway, Poland, Portugal, the Slovak Republic, Slovenia, Spain, Sweden, Switzerland, Turkey, the United Kingdom and the United States of America (USA))
TUBITAK	the Scientific and Technological Research Council of Turkey
TUIK	Turkish Statistical Institute of Turkey
UNECE	International Coal Classification of the Economic Commission for Europe
UNFCCC	the United Nations Framework Convention on Climate Change
WEC	World Energy Council
FBC	Fluidized Bed Combustion
BFB	Bubbling Fluidized Bed

CFB	Circulating Fluidized Bed
BFBC	Bubbling Fluidized Bed Combustor
CFBC	Circulating Fluidized Bed Combustor
Lab-CFBC	Laboratory-scale Circulating Fluidized Bed Combustor
λ	Excess air ratio (-)
SAR	Secondary Air Ratio (-)
T_{dp}	Temperature of the dense phase (^{o}C)
U_o	Superficial velocity in the combustor, m/s
EL_{mix}	Emission limit for the fuel mixture
EL_1	Emission limit for primary fuel
EL_2	Emission limit for supplementary fuel
P_{th-1}	Thermal power for primary fuel
P_{th-2}	Thermal power for supplementary fuel
PT	Pressure Transmitter
TT	Temperature Transmitter
IT	Initial deformation temperature
ST	Softening temperature
HT	Hemispherical temperature
FT	Fluid temperature
H	Hydrogen
C	Carbon
N	Nitrogen
Na	Sodium
Mg	Magnesium
Al	Aluminum
Si	Silicon
S	Sulfur
S_{ash}	Sulfur in ash
$S_{combustible}$	Combustible sulfur
S_{total}	Total sulfur
Cl	Chlorine
K	Potassium
Ca	Calcium
Cr	Chromium
Fe	Iron
Ni	Nickel
U	Uranium
CH_4	Methane
C_mH_n	Hydrocarbons
NH_3	Ammonia
HCN	Hydrogen cyanide
CO	Carbon monoxide
CO_2	Carbon dioxide
N_2	Nitrogen (gas)
NO	Nitrogen oxide

NO_2	Nitrogen dioxide
NO_x	Nitrogen oxides
N_2O	Nitrous oxide
SO_2	Sulfur dioxides
O_2	Oxygen
O_3	Ozone
MgO	Magnesium oxide
CaO	Calcium oxide
$CaSO_4$	Calcium sulfate
K_2SO_4	Potassium sulfate
Fe_2O_3	Iron (III) oxide
AFI	Ash fusibility index
B/A_R	Base-to-acid index
F_u	Fouling index
BA	bottom ash
FA-C	fly ash captured in the second cyclone
FA-BF	fly ash captured in the bag filter
DN	Nominal Diameter
ID	Inner Diameter
OD	Outer Diameter
HHV	Higher heating value
LHV	Lower heating value
SCR	Selective catalytic reduction
SNCR	Selective non-catalytic reduction
SEM-EDS	Scanning Electron Microscope-Energy Dispersive X-ray spectroscopy
XRD	X-ray diffraction
XRF	X-ray fluorescence
%MC	Moisture content of fuel, % by weight
%H	Hydrogen content of fuel, % by weight
h_{fg}	Latent heat of vaporization of water at 25^{o}C, 582.78 kcal/kg
MW_H	Molecular weight of hydrogen atom, 1 g/mole
MW_{H2O}	Molecular weight of water molecule, 18 g/mole
Nm^3	Volume (m^3) at normal atmospheric conditions (0^{o}C, 1 Atm)
L_{CO}	Combustion loss due to formation of CO in the flue gas, %
L_{HC}	Combustion loss due to formation of hydrocarbons in the flue gas, %
L_{BA}	Combustion loss due to unburnt carbon in the bottom ash, %
L_{FA-C}	Combustion loss due to unburnt carbon in the fly ash from 2nd cyclone, %
L_{FA-BF}	Combustion loss due to unburnt carbon in the fly ash from bag filter, %
η	Combustion efficiency (carbon-based), %
Gas Analyzer-1	ABB-AO 2000 flue gas analyzer
Gas Analyzer-2	GASMET-DX 4000 flue gas analyzer

CHAPTER 1

INTRODUCTION

1.1. General

World total primary energy supply (TPES) has been doubled in last 40 years because of the rapid increase in human population and dramatic increase in energy demand. While it was about 6.1 Giga tonnes of oil equivalent (Gtoe) in 1973, it increased to 12.7 Gtoe in 2010 (*IEA Key World Energy Statistics*, 2012). The increase in the world's population is the major triggering reason for the growth in energy demand. The world population was 6.8 billion in 2010 and it was estimated to be 8.6 billion in 2035 (*IEA World Energy Outlook*, 2012). In addition to the increase in total population, the number of people living in big cities will be increasing from 51% in 2010 to 61% in 2035 according to the International Energy Agency (IEA) estimates (*IEA World Energy Outlook*, 2012). There is no doubt that this will be followed by more and more energy demand because of the increase in people's living standards in cities.

Turkey's share in the world's TPES was 0.6% in 1990 and with the economic development within 20 years after 1990, it became 0.9% in 2010 (*WEC-TNC Energy Report (in Turkish)*, 2012). According to long-term plans and projections to meet increasing energy demand of Turkey, it was aimed to give priority to indigenous resources and to increase the energy variety in energy sector (*2010-2014 Strategic Plan (in Turkish)*, 2009). Turkey's primary energy supply in 2011 was 114 Million tonnes of oil equivalent (Mtoe) according to the Ministry of Energy and Natural Resource of Turkey and 72% of it was met by imports ("Energy Balances of Turkey," 2013). The high rate of imports does not seem sustainable in terms of economic development.

Turkey ratified The United Nations Framework Convention on Climate Change (UNFCCC) in 2004 and The Kyoto Protocol in 2009. Although there was no obligation for Turkey to mitigate greenhouse gas emissions until 2012, it is expected from Turkey to determine a reduction target under the Framework Convention on Climate Change. The total greenhouse gas emissions of Turkey were calculated to be 402 Million tonnes (Mt) Carbon dioxide (CO_2) equivalents for 2010 and the energy sector was responsible for 88.2% of this emission. The removal effect of the Land use, Land-use Change and Forestry (LULUCF) on greenhouse gas emissions (-78.7 Mt of CO_2 equivalent)) has been taken into account (*TurkStat National Greenhouse Gas Inventory Report 1990-2010*, 2012). If it is considered that the main greenhouse gas emissions were due to the energy sector in Turkey, the use of biomass resources which are defined as "CO_2 neutral"

(Baxter, 2005) in the energy sector is important for Turkey to fulfill the possible future commitments based on the Kyoto Protocol. Biomass is the most used energy source among the renewables. Its share in renewables was 75.2% for 2010 (*IEA Statistics Renewables Information*, 2012).

It seems the need for energy generation from biomass resources will increase because of the countries' future perspectives regarding usage of renewables in energy sector in terms of energy security and diversity. For example, the European Parliament made a decision in December 2008 supporting the climate targets which were set in EU's Climate Change Package (Bloem et al., 2010). According to the Climate Change Package, EU aimed to reduce greenhouse gas emissions by 20%, to improve the energy efficiency by 20%, and to increase the share of renewables in the EU energy mix to 20% by 2020 (*IEA World Energy Outlook*, 2012). World Energy Council (WEC)/Turkish National Committee (TNC) stated in their energy report (*WEC-TNC Energy Report (in Turkish)*, 2012) that it was very important to prepare energy and environmental policies which aimed to increase the share of indigenous and/or renewable energy resources in the energy production in Turkey for the energy supply security. With reference to the importance given in developed countries to renewables, it seems highly important to use indigenous and renewable energy resources in energy production.

Turkey is rich in coal reserves. Turkey was the twelfth biggest coal producer in the world with the production of 78.1 Mt in 2011. 95% of this production is lignite coals. Turkey was the fourth biggest lignite producer following Germany, China and Russia in 2011 (*IEA Statistics Coal Information*, 2012). Turkey's proved recoverable lignite reserves was estimated as 11.8 billion tonnes by 2011 according to the annual report known as "Blue Book" which was published by the Republic of Turkey, Ministry of Energy and Natural Resources in 2012 (*Enerji ve Tabii Kaynaklar Bakanlığı ile Bağlı ve İlgili Kuruluşlarının Amaç ve Faaliyetleri (in Turkish)*, 2012). In addition to lignite reserves, Turkey has also a high potential of biowastes. Biomass energy potential of Turkey is estimated as 8.6 Mtoe for 2011 in the "blue book" (*Enerji ve Tabii Kaynaklar Bakanlığı ile Bağlı ve İlgili Kuruluşlarının Amaç ve Faaliyetleri (in Turkish)*, 2012).

The use of indigenous resources such as coal and biowastes for energy production is of critical importance in reducing energy imports. However, there are some issues (storage problem of biomass; high sulfur, ash, moisture content and low heating value of Turkish lignites) for the usage of indigenous resources in energy production. The seasonal availability of biomass resources and storage problems are the challenges that are encountered. Therefore, thermal power plants (>300 Megawatt (electric) (MW_e)) using only biomass seem unpractical (Maciejewska et al., 2006). Another obstacle is the characteristics of Turkish lignites. Turkish lignites have high sulfur, ash and moisture content causing them to have low heating value. The average net heating value of Turkish lignites is about 2200 kcal/kg (*IEA Statistics Coal Information*, 2012). This value is less than the average lower heating value (4000 kcal/kg) of the forestry residues (Belen et al., 2009).

The use of advanced combustion technologies for low-quality fuels is more advantageous in terms of energy efficiency. Among the combustion technologies, fluidized bed technology becomes important because of the ability to burn different types of fuels due to the good mixing in the combustor and the high combustion efficiency achieved with less air in the combustor (Basu, 2006; Loo and Koppejan, 2008). Fluidized bed technology has many other advantages in addition to fuel flexibility as compared to pulverized coal combustion technology. High heat transfer rate is one of the other advantages. Thus, smaller surface areas for heat exchange are required. In situ SO_2 removal in the combustor is possible by using limestone. Also due to lower combustion temperature (850-870^oC) in the combustor, thermal nitrogen oxides (NO_x) formation is minimized. The combustor has a compact design as compared to pulverized coal technology because of lower surface area and volume requirement per unit energy produced (Hupa, 2008).

Utilization of biomass during combustion of coal for power generation (co-combustion) has many benefits in terms of environment and economy. First of all CO_2 emissions are reduced. Secondly, the cost for coal mining is reduced due to replacing coal with biomass. However, the use of biomass resources in energy generation may cause some operational problems due to the different characteristics of biomass fuel ash as compared with the coal ash. Agglomeration of the bed material is generally a problem observed in Bubbling Fluidized Bed Combustors (BFBCs) when a biomass with high alkali content is used in the combustor. In severe cases, it may cause total shut down of the system. If the biomass contains high chlorine, fouling and corrosion of the heat exchanger tubes are other problems encountered. In the case of co-combustion of different types of fuels in the same combustor, the interaction between fuel ashes may result in unexpected problems (Hupa, 2005). As it was stated in a study of Brus et al. (2005) that the mechanism of ash-related problems such as agglomeration could not be exactly determined, there is still a need to do more research in this subject. Co-combustion of high-sulfur coals with problematic biomass fuels seems to be one of the solutions to solve the ash-related problems in fluidized beds. Sulfur in coal ash may react with alkali species mainly originating from biomass, thus decreasing the formation of low melting point eutectics.

In the light of these needs and potentials, to use coal as the main fuel and various biomasses as supplementary fuel seem to be the promising choice for Turkey for energy production. Thus, low calorie coals can be used and the disposal of biowastes will be achieved. Additionally, the energy content of the biowastes will be used beneficially in the country's energy production, otherwise it will be wasted More important than these is the CO_2 emission reduction due to carbon dioxide neutral property of biomass which will provide the opportunity for a carbon credit in the future.

1.2. Aim of the Study

The biomass energy potential of Turkey was given to be 8.6 Mtoe for 2011 (*Enerji ve Tabii Kaynaklar Bakanlığı ile Bağlı ve İlgili Kuruluşlarının Amaç ve Faaliyetleri (in*

Turkish), 2012). However, this potential cannot be used for the energy demand of the country with conventional combustion technologies. On the other hand, Turkey is a country rich in lignite resources. Turkey's proved recoverable lignite reserves in 2011 was 11.8 billion tonnes (*Enerji ve Tabii Kaynaklar Bakanlığı ile Bağlı ve İlgili Kuruluşlarının Amaç ve Faaliyetleri (in Turkish)*, 2012). However, these lignite coals generally have high sulfur and ash content. Turkey imports 72% of its total primary energy. Energy demand is increasing every year because of a development rate of 5-7 %/year. Therefore, it will be wise to use lignite and biomass sources in energy production with a suitable combustion technology in Turkey.

A suitable technology for burning low calorie, high ash and high sulfur fuels can be fluidized bed technology, either bubbling (BFB) or circulating fluidized bed (CFB). Since the combustion rate is higher in CFB, in this study CFB is chosen to combust Turkish lignite coals and also to co-combust these lignite coals with biomass residues.

While burning biomass sources in fluidized bed combustors, some operational problems such as slagging, fouling and bed agglomeration can occur because of the formation of alkali oxides (Na_2O, K_2O) during combustion. The operational problems can be partially prevented by burning biomass with high-sulfur coals which lowers the total alkali metal content of ash produced.

The objectives of this study are;

1) to investigate the emission problems during combustion of Turkish lignite coals (Bursa/Orhaneli and Denizli/Kale lignites) and biomasses (olive cake and woodchips) in relation with different excess air ratios to achieve the lowest emissions and the highest combustion efficiency possible,
2) to investigate the possible ash related problems,
3) to investigate how co-combustion can help to solve these problem. (addition of Bursa/Orhaneli lignite (low S) and Denizli lignite (high S) to olive cake)

In order to achieve the objectives mentioned above, the parameters to be studied can be summarized as;

- flue gas emissions for combustion of biomasses and Turkish lignite coals with different excess air ratios,
- elemental composition and mineral content of ash for the combustion tests,
- partitioning tendency of sulfur and alkali metals (K, Na) between the phases, in bottom ash and in fly ash.

CHAPTER 2

THEORETICAL BACKGROUND

2.1. Fluidized Bed Combustion Technology

Fluidized bed combustion (FBC) technology is suitable for the combustion of fossil fuels as well as different types of biomasses and wastes. It is also possible to burn the problematic fuels such as plastics, municipal solid waste (MSW), and residue derived fuel (RDF) in fluidized bed combustors. Figure 2.1 shows FBC technology applications for several fuels based on their net heating values. As can be seen in the figure, the challenges faced with while burning fuels are increasing from right to left. While the FBC technology reaches its standard design for fossil fuels on the right of the figure, there are serious issues for the application of MSW, RDF and plastics in FBC technology. In terms of thermal power, the fluidized bed applications range between 30 and 900 Megawatt (thermal) (MW_{th}) for combustion. It is in the range of 8 and 10 MW_{th} for gasification. Contrary to the BFBCs, CFBCs are generally used for a wide variety of fuels and for the applications of higher thermal power (Winter and Szentannai, 2010).

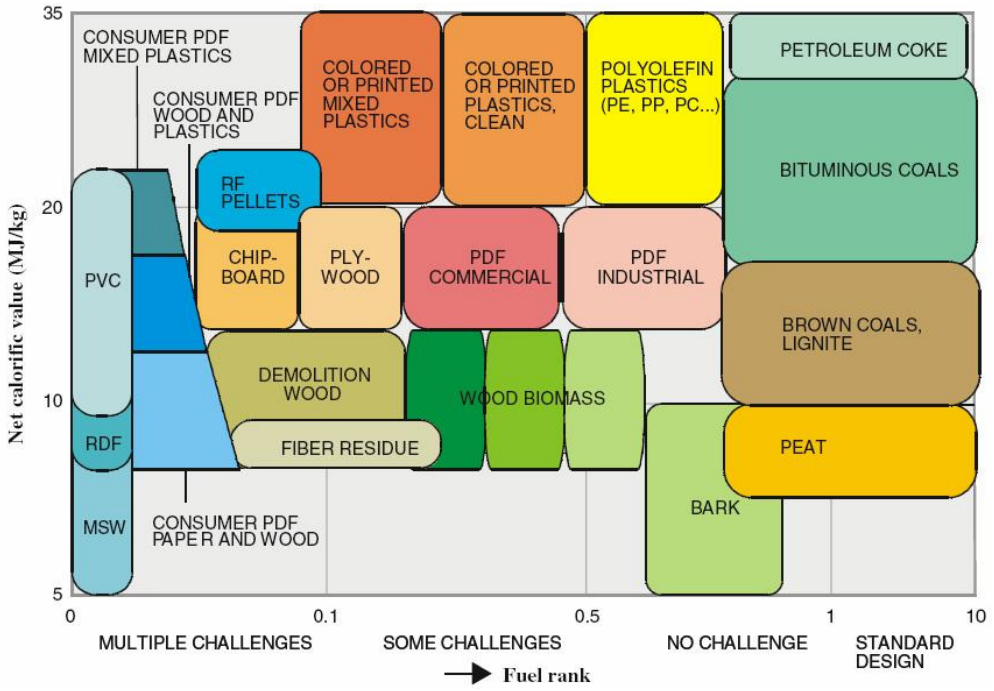

Figure 2.1 Different types of fuels used for FBC technology (Winter and Szentannai, 2010)

In general, fluidization is based on the principle of altering the status of solid particles in a vessel (or a combustor in our case) from stationary state to fluidized state by an upward flow of fluid which exceeds a critical flow rate (Werther et al., 2000). Solid particles in the combustor represent the bed. When a small amount of fluid flow is passed upward through the bed, the fluid runs through the voids between stationary particles. This is defined as "fixed bed". If the flow rate is increased up to a critical point where all the particles are kept in suspension by the upward force of fluid, the bed is considered as "bubbling fluidized bed" (Kunii and Levenspiel, 1991). As the fluid flow rate is increased further, the solid particles in the bed are started to be carried out of the combustor by the fluid. In this regime, there is no an apparent bed in the combustor. The solid concentration decreases along the combustor. If the particles entrained out of the combustor are collected by a cyclone and given back to the combustor along a return leg (downcomer), this is defined as "circulating fluidized bed" (Werther et al., 2000). Circulating fluidized bed regime has many advantages for heat and mass transfer by increasing the contact between fluid and solid phases (Kunii and Levenspiel, 1991).

2.1.1. Advantages of Fluidized Bed Combustion Technology

Fluidized beds have several advantages compared to other modes of contacting regimes. These advantages make them a good option for the combustion of coal and biomass in the same combustor. The advantages can be listed as follows:

1. It is easy to control the system because of smooth, liquid-like flow of particles (Kunii and Levenspiel, 1991).
2. Because of good mixing in the combustor, high heat transfer rate can be achieved between solid particles and the surface of heat exchangers (Bartels, 2008).
3. Due to the high heat transfer rate, smaller surface areas for heat exchangers are possible for FBC systems as compared to pulverized coal combustors (Kunii and Levenspiel, 1991). Therefore, FBC systems are more compact as compared to pulverized coal combustors.
4. The system can tolerate big changes in operational conditions and can resist rapid temperature changes due to the good-mixing in the combustor (Kunii and Levenspiel, 1991).
5. Uniform temperature distribution can be obtained in the combustor due to good solid mixing. No hot spots occur (Werther, 2007). This is a very important advantage as compared to pulverized coal combustors.
6. It is possible to burn different types of fuels with different sizes. It is also possible to burn the fuels with high moisture and low heating value because of the intense motion and high heat capacity of bed material (Werther et al., 2000).
7. Due to the low operational temperature (about 850^{o}C), formation of thermal and prompt NO_x can be minimized (Werther et al., 2000).
8. In-situ SO_2 removal is possible with the addition of limestone into the combustor. There is no need for a desulfurization unit (Winter and Szentannai, 2010).

There are some disadvantages:

1. Because of the entrained solid particles, gas/solid separators (cyclones, electrostatic precipitators, and bag house filters) are required for the flue gas especially when biomass is combusted (Werther, 2007).
2. High rate of solid mixing can result in a non-uniform residence times for solid particles in the combustor (Kunii and Levenspiel, 1991).
3. Erosion of the heat exchanger pipes or inner walls of the combustor can be encountered due to the high solid velocities especially for CFBCs (Kunii and Levenspiel, 1991).
4. Ash-related problems such as agglomeration are possible if biomass with high alkali content is combusted at temperatures higher than the melting temperature of biomass ash (Werther, 2007).

2.1.2. Types of Fluidized Bed Combustors

There are mainly two types of fluidized bed combustors concerning the fluidization regime. These are Bubbling Fluidized Bed Combustors (BFBC) and Circulating Fluidized Bed Combustors (CFBC). In BFBCs, the fluidization velocity is used in the range of 1 and 3 m/s. In CFBCs, higher gas velocities are used between 4 and 8 m/s. Because of the high velocity in CFBCs, there is no apparent bed in the combustor as compared to BFBCs. The particles leaving the CFBC are collected by a cyclone and returned back to the combustor above the distributor plate through a return leg. CFBCs have higher

combustion efficiency than BFBCs because of the higher velocity employed. However, the erosion rate is high due to the same reason (Khan, 2007). A schematic diagram of the two types of combustors is given in Figure 2.2. The fluidization regime in CFBCs is defined by high turbulence, solids back mixing, and no apparent bed height. Although there is no apparent bed height, the concentration of solid particles decrease along the combustor as one goes from bottom to top. Because of the high turbulence in the combustor, fuel particles are rapidly mixed with bed material and combustion efficiency is high. In BFBCs, small particles can escape from the combustor before complete combustion is done. Therefore, combustion efficiency is lower than BFBC. Moreover, it is necessary for BFBCs to have feeding points at every m^2 to achieve uniform fuel feeding and mixing. CFBCs do not have these limitations (Batu, 2008).

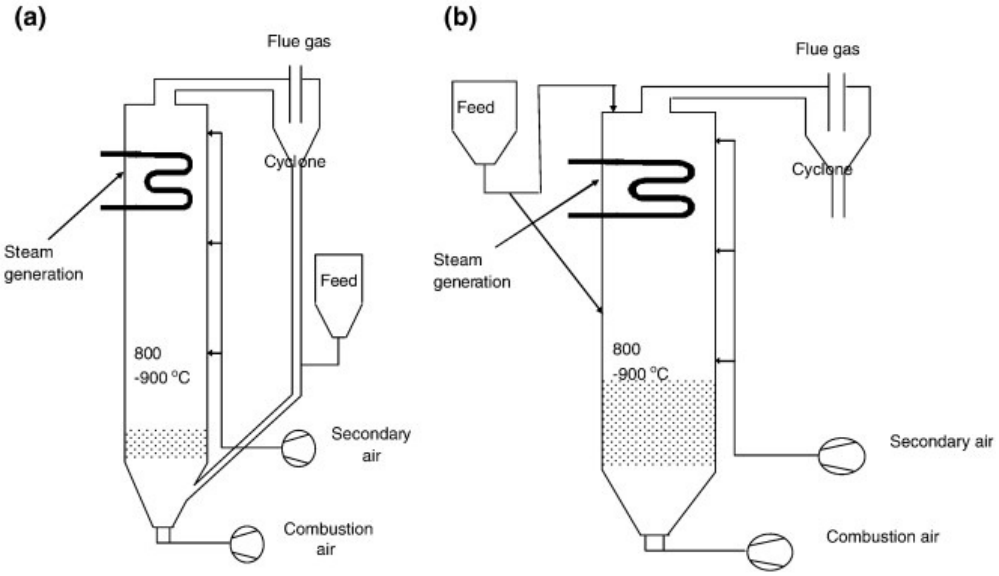

Figure 2.2 (a) Circulating fluidized bed combustor (b) Bubbling fluidized bed combustor (Khan, 2007)

2.2. Combustion and Co-combustion of Biomass with Coal in Fluidized Bed Combustors

There are several conversion processes and technologies for biomass feedstock according to the chemical and physical characteristics of biomass. The conversion processes and technologies may also vary based on the desired final product to be obtained such as heat, power, or biofuel. The biomass conversion technologies are mainly divided into two groups, bio-chemical and thermo-chemical. Bio-chemical conversion technologies are fermentation and anaerobic digestion. Thermo-chemical conversion technologies are combustion, gasification and pyrolysis. Among these three main thermal conversion

technologies, combustion of biomass is the most widely used when compared with the others. Because of low bulk density and high moisture content of biomass material, it is necessary to transport huge amount of biomass from source to the plant in which the biomass is utilized. This brings an extra transportation cost for biomass combustion. Preparation and storage of biomass are other issues increasing the operational cost (Khan, 2007). Therefore, co-combustion (also known as co-firing) of biomass with coal in power plants is the most cost-effective way of utilization of biomass resources in power generation (Iancu et al., 2010).

Co-combustion is generally defined as the simultaneous combustion of two or more fuels in the same system for heat or power generation. Generally, co-combustion of coal with other fuels such as biomass and waste derived fuels in the same combustor is very common. Fluidized bed combustors are known as the best solution for the co-combustion of different types of fuels because of its fuel flexibility (Winter and Szentannai, 2010). However, burning biomass in fluidized bed combustors may cause some ash-related operational problems such as agglomeration, slagging, fouling and corrosion. These problems are generally caused by properties of biomass fuels. Accumulation of Potassium (K) and Chlorine (Cl) in the deposits occurring on the surface of heat exchanger tubes may cause fouling and corrosion problems (Khan, 2007). The corrosion problem can be minimized if the biomass with high alkali content burns with a high-sulfur (S) coal. The S in coal reacts with the alkali chlorides from biomass forming alkali sulfates. Therefore, the alkali chlorides which are mainly responsible for corrosion of heat exchanger surfaces are converted into HCl and leave the system as HCl gas (*IEA Bioenergy Task 32 Biomass Combustion and Co-firing: An Overview*, 2002). Combustion of biomass containing high amount of alkali metals such as Sodium and Potassium (Na and K) may increase the agglomeration tendency (Winter and Szentannai, 2010). In order to prevent agglomeration, fluidized bed combustors are operated at the temperature lower than the melting temperature of biomass ash which in turn decreases the combustion efficiency (Khan, 2007). Besides the ash-related problems, high moisture content of biomass also decreases the combustion efficiency. If a high-moist biomass is dried prior to feeding, this increases the operational cost for drying. Despite the disadvantages biomass due to its physical and chemical characteristics, there are several advantages of burning biomass with coal in fluidized bed combustors. Low NO_x emission due to ammonia (NH_3) release from biomass is one of them. It is also possible to have low sulfur dioxide (SO_2) emission because of low Sulfur (S) content of biomass and high Calcium (Ca) content of some biomass (Winter and Szentannai, 2010).

2.2.1. Major Air Pollutants in the Flue Gas of a Fluidized Bed Combustor

It is unavoidable to have emissions of different air pollutants while burning solid fuels such as coal and biomass in producing heat or power. Among the air pollutants, PM, CO, NO_x, and SO_2 emissions are of interest and the major ones because of their high concentration in the flue gas when compared to other more dangerous air pollutants such as hydrocarbons, acid gases, dioxin and furans, and PAHs (Khan, 2007). The sources of the major air pollutants (PM, CO, NO_x, N_2O and SO_2), formation mechanisms and

significant operational parameters contributing their abundance in the flue gas are reviewed in the following sub-sections.

2.2.1.1. CO Emission

CO emission is the product of incomplete combustion process. There are three important operational parameters for the complete combustion. These are Temperature, Time and Turbulence (three T's). It is necessary for the combustion gases to spend enough time in the combustor having a temperature of 720^{o}C or above for the oxidation of CO to CO_2 (Baumbach, 1996). The turbulence in the combustor is also significant in order to increase the number of CO and O_2 molecules having a successful contact for the oxidation reaction. In the case of low temperature or residence time or insufficient mixing of fuel with air in the combustor, some portion of CO formed can leave the combustion system as a product of incomplete combustion lowering the overall combustion efficiency. Fuel composition is also important for the generation of high CO emission. CO emission for the biomass combustion is always higher than that for coal combustion. This is mainly because of the higher volatile matter content of biomass than coal (Kaynak et al., 2005; Varol and Atimtay, 2007; Munir et al., 2011; Vamvuka et al., 2012). The biomass with high volatiles needs more residence time in the freeboard in order to totally oxidize to the final combustion product of carbon, CO_2. Lab-scaled or pilot-scaled fluidized bed combustors generate high CO emission because of the smaller residence time (Khan, 2007). CO emission originated from industrial scale fluidized bed boilers is not a big issue; they are generally below the emission limits (Basu, 2006).

2.2.1.2. NO_x Emission

There are three main oxides of nitrogen in the flue gas. These are nitrogen oxide (NO) and nitrogen dioxide (NO_2) which are both defined as nitrogen oxides (NO_x) emission and nitrous oxide (N_2O). NO_x emission is produced during combustion. NO accounts for the most of the NO_x emission in the flue gas. Almost 95% of NO_x emission is NO. NO reacts with oxygen in the stack and eventually in the atmosphere and turns into NO_2. NO is a colorless gas and has some adverse effects on health but these effects are less than that of NO_2. The main concern with NO_x emission is the contribution of them to the formation of ozone (O_3) and photochemical smog. NO_2 is photodissociated by sun light producing NO and oxygen radical. The oxygen radical reacts with O_2 to form O_3. O_3 then reacts with NO forming NO_2 and O_2 molecules. These three reactions represents the photochemical cycle for NO, NO_2, and O_3 and there is an equilibrium between the molecules. If there are hydrocarbons in the atmosphere, they convert NO to NO_2. In that case, there is not enough NO to react with O_3 and O_3 starts to accumulate in the atmosphere (in the troposphere indeed). O_3 is a strong respiratory irritant and one of the other strong irritant components of the photochemical smog (Boubel et al., 1994; Nevers, 1995).

NO is formed through three mechanisms, namely thermal-NO, prompt-NO, and fuel-NO during combustion depending on the temperature and residence time. Thermal-NO

formation is known as Zeldovich mechanism and according to the mechanism, NO is produced by the oxidation of molecular nitrogen in the air at high temperature over 1300^{o}C. NO can also be formed by the reaction of fuel radicals (CH, C, CN, HCN) and molecular nitrogen at high temperatures in flame where there is low oxygen concentration. This was discover by Fenimore and is known as prompt-NO. Organic nitrogen compounds in the fuel can also be oxidized to NO at lower temperature which is termed as fuel-NO (Baumbach, 1996).

Because of the low operational temperatures (800-900^{o}C) in fluidized beds, the oxidation of nitrogen in the fuel (fuel-N) is the main contributor to NO emission. NO formation can take place via homogenous gas phase reactions (oxidation of fuel-N released with volatiles so called volatile nitrogen oxidation) or heterogeneous reactions (oxidation of fuel-N in the char so called char nitrogen oxidation) in fluidized bed combustors. The homogenous reactions occur in the freeboard region of BFBCs and in the upper parts of CFBCs where there are fewer particles (Afacan, 2005). NH_3 and hydrogen cyanide (HCN) are two important volatile species for the homogenous reactions (Miller and Bowman, 1989; Werther et al., 2000). Werther et al. (2000) in their review study stated that NH_3 may react with oxygen or NO and hydroxyl OH radicals to form NO and Nitrogen (gas) (N_2), respectively; referring to the study of Johnsson (1994). In this case, NH_3 participates into the formation and reduction reactions for NO (Khan, 2007). Although NH_3 is the main source for NO, HCN is a responsible for the formation of N_2O (Miller and Bowman, 1989; Afacan, 2005).

For the formation of NO, there are several heterogeneous reactions occurring in fluidized bed combustors due to the existence of different types of solid particles such as char, ash and limestone. These can be divided into two groups, namely gas-solid phase and catalytic heterogeneous reactions. NH_3 and HCN react with oxygen on the surface of char, ash or limestone forming NO and N_2. Char-N is oxidized to NO along with the carbon oxidation during char combustion (Afacan, 2005). Char-N oxidation is the major reason for NO formation during coal combustion in fluidized beds (Glarborg et al., 2003). Because of the high volatile matter content and low fixed carbon of biomasses, it seems heterogeneous reactions on char may not be the main responsible mechanism for the formation of NO during biomass combustion (Werther et al., 2000). In biomass combustion, most of the fuel-N is released with the volatiles (Glarborg et al., 2003).

NO reduction on char is a complex process. Char can provide a catalytic surface for the reduction of NO in the presence of reducing agents like carbon monoxide (CO) (Glarborg et al., 2003). This reduction step is estimated to be responsible for the half of the NO reduction during bituminous coal combustion (Johnsson, 1994). This mechanism is not likely to occur for biomass combustion because of the lower char content of biomass but it is possible for co-combustion applications (Khan, 2007). It was also mentioned in the review of Werther et al. (2000) referring the study of Johnsson and Dam-Johansen (1991) that the presence of calcium oxide (CaO), magnesium oxide (MgO) and iron (III) oxide (Fe_2O_3) in the fuelcan behave as a catalyst for NO and N_2O reduction under fuel-rich combustion conditions.

NO reduction on char surface may not take place due to the low fixed carbon and insufficient CaO content of biomass for the combustion of biomass in fluidized bed combustors. Therefore, it is possible for biomass combustion to have higher NO_x emission than coal combustion when both fuels have the same amount of fuel-N. In the case of high NO_x emission, it may be necessary to use emission reduction measures for NO_x emission (Werther et al., 2000). There are basically two measures; primary and secondary. The primary measures are used to reduce NO_x emission by changing or modifying some parameters (secondary air, excess air, or temperature) during combustion. The secondary measures are removal techniques that are used to transform the NO_x formed during combustion into other compounds (Baumbach, 1996). Air staging is the most effective one among the primary measures. In air staging; the combustion air as well as the fluidization air in fluidized beds, is given into the combustor from two different locations. While some part of it introduces into the combustor from the bottom of the combustor through distributor plate, the rest is given from specific locations along the combustor; it can be even given into the cyclone. Air staging has a good advantage for the NO_x reduction, especially for the highly volatile fuels (Basu, 2006). Khan (2007) in his Ph.D. thesis reported that it was recommended by Nussbaumer (2003) to increase the temperature up to 1150^oC in order to achieve high reduction efficient by air staging. Otherwise, it did not give good results at lower temperatures according to the studies in the literature reported by Khan (2007). Lowering excess air given into the combustor and lowering the temperature are the other primary operational measures that were mentioned by Basu (2006) for NO_x reduction but these measures bring the risk of high level of CO as well. Other reduction techniques are selective catalytic reduction (SCR) and selective non-catalytic reduction (SNCR). While ammonia or urea is injected over a catalyst in a temperature range of 250-450^oC for SCR, ammonia is injected over the gas in a separate chamber at temperatures of 850-950^oC (Khan, 2007).

2.2.1.3. N_2O Emission

During the combustion of coal or biomass in fluidized beds, it is likely to have N_2O emission as well as NO_x emission. Although its percentage in the flue gas may be negligible as compared to NO_x emission, it is one of the important components of the flue gas in terms of global warming. N_2O is one of the greenhouse gases. Its global warming potential is 280 times higher than CO_2 over 20 years ("Global Warming Potentials", 2013). Therefore, it is important to understand the formation mechanism and to take some measures in order to minimize N_2O emission in terms of global warming and stratospheric ozone depletion issues.

Volatile nitrogen oxidation is the main mechanism for the formation of N_2O in fluidized bed combustors. N_2O can form by the reaction of NO with NCO which is produced by HCN (Afacan, 2005). Excess air ratio and operational temperature are two important parameters that affect the formation of N_2O emission. N_2O emission can be reduced by increasing the operational temperature or decreasing the excess air ratio (Werther and Ogada, 1999). At temperatures higher than 900^oC, N_2O decomposes to N_2 (Werther et al.,

2000). While air staging has a reducing effect on NO_x emission, it is not significantly important for the reduction of N_2O emission (Khan, 2007). Air staging leads the temperature of the bed in a BFBC to increase. The formation of O and OH radicals at high temperature increases as well, resulting in N_2O destruction. But, at the same time, OH radicals are more reactive to oxidize carbon in char, CO and methane (CH_4) when compared to N_2O reduction reaction. Therefore, it seems this patway is not dominant for the destruction of N_2O. In addition to that, N_2O formation from NO may also be reduced because of the NO reduction by air staging (Suksankraisorn et al., 2004).

Leckner et al. (2004) studied the co-combustion of sewage sludge with wood and coal in two circulating fluidized bed plants. They stated that N_2O emission for the co-combustion of sewage sludge and wood was lower than sewage sludge and coal mixture. Löffler et al. (2002) in their study reported no N_2O emission for wood combustion. This was explained by the catalytically activity of wood ash. The importance of char for the catalytic reduction of N_2O was also stated by Werther et al. (2000). Werther et al. (2000) also mentioned the catalytic effect of bed containing CaO, MgO and Fe_2O_3 for N_2O reduction. On the other hand, it was stated by Khan (2007) that the char oxidation was not important for biomass because of the low char content but it might be effective for co-combustion.

2.2.1.4. SO_2 Emission

The main source of SO_2 emission is the combustion of sulfurous fuels, particularly coal in thermal power plants and industrial furnaces. Sulfur in coal can be present in three forms, namely pyritic, organic and sulfate. SO_2 emitted from tall stacks into the upper troposphere has long residence time and can travel long distances. In the atmosphere, it can oxidize to sulfuric acid leading to the formation of acid rain problem. Therefore, it is very crucial to take necessary measures to capture SO_2 in the flue gas or in the combustor.

In-situ usage of limestone is one of the effective and most commonly used ways for the control of SO_2 emissions in fluidized bed combustors. SO_2 is captured by calcium carbonate ($CaCO_3$) in limestone forming calcium sulfate ($CaSO_4$) via the two following reactions (Rxn. 2.1and Rxn. 2.2). $CaSO_4$ is a solid product which is discharged from the combustor with ash material. SO_2 capture by limestone occurs in two consecutives steps. The first one is calcination. It is an endothermic reaction where $CaCO_3$ in limestone decomposes into CaO and CO_2 at the combustion temperature range of 800-900^oC. The CO_2 released during the calcination reaction creates many pores in the limestone and increases the surface area available for the SO_2 capture. The second step is the sulfation reaction where SO_2 is captured by CaO forming solid $CaSO_4$ (Anthony and Granatstein, 2001).

Calcination: $CaCO_3\ (s) \leftrightarrow CaO\ (s) + CO_2\ (g)\ \Delta H = 182.1$ kJ/gmol Rxn. 2.1

Sulfation: $CaO\ (s) + SO_2\ (g) + 1/2\ O_2\ (g) \leftrightarrow CaSO_4\ (s)\ \Delta H = -481.4$ kJ/gmol Rxn. 2.2

According to the calcination (Rxn. 2.1) and sulfation (Rxn. 2.2) reactions above, one mole of Ca is required for one mole of S to be captured and one mole of $CaSO_4$ is

formed. However, sulfur capture efficiency in reality is lower than in theory. The limiting step for SO_2 capture by limestone is the sulfation. Although the calcination reaction is relatively fast as compared to sulfation reaction, all the CaO formed by calcination cannot be converted into $CaSO_4$. This is mainly because of the plugging of pores and pore entrances in limestone during sulfation process. When $CaSO_4$ is started to build up at the outer surface of the pores and plugs the entrance, SO_2 as well as O_2 cannot diffuse into the pores and the interior surface of the pores cannot be used for SO_2 capture. Due to the larger molar volume of $CaSO_4$ than CaO, $CaSO_4$ plugs the entrance of the pores. Therefore, this decreases the sulfur capture efficiency of limestone (Basu, 2006). Sulfur capture was reported as maximum at the range of temperature between 800 and 850^oC by Khan (2007) giving the study of Lyngfelt and Leckner (1993) as reference.

Co-combustion of sulfuous coals with biomasses is a good application in terms of CO_2 emission but it is also beneficial for SO_2 reduction. It decreases SO_2 emission due to the two main reasons. SO_2 emission is expected to decrease as much as the share of biomass in the fuel mixture due to the low sulfur of biomass. Moreover, CaO and MgO content of biomass ash can also capture SO_2 in the combustion gas (Khan, 2007).

2.2.2. Ash Related Operational Problems in Fluidized Bed Combustors

Fluidized bed combustion technology has an advantage that it is possible to burn different types of fuels in the same combustor. Due to this advantage, most of the fluidized bed combustors all over the world are recently designed to operate with different solid fuels. However, mixing different fuels may cause some operational problems in the system and may also lead to completely shut down of the system. When two or more fuels are burned in the fluidized bed combustor, because of their different ash characteristics, chemical reactions and/or physical interactions may occur between ash particles resulting operational problems such as agglomeration of bed material, slagging, fouling and corrosion of heat exchanger tubes (Hupa, 2008). Although these operational problems are the main concerns for the combustion of all types of solid fuels, they are particularly important for the combustion of biomass having ash rich in alkali and alkaline earth metals (Szemmelveisz et al., 2009).

2.2.2.1. Ash Deposition Mechanisms

Deposits can form on the heat transfer surfaces due to the five mechanisms. These are inertial impaction, eddy impaction, thermophoresis, condensation, and chemical reaction. The inertial impaction is the main mechanism responsible for the ash deposition on the heat transfer surfaces. The inertial impaction happens when a gas flow carrying particles hits and moves around the heat exchanger tubes. The particles moving with their inertia cannot follow the gas flow pathway, hit the tube surface and stay on it. Eddy impaction is more effective for the fine particles. Because of small sizes of fine particles, their inertia is small. After a few collisions with other particles in the turbulent regime of the combustor or boiler, they may hit the heat exchanger tubes and deposit on the surface. Temperature gradients in local size can affect the motion of particles in the carrying gas.

This effect is named as thermophoresis. Condensation is another important ash deposition mechanism. It happens while hot gases pass thorough or across the cooled heat transfer surfaces. Vapors of some metals like alkali chlorides can condense on the cooled surface. Condensation is mostly responsible for ash deposition in the case of biomass or low-grade coal combustion. Chemical reactions between the gas and the particles on char surfaces, for sure, are very important for ash deposition. Sulfation of alkali metals such as K or Na is one of the important chemical reactions for the formation of deposits. On the other hand, reactions of these alkali metals with silica (SiO_2) to form alkali silicates are also responsible for ash deposition (Lokare, 2008). Cl has an important role for the formation of alkali silicates. It enhances alkali metals to release as alkali chlorides and hydroxides in the gas phase by increasing the volatility of alkali metals. When the flue gas contacts with the cold surfaces, these alkali compounds condense on the surfaces of the heat exchanger. If there is SO_2 in the flue gas, then alkali compounds react with SO_2 forming alkali sulfates in the tube surface. If there is no SO_2, they remain as alkali chlorides on the surface. These alkali compounds make a sticky layer on the tube surfaces which in turn accelerates the deposit build-up by inertial impaction (Khan, 2007).

2.2.2.2. Agglomeration of Bed Material

Agglomeration of bed material is one of the main operational problems encountered in fluidized bed combustors. If necessary measures are not taken, it can lead to total defluidization of the bed material and eventually shut down of the system. Agglomeration problem is mostly seen in BFBCs because the ash formed during combustion process makes layers between the particles of the bed material which is generally quartz (silica sand) (Khan, 2007). It is not commonly observed in CFBCs because there is no apparent bed in the combustor. Due to the high velocity in the combustor and the presence of a downcomer, the ash particles and bed material are circulated between the combustor and the downcomer, reducing the possibility of the ash particles form a sticky layer between bed materials.

Although the agglomeration problem was firstly studied for coal combustion (Reddy and Mahapatra, 1999; Vuthaluru, et al., 1999; Vuthaluru and Zhang, 1999; Vuthaluru et al., 2000), it became one of the main concerns when several biomass fuels was co-combusted with coals (Zevenhoven-Onderwater et al., 2000; Arvelakis et al., 2001; Robinson et al., 2002; Arvelakis et al., 2003; Lin et al., 2003; Fernández Llorente and Carrasco García, 2005; Zheng et al., 2007; Vamvuka et al., 2008; Toscano and Corinaldesi, 2010; Yang et al., 2011; Silvennoinen and Hedman, 2013).

It was reported that there were at least three different mechanisms for the formation of agglomeration. These are due to (1) the presence of a liquid phase (molten phase), (2) the solid-state sintering, and (3) chemical reactions. Sintering through the first two mechanisms can be classified according to the melt. If there are alkali metals (Na, K) or alkaline earth metals (Ca, Mg) in the ash, low viscous melts may result in the form of alkali or alkaline earth salt mixtures such as sulfates, chlorides or carbonates. In this case, sintering is dependent on the amount of melt and is a function of operational temperature

and chemical composition. If there is Si in the ash, highly viscous melts may form. They may cause big problems because they may form a glassy phase and don't crystallize when the temperature is decreased below the melting points of the silicates (Skrifvars et al., 1998b).

Alkali metals, K and Na, play an important role in the formation of agglomeration during the fluidized bed combustion of biomass (Hupa, 2012; Silvennoinen and Hedman, 2013). These alkali metals can react with silica sand (bed material) at temperatures of 700-900^{o}C forming low-melting point eutectics (Valmari et al., 1999; Scala and Chirone, 2006, Scala and Chirone, 2008; Lokare, 2008). Silica sand is the most commonly used bed material in fluidized bed combustors. It is mainly responsible for the formation of silicate compounds. K, for example, can easily volatilize during char combustion and form gaseous compounds such as potassium chloride (KCl) or potassium hydroxide (KOH). These gaseous compounds can react silica in the bed to form alkali silicates which have a melting temperature range of 930-980^{o}C (Hupa, 2008). Alkali silicates can form a molten layer on the particle surfaces making the particles sticky in the combustion of biomass having high alkali content (Hupa, 2012). When the system is operated for a long time, the sticky layer on the surface of the particles results in the formation of permanent bonds between sand particles (Scala and Chirone, 2008). Due to the sticky layer, the particles in the bed hit and adhere onto each other, increasing both the size and the number of the agglomerated particles. If it is allowed, agglomeration of the whole bed material and total shutdown cannot avoidable. Although the formation of silicate is not well defined, Rxn. 2.3 is given as possible way. It is a solid-gas reaction between quartz and alkali chloride vapors (Hupa, 2012).

$$SiO_2\ (s) + 2KCl\ (g) + H_2O\ (g) \leftrightarrow K_2SiO_3\ (l) + 2HCl\ (g) \qquad \text{Rxn. 2.3}$$

If there is no Cl available for the Rxn. 2.3 above, quartz can react with other alkali vapors such as alkali hydroxide according to the Rxn. 2.4 (Hupa, 2012).

$$SiO_2\ (s) + 2KOH\ (g) \leftrightarrow K_2SiO_3\ (l) + H_2O\ (g) \qquad \text{Rxn. 2.4}$$

For the combustion of biomass with ash containing high K or Na, following two reactions (Rxn. 2.5 and Rxn. 2.6) are possible. Quartz, which is mainly composed of SiO_2, has a melting point temperature around 1450^{o}C (Lin et al., 1997). SiO_2 can react with alkali oxides or salts in the ash forming eutectic mixtures with melting temperatures of 874^{o}C and 764^{o}C, respectively (Grubor et al., 1995). These are lower than the melting temperature of SiO_2 as well as the melting temperatures of individual components (891^{o}C for K_2CO_3 and 851^{o}C for Na_2CO_3).

$$2SiO_2 + Na_2CO_3 \rightarrow Na_2O \bullet 2SiO_2 + CO_2 \qquad \text{Rxn. 2.5}$$

$$4SiO_2 + K_2CO_3 \rightarrow K_2O \bullet 4SiO_2 + CO_2 \qquad \text{Rxn. 2.6}$$

If there is enough Fe_2O_3 in the ash, Fe_2O_3 can react with alkali oxides or salts according to the Rxn. 2.7 and Rxn. 2.8 by competing with the reactions SiO_2 with alkali salts (Rxn.

2.5 and Rxn. 2.6). Thus, the eutectic mixtures formed as a result Rxn. 2.7 and Rxn. 2.8 can reduce the tendency of the formation of agglomeration because these mixtures have a melting point temperature higher than 1135°C. X in Rxn. 2.5 and Rxn. 2.6 is Na or K elements (Grubor et al., 1995).

$$Fe_2O_3 + X_2O \rightarrow X_2Fe_2O_4 \qquad \text{Rxn. 2.7}$$

$$Fe_2O_3 + X_2CO_3 \rightarrow X_2Fe_2O_4 + CO_2 \qquad \text{Rxn. 2.8}$$

Since the interaction between ash and bed material (silica sand) is not well understood and is not clear enough, the main precaution to prevent total agglomeration is lowering the alkali content in the combustor by continuously removing the ash formed and replacing the bed material with fresh silica sand (Hupa, 2012). It is also important to use alternative bed materials in order to minimize the silica content which eventually reacts with alkalis (Hiltunen et al., 2008). Different types of materials are used as an alternative to silica sand. These are dolomite, magnesite, ferric oxide, feldspar (Werther et al., 2000). Porous alumina (Shimizu et al., 2006), blast-furnace slag (Brus et al., 2004; Davidsson et al., 2008) and olivine sand (Davidsson et al., 2008) are the other ones to be used as alternative bed materials. The formation of molten silicates may be eliminated by using these alternative bed materials. Due to the high cost of the alternative bed materials, silica sand is the commonly used as bed material even with the high-alkali fuels (Hupa, 2012). Moreover, some problems such as high attrition and entrainment rates, chemical stability, and plugging of air nozzles and windbox were reported during the usage of these alternative bed materials (Khan, 2007). Another measure is the usage of some additives such as kaolin, dolomite, lime, and alumina. However, they have limited usage due to the low efficiency and high operational cost.

Co-combustion of high-alkali biomass with high-sulfur coals seems another solution to solve the bed agglomeration problem mainly resulted from high-alkali biomass. Sulfur in coal may react with alkali oxides forming alkali sulfates. By this way, Si cannot find enough alkali metals to form viscous alkali silicates according to Rxn. 2.5 and Rxn. 2.6. Mixing high-alkali biomass with high-sulfur high-ash coals is also good application to dilute the alkali content of the mixture (Werther et al., 2000).

Before using any fuel in real applications, it is a good practice to estimate the tendency of the fuel ash to agglomerate. The agglomeration tendency of a fuel can be estimated in terms of some indices. Bed Agglomeration Index (BAI) is the one which is commonly used. It is the ratio of iron oxides to the sum of potassium and sodium oxides in the fuel ash. The ratio is given in Eq. 2.1. If the ratio is less than 0.15, it is possible the agglomeration to be seen (Bapat et al., 1997).

$$BAI = \frac{\%(Fe_2O_3)}{\%(K_2O + Na_2O)} \qquad \text{Eq. 2.1}$$

The BAI is directly related to the melting temperature of the fuel ash. If K and Na are high in fuel ash, this lowers the BAI increasing the tendency to have agglomeration. The presence of K and Na in the fuel ash decreases the melting temperature of it as it was

stated in the book of Loo and Koppejan (2008). On the other hand, Ca and Mg were reported having an increasing effect on the melting temperature of the fuel ash (Loo and Koppejan, 2008).

2.2.2.3. Slagging, Fouling and Corrosion

The ash formed during the combustion in the combustor can interact each other or can react with the combustion gases forming different compounds in gaseous, liquid or solid phase (Bapat et al., 1997). When these compounds, particularly molten ash particles, hit the cooled surfaces of heat exchangers, they accumulate on the cooled surfaces forming layers of deposits. The deposits on the cooled surfaces depend on the section of the boiler. If the cooled surfaces are exposed to radiant heat in the fire-side section of the boiler like the furnace walls, the deposits are referred as "slagging". If they are in the steam-side (heat recovery) section in which superheaters, evaporators, or economizers are present, the deposits are named as "fouling" (Werther et al., 2000). Fouling and slagging can occur due to the transformation of inorganic constituents of fuel ash and heterogeneous reactions between gaseous, liquid, and solid phases. Reaction kinetics and transport rates of species are two important parameters for the formation of fouling and slagging (Lokare, 2008). Corrosion, as its name implies, is the erosion or deterioration of the heat transfer tube materials because of the reaction with the gases or deposits. Slagging and fouling cause heat transfer rate to reduce as well as the corrosion to increase (Khan, 2007).

The deposit formation on heat transfer surfaces is mainly due to the presence of alkali and alkaline earth metals in the fuel ash. While K is the important one for the biomass combustion, Na is the main concern for the coal combustion. Both K and Ca plays major role for the formation of sulfate deposits in heat transfer surfaces. Si, reacting with alkali and alkaline earth metals, contributes to the formation of alkali silicates with low melting temperatures at the temperature range of fluidized bed combustors 800-900^{o}C (Baxter et al., 1998). These alkali silicates can melt at the temperatures as low as 700^{o}C and provides a surface for the deposition (Khan, 2007). These compounds then enhance the formation of both slagging and fouling (Baxter et al., 1998). In the case of biomass combustion, especially woody biomass or olive cake with ash rich in Ca and K, the ash can easily deposit on the heat transfer surfaces causing fouling. The deposit may contain these elements in the form of CaO, $CaSO_4$ or K_2SO_4. While it is easy to remove the deposits from the surface of the economizer by soot blowing, it may be more problematic to remove the deposits on the superheater surface because of the high temperature above 500^{o}C in that region (Hiltunen et al., 2008).

Slagging is also another serious ash related problem encountered in the biomass-fired power plants. Slagging may form at high temperatures. The ash particles which are softened or partially melted can stick onto the heat transfer surfaces in the combustion section. After long operations, the slag formation may grow in size and prevent the homogenous distribution of combustion air. It is possible that unburnt fuel particles can stay in the slag increasing the unburnt C loss, which in turn results in a decrease in boiler

efficiency. The slag can also erode the heat transfer surfaces as well as the refractory material in the combustion section. If molten ash particles are carried to the heat recovery section, they can hit the heat transfer surfaces and stick on them forming a molten slag layer. The layer can easily grow with the accumulation of dry ash particles on this molten slag layer. This also decreases the heat transfer rate (Szemmelveisz et al., 2009).

Temperature, concentration of Cl, S, alkali metals and O_2 are main parameters affecting the corrosion. Cl plays an important role on corrosion getting involved into the condensation of alkali chlorides on heat transfer surfaces (Baxter et al., 1998). Alkali chlorides then react with SO_2 in the flue gas and form sulfates releasing Cl_2. Cl act as a catalyst accelerating the oxidation of the heat transfer material (Loo and Koppejan, 2008). The metal surfaces in the boilers are exposed to gases such as Cl_2 and compounds such as sulfates and chlorides. Due to the high exposure time, the metals in the heat exchanger tubes are released in different types such as metal chlorides or sulfites leading the tubes to corrode (Khan, 2007). Loo and Koppejan (2008) stated that combustion of biomass with S/Cl ratio less than 2 can cause serious corrosion problems, referring to the study conducted in 2000 (Salmenoja and Mäkelä, 2000). Werther et al. (2000) in their review paper cited a study (Petersen et al., 1991) which investigated the corrosion rates in three straw-fired boilers. Werther et al. (2000) summarized the study stating that the corrosion rate of steel material of heat transfer exchangers was strongly dependent on the surface temperature of the heat exchanger.

There are many indices have been used for the fuels to estimate the fouling and slagging tendencies of their ashes. Among the indices, the base-to-acid index (B/A_R) is the most commonly used fouling index. It is used by Babcock and Wilcox Company for all types of coal. A modified version of the B/A_R index is used for bituminous type ashes (Su et al., 2003; Namkung et al., 2013). It is the product of B/A_R index and the percentage of Na_2O in ash and given as B/A x Na_2O_R below.

$$B/A\_R = \frac{\%(Fe_2O_3 + CaO + MgO + K_2O + Na_2O)}{\%\,(SiO_2 + AlO_3 + TiO_2)} \quad \text{Eq. 2.2}$$

$$B/AxNa_2O\_R = B/A\_R * \%Na_2O \quad \text{Eq. 2.3}$$

Total alkali content is another index used for the fuel ashes having high alkali and alkaline earth metals (Na, K, or Ca) and their sulfates ashes (Su et al., 2003; Namkung et al., 2013). The total alkali content index is given in Eq. 2.4 below. The term "0.6589%K_2O" is the molar equivalent of Na_2O. This index seems more applicable for biomass ashes. Su et al. (2003), referring to Couch (1994), reported that there could be less probability of fouling formation if this index was less than 0.3.

$$Total\ alkali\ content = (\%Na_2O + 0.6589\%K_2O) * \frac{\%Ash}{100} \quad \text{Eq. 2.4}$$

Another index which can be used for biomass ashes is Fouling index, F_u which is given in Eq. 2.5. This is based on the B/A_R index. The potential of fouling formation was given

to be low for $F_u \leq 0.6$, high for $0.6 < F_u \leq 40$, and extremely high for $F_u > 40$ (Pronobis, 2005).

$$Fouling\ index, Fu = B/A\_R * \%(Na_2O + K_2O) \quad \text{Eq. 2.5}$$

Alkali index is generally applicable for biomass fuels such as straw and wood. It is defined as the amount of alkali oxides (Na_2O+K_2O) in the fuel per unit energy gained from the fuel and presented in Eq. 2.6 (Jenkins et al., 1998).

$$Alkali\ index = \%(Na_2O + K_2O) * \frac{\%Ash}{Q} \quad \text{Eq. 2.6}$$

In the Eq. 2.6 above, Q is the higher heating value (GJ/kg dry basis), %Ash is the mass fraction of ash in the fuel, $\%Na_2O$ and $\%K_2O$ are the mass fractions of Na_2O and K_2O in the ash, respectively (Jenkins et al., 1998). Miles et al. (1995) reported that the slagging risk was high when alkali index was above 0.17 kg alkali/GJ and it was almost certain to have slagging and fouling when it was above 0.34 kg alkali/GJ. Another Alkali index is from Hulkkonen et al. (2003) and Guanyi et al. (1997). It is the ratio of alkali metal oxides to silica oxide. It is defined as AI and given in Eq. 2.7 below. If the index is higher than 1, it is possible to have severe fouling on the heat transfer surfaces (Hulkkonen et al., 2003).

$$AI = \frac{\%(K_2O + Na_2O)}{\%\ (SiO_2)} \quad \text{Eq. 2.7}$$

The ash fusibility index (AFI) is used as an alternative index. It is different than the other indices given above because it is defined according to the ash fusion temperatures rather than ash composition. Therefore, it is highly possible that the result of this index can give more realistic estimates than the other indices regarding fouling and slagging. There are four ash fusion temperatures; Initial deformation temperature (IT), softening temperature (ST), hemispherical temperature (HT), and fluid temperature (FT). These ash fusion temperatures are determined according to the American Society for Testing and Measurement (ASTM) standard (*ASTM Standard D1857 Standard Test Method for Fusibility of Coal and Coke Ash*, 2004) and they are given in Figure 2.3. The IT is the temperature when the first rounding of the apex of the cone observed (second cone in Figure 2.3). The ST is the temperature when the cone takes a spherical shape in which the height is equal to the width (third cone in Figure 2.3). HT is the temperature when the cone takes a hemispherical shape in which the height is equal to one half of the width (forth cone in Figure 2.3). FT is the temperature at which the cone is spread out in a nearly flat layer with a maximum height of 1.6 mm (fifth cone in Figure 2.3) (*ASTM Standard D1857 Standard Test Method for Fusibility of Coal and Coke Ash*, 2004). AFI is based on the IT and HT and it is presented in Eq. 2.8. The slagging potential was reported as low for AFI > 1343°C, medium for when 1232°C < AFI ≤ 1343°C, high for 1149°C ≤ AFI ≤ 1232°C, and sever for AFI < 1149°C (Teixeira et al., 2012).

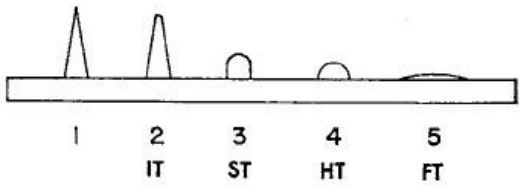

Figure 2.3 Ash Fusion Temperatures (*ASTM Standard D1857 Standard Test Method for Fusibility of Coal and Coke Ash*, 2004)

$$AFI = \frac{(4 * IT + HT)}{5} \qquad \text{Eq. 2.8}$$

Another important data obtained from the determination of ash fusion temperatures is related with the deposit formation on tube surfaces. The temperature differential between the IT and the FT gives an indication of the type of deposit formation on the furnace tube surfaces. If the temperature differential is small, this indicates that the surface slag will be thin and tenacious. If the temperature differential is large, this indicates that the slag deposit may build up in thicker layers (Borman and Ragland, 1998).

These indices are firstly developed to predict the behavior of coal ashes in the boilers in terms of fouling and slagging issues. With the usage of biomass fuels with coal or alone in combustors for the energy generation, these indices have been tried to be used for the prediction of ash-related problems of biomass fuels. However, Teixeira et al. (2012) presented some limitations for their applications to biomass fuels. They criticized the B/A_R index because it considered that alkali oxides (Na_2O, K_2O) and alkaline earth oxide (CaO) had the same effect on the reaction with SiO_2 in terms of fouling, indicating the study of Risnes et al. (2003) as a reference. Risnes et al. (2003) stated that Ca may affect the equilibrium reactions between K_2O, CaO, and SiO_2. Risnes et al. (2003) showed that if there was abundance of Ca, this increased the calcium silicates formation and decreased the formation of K-rich slag. All the indices based on the ash composition ignore any possible synergistic effect between ash samples. However, AFI is calculated according to the thermal behavior of the ash sample. Therefore, it may give more reliable estimates for the fouling and slagging. However, there are some limitations of AFI which in turn affect the accuracy of the prediction. These are related with the ash production. Production of the ash from its fuel in laboratory to perform ash fusibility test may differ ash produced in the combustor in terms of temperature gradients, changes on combustion conditions, interactions between ash particles and bed material (Teixeira et al., 2012).

Werther et al. (2000) made a wise conclusion for the discussion about the indices, referring to the study of Skrifvars et al. (1998a). Werther et al. (2000) stated that measurements of ash melting point temperatures in the laboratories and calculations of several indices from the ash compositions were not enough to provide sufficient information for the prediction of ash behaviour in a technical plant.

2.3. Circulating Fluidized Bed Combustors

The fluidized bed technology has been used for several physical and chemical processes in industry. Some of the application areas are physical operations like heat exchange, drying, and coating; synthesis reactions like Fischer-Tropsch synthesis; Fluid Catalytic Cracking; combustion; gasification; carbonization; calcination (Kunii and Levenspiel, 1991). Among the several applications, the fluidized beds are most widely used for the thermal conversion (combustion, gasification and pyrolysis) of biomasses and low-grade coals. The most of the power plants in the world uses combustion method for the utilization of that kind of fuels in order to get energy. There are basically two types of fluidized bed combustors; bubbling fluidized bed combustors (BFBCs) and circulating fluidized bed combustors (CFBCs). BFBCs are the first applications of fluidized bed combustion of coal. The first example of BFBC was seen in the early 1960s. The CFBCs are the next generation of BFBCs. For the some disadvantages encountered at BFBCs, CFBCs have rapidly taken the place of BFBCs. The main disadvantage of BFBCs compared to CFBCs is the low heat release rate per unit area. While it is between 0.5 MW_{th}/m^2 and 1.5 MW_{th}/m^2 for BFBCs, it is between 3 MW_{th}/m^2 and 5 MW_{th}/m^2 for CFBCs (Grace et al., 1997). The first CFB boiler was built in 1982 for the combustion of low-grade coal with the total capacity of 84 MW (Basu and Fraser, 1991). The CFB units have been developed in size and capacity since 1980s. According to the Pai and Engström (1999), there were around 300 atmospheric CFB units in operation or under construction by the 1999. CFB plants have been competing with the pulverized coal plants for the units up to 500 Megawatt (electric) (MW_e) (Pai and Engström, 1999). In the case of biomass co-firing, there were over 228 installations in the capacity range from 50 MW_e to 700 MW_e in the world, of which more than 100 of them were located in Europe (Al-Mansour and Zuwala, 2010). According to the IEA database, there are 87 fluidized bed units in the world co-firing biomass with different types of fuels, of which 40 are CFB units. The total global capacity of installed CFB or BFB units was 13.2 GW_{th} (3.6 MW_e) ("IEA Bioenergy Task 32: Biomass Combustion and Co-firing, Database of Biomass Co-firing initiatives," 2013).

2.3.1. Circulating Fluidized Bed Combustors in Turkey

The studies about the fluidized bed combustion were started in early 1980s in Turkey. The first attempt was under the leadership of the university. A BFBC with the thermal capacity of 0.3 MW_{th} was established at the Department of Chemical Engineering in Middle East Technical University (METU). The studies conducted in this test unit have provided useful know-how and experience as to the application of the fluidized bed combustion for Turkish lignites. A fluidized bed boiler which was established in 2001 by Alkim Inc. was a successful application of the studies done in 0.3 MW_{th} BFBC ("Akışkan Yataklı Kazanlar (in Turkish)," 2013). Because of the disadvantages encountered in industrial scale BFBCs such as low heat generation per unit surface area of heat exchangers, the fluidized bed technology in Turkey as well as in the world has shifted from bubbling to circulating fluidized bed combustion. The first CFBC was again coming from a university. It was established late 1980s at the department of Mechanical

Engineering, Gazi University. It was 125 mm in diameter and 1.8 m in height (Topal et al., 2003). Other one was established at the department of Chemical Engineering in METU in the second half of the 2000s. It had an inside diameter of 250 mm and a height of 6.5 m (Batu, 2008). The Laboratory-scale Circulating Fluidized Bed Combustor (Lab-CFBC) used in this study was established in 2009 in Marmara Research Center-Energy Institute (MRC-EI) of the Scientific and Technological Research Council of Turkey (TUBITAK) on the scope of a TUBITAK project which was proposed by Prof. Dr. Aysel Atimtay from Department of Environmental Engineering at METU. This system is one of the three lab-scale systems established at research centers or universities in Turkey.

There is only one power plant operating as CFBC which is owned by the Turkish government. It has two CFBC units. The total capacity is 320 MW_e. It uses Turkish lignite and has been operated by the Turkish Electricity Generation Company (EÜAŞ) since 2004. Other than that, there are a few fluidized bed power plants on industrial scale in Turkey. These are listed in Table 2.1. These plants were designed for Turkish lignite, imported coal and indigenous asphaltite. However, there is already no industrial-scale biomass-fired fluidized bed boiler in Turkey. In Table 2.1, the companies, the location of the power plants, capacity and capacity in operation as well as licensing date and period are also presented. Total construction capacity is 767 MW_e of which 460 MW_e are in use. The power plant in Şırnak has total capacity of 450 MW_e; three units with the capacity of each 150 MW_e. The first unit was put into service in March, 2013. The other two are still in construction. The power plant licensed by Çobanyıldızı Inc. is also in construction. The facility of İçdaş Inc. has three units; each has a capacity of 135 MW_e. The facility has started to produce electricity in 2005. The primary fuel used in the facility is imported coal. Natural gas is used as supplementary fuel.

Table 2.1 Fluidized bed power plants owned by the legal entities who have electricity production license in Turkey ("Üretim Lisansı Verilen Tüzel Kişiler (in Turkish)," 2013)

Company Name	**Place of Facility**	**Facility Type**	**Capacity [MW_e]**	**Capacity in Operation [MW_e]**	**Licensing Date**	**Licensing Period [year]**
Çolakoğlu Inc.	Gebze/ Kocaeli	Imported coal	190	190	16.10.2003	15
İçdaş Inc.	Biga/ Çanakkale	Imported coal	405	270	27.12.2007	49
Çobanyıldızı Inc.	Çumra/ Konya	Lignite/ Natural Gas	37	0	08.04.2011	49
Şırnak Inc.	Silopi/ Şırnak	Indigenous Asphaltite	135	0	03.01.2012	30

There are also two low-capacity applications of fluidized bed plants. ETİ SODA Inc. is the owner of the first one. It has two CFB units; each has a capacity of 10.5 MW_e. However, one of them is kept out of operation, they are not simultaneously operated. The other one has two CFB units and a total capacity of 16 MW_e. It is located in Çumra/Konya and established by Konya Sugar Factory. The power plant was constructed by Gama Power Systems Inc. in 2004 with the Babcock and Wilcox license.

2.4. Emission Limits in EU and Turkey

The emission of major pollutants in the flue gas of the large combustion plants has been regulated by the Directive 2001/80/EC of the European Parliament and of the Council of 23 October 2001 on the limitation of emissions of certain pollutants into air from large combustion plants (EU Directive) ("Directive 2001/08/EC of the European Parliament and of the Council of 23 October 2001 on the limitation of emission of certain pollutants into air from large combustion plants," 2001). The EU Directive aims to limit SO_2, NO_x and dust emissions from large combustion plants with thermal power equal to or greater than 50 MW. The definition of biomass in the EU Directive includes agricultural or forestry products containing vegetable matter, vegetable waste from agriculture and forestry, and from food processing industry, fibrous vegetable waste from pulp and paper industry, cork waste, wood waste does not contain halogenated organic compounds or heavy metals.

NO_x (measured as NO_2) and SO_2 emission limits for the new combustion plants using solid fuels are given in Table 2.2. In the EU Directive, the new combustion plants are defined as the plants which had a construction licence or an operating licence on or after 1 July 1987. Limit values here are expressed in mg/Nm^3 based on 6% O_2 in the flue gas and they are valid for the new combustion plants which have been put into operation after 27 November 2003. There is no emission limit for CO in the EU Directive.

Turkey was accepted as a candidate country to EU by EU members in 1999 and has started to negotiate on full membership since 2005. During this adaptation process, Turkey has prepared some regulations and directives regarding the control of air pollution by mostly translating equivalent ones in EU. The first regulation of Turkey in terms of air quality control was prepared and put into force in 1986. This regulation was legislated away by the Regulation for Industrial Air Pollution Control which was put into force in 2004. Following a modification of the regulation in 2006, the final version of the regulation was published in 2009. The emission limits for CO, NO_x (measured as NO_2) and SO_x (measured as SO_2) in the Turkish Regulation ("Turkish Regulation for Industrial Air Pollution Control," 2009) for both coal and biomass burning plants are given in Table 2.2 together with limits in EU Directive for the purpose of comparison. The biomass was defined in the Turkish regulation as same as in the EU Directive. Emission limits in the Turkish regulation was given at 0^oC temperature and 1 atm pressure based on 6% O_2 in the flue gas. Although the Turkish Regulation has higher limits than the EU Directive in terms of coal combustion, they have closely the same limits for biomass combustion.

Table 2.2 CO, NO_x (measured as NO_2) and SO_x (measured as SO_2) emission limits for the combustion plants using solid fuels according to the EU Directive ("Directive 2001/08/EC of the European Parliament and of the Council of 23 October 2001 on the limitation of emission of certain pollutants into air from large combustion plants," 2001) and the Turkish Regulation ("Turkish Regulation for Industrial Air Pollution Control," 2009)

Fuel Type	CO		NO_x as NO_2		SO_x as SO_2	
	Emission Limits (mg/Nm^3) [6% O_2]					
	EU	TR	EU	TR	EU	TR
Coal	-	200	400[a]	800[b]	850[c]	2000[d]
Biomass	-	460[e]	400[f]	400[g]	200[h]	200[e]

EU: EU Directive, TR: Turkish Regulation.
[a]50-100 MW_{th}; the limit is 200 mg/Nm^3 for the plants ≥100 MW_{th},
[b]≥50 MW_{th},
[c]the limit is given as SO_2 (50-100 MW_{th}); the limit is 200 mg/Nm^3 for the plants ≥100 MW_{th},
[d]<100 MW_{th}; the limit is 1300 mg/Nm^3 for the plants 100-300 MW_{th} and 1000 mg/Nm^3 for the plants ≥300 MW_{th},
[e]≥0.5 MW_{th},
[f]50-100 MW_{th}; the limit is 300 mg/Nm^3 for the plants 100-300 MW_{th} and 200 mg/Nm^3 for the plants ≥300 MW_{th},
[g]the limit is given as NO (≥50 MW_{th}),
[h]the limit is given as SO_2 ((≥50 MW_{th}).

The Turkish regulation is a transposition of the EU Directive and they have the same limits in terms of biomass combustion. Therefore, keeping the EU limits in mind, results of this study were compared to the limits of the Turkish regulation ("Turkish Regulation for Industrial Air Pollution Control," 2009). According to the Turkish Regulation, the emission limits, for the plants burning two fuels simultaneously -like in the case of co-combustion of coal and biomass- are calculated in terms of thermal power obtained from each fuel. In order to determine the emission limit, the emission limit of each fuel is multiplied by its thermal power. They are summed up and divided by the total thermal power coming from the fuels. The formula is given in Eq. 2.9 below.

$$EL_{mix} = \frac{(P_{th-1} * EL_1 + P_{th-2} * EL_2)}{(P_{th-1} + P_{th-2})} \quad \text{Eq. 2.9}$$

where,

EL_{mix}: Emission limit for the fuel mixture
P_{th-1} : Thermal power for primary fuel
EL_1 : Emission limit for primary fuel
P_{th-2} : Thermal power for supplementary fuel
EL_2 : Emission limit for supplementary fuel

This calculation is only valid for the case that the thermal power from one fuel is at least 10% of the total thermal power. Otherwise, the emission limits are determined as if the plant burns only one fuel which gives more power.

CHAPTER 3

LITERATURE SURVEY

3.1. Energy Review

3.1.1. World's Energy Outlook

The trend of world's TPES between 1971 and 2010 is given in Figure 3.1. The World's TPES in 2010 was 12700 Mtoe. It was 5.6% more than the previous year. The fossil fuels were the main sources for the energy supply. According to the Current Policies Scenario of International Energy Agency, it was estimated that the world's TPES will rise by 1.5% per year in the period between 2010 and 2035 and will reach to 18 700 Mtoe in 2035 (*IEA World Energy Outlook*, 2012). It was also estimated by IEA that the fossil fuels will remain as the most important energy source until 2035. The share of coal in TPES was estimated to be 29.6% followed by oil and natural gas with the contributions of 27% and 23.5%, respectively (*IEA World Energy Outlook*, 2012). While oil was the main fuel in world's TPES in 2010, it was predicted that the main fuel will be coal in 2035 (Tamzok et al., 2012).

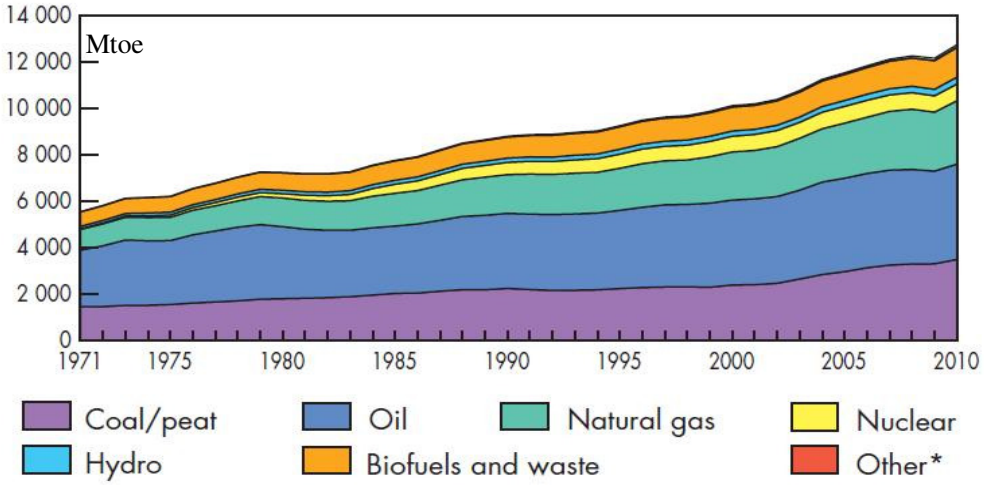

* Other includes geothermal, solar, wind, heat, etc.

Figure 3.1 World's TPES (Mtoe) from 1971 to 2010 (*IEA Key World Energy Statistics*, 2012)

World's total primary energy supply (TPES) has been doubled in last 37 years While it was about 6100 Mtoe in 1973, it increased up to 12700 Mtoe in 2010 (*IEA Key World Energy Statistics*, 2012). Within this period, the share of oil in world's TPES decreased from 46% to 32%. However, the share of natural gas and nuclear increased to 21% from 16% and 6% from 1%, respectively (Tamzok et al., 2012). As can be seen in Figure 3.2, 81% of the world's TPES was met by fossil fuels in 2010; shares of oil, coal, and natural gas were 32%, 27% and 22%, respectively (*WEC-TNC Energy Report (in Turkish)*, 2012). The share of renewable energy sources in 2010 was 13.2% including hydro, biofuels and waste, geothermal, solar and wind. Among the renewables, solid biofuels (excluding wastes), were the largest contributor, providing 69.2% of world's renewables (*IEA Statistics Renewables Information*, 2012).

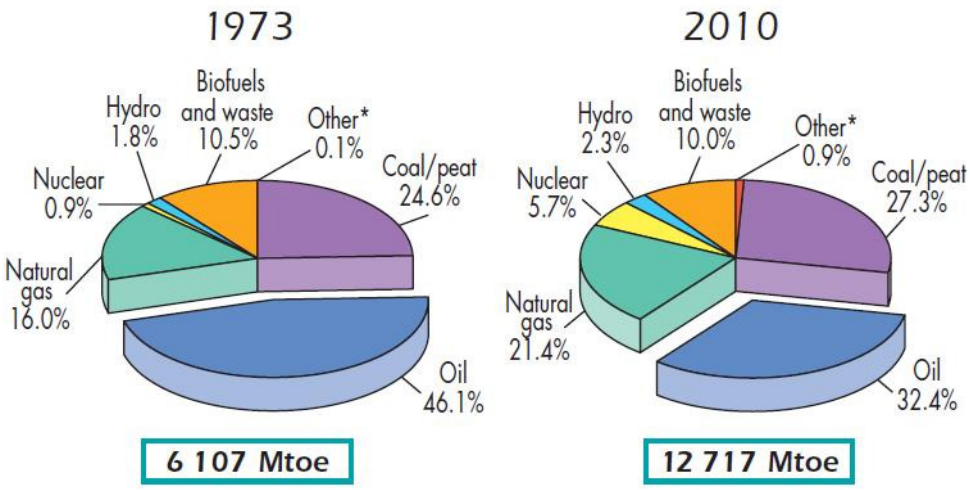

* Other includes geothermal, solar, wind, heat, etc.

Figure 3.2 Shares of world's TPES for the years 1973 and 2010 (*IEA Key World Energy Statistics*, 2012)

3.1.2. Turkey's Energy Outlook

Turkey's TPES are given in Figure 3.3. While Turkey's TPES was 84 Mtoe in 2003, it increased in parallel with the economic development over 9 years and reached to 114.5 Mtoe in 2011. 90% of Turkey's TPES was supplied from fossil fuels out of which 32% is from natural gas, 31% from coal, and 27% from oil. The percentage of fossil fuels in TPES in 2003 was almost the same, 88%. While oil was leading in 2003, the leadership shifted to natural gas in 2011. The share of renewable energy sources (biomass (wood, animal waste and vegetable residues), hydropower, geothermal, solar, wind, and biofuels) in total TPES was 12% in 2003. It decreased to 10% in 2011 because of the decrease in biomass usage from 7% in 2003 to 3% in 2011.

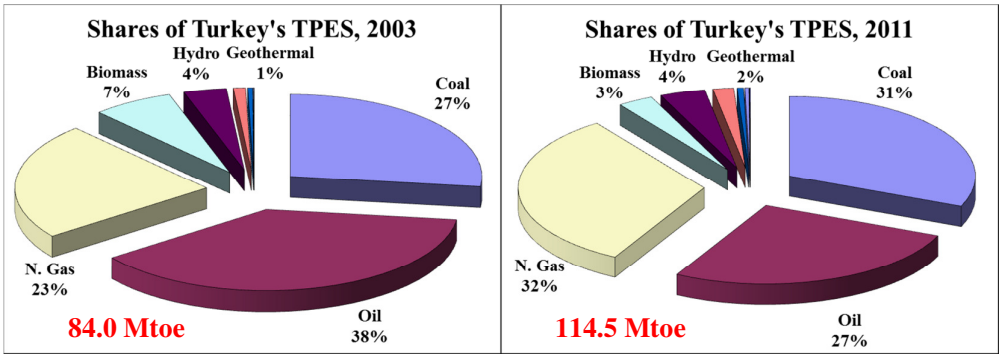

Figure 3.3 Turkey's TPES for the years 2003 and 2011 ("Energy Balances of Turkey," 2013)

Turkey's total energy production in 2003 and 2011 and the distribution of the production among different types of fuels are given in Figure 3.4. Increase in the total energy production for this period was 35%, namely total energy production increased from 23.8 Mtoe in 2003 to 32.2 Mtoe in 2011. The import rate was in the range of 70-75% for the last 9 years. It can be seen from Figure 3.4 that coal is the main fuel used in the energy production. Share of coal in the production was 45% in 2003, the share rose to 56% in 2011. The government's policy about the use of indigenous resources, particularly lignite resources, in the energy production is the main reason for the increase of coal share in the energy production (*2010-2014 Strategic Plan (in Turkish)*, 2009). On the other hand, the share of biomass decreased from 24% to 11% between the years 2003 and 2011. The biomass resources were mainly used for residential heating in rural areas. The share of biomass in energy production decreased mostly due to the replacement of biomass with natural gas for heating purposes. Hydropower is another important energy source in Turkey for many years. Its share in energy production did not change much over 9 years. It was 13% in 2003 and 14% in 2011.

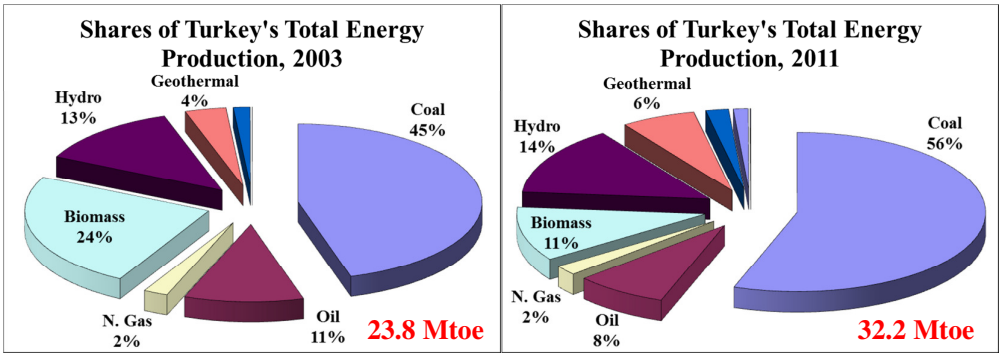

Figure 3.4 Turkey's Total Energy Production between the years 2003 and 2011 ("Energy Balances of Turkey," 2013)

Total energy production, TPES and imports in Turkey from 1985 to 2011 is given in Figure 3.5. TPES in 1985 was 39 Mtoe, of which 44% was met by imports. The total energy production in that year was 21.7 Mtoe. There was a rapid increase in energy demand of Turkey in years between 1985 and 2000. Because of not giving importance for the energy production investments over the 15-year period, energy production was almost constant and the increase in energy demand was mainly met by imports. While the rate of increase in TPES was 107%, the rate of increase in imports was 212% in the same period. After the two-year recession in energy sector following the economic crisis in 2001, energy demand started to increase again. 2003 was the first year that the import share in TPES was over 70% and it never came back again. On the other hand, it did not pass 75% between 2003 and 2011 due to the increase in energy production.

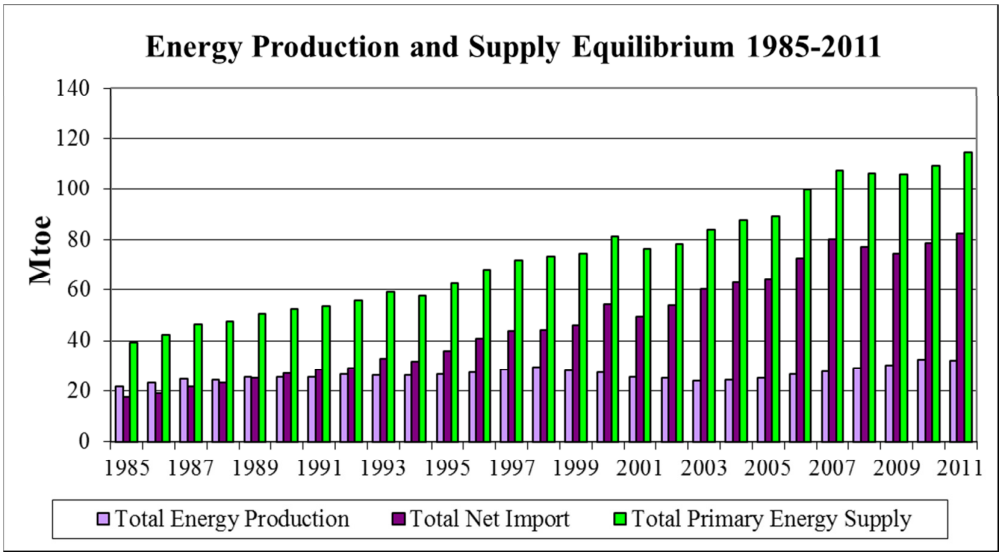

Figure 3.5 Total energy production, net imports and primary energy supply between 1985 and 2011 in Turkey ("Energy Balances of Turkey," 2013)

Total energy production, total net imports and TPES of Turkey between 1985 and 2011 are presented in Table 3.1. It can be seen from the table that Turkey's TPES increased by 193% over the 26 years between 1985 and 2011. However, increase in the total energy production was only 48.5% for the same period. The gap between the demand and production was met by imports. While the share of total net imports in TPES was 44% in 1985, it became 72% in 2011.

Table 3.1 Energy outlook of Turkey between 1985 and 2011 ("Energy Balances of Turkey," 2013)

	1985	1990	1995	2000	2005	2010	2011
Total Energy Production, Mtoe	**21.70**	**25.23**	**26.34**	**27.14**	**25.19**	**32.49**	**32.23**
Total Net Import, Mtoe	**17.39**	**27.07**	**36.00**	**54.23**	**63.91**	**78.68**	**82.26**
TPES, Mtoe	**39.09**	**52.30**	**62.34**	**81.10**	**89.10**	**109.27**	**114.48**
Total Energy Production, %	**55.52**	**48.24**	**42.25**	**33.46**	**28.27**	**29.74**	**28.15**
Total Net Import, %	**44.48**	**51.76**	**57.75**	**66.87**	**71.73**	**72.01**	**71.85**

3.2. Coal Review

Coal is defined as *combustible sedimentary rock materials*. Because of its wide range of quality scale in terms of heating value, it is classified by the International Coal Classification of the Economic Commission for Europe (UNECE) into two groups which are divided into two subgroups (*IEA Statistics Coal Information*, 2012):

- Hard Coal (gross calorific value more than 5 700 kcal/kg on ash-free basis)
  - Anthracite
  - Bituminous coal
- Brown Coal
  - Sub-bituminous coal (gross calorific value between 4 165 kcal/kg and 5 700 kcal/kg on ash-free basis)
  - Lignite (gross calorific value less than 4 165 kcal/kg on ash-free basis)

3.2.1. World's Coal Review

3.2.1.1. Coal Reserves

There are three main estimates in the IEA's report (*IEA Statistics Coal Information*, 2012) regarding coal reserves in the world. The first one is from World Energy Council (WEC) which was published in 1978. It estimated that the proved coal reserves were 636.4 billion tonnes. The second one is from WEC. It predicted the proved coal reserves were 909.1 billion tonnes in 2002. The last one is from the German Federal Institute for Geosciences and Natural Resources (BGR). According to BGR, the proved recoverable coal reserves were 1003.8 billion tonnes in 2010. According to another estimate of WEC, the world coal reserves are 861 billion tonnes for 2008 of which 47% is hard coal, 30% is sub-bituminous and 23% is lignite (Iancu et al., 2010). It can be seen from the estimates that the amount of coal reserves is increasing over time. As the coal prices increase, some

part of the coal resources becomes economically feasible to bring them to the surface (*IEA Statistics Coal Information*, 2012). According to the WEC's estimate in 2008, USA was leading the way with the share of 27.6% in global coal reserves. USA was followed by Russian Federation (18.2%) and China (13.3%). Other countries in the top rank were Australia (8.9%), India (7%) and Germany (4.7%) (Tamzok et al., 2012).

Among the fossil fuels, coal is plentiful and widely distributed all around the world. Proved coal reserves are much more than the total of oil and natural gas reserves. BGR estimates that coal reserves are enough to meet the demand about 130 years with the production rates in 2011. Almost half of the world's energy demand was met by coal over the past 10 years. It is expected that coal consumption in the energy sector will be still important, particularly for the countries of Organization for Economic and Co-operation Development (OECD) (*IEA World Energy Outlook*, 2012).

3.2.1.2. Total Coal Production

Total coal production in the world was 7783 Mt in 2011 (*IEA Key World Energy Statistics*, 2012). The major coal producers, net exporters and net importers were shown in Table 3.2. China was seen at the top of the list with the production of 3576 Mt. China met almost the half of the need by itself. China was followed by USA (1004 Mt), India (586 Mt), Australia (414 Mt) and Indonesia (376 Mt) (*IEA Key World Energy Statistics*, 2012). China not only consumed all the coal produced by itself but also imported some in order to meet its energy demand in 2011. China was one of the major coal importers with Japan, Korea and India as can be seen in Table 3.2. It was also same for the other developing country in Asia, which is India. India produced 586 Mt of coal in 2011. That amount was not enough for its demand and India imported as much coal as 17% of its production. Australia and Indonesia were the major coal exporters in 2011. It seems from Table 3.2 that these two countries mine the coal mainly to sell them to the neighboring countries such as China, India, Japan, and Korea. Indonesia and Australia shipped 82% and 69% of their total productions in 2011, respectively.

Table 3.2 Major coal* producers, net exporters and net importers in 2011 (*IEA Key World Energy Statistics*, 2012)

Producers	**Production, Mt**	**Production Share, %**	**Net exporters**	**Mt**	**Net importers**	**Mt**
China	3576	45.9	Indonesia	309	China	177
USA	1004	12.9	Australia	285	Japan	175
India	586	7.5	Russian Fd.	99	Korea	129
Australia	414	5.3	USA	85	India	101
Indonesia	376	4.8	Colombia	76	Chin. Tai.	66
World	**7783**	**100.0**	**World**	**1041**	**World**	**1002**

*Includes steam coal, coking coal, lignite and recovered coal.

The world coal production by region between 1971 and 2011 is given in Figure 3.6. The total coal production has increased 2.5 times as much over 40 years. This was because of the increasing energy/electricity demand coming from the developing countries in Asia, particularly China. When the figure was examined, it can be easily seen that there was not too much change in the total coal production of OECD countries. Total coal production of OECD countries in 2011 was 10 Mt lower than that is in 1998. On the other hand, total coal production of non-OECD countries increased by 115% in the same period (*IEA Statistics Coal Information*, 2012). While OECD countries were leading the coal production in 1970s, Asian countries (e.g. China being the first) have started to take the leadership by 1980. There might be two main reasons for that shift. Coal is still the cheapest resource to produce electricity compared to the other energy resources and the developing countries in Asia are rich in coal resources. They use coal in energy production in order to meet the increasing energy demand. On the other hand, developed countries, mainly European Union members, prefer natural gas for electricity generation rather than coal because of the public concerns in air pollution problems (Tamzok et al., 2012).

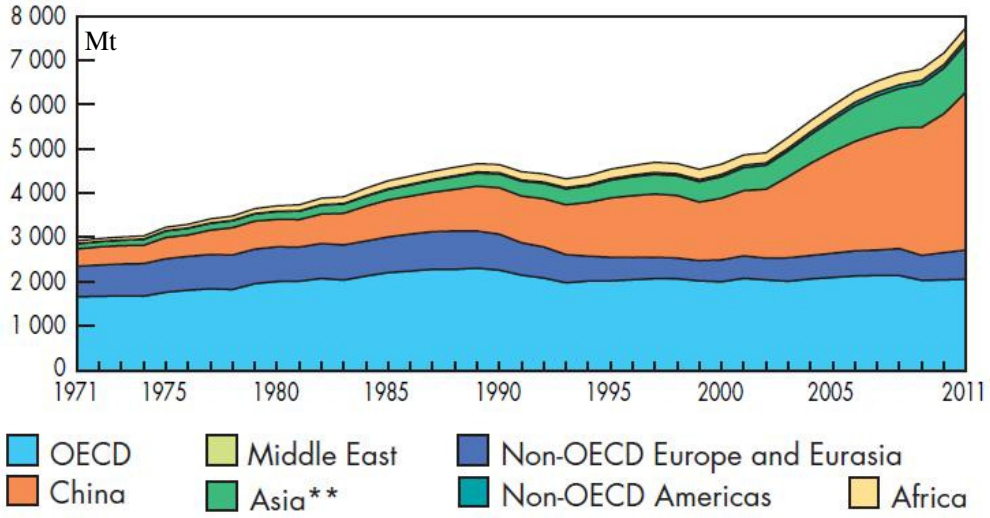

** Asia excludes China.

Figure 3.6 World coal production by region (Mt) (*IEA Key World Energy Statistics*, 2012).

The change in the contributions of different regions in coal production is presented in Figure 3.7. The main coal producers were OECD countries and non-OECD Europe and Eurasia countries like Russian Federation, Bulgaria and Turkmenistan in 1973. 80% of the coal demand in the world was met by these countries in 1973. Since 1979 when economic reforms and globalization process started in China, China has started to use its indigenous resources in energy sector. The new developing countries like China and India became the world leaders in coal production. While the share of China in coal production

was 13.7% in 1973, it increased to 45.9% in 2011. In 2011, Asian countries met 60.2% of the coal demand of the world.

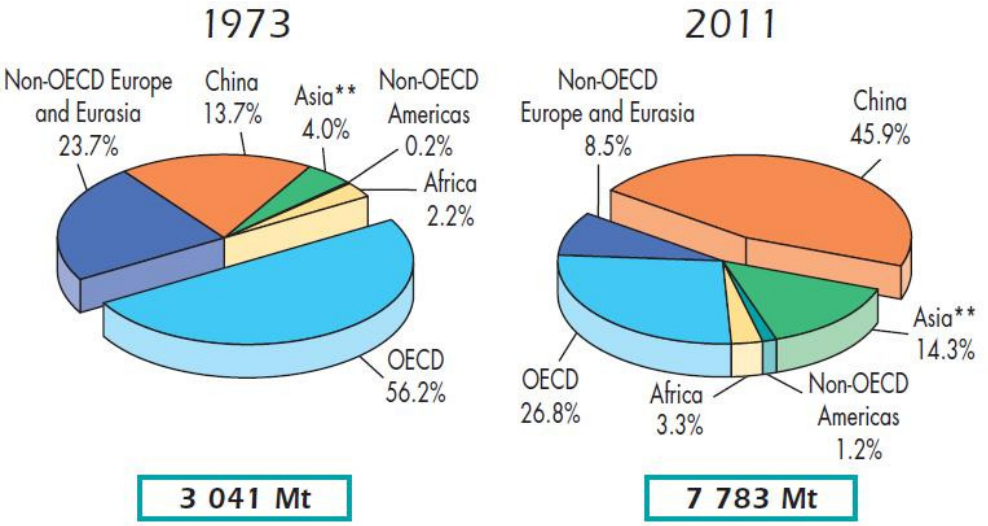

** Asia excludes China.

Figure 3.7 Coal production in different regions of the world for the years 1973 and 2011 (*IEA Key World Energy Statistics*, 2012)

3.2.1.3. Total Coal Consumption

The world's coal consumption has gone up at 4.9% per year since 2000 (Iancu et al., 2010). The major coal producers in 2011 were also the major coal consumers. Those countries were China, USA and India. With Russia and Japan, these five coal consumers accounted for 76.4% of the world coal consumption in 2011 (*IEA Statistics Coal Information*, 2012). IEA predicts that coal consumption will rise by over 60% by 2030 and China and India will account for 85% of this increase (Iancu et al., 2010).

3.2.1.4. Lignite Reserves, Production and Consumption

The world's total lignite reserves were estimated as 195 billion tonnes at the end of 2008 according to the WEC (Iancu et al., 2010). The largest portion, 21% of these reserves are present in Germany. Germany is followed by Australia and USA with the shares of 19% and 16%, respectively. Other countries having high lignite reserves were China (9.5%), Serbia (7%), Kazakhstan (6%), and Russian Federation (5%).

The total lignite production in the world and the major producers in 2011 are given in Table 3.3. The total lignite production was 1041 Mt in 2011. It increased by 5.9% in

2010. Lignite production in OECD countries increased to 604 Mt which was mainly led by the production increases in Germany, Poland and Turkey, there was much more production increase in non-OECD countries. The total production was 437.1 Mt in 2011, rising by 9.4% compared to that in 2010 (*IEA Statistics Coal Information*, 2012). 75% of the total lignite production in 2011 was only done by 10 countries. Germany was leading with the production of 176.5 Mt. Germany accounted for 17% of the total production. China was the second largest lignite producer. China mined 13.1% of the total lignite produced in 2011. China was followed by Russian Federation, having 7.5% share in total production (*WEC-TNC Energy Report (in Turkish)*, 2012). Turkey produced 74.4 Mt of lignite in 2011 being the 4th largest producer in the world. Turkey's share in the total production was 7.1% (Tamzok et al., 2012). The lignite producers are at the same time the main consumers. Therefore, annual production amounts are nearly equal to the annual consumption amounts.

Table 3.3 Major lignite producers in 2011 (*IEA Statistics Coal Information*, 2012)

Country	Production*, Mt	Production Share, %
Germany	176.5	17.0
China	136.3	13.1
Russian Fd.	77.6	7.5
Turkey	74.4	7.1
USA	73.4	7.1
World	**1041.0**	**100.0**

*preliminary estimates based on IEA member countries; includes also oil shale.

3.2.1.5. World's CO_2 Emissions from Fuel Combustion

World CO_2 emissions from fuel combustion within 40 years between 1971 and 2010 are given in Figure 3.8 (*IEA Key World Energy Statistics*, 2012). The increase on CO_2 in the period of 1971 and 2010 was 115% going from 14.1 Giga tonnes (Gt) in 1971 to 30.3 Gt in 2010. Within the same period, coal related CO_2 emissions increased by 152% from 5.2 Gt in 1971 to 13.1 Gt in 2010 (*IEA Statistics Coal Information*, 2012). CO_2 emissions increased by 4.6% in 2010 as compared to that in 2009 because of the economic crisis, particularly in USA and EU countries (*IEA Statistics CO_2 Emissions from Fuel Combustion*, 2012).

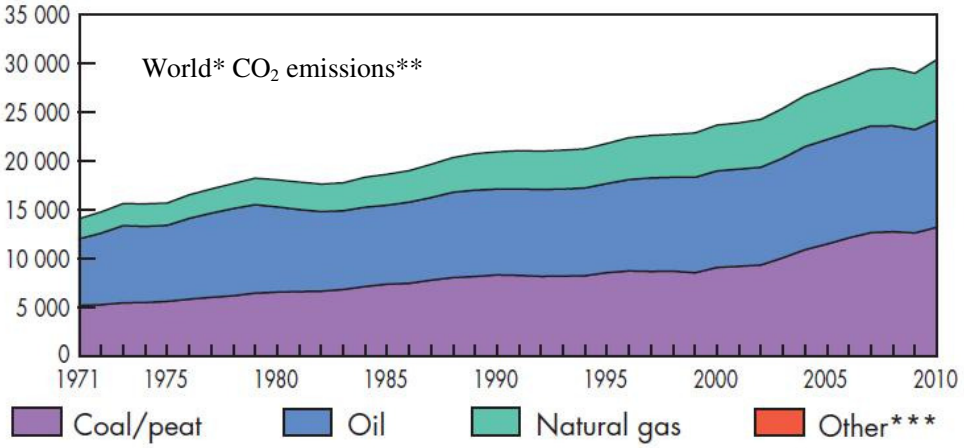

* World includes international aviation and international marine bunkers.
** Calculated using the IEA's energy balances and the Revised 1996 IPCC Guidelines. CO_2 emissions are from fuel combustion only.
*** Other includes industrial waste and non-renewable municipal waste.

Figure 3.8 World CO_2 emissions from fuel combustion between 1971 and 2010 by fuel (Mt of CO_2) (*IEA Key World Energy Statistics*, 2012)

The contribution of coal combustion to the CO_2 emissions was 43.1% in 2010 as can be seen in Figure 3.9. Coal has been the main source for CO_2 emissions since 2005. Coal-related CO_2 emissions have increased by 4.7% per year since 2002 (*IEA Statistics Coal Information*, 2012). While CO_2 emissions were 15.6 Gt in 1973, they reached to 30.3 Gt in 2010. According to the IEA estimates mentioned in World Energy Outlook 2012 (*IEA World Energy Outlook*, 2012), CO_2 emissions were expected to be 31.2 Gt in 2011 and this was attributed to China because of its rising emissions by 9% per year.

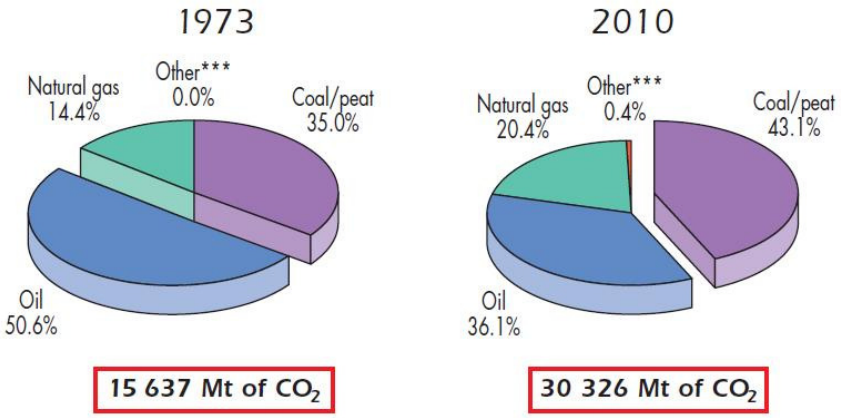

*** Other includes industrial waste and non-renewable municipal waste.

Figure 3.9 world CO_2 emissions for the years 1973 and 2010 (*IEA Key World Energy Statistics*, 2012)

Total CO_2 emission in 2010 was 30.3 Mt of CO_2, of which 65% (19.8 Gt) originated from 10 countries. Among these ten countries, China and USA were the two main emitters, responsible for the 41.5% of CO_2 emissions in 2010 with the contribution of 23.8% and 17.7%, respectively (*IEA Statistics CO_2 Emissions from Fuel Combustion*, 2012).

3.2.2. Turkey's Coal Review

According to the WEC report published in 2010 (Iancu et al., 2010), Turkey's total proved recoverable coal reserves at the end of 2008 were estimated to be 2.3 billion tonnes, of which 1.8 billion tonnes were lignite reserves. On the other hand, in Turkish official sources, it was underlined that Turkey had 11.8 billion tonnes of proved recoverable lignite reserves in 2011 according to the annual report known as "Blue Book" which was published by The Republic of Turkey, Ministry of Energy and Natural Resources in 2012 (*Enerji ve Tabii Kaynaklar Bakanlığı ile Bağlı ve İlgili Kuruluşlarının Amaç ve Faaliyetleri (in Turkish)*, 2012). The same amount of reserves was also mentioned in the report of General Directorate of Turkish Coal Enterprises which was published in 2012 (Tamzok et al., 2012). This amount accounted for 6% of the world's lignite reserves (195 billion tonnes by 2008) (Iancu et al., 2010). However, heating values of Turkey's lignite reserves are pretty low. The heating values are in the range of 1000 kcal/kg and 4200 kcal/kg. 90% of lignite reserves have lower heating value less than 3000 kcal/kg (Tamzok et al., 2012). For example, the lignite mined in Afşin-Elbistan basin which has the largest lignite reserves, has the lower heating value between 900 and 1250 kcal/kg (*WEC-TNC Energy Report (in Turkish)*, 2012).

Turkey's coal map by 2011 is shown in Figure 3.10. The Afşin-Elbistan basin accounts for about 40% of all lignite reserves in Turkey (Akdeniz et al., 2002; Kiliç and Kaya, 2007). The other lignite reserves are located in Soma, Tunçbilek, Seyitömer, Bursa/Orhaneli, Çan, Muğla, Ankara-Beypazarı, Sivas-Kangal and Konya-Karapınar basins. As can be seen from the figure that although lignite deposits are spread all over the country, hard coal is only extracted from Zonguldak basin in the northwest of Turkey (*U.S. Energy Information Administration, Country Briefs, Turkey*, 2013).

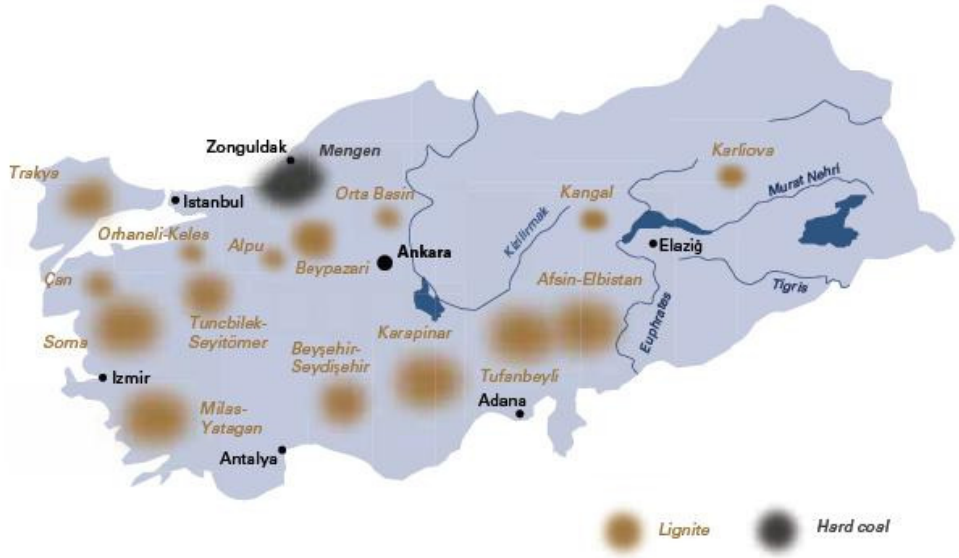

Figure 3.10 Turkey's coal map by 2011 ("Coal, Country Profiles, Turkey," 2011)

Turkey is a rich country in coal reserves and it is among the big coal producers in the world. When coal productions in the world given in Table 3.2 are examined, it is seen that 7783 Mt of coal was produced in the world in 2011 (*IEA Key World Energy Statistics*, 2012). While China was the biggest coal producer with the production of 3 576.1 Mt coal, it was followed by USA with the production of 1004 Mt. Turkey was the twelve biggest coal producers with the production of 78.1 Mt in 2011 (*IEA Statistics Coal Information*, 2012). With this production, Turkey met 1% of the world coal production in the same year. The majority of the total coal production (95%) was coming from lignite in Turkey. The lignite production was 74.4 Mt in 2011 (*IEA Statistics Coal Information*, 2012). It accounts for 7.1% of world's lignite production (1041 Mt). Turkey was the fourth biggest lignite producer, following Germany, China and Russia (*IEA Statistics Coal Information*, 2012). As can be seen from the data above, Turkey is a rich in coal -particularly lignite- reserves and it is very important to use this potential in energy production in order to minimize the foreign-source dependency.

The total capacity of power plants in Turkey by the end of 2011 was 52911 MW_e, of which 64% (33931 MW) was met by thermal power plants (*Enerji ve Tabii Kaynaklar Bakanlığı ile Bağlı ve İlgili Kuruluşlarının Amaç ve Faaliyetleri (in Turkish)*, 2012). Although Turkey mined both hard coal and lignite, the production was only enough for the half of its consumption in 2010. While all the lignite production was used in the country, Turkey imported almost 90% of its hard coal requirement (*OECD "Turkey", in Inventory of Estimated Budgetary Support and Tax Expenditures for Fossil Fuels 2013*, 2013). The amount of hard coal imported was 26.9 Mt in 2010. 38.3% of it was imported from Russian Federation, 10.6% from Colombia, 9% from USA, and 7.6% from South Africa. The total capacity of thermal power plants using imported coal was 3881 MW_e in

2011, of which 1200 MW_e was generated in Iskenderun in the southern part of Turkey. The power plant in Iskenderun has been operated since 2004 ("Coal, Country Profiles, Turkey," 2011). There is only one power plant with the capacity of 300 MW_e using the indigenous hard coal in Zonguldak basin. Lignite production is being mainly done for three sectors, namely energy sector (thermal power plants), industry, and heating. Total capacity of lignite-fired power plants was 8140 MW_e in 2011 (*WEC-TNC Energy Report (in Turkish)*, 2012). In 2011, 82% of total lignite production was consumed in thermal power plants (*WEC-TNC Energy Report (in Turkish)*, 2012). 7.5 % of it was used in industry and 8.6% of it was consumed for heating purposes (Tamzok et al., 2012).

3.2.2.1. Turkey's Greenhouse Gas Emissions

Turkey ratified The United Nations Framework Convention on Climate Change (UNFCCC) in 2004 and The Kyoto Protocol in 2009. As required by the Convention, Turkey prepares national inventory on greenhouse gas (GHG) emissions according to the Intergovernmental Panel on Climate Change (IPCC) methodology (*TurkStat National Greenhouse Gas Inventory Report 1990-2010*, 2012). Turkey's GHG emissions by sectors and by greenhouse gases for the years 1990 and 2010 are shown in Table 3.4. GHG emissions are expressed in CO_2 equivalent and the sector of Land Use, Land Use Change and Forestry (LULUCF) is not taken into account. GHG emissions increased by 115% over 20 years from 187 Mt of CO_2 eq. to 402 Mt of CO_2 eq. as can be seen from Table 3.4. Energy sector was responsible for 71 % of the GHG emissions in 2010. The contributions of industrial processes, agriculture and waste sectors were 13.4%, 6.8%, and 8.9% in 2010, respectively. Among the GHG, the major contribution was from CO_2. While it was 76% in 1990, it made up more than 80% of GHG emissions in 2010.

Table 3.4 Turkey's GHG emissions by sectors and gases for the years 1990 and 2010 (*TurkStat National Greenhouse Gas Inventory Report 1990-2010*, 2012)

	1990	**2010**
	(Million tonnes CO_2 eq.)	
Total (excluding LULUCF)	**187.03**	**401.92**
Sector		
Energy	132.13	285.07
Industrial processes	15.44	53.90
Agriculture	29.78	27.13
Waste	9.68	35.83
Gas		
CO_2	141.36	326.47
CH_4	33.50	57.54
N_2O	11.57	13.03
HFCs	0.00	4.01
PFCs	0.60	0.00
SF_6	0.00	0.88

The fossil fuel combustion used in energy sector for power generation was the main source for the GHG emissions in Turkey. CO_2 was the major gas among the GHG emitted to the atmosphere and almost 90% of CO_2 emissions was coming from the combustion of fossil fuels (*TurkStat National Greenhouse Gas Inventory Report 1990-2010*, 2012).

3.2.2.1.1. Turkey's CO_2 Emissions from Fuel Combustion

The changes in CO_2 emissions from fuel combustion over 20 years between 1990 and 2010 for the world are given in Table 3.5. The contribution of OECD and non-OECD countries to the CO_2 emissions is presented in Table 3.5. The emissions of USA and China, major contributors among the OECD and non-OECD countries, respectively are also given in Table 3.5 for the years 1990 and 2010 in order to see the contribution of Turkey to the total CO_2 emissions in the world. CO_2 emissions presented here are the values calculated according to the sectoral approach of IEA (*IEA Statistics CO_2 Emissions from Fuel Combustion*, 2012). The recent CO_2 emissions in 2010 are compared with the CO_2 emission in 1990 because 1990 was stated as a reference year for the emission reduction targets in Kyoto Protocol. When the CO_2 emissions are examined in the table, it can be seen that the total increase in the CO_2 emissions of the world over 20 years was 44.4%. The non-OECD countries are seen to be the main contributor for that increase with 81.9% increase in their total CO_2 emissions over the same period. Among the non-OECD countries, China led the way by generating 223% more CO_2 emissions in 2010 compared to that in 1990. In the same period, OECD countries increased the global CO_2 concentration by 11.5%. The major contribution among the OECD countries was from USA with 5369 Mt of CO_2. The increase in CO_2 emissions was 10.3% within 20 years. Turkey's CO_2 emission can be neglected when it is compared with the emissions of USA but the total increase of CO_2 emissions in Turkey cannot be ignored. Turkey produced 266 Mt of CO_2 in 2010. When it was compared with the emission in 1990, the total increase was more than the double. Turkey was the one who has the highest increase in CO_2 emissions among the OECD European countries in 2010. Turkey, with the 266 Mt of CO_2 emissions in 2010, was the 7th biggest contributor among the OECD European countries. The major contribution was from Germany among the OECD European countries in 2010. Germany emitted 761.6 Mt of CO_2 from fuel combustion to the atmosphere in 2010.

Table 3.5 CO_2 emissions (sectoral approach) from fuel combustion for the years 1990 and 2010 (million tonnes of CO_2) (*IEA Statistics CO_2 Emissions from Fuel Combustion*, 2012)

	1990	**2010**	**% change**
World	20973.9	30276.1	44.4
Non-OECD	9199.3	16736.8	81.9
OECD	11156.8	12440.3	11.5
China	2244.1	7258.5	223.5
USA	4868.7	5368.6	10.3
Turkey	126.9	265.9	109.5

China was the main contributor of CO_2 emissions originated from fuel combustion in 2010 with 24%. China was followed by USA with 17.7% as can be seen in Table 3.5. According to the IEA report (*IEA Key World Energy Statistics*, 2012), Turkey's population was 72.85 million in 2010. This accounts for 1.1% of the world's population. In line with the population, Turkey's share in the world's TPES was 0.8% for the same year (World's TPES was 12717 Mtoe in 2010, including international aviation and international marine bunkers as well as electricity and heat trade). As a result of this, Turkey, having 266 Mt of CO_2 emissions, was only responsible for the 0.9% of the world's total CO_2 emissions from fuel combustion in 2010. Turkey's share of CO_2 emissions among the OECD countries was 2.1%. Although Turkey's CO_2 emissions from fuel combustion have been doubled over 20 years, Turkey's contribution to the global CO_2 emissions in total amount can be negligible (*WEC-TNC Energy Report (in Turkish)*, 2012). Turkey ratified the Kyoto Protocol in 2009. It is expected Turkey to take some cautions and make investments in order to decrease total GHG emissions after 2012. It is obvious that all these efforts put an extra financial burden on the Turkish economy.

3.3. Biomass Review

3.3.1. World Biomass Potential

In 2012, biofuels and wastes accounted for 10 % of the world's TPES as can be seen in Figure 3.2. This corresponded to about 50 EJ global energy demand. 85% of this demand was mainly traditional biomass which was used mostly for cooking and heating purposes (*REN21 Renewables 2012 Global Status Report 2012*, 2012). Considering the different types of biomass feedstock, the technical biomass potential was estimated as much as 1 500 EJ/yr by 2050 in the literature. However, most of the biomass supply scenarios taking into account the sustainability limitation predicted the potential in the range of 200-500 EJ/yr. (Iancu et al., 2010). The German Government's Integrated Energy and Climate Programme (IEKP) estimated the total biomass potential between 68 and 116 PJ per year for 2020, of which 30 EJ/yr was from residues and waste (Thrän et al., 2011).

3.3.2. Turkey's Biomass Potential

Table 3.6 shows the TPES of the world, OECD countries and Turkey for 2010. It also gives the share of renewables in TPES and the share of biofuels and wastes in renewables for the world, OECD countries and Turkey in order to see the Turkey's position on biomass usage in energy and heat production. According to IEA, the world's TPES in 2010 was 12782 Mtoe, of which 13% was met by renewable resources (*IEA Statistics Renewables Information*, 2012). The share of biofuels and wastes in renewables was 75.2%. Because of the widespread usage of biomass in developing countries, biofuels and waste were the biggest source among the renewable energy sources. The share of biofuels and wastes in total renewables were 57.4% and 38.9% for OECD countries and Turkey, respectively. Following biofuels and wastes, the second largest renewable source was hydro for OECD countries as well as Turkey (*IEA Statistics Renewables Information*, 2012).

Table 3.6 Renewables indicators in 2010 (*IEA Statistics Renewables Information*, 2012)

	TPES, Mtoe	Share of renewables in TPES, %	Share of biofuels and wastes in total renewables, %
World	12782.0	13.0	75.2
OECD	5405.9	7.8	57.4
Turkey	105.1	11.1	38.9

Turkey has also a high production potential of biowastes. In the current study (Melikoglu, 2013), the biomass energy potential of Turkey was estimated to be around 32 Mtoe. The total recoverable potential was estimated to be about 16.9 Mtoe according to the previous studies (Evrendilek and Ertekin, 2003; Balat, 2005). The annual biomass energy potential of Turkey which was estimated as 32 Mtoe was also mentioned in the study (Balat, 2005) and this estimate belonged to the year 2001. The recoverable potential given as 16.9 Mtoe in the study (Evrendilek and Ertekin, 2003) was referred to the study (Kaygusuz and Türker, 2002) and this value was for 1998. In another recent study (Toklu, 2013), the total recoverable biomass energy potential was expected to be 16.8 Mtoe in 2000 and 14.2 Mtoe in 2008. These estimates were done according to the amounts of agricultural, forestry and wood processing residues. Total biomass production was estimated as 12.6 Mtoe in 2020 in the same study (Toklu, 2013). In the study of Ozgur (2008), the potential of biomass energy was classified as classic and modern and technical and available potentials of each were presented. After stating that usage of modern biomass term for the potential was better than classic biomass, technical and available potential of modern biomass was given as 40 Mtoe and 25 Mtoe, respectively (Ozgur, 2008). The data in Ozgur (2008) was taken from the study (Ozdamar et al., 2004) which used the data of Ültanır (1998). All these studies were used the data of years 1998 and 2001. In the "blue book" (*Enerji ve Tabii Kaynaklar Bakanlığı ile Bağlı ve İlgili Kuruluşlarının Amaç ve Faaliyetleri (in Turkish)*, 2012), the biomass energy potential of Turkey was given to be 8.6 Mtoe for 2011. The Republic of Turkey, Ministry of Energy and Natural Resources, General Directorate of Renewable Energy estimated the forestry biomass potentials as 1.5 Mtoe (4.8 Mt) ("Forestry-based Biomass Potential of Turkey," 2013). Its estimate about the agricultural biomass energy potential was 303.2 PJ (15.3 Mt/7.2 Mtoe) ("Agricultural Biomass Potential of Turkey," 2013).

3.3.2.1. Olive and Olive Cake Production

According to the data updated in 04.03.2013 by Turkish Statistical Institute of Turkey (TUIK), the number of olive trees in 2012 was 157904, of which 120820 trees were bearing type. The total olive production in 2012 was 1.82 Mt of which 1.34 Mt (74%) was used for olive oil production. The data given above was given by the TR Ministry of Food, Agriculture and Livestock by TUIK. Turkey had a total agricultural land of 38.2 million hectares (by TUIK), of which 798493 hectares (by the Food and Agriculture Organization of the United Nations (FAO)) was used for olive production in 2011.

World's olive production and the major olive producers for the years between 2008 and 2011 are given in Table 3.7. The annual olive productions for ten years between 2002 and 2011 are also shown in the table. The shares of the countries in the average olive production between 2002 and 2011 are depicted in Figure 3.11. The world's annual olive production for 10 years between 2002 and 2011 was 17.8 Mt as an average. Olive is generally produced in the Mediterranean countries. Spain was the leader in olive production with the production share of 5.8 Mt. Spain was followed by Italy, Greece, Syria and Tunisia. Turkey was the 6th biggest olive producer in the world. Turkey's olive production was 859 kilotonnes for the years between 2002 and 2011. The Turkey's share in the total production was 5% as can be seen in Figure 3.11. Almost 65% of the olive production was only met by three European Union countries, Spain, Italy and Greece.

Table 3.7 World olive production between 2008 and 2011 and the average production for 10 years between 2002 and 2011 ("FAOSTAT Crop Productions," 2013)

	Olive Production (kilotonnes)					
	2008	**2009**	**2010**	**2011**	**2002-2011 (Average)**	**2002-2011 % share**
World	18078	17583	18967	19845	17807	
Spain	5571	5701	6682	6940	5790	32.5
Italy	3474	3287	3171	3182	3487	19.6
Greece	2575	2286	1810	2000	2282	12.8
Syria	1464	1291	1415	1750	1421	8.0
Tunisia	1183	800	750	863	926	5.2
Turkey	827	886	960	1095	859	4.8
Morocco	765	850	1484	1365	829	4.7
Portugal	344	423	445	444	325	1.8
Algeria	254	475	410	420	318	1.8
France	32	28	31	21	24	0.1

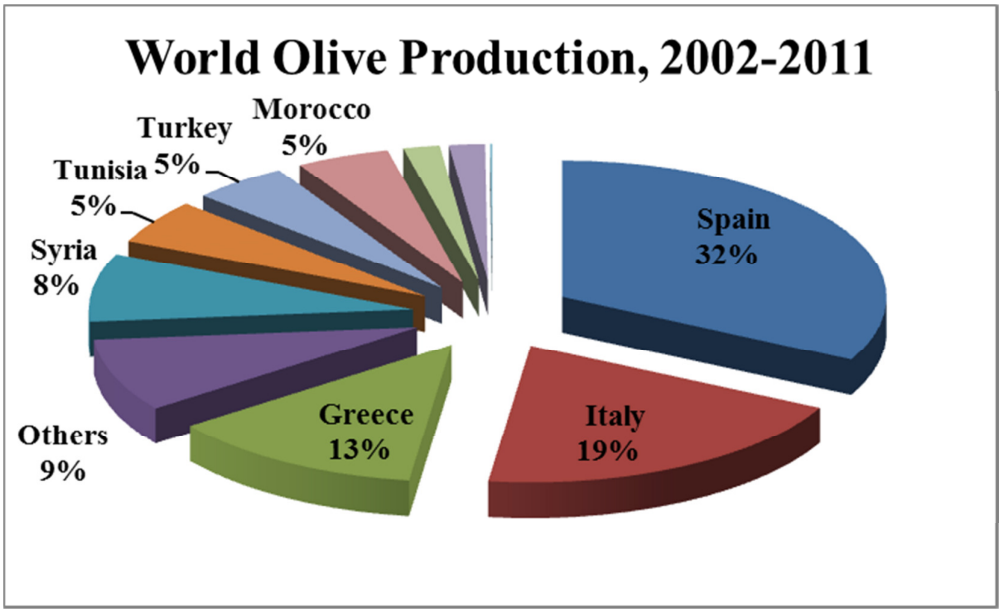

Figure 3.11 World olive production by countries between 2002 and 2011 ("FAOSTAT Crop Productions," 2013)

In order to determine the olive cake production in Turkey, data provided by Olive Research Institute was used. Olive Research Institute stated that 15-22 kg of olive oil and 35-45 kg of olive cake are obtained from 100 kg of olive. About 60-70 kg of dry olive cake is obtained from 100 kg of wet olive cake ("Olive Black Water and Olive Cake (in Turkish)," 2013). As mention in the first paragraph of this section, almost 70% of the total olive produced was used for the olive oil production. If it is assumed that 40% of olive cannot be used for olive oil production and leaves the process as olive cake, approximately 240 kilotonnes per year (Table 3.7: 859 kilotonnes * 0.7 *0.4) of olive cake is formed at the end of the olive oil production. With the assumption of 35% moisture for olive cake, the total dry olive cake production is estimated to be 155 kilotonnes per year. The lower heating value of olive cake is about 20 MJ/kg. Therefore, the total energy that can be obtained from olive cake combustion is calculated as 3.1 PJ. This is almost equal to 74 ktoe (1 toe = 41.87 GJ, (*IEA Statistics Renewables Information*, 2012)).

3.3.2.2. Forestry Biomass and Woodchips Potentials

Among the biomass resources, forestry residues are important to prevent forest fires and to regenerate the forests. General Directorate of Renewable Energy of Turkey recently estimates the biomass potential of forestry wastes to be 4.8 Mt which is equivalent to 1.5 Mtoe ("Forestry-based Biomass Potential of Turkey," 2013). The forestry residues are defined as roots and stumps of trees, small tree branches and barks, and smashed trees left over in the zone during chopping down and transportation processes. These residues are all left in the forest areas during the wood production because they cannot be used for

industrial purposes. Moreover, trees, shrubs and bushes removed from the forest area as a result of some forest tending methods such as zone cleaning for forestation and regeneration of the forest area are also named as forest residues (Belen et al., 2009). It would be beneficial to use forestry residues in energy production to minimize the foreign-source dependency as well as for sustainable forest management.

The forest area in Turkey is about 21.2 Million hectares (Taşkıran, 2009). The forest tending and wood production in this area is done by The General Directorate of Forestry (GDF). According to the GDF data, the annual amount of biomass based on the forest residues generated in the forests is about 7 Mt (Belen et al., 2009). If it is assumed that the forest residues have average lower heating value of 4000 kcal/kg (Belen et al., 2009), this amount corresponds to the approximately 3 Mtoe biomass energy potential. It might be beneficial to use the forestry residues in energy production for lowering the foreign-source dependency. It might be useful for sustainable forest management as well. Moreover, it is necessary to remove these residues from the forest areas to fight against forest fires. Additionally, Turkey, under the umbrella of FOREST EUROPE (The Ministerial Conference on the Protection of Forests in Europe), commits to use woody biomass as renewable energy source in energy production and to remove the residues from forests to reduce risk of fires according to the Warsaw Resolution 1 (*Fifth Ministerial Conference on the Protection of Forest in Europe Warsaw Resolution 1 Forests, Wood and Energy*, 2007). GDF in Turkey aims to increase the use of biomass and to reduce the share of fossil fuels in new power plants in electricity production (Belen et al., 2009). Among the forestry residues, Rhododendron is an important biomass source due to its high potential. Rhododendron is a genus of woody plants. It is stated by GDF (Acar et al., 2011), that 500000 hectares of area in the Black Sea region is covered by Rhododendron spp. (a species of Rhododendron genus) and its potential as a biomass resource is estimated as 50 Million tons (*The Master Planning of Forestry Research of Ministry of Forestry for 1995-1998 (in Turkish)*, 1995; Acar et al, 2001). Rhododendron is an easy-growing plant covering the entire land in a short period of time. Due to this property, it plays an important role to prevent soil erosion. However, regeneration of the forests becomes impossible due to this easy growing plant. Therefore, Rhododendron is undesirable in the forest areas (Gündüz, 1996). GDF removes Rhododendron residues (it will be mentioned as “woodchips” in the text below) from the forests due to adverse effect of them on the regeneration of trees and wants to use them in the energy production. Therefore, it will be wise to use them as biomass energy source (Acar et al., 2011).

3.4. Emission Characteristics of Combustion and Co-combustion of Coal and Biomass in Fluidized Bed Combustors

Coal has been used for power and electricity generation in pulverized combustion power plants for about 100 years. After the development of fluidized bed combustion technology, it was possible to burn different ranks of coals with having higher thermal efficiencies. There are basically two types of fluidized bed combustors; bubbling fluidized bed combustors (BFBCs) and circulating fluidized bed combustors (CFBCs).

BFBCs are the first applications of fluidized bed combustion of coal. The CFBCs are the next generation of BFBCs. Because of its advantages over BFBCs, CFBCs are mostly preferred for coal combustion. There are several studies in the literature about the combustion of different types of coals in the fluidized bed combustors to investigate the effect of operational parameters such as excess air ratio and secondary air ratio on the temperature profiles along the combustor and flue gas emissions. Some studies are presented here giving priority to the studies on emission characterization. Four coals; an anthracite, a high-sulfur bituminous, a sub-bituminous and a lignite, and a petroleum coke were studied in a circulating fluidized bed combustor by **Zhao et al.** (1997) in order to investigate the NO_x formation and destruction mechanisms. NO_x concentration as well as O_2, CO, and CH_4 concentration profiles were obtained both longitudinally and laterally. It was stated the NO_x formation was occurred at higher levels close to the bottom of the combustor where there was higher solid and oxygen concentrations compared to the upper parts of the combustor. At the upper part of the combustor, NO_x reduction reactions on char and by CO (limestone catalyzed) were dominant over volatile and char nitrogen oxidation. Due to the complex reactions taking place in the combustor in the case of limestone addition for high volatile-coals, a clear explanation of limestone usage for NO_x formation could be done and it was concluded that limestone usage could increase or decrease overall NO_x formation depending on the volatile matter content of the fuel. **Hayashi et al.** (2002) also studied the effect of flue gas recycle ratio on the NO and N_2O emissions and relationship between NO/N_2O reduction and O_2 consumption during the combustion of a sub-bituminous coal in a bubbling fluidized bed combustor. It was observed that the increasing O_2 concentration at inlet, thus increasing the O_2 consumption rate and decreasing the flue-gas recycling ratio decreased the conversion of nitrogen to N_2O without making any change on the conversion to NO. The recycled NO was reduced to N_2 either directly or via N_2O. It was stated that while direct NO reduction to N_2 was governed by char combustion, NO conversion to N_2O was attributed to the volatile combustion. It was also found that H_2O enhanced NO-to-N_2 reduction over char surface. It was also effective for homogenous NO-to-N_2O conversion, in turn limiting the N_2O-to-N_2 reduction over the char surface. Another study on the effect of temperature, excess air and limestone addition on N_2O emission during the combustion of a bituminous and a sub-bituminous coal in a circulating fluidized bed pilot plant (CFBC-CIEMAT) was conducted by **Armesto et al.** (2003b). They also used the findings from pyrolysis tests in a laboratory- scale circulating fluidized bed to support their results. It was stated that char-N conversion was the dominant mechanism for N_2O formation. It was also determined that N_2O formation was strongly affected by the temperature profile of the combustor and the limestone addition. N_2O emissions decreased with increasing temperature due to the conversion of nitrogen radicals such as •NCO and •NH directly to NO and N_2 rather than N_2O at high temperatures. The formation of hydrogen radicals (•H and •OH) was also given as a reason for the N_2O destruction. Increasing Ca/S ratio decreased SO_2 emission as well as N_2O emissions. The decreased in N_2O was explained by the catalytic effect of CaO on the destruction of N_2O.

Ersoy et al. (2004) studied the effect of secondary air on the hydrodynamics of circulating fluidized beds. A 0.23-m ID combustor was used for tests and it was noted

that injection of secondary air created two different sections in the combustor: a dense and turbulent section below the location of secondary air injection and a dilute section above the injection point. **Gungor** (2008) conducted a modeling study in order to estimate the effect of excess air, bed operational velocity, coal particle size, and coal feeding rate on the carbon combustion efficiency using a dynamic 2D model. He used the results of two studies in the literature (Adanez et al., 2001; Atimtay and Topal, 2004) to validate his model in terms of combustion efficiency. It was stated that increasing excess air had a decreasing impact on the combustion efficiency. This was explained by the heat loss due to the increasing flue gas flowrate and by the decrease of the bed temperature due to the decrease in reaction rates. However, his conclusion about the effect of excess air on the combustion efficiency contradicted with the experimental results in the 300 kW pilot scale circulating fluidized bed combustor (Adanez et al., 2001) since it was obvious that combustion efficiency slightly increased with excess air. The combustion efficiency increased with bed operational velocity. This was explained by the increase rate of solid circulation and consequently the decrease in the mean bed temperature which resulted in high CO emission.

Zhu et al. (2009) introduced high temperature air from a circulating fluidized bed combustor into the down-fired combustor and studied the effect of residence time, excess air, furnace temperature, oxygen concentration in high temperature air and air-staging on NO emission for the combustion of pulverized coal. They stated that air-staging with high temperature air had a reducing effect on nitrogen oxide emission. **Li et al.** (2010) investigated the effect of declivitous secondary air on combustion performance of a 300 MW_e down-fired boiler. An anthracite coal was used for the experiments. The modification of the boiler consisted of F-tier secondary air with an angle of declination of 25^o. It was concluded that the modification on the system lowered the NO_x emissions and the carbon content in the fly ash.

With the increase of the public concern about the air pollution originated from energy production sector burning fossil fuels, particularly coal, different types of biomasses have been tried to be burned in the fluidized bed combustors. The main goal is to decrease the share of coal in energy production by shifting them with biomass fuels. Because of high energy content of biomasses, combustion of biomass is a good way to obtain clean energy by minimizing environmental pollution, especially air pollution. Burning biomass is also very beneficial way to dispose the biomass waste. Shifting fossil fuels by biomass fuels in the energy production can help to reduce CO_2 emissions released to the atmosphere. It is important in terms of SO_2 emissions because biomass fuels generally do not have sulfur. There are many investigations and research about the combustion of biomass in fluidized bed combustors. Here, some of them were summarized. Since olive cake and woodchips were used in the experiments of this study, the studies conducted with these biomass fuels as a priority were covered in the literature survey.

The most known study in the literature about the combustion of olive cake in fluidized beds was from **Abu-Qudais** (1996). Since it was accepted as the one of the first studies on the subject, it just investigated the combustion characteristics of olive cake in terms of

combustion efficiency. The combustion efficiency between 86% and 95% was reported. Another study about the olive cake was conducted by **Alkhamis and Kaplan** (1999). They investigated the effect of grain size of olive cake on its calorific value. It was stated that combustion of olive cake with oil shale was helpful to ignite the oil shale due to high energy content of olive cake. In Turkey, olive cake was first burned in a circulating fluidized bed combustor by **Topal et al.** (2003). In their study, the effect of excess air ratio on the combustion efficiency and emissions for the combustion of olive cake was investigated in a circulating fluidized bed combustor having 125 mm diameter and 1800 mm height. The results obtained from that combustor were compared with the coal combustion. It was found that the combustion efficiency decreased to 94-95% due to the formation of CO and hydrocarbon emissions in the case of excess air ratio < 30%. The minimum emissions were measured at excess air ratio of 1.35. The combustion performance and emission characteristics of olive cake were also studied in a bubbling fluidized bed combustor by **Varol and Atimtay** (2007). The effect of excess air ratio and secondary air ratios on the flue gas emissions was investigated for the combustion of olive cake and the results were compared with the results obtained from the combustion of Tunçbilek lignite (Turkish lignite). Thus, combustion characteristics of olive cake produced in Turkey was covered in both bubbling and circulating fluidized bed combustors. It was reported that high volatiles content (71.2 % by wt.) in olive cake was the reason for the maximum temperatures observed in the freeboard rather than in the bed for the combustion of olive cake. Olive cake particles released their volatiles as they entered into the combustor due to the rapid heating and volatiles were mostly burned in the freeboard. The major losses for the carbon combustion efficiency were shown to come from the flue gas which contains high concentrations of hydrocarbons and CO. Optimum operational conditions were given as 1.2 of excess air ratio, 50 L/min of secondary air flowrate for the combustion of olive cake in terms of NO_x and SO_2 emissions.

Combustion of woodchips was studied by **Lyngfelt and Leckner** (1999). They studied the effect of temperature and air-staging on CO and NO emissions for the combustion of woodchips in a 12 MW circulating fluidized bed boiler. They tested secondary air addition in the cyclone outlet in combination with SA addition in the cyclone inlet and/or at 2.2 m height for three loads. They achieved a significant NO reduction without high CO emissions. They also found that increasing temperature of cyclone outlet had a decreasing effect on CO emissions. **Werther et al.** (2000) in their review study discussed several issues about the combustion and co-combustion of agricultural residues such as straw, bagasse, coffee husks, and rice husks and forest residues such as woodchips, sawdust and bark from the perspective of ash-related problems and emissions. The physical and chemical properties of different biomass residues were given. Due to the low bulk density of the most of the biomass residues, the need for densification was pointed out in term of transportation, storage, fuel feeding, and combustion efficiency. It was stated the high volatile matter content of residues was significant for the combustion performance and design of the combustion systems. For the biomass residues having low ash melting points, it was suggested to design and operate a system at the temperatures below the melting point of the biomass ash and to remove the ash periodically. Moreover,

secondary air injection from the upper parts of the combustor where high temperatures were achieved was advised to burn the volatiles. By this way, it was stated that it was possible to minimize the ash-related problems such as fouling, slagging and corrosion in the high temperature zones due to the low ash concentration. It was remarked that the NO_x reduction mechanisms on char surfaces was expected to be negligible due to the low fixed carbon and CaO contents of biomass residues. Therefore, more NO_x emissions were be expected for the combustion of biomass residues rather than the combustion of coal of comparable nitrogen contents.

Permchart and Kouprianov (2004) made an experimental study about the combustion of sawdust, rice husk and per-dried sugar cane bagasse in a single fluidized bed combustor in order to investigate the effect of load and excess air on the temperature, CO, NO, and O_2 profile along the combustor and CO and NO emissions in the flue gas as well. By means of emissions, CO emissions for rice husk were measured much greater than those for sawdust and bagasse for similar operating conditions. This was explained by the coarser char particles and higher ash concentration for rice husk: up to 200 μm, against 5 μm for sawdust and 10 μm for bagasse. The rate of NO reduction for rice husk was found much greater than the others. The heterogeneous reactions on the char surface in the freeboard and cyclone were given as a cause for that reduction. **Sun et al.** (2008) studied the effect of fluidizing velocity, air split ratio (secondary air) and air injection to the loop seal on the bed temperature during the combustion of cotton stalk in a circulating fluidized bed combustor. The combustor had a 12 m height. The inner diameters of the combustor were 300 mm and 400 mm for dense phase and dilute phase regions, respectively. Due to the high volatile content of cotton stalk, it was observed that combustion was occurred mainly in the upper part of the combustor. The secondary air was introduced into the combustor at a height of 1.8 m. While the primary air flowrate was kept constant at 267 Nm^3/h, the secondary air flowrate was 150 Nm^3/h, 235 Nm^3/h, and 318 Nm^3/h corresponding to the air split ratios of 1:0.56, 1:0.88, and 1:1.19, respectively. The effect of secondary air ratio on bed temperature was studied but the change in the total flowrate, and in turn the effect of excess air on the temperature profile was ignored. The highest temperature profile was obtained at air split ratio of 1:0.88. It was suggested to burn the cotton stalk at excess air ratio at about 1.3 and air split ratio of 1:0.88 to have highest combustion efficiency.CO, NO, and SO_2 emissions in the flue gas were measured during the combustion of cotton stalk but the effect of the operational parameters on the emission did not studied. They used the alumina as an alternative bed material to silica sand in order to prevent bed agglomerates. After 26 hours operation, no bed agglomeration was observed. When the silica sand was used as a bed material, agglomerated particles were seen. They showed the pictures of bed materials after combustion tests, but they could not support their findings with ash analyses such as XRF, XRD or SEM-EDS.

Youssef et al. (2009) conducted the combustion of four different kinds of biomass (wheat straw, sawdust-wood, cotton seed burs, and corn cobs) in a circulating fluidized bed with 145 mm inner diameter and 2 m height. They just shared the emission findings. There was a lack of comprehensive explanation for the effect of operational parameters such as

excess air and secondary air on the flue gas emissions. **Kuprianov et al.** (2011) studied air-staged combustion of rice husk in a swirling fluidized-bed combustor. It was reported that while secondary air had almost no effect on CO and NO emissions, its effect on C_xH_y emissions was apparent. **Vamvuka et al.** (2012) investigated emission characteristics of orange tree pruning, leaves, peels and their mixtures in a lab-scale fluidized bed (1.5 m high, an inner diameter (ID) of 70 mm)). The effects of excess air ratio, fuel feeding rate, and fuel mixture on the temperature profile in the combustor and on the CO and NO_x emissions were studied. It was reported that increasing excess air ratio from 1.3 to 1.7 in the case of combustion of orange tree pruning decreased the temperature in the combustor and the CO emission in the flue gas as well. However, the decrease observed in CO emission could not be explained.

After the review study of **Werther et al.** (2000), the need for the current developments on the biomass combustion was met by the review study of **Williams et al.** (2012). They specifically focused on the pollutants originated from biomass combustion. The chemical mechanism responsible for the formation of pollutants such as NO_x, SO_x, unburned hydrocarbons, and Cl compounds were outlined. The studied in the literature conducted not only in the fluidized bed combustors but also in the fixed beds and pulverized biomass combustors were reviewed. They also presented the co-combustion studies in the field. The potential of biomass feedstocks and the characterization techniques was also discussed and covered. The current developments in the fluidized bed combustion of waste fuels including biomass fuels as well was reviewed by **Caneghem et al.** (2012). They stated that gasification and pyrolysis were under development. Among the thermal conversion technologies, fluidized bed combustion has been reported as growing in applications. They also reviewed the studies in the literature regarding the ash-related problems. The feeding problems of waste fuels were also covered.

The co-combustion of biomass with coal is also another application to generate cleaner energy. In the literature, the research trend is on the co-combustion of coal with several biomass types. Co-combustion of coal and biomass has an advantage for disposal of waste products. Besides, using biomass instead of coal for energy production is another advantage reducing the cost of fuel. Therefore, co-combustion seems to be the most cost effective method of biomass utilization. Co-combustion of biomass with coal is also an effective way to reduce CO_2 emissions (McIlveen-Wright et al., 2011). Moreover, co-combustion of biomass with high-sulfur coals is also an effective way to prevent some ash-related operational problems. In this part, the studies covering co-combustion of olive cake with coal was firstly reviewed. And then, the literature survey was followed by reviewing the studies about the co-combustion of woody and agricultural biomass fuels with coal.

The one of the important study about the co-combustion of olive cake and coal was conducted by **Cliffe and Patumsawad** (2001). They studied the co-combustion of olive oil waste and coal mixture in a bubbling fluidized bed combustor. The co-combustion tests included 10% and 20% olive oil waste by weight. They concluded that it was possible to burn olive oil waste and coal mixtures containing olive oil waste up to 20%.

When the olive oil waste share was greater than 20%, there were seen a temperature drop in the bed and the combustion could not sustained. They also reported that CO emission increased with excess air due to the decrease in the bed temperature. While CO emission for the combustion of 10% olive oil waste was lower than that for the combustion of 20% olive oil waste, the combustion efficiency for 20% case was higher than that for 10% case. One study of **Armesto et al.** (2003b) which was conducted in 2003 to investigate the effect of temperature, excess air and limestone addition on N_2O emission during the combustion of two types of coal in CFBC-CIEMAT was mention before in this section. In the same year, **Armesto et al.** (2003a) published another study regarding the co-combustion of Spanish lignite and an anthracite with foot cake conducted in a bubbling fluidized bed combustor (BFBC-CIEMAT). They named the olive cake as foot cake in their study. The effect of furnace temperature, share of foot cake in the fuel mixture and coal types on the emissions and combustion efficiency for the co-combustion of coal and foot cake mixtures were studied. The foot cake share in the fuel mixture was 10%, 15%, 20%, and 25%. It was observed that NO_x emissions decreased as the share of foot cake in mixtures increased. This was explained by the increasing volatile matter content of the fuel mixtures as the share of foot cake increased because all fuels had the similar nitrogen content. It was stated that the fast release of volatiles formed high levels of hydrocarbon radicals which were responsible for NO reduction. It was found that while NO_x emissions decreased with increasing foot cake share in the fuel mixture, N_2O emissions increased. The increased observed in N_2O emissions were explained by the decrease in the flame temperature due to the high moisture content of the foot cake. **Atimtay and Topal** (2004) studied the co-combustion of olive cake with the Tunçbilek lignite in a circulating fluidized bed combustor. Experiments were conducted in the same bed used in the previous work by **Topal et al.** (2003). Various runs were conducted with mixtures of olive cake and lignite, namely 25, 50 and 75 % by wt. olive cake mixed with lignite. These mixtures were burned with various excess air ratios. It was found that if excess air ratio was less than 40-50%, appreciable amounts of CO and unburned hydrocarbons were formed and the combustion efficiency dropped to 84-87%. CO and C_mH_n emissions were lower for coal than the emissions for olive cake and coal mixtures at the same excess air ratio and temperature. The minimum emissions were observed at about excess air ratios of 1.5. In order to meet the EU emission limits, less than 50 % by wt. olive cake mixture was suggested. Another experimental study on the co-combustion of olive cake and Tunçbilek lignite was conducted in a bubbling fluidized bed combustor by **Atimtay and Varol** (2009). The share of olive cake in the fuel mixture was 25, 50, and 75% by wt. The effect of excess air ratio and the secondary air injection on the carbon combustion efficiency and flue gas emissions were studied. It was reported that the temperature was taken place in the freeboard as the share of olive cake in the fuel mixture increased. As the olive cake share increased, high CO and hydrocarbon emissions were measured due to the increasing volatile matter content of the fuel mixture. Excess air ratio of 1.35 and secondary air flow rate of 30 L/min was suggested for the co-combustion of fuel mixtures containing 25 and 75% by wt. olive cake.

Co-combustion of woody biomass with coal and also with sludge was studied by **Laursen and Grace** (2002). They studied the co-combustion of hog fuel, sludge and sub-

bituminous coal mixtures in a fixed bed reactor. The study was done to investigate some implications that could be happened if this mixture was combusted in a bubbling fluidized bed boiler using hog fuel and sludge mixtures in present conditions. Hog fuel was composed of forest residues such as bark, twigs, and low-quality wood left on the forest floor after harvesting. The conditions present in the boiler (at low operational temperature due to the high alkali ash content of hog fuel and sludge mixture and under high moisture atmosphere) were simulated in the fixed bed and it was tried to find out an answer to the question "will coal ignite at the conditions present in the boiler?" It was conclude that no ignition problem was observed for the combustion tests in the fixed bed at the condition ranging temperature from 675 to 825^{o}C, moisture content of hog fuel and sludge mixtures from 55 to 70%, and oxygen concentration in the flue gas from 4.9 to 5.6%. Limestone addition to fuel mixture was also studied to determine the required Ca/S ratio to keep the SO_2 emissions at an acceptable level. Sulfation tests were done in a packed bed quartz reactor. Ca/S ratio of 2.5 was suggested to prevent an increase in SO_2 emissions.

Gayan et al. (2004) analyzed the circulating fluidized bed combustion performance burning coal and biomass together. Two kinds of coal and a forestry residue (pine bark) were used in experiments. Two circulating fluidized bed pilot plants with the power 0.1 and 0.3 MW_{th}, respectively were used. The effect of combustion temperature, biomass share in the fuel mixture, excess air, secondary air and particle size distribution of coal on the combustion efficiency was studied. A mathematical model was developed which can predict the different gas concentrations (O_2, CO, CH_4, etc.) and the carbon combustion efficiency along the bed column. The results of the experiments conducted in the two pilot plants were compared with the model predictions and a good correlation was found for all the conditions used. **Xie et al.** (2007) performed a study to see the influence of excess air, air staging, biomass share and feeding position of fuel on SO_2, NO and N_2O emissions in a 30 kW_{th} bench scale circulating fluidized bed combustor for a bituminous coal combustion and co-combustion of coal and rice husk. While NO emission increased with the excess air ratio for the co-combustion of 22% by wt. rice husk with coal, it was seen that CO emission decreased. The lower NO emission measured at excess air less than 10% was attributed to the presence of char and high CO concentration. They remarked that an increase in the biomass share in the fuel resulted in an increase of CO emissions in the flue gas because of high volatile matter content of biomass. They reported that air-staging decreased NO emission without an increase in SO_2 emission. Although the change of the fuel feeding position from riser to downer resulted in a decrease in the NO emission level, no obvious change was observed for the SO_2 emissions.

Munir et al. (2011) performed co-combustion tests of pulverized Russian coal with different biomasses such as shea meal (SM), cotton stalk (CS), sugarcane bagasse (SB_T), sugarcane bagasse (SB_R) and woodchips (WC) in order to see the effect of air-staging on NO_x emission and combustion efficiency. A 20 kW down-fired combustor was used and the biomass shares in fuel mixture were determined to be 5, 10 and 15% by thermal power. It was found that biomass addition had a positive impact on carbon burnout and NO reduction under optimum conditions. 10% of biomass addition was suggested in

terms of NO reduction since 10% of SB_R, SM, WC, CS and SB_T in fuel mixture resulted in 49%, 51%, 53%, 60% and 72% NO reduction, respectively. **Saikaew et al.** (2012) studied NO_x and N_2O emissions for the co-combustion of sub-bituminous coal with four biomasses, palm shell, coconut shell, sawdust and rice husk in a circulating fluidized bed combustor. They stated that biomass addition in fuel mixture cause NO_x and N_2O emissions to decrease and they presented that the location of secondary air had an influence on NO_x and N_2O emissions. The secondary air was introduced into the combustor (Height: 3 m, ID: 0.1 m) from three different locations; 1 m, 2 m, and 2.4 m above the distributor plate. For the case of coal combustion, it was observed that NO_x and N_2O emissions decreased when the location of secondary air moved upward from 1 m to 2.4 m. The decrease in NO_x (from 235ppm to 195 ppm) emissions was explained by the excess air promoting fuel-nitrogen oxidation in the high temperature region of the combustor when it was given at 1 m. When it was introduced from 2.4 m, the effect of excess air on the fuel-nitrogen oxidation did not seem too much due to the lower temperature in the upper part of the combustor.

There are also several studies in the literature concerning the co-combustion of refused-derived fuels and municipal solid wastes with coals in fluidized bed combustors. Here, some studies of them were here shared. **Desroches-Ducarne et al.** (1998) investigated the NO, N_2O, HCl, SO_2 and CO emissions during the combustion of an American bituminous coal and municipal solid waste (MSW) mixtures in a 25 kW circulating fluidized bed boiler. While N_2O and SO_2 emissions decreased with the increasing share of the municipal solid waste in the fuel mixture, HCl and NO emissions increased. The increase on the NO emission with MSW share in the fuel mixture was explained by the nitrogen functionality in the fuel. While the most of the nitrogen remained in the char and released nitrogen converted to HCN which then turned into N_2O for the high-rank coal, the nitrogen in the MSW were generally proteins and they were released as NH_3 which was the main source of NO. Lower NO emission for coal combustion than MSW combustion was related with the solid reduction of NO on char surfaces under the reducing atmosphere promoted by high CO concentration. In 2000, **Piao et al.** (2000) studied the combustion characteristics of two types of refused derived fuel (RDF) in a bubbling fluidized bed combustor. They stated that secondary air addition decreased both CO and NO emissions for both types of RDFs. **Suksankraisorn et al.** (2004) investigated co-combustion of municipal solid waste (MSW) with and Thai lignite in a laboratory scale bubbling fluidized bed. The share of MSW, excess air, secondary air on the temperature profile, and fuel gas emissions were studied. NO and N_2O emissions increased with the increase of the share of MSW in the fuel mixture. In terms of CO, NO, and N_2O emissions, the optimum conditions were given as 20% MSW, 40% excess air, and 0.2 secondary air ratio. They stated that NO emission increased with increasing excess air ratio due to the increase O_2 concentration for conversion of fuel N to NO. They also reported that NO emission decreased by the increase in secondary air ratio. When the secondary air was introduced to the combustor, it created a reducing atmosphere in the bed leading the NO reduction by the char in the bed and such species as CO and CH_4.

Although there are several studies as to effect of operational parameters on emissions in the literature, a limited number of studies concerning co-combustion of biomass and Turkish lignites in fluidized bed combustors are noticeable. As well as there are few studies in this subject, the effect of operational parameters such as excess air ratio and secondary air ratio on flue gas emissions, while co-firing Turkish lignite and biomass resources, have not been studied in circulating fluidized bed combustors in a detailed manner. In this respect, co-combustion of Bursa/Orhaneli lignite with two biomasses from Turkey (olive cake and woodchips) in a circulating fluidized bed combustor was carried out in order to investigate the effect of excess air ratio, secondary air ratio and its location on the major emissions (CO, NO, and SO_2) of the flue gas in the scope of this study. While the effect of excess air ratio on the flue gas emissions are presented in Section 5.1 "Assessment of Experiments for SET#1", the study conducted to investigate the effect of secondary air on the emissions is given in Section 5.2 "Assessment of Experiments for SET#2". The study covering the determination of optimum Ca/S ratio for Bursa/Orhaneli and Denizli/Kale lignites can be found in Section 5.3 "Assessment of Experiments for SET#3".

3.5. Ash-related Problems during Fluidized Bed Combustion

In the literature, while burning biomass itself or co-combustion of several biomasses with coal, some operational problems regarding bed agglomeration or defluidization of the bed have often been reported. The defluidization of the bed is an operational problem occurring when a sudden pressure drop is observed across the bed accompanying with a local temperature increase within the bed. This situation creates uncontrolled combustion conditions and leads to the shutdown of the combustor or boiler (Scala and Chirone, 2008). In this section of this chapter, the studies previously conducted which investigate the ash-related problems encountered while burning biomass and biomass and coal mixtures in fluidized bed combustion systems are summarized.

Vuthaluru and Zhang (1999) carried out experiments to study controlled methods for mitigating particle agglomeration and bed defluidization during fluidized bed combustion of low-rank coals. A laboratory scale spouted bed was used. Using alternative bed materials (sillimanite, bauxite, calcite, and magnesite), mineral additives (clay, kaosil, and bauxite), pre-treatment (water washing, Al and Ca pre-treatment) of coal and coal blending were studied. Test results showed that all control methods were effective to different extents in reducing ash problems. Tests with alternative bed materials and mineral additives showed trouble free-operation for longer periods (7–12 h at 800^{o}C) than with sand runs at the same bed temperature. Wet pre-treatment and coal blending were also found to be effective and resulted in extended combustion operation (9–12 h at 800^{o}C). Chemical analyses indicated that formation of low temperature eutectics was suppressed by Al/Ca/Mg-rich phases in ash coating of bed particles. This was identified as the main mechanism for prevention of ash problems observed with the use of alternative bed materials, mineral additives, pretreated coals and coal blends.

Anthony and Jia (2000) studied agglomeration tendency of fluidized bed combustor ashes from high-sulfur, low-ash fuels. They stated that these ashes could agglomerate if subjected to sulfating conditions for long enough time. The degree of sulfation increased with both temperature and time under these conditions, and at a conversion equivalent to the production of 50–60% or more of $CaSO_4$ in the deposit the ashes agglomerate. The potential for agglomeration increased if the temperature was increased from 850 to 950°C. Agglomeration also occurred at lower temperatures (down to at least 750°C), but the mechanism might be via carbonation and then sulfation of the ash. Two bed materials with strong and weak agglomerating tendencies were studied. These were shown to have very similar particle shapes and only slightly different angles of repose, but quite different bulk densities. Residues with a greater bulk density appeared to have a stronger tendency to agglomerate. **Tangsathitkulchai and Tangsathitkulchai** (2001) investigated agglomeration propensity of Thai low-rank coal ashes by measuring the compressive strength of sintered ash pellets over the temperature range of fluidized bed combustion. Physical and chemical changes of the sintered products were ascertained from scanning electron microscope-energy dispersive X-ray spectroscopy (SEM-EDS) and X-ray diffraction (XRD). A clear difference existed in the strength–temperature relationship between these ashes. This difference was attributed to the role and relative amounts of clays and anhydrite components that form the low temperature melting eutectics. The bed materials (sand, CaO, $CaCO_3$, and $CaSO_4$) and additives (gibbsite and andalusite) when combined with the ashes caused a strength reduction due to the inert dilution effect that prevented the interaction of anhydrite and clays.

Arvelakis et al. (2001) studied effect of leaching on the ash behavior of wheat straw and olive residue during fluidized bed combustion. Leaching pre-treatment technique showed to have different effect as far as it concerns the ash thermal behavior of olive residue and wheat straw samples. In specific, leaching proved to significantly improve the ash thermal behavior of olive residue samples securing the unproblematic operation of the combustor during all tests with the leached treated samples. Leaching resulted in an almost total expulsion of alkali metals and chlorine from the materials ash ensuring its neutral behavior at elevated temperatures. On the other hand, the effect of leaching on the ash thermal behavior of straw samples proved to be insufficient to prevent the formation of deposits/agglomerates during the fluidized combustion tests.

Brus et al. (2005) carried out controlled agglomeration tests, using six representative biomass fuels (bark, Lucerne, reed canary grass, bagasse, olive flesh, and cane trash) were performed in a bench-scale fluidized bed (5 kW) during both gasification and combustion conditions. The resulting bed materials were analyzed using scanning electron microscopy/energy-dispersive spectroscopy (SEM/EDS), and chemical equilibrium calculations were performed to facilitate the interpretation of the experimental findings. Layers of fuel-ash-derived compounds were built up on the bed particles during processing of all studied fuels. The accumulated material was determined to consist of two layers: (i) an inner thicker and more homogeneous layer that consisted of mainly K-Ca-silicates and (ii) a thinner, particle-rich outer layer. For all fuels except Lucerne, no major differences in bed agglomeration tendencies or bed particle layer

characteristics could be detected between gasification and combustion. **Zevenhoven-Onderwater et al.** (2006) studied the agglomeration tendency of five Scandinavian forest-derived biomasses by using chemical fractionation analysis, controlled bed defluidization tests, and SEM/EDS analysis. It was stated that all biomasses had a tendency of agglomeration when they were burned in a fluidized bed with silica sand as bed material. The agglomeration appeared to proceed by formation of a sticky layer on the bed particles and this layer contained Si, Ca, and K. They concluded that the soluble fraction of Ca and K might be responsible for the formation of this layer.

Liu et al. (2007) used two kinds of bed materials, silica and aluminous, when cotton stalk was burnt in circulating fluidized bed combustor (CFBC). XRF, XRD, and SEM/EDS analyses were performed on the ash samples. The results showed that both of the bed materials enriched with alkali metals but the changing speed of aluminous particles was much slower than that of silica particles. **Vamvuka et al.** (2008) examined the thermal behavior of the ashes of olive kernel and olive tree wood during lab-scale fluidized bed combustion tests. They used some control methods such as leaching the raw fuels with water and using different mineral additives during combustion for mitigating ash problems. Leaching raw fuels with water resulted in a significant reduction of the problematic elements K, Na, Cl, and S in the fly ashes. The usage of fuel additives decreased the concentrations of alkali and iron minerals in the fly ashes. With clay additives calcium compounds were enriched in the bottom ash, while with carbonate additives they were enriched in the fly ash. Fuel additives or water leaching reduced the slagging/fouling potential due to alkali.

Scala and Chirone (2008) carried out experiments to determine the agglomeration behavior of three biomass fuels (exhausted and virgin olive husk and pine seed shells) in a lab-scale fluidized bed combustor. Virgin husk was obtained after mechanical extraction of oil by olive pressing, while exhausted husk was obtained after solvent extraction of residual oil from virgin husk. The particle size of the husk used in the experiments was in the range of 20-4000 μm and it was 1-3.3 mm for pine seed shells. The combustor has an inside diameter of 0.102 m and a height of 1.625 m. All the experiments are done in a bubbling fluidized bed regime. Quartz sand, sieved in the two size ranges 211-400 μm and 600-850 μm, was used as a bed material. The bed height was kept constant as 0.3 m at minimum fluidization conditions. Experiments were conducted at a fluidization velocity varying between 0.38 and 0.92 m/s. Bed temperature was fixed at either 850 or 900^{o}C. Fuel feeding rate was adjusted between 0.33 and 0.82 kg/hr. After each run, agglomerate samples were selected. SEM/EDS analysis of bed agglomerate samples was conducted and the effect of the fuel ash composition, bed temperature and sand particle size on agglomeration was investigated. **Sun et al.** (2008) studied the effect of alternative bed material on the agglomeration was used as an alternative bed material to silica sand in order to prevent bed agglomerates. After 26 hours operation, no bed agglomeration was observed. When the silica sand was used as a bed material, agglomerated particles were seen. They showed the pictures of bed materials after combustion tests, but they could not support their findings with ash analyses such as XRF, XRD or SEM-EDS.

Yang et al. (2011) studied the influence of inorganic sulfur FeS_2 addition on the fate of alkali metals and the effect of sulfur on the alkali chloride sulfation during the co-combustion of rice straw (K content in fuel was 1.6% by wt. on dry basis) and low-sulfur sub-bituminous coal (0.4% sulfur by wt. on air-dried basis) in a laboratory scale reactor. They stated the FeS_2 addition enhanced the potassium sulfate formation when S/K molar ratio was less than 2. When the ratio was greater than 2 by adding more FeS_2, the release of SO_2 was observed and it was concluded that this had a limited effect on the alkali sulfate formation. The ash-related problems for the combustion of some problematic agricultural biomasses were also investigated in the study of **Silvennoinen and Hedman** (2013). They conducted co-combustion tests of up to 30% share of agricultural mixture (sunflower seed hull pellets and oat seeds) with woodchips in a fluidized bed boiler. Deposit sampling probes, gas and solid samplings were used to monitor the risk of corrosion, slagging, and fouling. The potassium silicate formation was detected in the ash samples collected on the surface of the deposit probe. They suggested sulfur addition in order to eliminate or mitigate the risk of corrosion.

Although there are several studies about the ash-related problems for fluidized bed combustion of biomass fuels in the literature, there is no study conducted with olive cake and Turkish lignites to investigate ash characterization of these fuels. The co-combustion tests of olive cake with Bursa/Orhaneli lignite and Denizli/Kale lignite in a circulating fluidized bed combustor was carried out in order to investigate the effect of sulfur on the ash composition and to investigate the effect of biomass and limestone interaction on the ash composition and flue gas emissions. The results of the study are presented in Section 5.4 “Assessment of Experiments for SET#4” and Section 5.5 “Assessment of Ash Analysis for Experiments in SET#4”.

CHAPTER 4

MATERIALS AND METHODS

4.1. Characteristics of Fuels and Limestone

4.1.1. Fuels Characterization

Two types of Turkish lignites and two types of biomass fuels were used in this study. Bursa/Orhaneli/Gümüşpınar (Bursa/Orhaneli) and Denizli/Kale lignites were selected by taking into account their potential reserves and sulfur contents. According to the General Directorate of Mineral Research and Exploration, total reserves of Bursa/Orhaneli and Denizli/Kale lignites were 34 Mt and 20 Mt in 2010, respectively (*Mineral and energy resources in Bursa (in Turkish)*, 2010, *Mineral and energy resources in Denizli (in Turkish)*, 2010). Bursa/Orhaneli lignite represents the low-sulfur coal ($S_{total} < 2.7\%$ by wt. on dry basis, see Table 4.1) and Denizli/Kale represents the high-sulfur coal ($S_{total} > 3.6\%$ by wt. on dry basis, see Table 4.1). Olive cake and Woodchips were decided to be used as biomass sources because of their high production rates (See Section 3.3.2). The fuels were analyzed according to the standards given in Table 4.1 in order to determine the characteristics of them.

Table 4.1 List of standards used in the analyses

Standard #	Date	Title	Parameter
ASTM D 5142-04	2004	Standard Test Methods for Proximate Analysis of the Analysis Sample of Coal and Coke by Instrumental Procedures	Moisture Volatile Matter Ash
ASTM E 1755-01	2001	Standard Test Method for Ash in Biomass	Ash
ASTM D 5865-07a	2007	Standard Test Method for Gross Calorific Value of Coal and Coke	Higher and Lower Heating Values
ASTM D 5373-08	2008	Standard Test Methods for Instrumental Determination of Carbon, Hydrogen, and Nitrogen in Laboratory Samples of Coal	Carbon Hydrogen Nitrogen
ASTM D 4239-08	2008	Standard Test Methods for Sulfur in the Analysis Sample of Coal and Coke Using High-Temperature Tube Furnace Combustion Methods	Total Sulfur
ASTM D 5016-08	2008	Test Methods for Sulfur in Ash from Coal, Coke and Residues from Coal Combustion Using High-Temperature Tube Furnace Combustion Method with Infrared Absorption	Sulfur in Ash
ASTM D 1857-87	1994	Standard Test Method for Fusibility of Coal and Coke Ash	Ash fusion temperatures
TS 644/ISO 587	2001	Solid Mineral Fuels – Determination of Chlorine using Eschka Mixture	Chlorine

Proximate Analysis

Proximate analysis of fuel samples were done by the accredited laboratory in MRC-EI of TUBITAK. Proximate analysis includes the determination of moisture, volatile matter, fixed carbon and ash content of fuel samples. Fixed carbon content of the fuel samples is calculated by difference. Proximate analysis of coal sample is done according to the ASTM D 5142-04. For moisture determination, sample is heated to 105^{o}C until constant weight is reached. For volatile matter determination, sample is heated to 950^{o}C and held at this temperature for 7 min in a closed crucible. For the determination of ash, the furnace is cooled from 950^{o}C to 600^{o}C and the temperature is gradually raised to 750^{o}C. Ash content is determined at 750^{o}C when sample reaches a constant weight. Moisture and volatile matter content of olive cake is done according to the ASTM D 5142-04 standard with the same method but the ash content is determined at 575^{o}C until constant weight is reached according to the ASTM E 1755-01. Proximate analyses of coals and biomasses used in each test are given in Table 4.2.

Heating Values

Fuel samples were analyzed both by the accredited laboratory of in MRC-EI of TUBITAK in order to determine their heating values. Heating value determination of fuels was done according to the ASTM D 5865-07a. Lower heating value (LHV) was calculated according to the formula given below.

$$LHV = HHV - \frac{\left[\%\mathrm{MC} + \left(\frac{\%H}{MW_H}\right) * \left(\frac{1\,mole\,H_2O}{2\,moles\,H}\right) * MW_{H_2O}\right] * h_{f_g}}{100} \qquad \text{Eq. 4.1}$$

where,

LHV : Lower heating value, kcal/kg
HHV : Higher heating value, kcal/kg
%MC : Moisture content of fuel, % by weight
%H : Hydrogen content of fuel, % by weight
MW_H : Molecular weight of hydrogen atom, 1 g/mole
MW_{H2O}: Molecular weight of water molecule, 18 g/mole
h_{fg} : Latent heat of vaporization of water at 25°C, 582.78 kcal/kg

Higher and lower heating values of fuels used in each test are given in Table 4.2.

Heating values, proximate and ultimate analyses of fuels used in each test are given according to their test codes. Detailed information about the test codes is presented in Section 4.4.

Table 4.2 Proximate analysis and heating values of coals and biomasses

Proximate analysis	**FC**	**VM**	**Ash**	**Moisture**	**HHV**	**LHV**
	%, by weight (as fired)				**kcal/kg (as fired)**	
Bursa/Orhaneli						
C1-1/2/3/4; C1-B1-1/2/3; C1-B2-1/2/3	20.18	34.40	23.09	22.33	3098	2827
C1-B1-4	29.19	35.69	17.02	18.10	4236	3959
C1-B1-5	32.63	36.61	10.64	20.12	4566	4270
C1-B2-4	32.71	36.23	13.24	17.82	4525	4244
C1-B2-5	28.94	36.19	16.43	18.44	4252	3971
C1-B1-6	32.62	35.50	11.45	20.43	4503	4210
C1-B1-7	31.73	33.49	7.94	26.84	4435	4112
Denizli/Kale						
C2-1/2/3/4	29.02	36.88	16.23	17.87	4181	3904
C2-B1-1	28.66	37.71	17.19	16.44	4137	3867
C2-B1-2	28.49	37.46	17.13	16.92	4125	3854
Olive Cake						
B1-1; C1-B1-1/2/3	15.30	59.91	5.47	19.32	3913	3573
C1-B1-4	17.23	67.09	5.71	9.97	4667	4340
C1-B1-5	16.13	64.33	7.72	11.82	4924	4583
C1-B1-6	15.26	70.93	5.67	8.14	4788	4456
C1-B1-7	16.07	69.18	5.64	9.11	4867	4533
C2-B1-1/2	17.59	61.64	9.69	11.08	4120	3818
Woodchips						
C1-B2-1/2/3	16.97	75.20	1.27	6.56	4361	4046
C1-B2-4	15.72	69.08	2.90	12.30	3962	3640
C1-B2-5	17.37	74.03	1.08	7.52	4398	4080

FC: Fixed Carbon, VM: Volatile Matter, HHV: Higher Heating Value, LHV: Lower Heating Value

Ultimate Analysis

Ultimate analysis of fuel samples were done by the accredited laboratory of in MRC-EI of TUBITAK. Ultimate analysis includes determination of carbon (C), hydrogen (H), nitrogen (N), and total sulfur (S_{total}) content of fuel samples. The combustible sulfur ($S_{combustible}$) is calculated by subtracting sulfur content in ash from total sulfur in fuel. Oxygen (O) content is determined by difference. C, H, and N content are determined according to the ASTM D 5373-08. Total sulfur content of fuels is determined according to the ASTM D 4239-08 and sulfur content in ash is determined according to the ASTM D 5016-08. Ultimate analyses of fuels used in each test are given in Table 4.3.

Table 4.3 Ultimate analysis of coals and biomasses

Ultimate analysis	**C**	**H**	**N**	**O**	**$S_{combustible}$**	**S_{total}**	**Ash**
	%, by weight (dry basis)						
Bursa/Orhaneli							
C1-1/2/3/4; C1-B1-1/2/3; C1-B2-1/2/3	41.48	2.37	0.54	24.12	n.a.	1.76	29.73
C1-B1-4	59.38	6.25	0.98	11.71	0.91	2.38	20.78
C1-B1-5	64.06	4.11	1.14	16.26	1.11	2.42	13.32
C1-B2-4	66.59	4.20	0.96	11.09	1.05	2.28	16.11
C1-B2-5	63.98	6.40	0.88	7.52	1.07	2.48	20.14
C1-B1-6	66.35	4.47	1.35	12.34	1.10	2.43	14.39
C1-B1-7	70.62	4.66	1.66	10.85	1.36	2.61	10.85
Denizli/Kale							
C2-1/2/3/4	57.32	3.81	1.38	15.63	2.10	4.23	19.76
C2-B1-1	56.26	3.48	1.47	16.75	1.47	3.69	20.57
C2-B1-2	55.23	3.36	1.45	17.41	1.94	3.79	20.62
Olive Cake							
B1-1; C1-B1-1/2/3	54.72	5.24	1.14	31.98	n.a.	0.14	6.78
C1-B1-4	56.08	5.52	1.05	30.87	0.14	0.20	6.34
C1-B1-5	51.32	5.29	1.24	33.22	0.18	0.32	8.75
C1-B1-6	55.57	5.68	1.32	30.71	0.54	0.65	6.17
C1-B1-7	57.31	5.79	1.19	28.84	0.67	0.84	6.21
C2-B1-1/2	49.80	4.90	1.64	32.13	0.63	0.84	10.90
Woodchips							
C1-B2-1/2/3	53.72	6.93	0.29	37.70	n.a.	0.00	1.36
C1-B2-4	50.66	5.22	0.06	40.14	0.61	0.68	3.31
C1-B2-5	53.75	6.36	-	38.65	0.07	0.12	1.17

n.a.: not applicable

Chlorine content

Chlorine (Cl) content of fuel samples were determined by the accredited laboratory of Marmara Research Center-Chemistry Institute (MRC-CI) of TUBITAK. Chlorine content was determined according to TS 644 ISO 587 standard and the results are given in Table 4.4 for fuel samples.

Table 4.4 Chlorine contents of fuel samples

	Cl, % by weight (dry basis)
Bursa/Orhaneli	0.00059
Denizli/Kale	0.00035
Olive Cake	0.088
Woodchips	0.0034

4.1.2. Limestone Characterization

In order to choose the limestone to be used in the combustion tests for SO_2 capture, five different limestones were tested for their reactivity and reactivity index analyses. The analyses were done in Çan Thermal Power Plant laboratories. Since Çan limestone had the highest reactivity index among the other five limestones, it was selected to be used in the experiments. The reactivity indexes of five limestones are given in Table 4.5.

Table 4.5 Reactivity index of different limestones

Limestone	**Reactivity (g S/kg limestone)**	**Reactivity Index (g S/kg $CaCO_3$)**
Öztüre	25.73	27.43
Başta ş	56.05	57.78
Sedef	76.58	76.81
Çumra	75.33	79.56
Çan	116.85	120.73

After the selection of the limestone to be used in the tests, total porosity and BET surface area analysis were conducted for the chosen limestone, Çan. The analyses were repeated after the limestone was calcined at 900°C. The total porosity and BET surface area results are given in Table 4.6. As can be seen in Table 4.6, the porosity and BET surface area of Çan limestone increased about 10 and 50 times, respectively after calcination. The CO_2 released during calcination making the limestone more porous.

Table 4.6 Total porosity and BET surface area of Çan limestone

Limestone	Total porosity	BET surface area
	%	m^2/g
Çan-before calcination	3.15	0.31
Çan-after calcination@900^oC	29.88	14.93

The Çan limestone was also subjected to chemical analysis. The analysis was conducted according to the EN 12485 standard (Chemicals used for treatment of water intended for human consumption-Calcium Carbonate_Test Methods-2010) by the accredited laboratory of MRC-CI in TUBITAK. The chemical composition is given in Table 4.7.

Table 4.7 Chemical composition of Çan limestone

Component	Chemical Analysis (wet) % by weight
Moisture	0.66
$CaCO_3$	96.89
$MgCO_3$	0.313
Al_2O_3	0.154
Na_2O	0.0280
K_2O	0.0094
SiO_2	0.31
Loss on Ignition	44.06

4.2. A Laboratory-Scale Circulating Fluidized Bed Combustor

A Laboratory-scale Circulating Fluidized Bed Combustor (Lab-CFBC) was designed and installed for the combustion and co-combustion of 1-2 mm fuel particles. The design of the Lab-CFBC was based on the characteristics of the Bursa/Orhaneli lignite (C1-1 in Table 4.2 and Table 4.3). However, it was also possible to burn different types of fuels with a wide range of moisture, ash, volatile matter contents. Its thermal capacity was about 30 kW_{th} and it was used in this study for the combustion and co-combustion of Bursa/Orhaneli and Denizli/Kale lignites with olive cake and woodchips at different mixing ratios. The experimental setup consists of a circulating fluidized bed combustor, a fuel feeding system (two fuel hoppers), a return leg, air feeding systems (primary and secondary air), electrical heaters, ash hoppers, a flue gas cooling system, two cyclones and a bag filter. The schematic diagram of the experimental setup is shown in Figure 4.1.

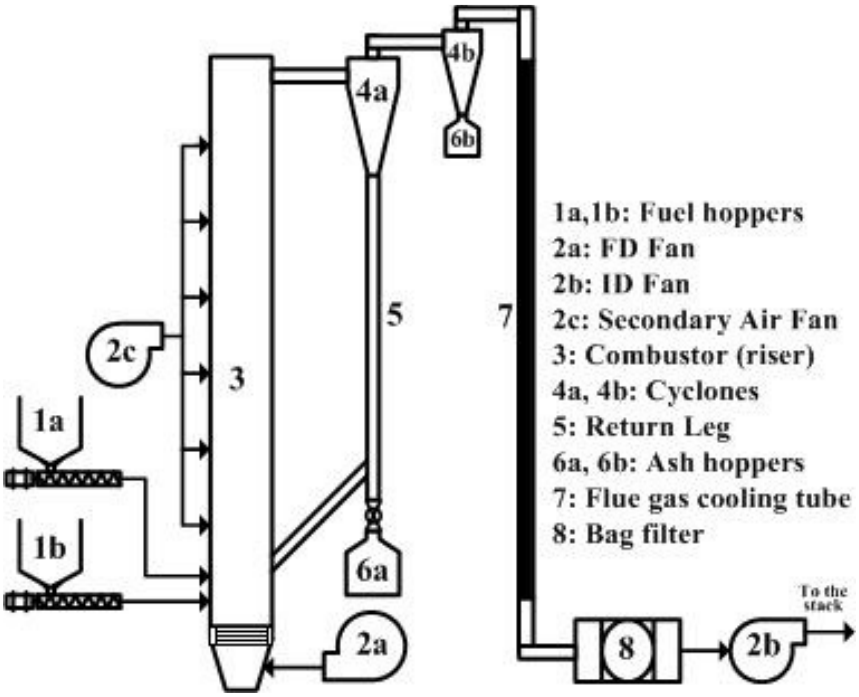

Figure 4.1 Schematic diagram of the combustion system

In order to control the combustion system from a computer, a control system and an interface was installed. The interface shown in Figure 4.2 is used as a control screen on a computer in order to observe the temperatures and pressures in the system, and to control the air and fuel feeding rates during experiments. The data is continuously measured and recorded. The flue gas composition measured by ABB-AO 2000 and GASMET-DX 4000 flue gas analyzers. The results are also observed on the control screen and recorded during the tests.

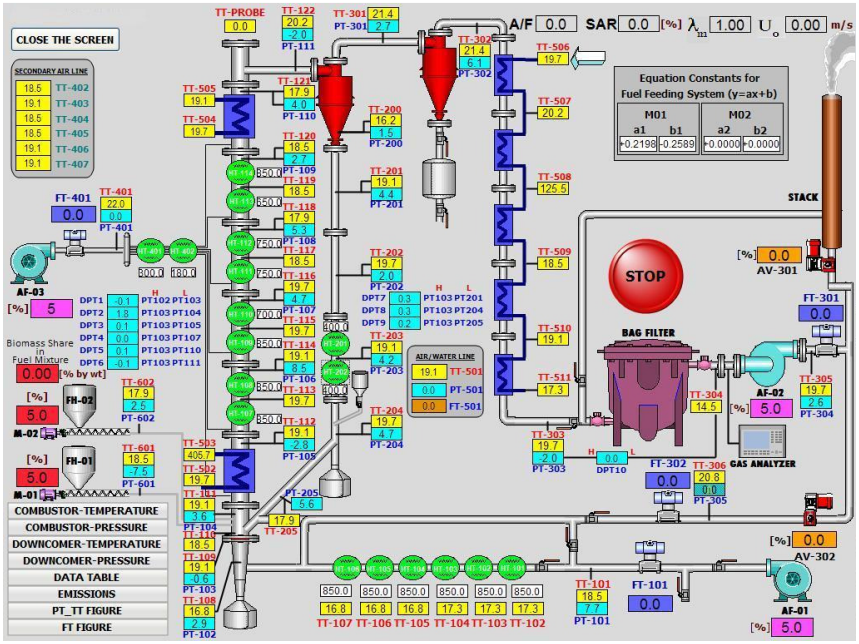

Figure 4.2 Control screen of the combustion system

The combustor has an inside diameter of 108 mm and a height of 6 m. It consists of 8 modules. Two modules (Module 102 and Model 107) are used to take the heat away from the combustor. Design details of each module are described in section 4.2.2. Eight electrical heaters are used along the combustor in order to maintain temperature of the combustor at the desired value. Additionally, two electrical heaters are used on the return leg. The combustor is connected to the first cyclone with a pipe which has a nominal diameter (DN) of 32. The solids separated from the flue gas on the cyclone are given back to the combustor through a downcomer. The fuel feeding system consists of two hoppers, two screw feeders, two electrical motors and a compressed air connection. A photograph of the system is given in Figure 4.3.

The fluidizing air is given by a force draft (FD) fan and it is heated by six primary air preheaters. The pressure inside the combustor can be controlled by adjusting the flowrate and the operating pressure of the induced draft (ID) fan. It is possible to operate the system both at positive and negative pressures by adjusting the flowrate and the operational pressures of these two fans (FD and ID). During combustion tests, the system was operated keeping the pressure zero (gauge) at the exit of the second cyclone. By this way, the pressure in the combustor was above the atmospheric pressure and the system was operated under vacuum after the first cyclone. While the combustor is operated at positive pressure, there may be some fuel feeding problems due to the positive pressure inside the combustor. In order to prevent the feeding problem, compressed air is blown into the fuel feeding lines. The first cyclone is used to separate the solids from the gas and to maintain the recirculation of solid by returning them into the combustor via a return leg. The second cyclone, which is design smaller than the first one, is used to keep finer

particles escaping from the first cyclone. The ash particle accumulated at the ash hopper under the second cyclone was collected, sampled and subjected to the ash analyses for the co-combustion tests in SET#4. The flue gas leaving the second cyclone was passed through five water-cooled tubes in order to decrease the flue gas temperature below 200°C. The temperature of the flue gas is decreased below 200°C to protect the bag filter and ID fan. The bag filter is located after the flue gas cooling tubes to catch the finest particles and to protect the ID fan from the flue gas having high solid concentration. There are six ports for the secondary air injection along the combustor. The temperatures along the combustor and the return leg are continuously measured with thermocouples located at specific heights (see Table B.5). The temperature of the combustor is kept at about 850°C during combustion experiments. The pressure drops along the combustor, cyclone, and return leg are continuously measured and observed in order to determine the solid mass flux within the combustor.

Figure 4.3 A photograph of the combustion system

Process and Instrumentation Diagram (P&ID) of the combustion system was drawn. P&ID consists of two separate drawings, flue gas path and water/air path. These drawings are given in Figure 4.4, and Figure 4.5, respectively. As can be seen from the P&IDs, there are 3 air fans (two FD fans for primary and secondary airs, an ID fan to exhaust the flue gas), 5 orifice type flowmeters, 14 rotameters, 21 pressure transmitters (PT) and 49 thermocouples (temperature transmitters (TT)) on the combustion system. The codes used in P&IDs for temperature and pressure transmitters and locations of them on the combustion system are given in Table B.3 and Table B.4 in Appendix B, respectively. 18 electrical heaters are used, 6 of them are 2.5 kW in power and used to heat the primary air to a temperature for fuels to be ignited. 8 of them are 4.5 kW in power and located on the combustor column to keep the combustor temperature at about 850^{o}C which is generally operating temperature of fluidized bed combustors. Two of them are 4 kW in power and used on the downcomer in order to keep up the temperature of the material in the return leg. Last two are 2.5 kW in power and used to heat the secondary air given to the combustor.

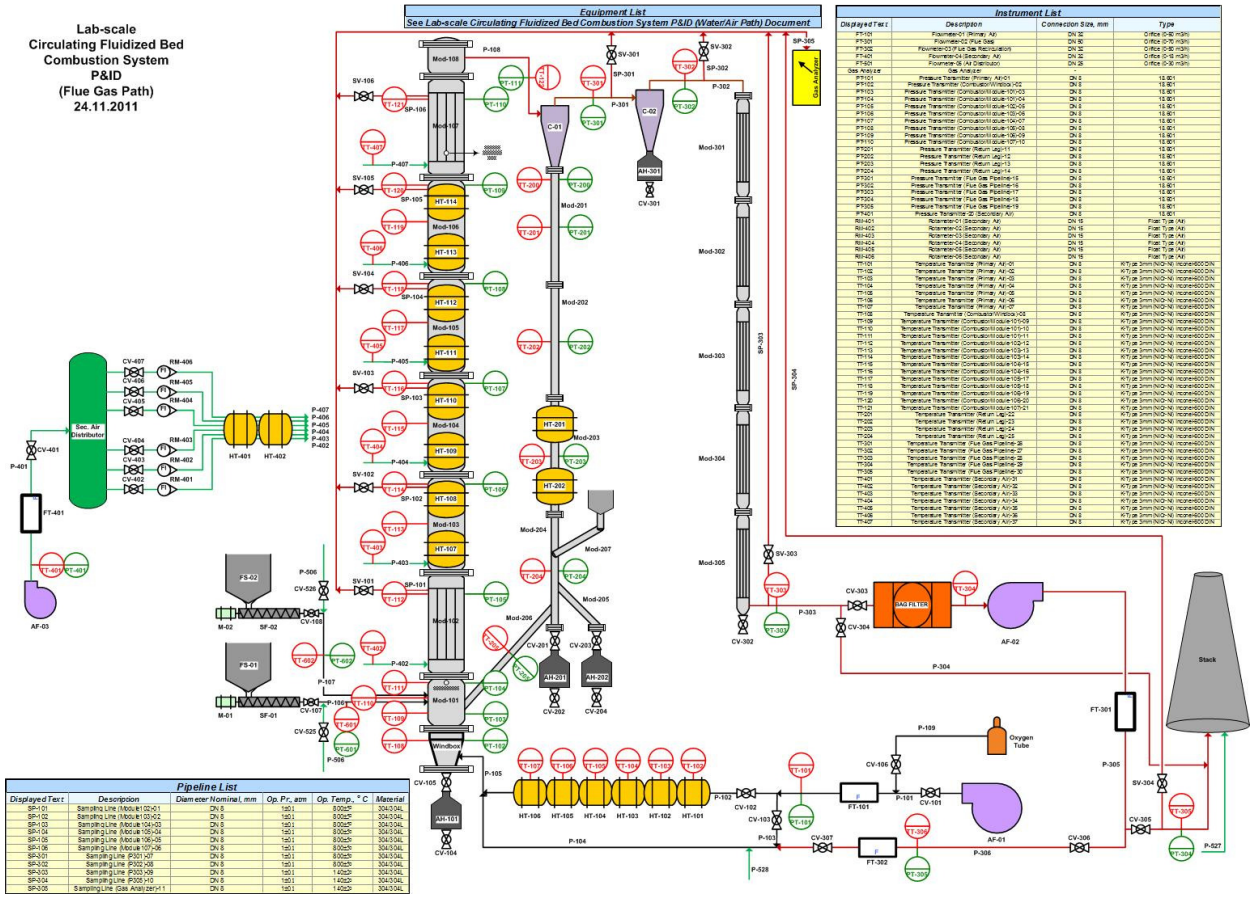

Figure 4.4 Process and instrumentation diagram of the circulating fluidized bed combustion system (flue gas path)

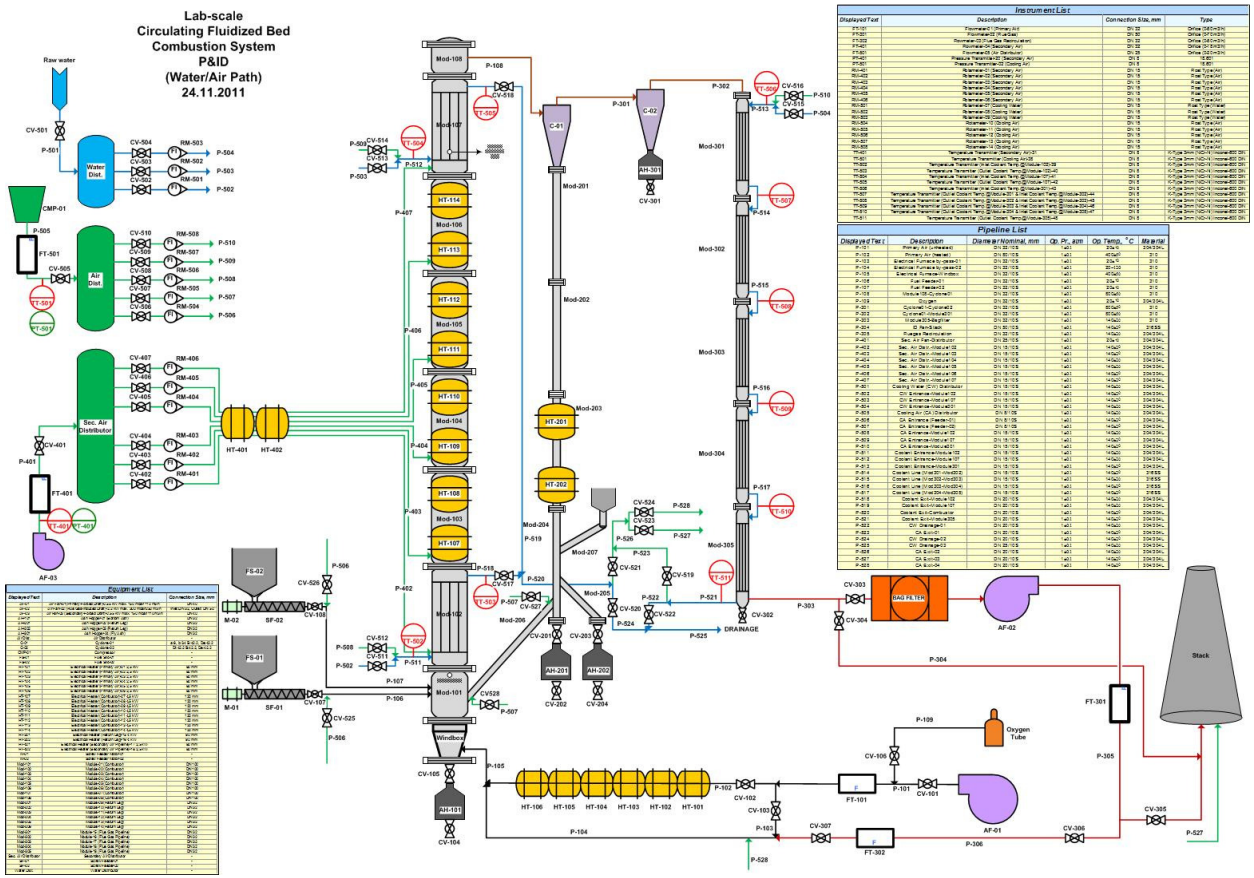

Figure 4.5 Process and instrumentation diagram of circulating fluidized bed combustion system (water/air path)

4.2.1. Fuel Feeding System

4.2.1.1. Calibration of the Fuel Feeding System

The fuel from the hopper was fed to the combustor by a screw feeder. The calibration curves of the screw feeders for each fuel (1-2 mm diameter) were done before combustion tests. Calibration curves of the feeding system for these fuels were given in Figure C.1 to Figure C.4 in Appendix C. The calibration curve of the fuels was a straight line which is very easy to use.

4.2.2. Design Details of Components of Combustor

4.2.2.1. Windbox

Windbox is a pipe with a size of DN 100 (SCH 10) and the height of the windbox is 150 mm. There is a conical item which connects the windbox to the bottom ash removal pipe with a size of DN 32 (SCH 10). The primary air enters the windbox from sides through a pipe with a size of DN 32 (SCH 10). There are two ports on the windbox, one is for temperature and the other is for pressure measurement. Technical drawings of the windbox and its specifications are given in Figure B.1 and Table B.1, respectively, in Appendix B.

4.2.2.2. Distributor Plate

The distributor plate used in the combustor was located between two flanges. It has 2472 holes on it and each hole has a diameter of 0.5 mm. The diameter of the holes was determined to have a gas velocity of 30 m/s in the holes. A photograph of the distributor plate is given in Figure 4.6.

Figure 4.6 The distributor plate used in the combustor

4.2.2.3. Module-101

Module-101 is a pipe with a size of DN 100 (SCH 10) and the height of the module-101 is 415 mm. Module-01 is connected to the windbox at the bottom and to Module-102 at the top with flanges with a size of DN 100. The total height of the module with flanges is 425 mm. There is a distributor plate between the windbox and the Module-101. The fuels in the two fuel hoppers are fed to the combustor from Module-101. The fuel coming from the Fuel Hopper-01 and Fuel Hopper-02 enters into the Module-101 at the height of 62.64 mm and 126.13 mm over the distributor plate, respectively. This is the height of the center of the pipe over distributor plate. Technical drawings and specifications of Module-101 are given in Figure B.2 and Table B.2, respectively, in Appendix B.

4.2.2.4. Module-102 and Module-107

Module-102 and Module-107 are identical. These modules are used for cooling purpose. The module is consisted of two concentric pipes. The pipe inside has a diameter of DN 100 (SCH 10) and a height of 900 mm. The material is stainless steel type 310. The pipe outside has a diameter of DN 125 (SCH 10) and a height of 680 mm. It is also made of stainless steel type 304. Between these two concentric pipes, water or air flows in order to remove heat from the combustor. There are two flanges at the top and bottom of the module. With the flanges, the total height of the module is 910 mm. There are two ports for inflow and outflow of the coolant. The diameter of these ports is DN 15 (SCH 10) and they are 150 mm in length. The temperature of the coolant inflow and outflow is measured by two temperature transmitters. There are also six ports; one for temperature measurement, one for pressure measurement, one for gas sampling and one for secondary air injection. The deposit sampling probe is located on Module-107. Technical drawings and design details are given in Figure B.3 in Appendix B.

4.2.2.5. Module-103, Module-104, Module-105 and Module-106

Module-103, Module-104, Module-105, and Module-106 are identical. These modules have a diameter of DN 100 (SCH 10) and a height of 900 mm. The material is stainless steel type 310. There are two flanges at the top and at the bottom of the module. With the flanges, the total height of the module is 910 mm. There is one port for temperature measurement and one port for pressure measurement, one port for gas sampling and one port for secondary air injection. Technical drawings and design details are given in Figure B.4 in Appendix B.

4.2.2.6. Module-108

The module has a diameter of DN 100 (SCH 10) and a height of 250 mm. The material is made of stainless steel type 310. There are two flanges at the top and at the bottom of the module. With the flanges, the total height of the module is 260 mm. There is an observation window at the top of the module. Technical drawings and design details are given in Figure B.5 in Appendix B.

4.3. Operational Procedure

The first step to operate the system is to turn on FD and ID fans. The FD fan (AF-01 in Figure 4.2) and the ID fan (AF-02 in Figure 4.2) are run at low flowrates (less than 25% of their total capacities). Air supplied from the FD fan is preheated by six electrical heaters which are located between the FD fan and the combustor and by eight electrical heaters on the combustor. Electric heaters are operated in series and used to increase the combustor temperature over the ignition temperature of the fuel. Air is uniformly fed into the combustor with a distributor plate. This air supplied to the combustor is used both as fluidization air and primary air for combustion. Six electrical heaters for preheating the air are set to 800°C and the eight electrical heaters on the combustor are set to 700°C.

Sand is used as the bed material in the combustor. 6 kg of sand (250µm-350µm) is fed into the combustor in each experiment from the return leg. While sand is being fed into the combustor, the FD fan is operated at a low capacity to make feeding easy. After the bed material is fed into the combustor, the FD fan is set to 45-50% of its capacity and the ID fan is set to 30-40% of its capacity to provide an air flowrate a little above 15 m^3/h. If the flowrate is less than 15 m^3/h, it is possible to plug the holes of the distributor plate.

The fuel prepared in advance is stored in the fuel hoppers. The fuel hopper (FH-01) and the fuel hopper (FH-02) are generally used for coal and biomass fuels, respectively. The fuel feeding lines are cooled by injecting compressed air to prevent ignition of fuel particles in the feeding line. Feeding air into fuel feeding lines is also required to generate positive pressure in the lines and thus to prevent hot gases from the combustor enter the feeding lines. There is one temperature transmitter in each feeding line (TT601 for FH-01 and TT602 for FH-02 in Figure 4.2) to observe the temperature. The temperature of these transmitters should be kept at less than 200°C to feed the fuel into the combustor safely. When the temperature at 24 cm above the distributor plate (thermocouple TT110 is located at the same level of fuel feeding ports) is reached 420-430°C which is higher than the ignition temperatures of all fuels, the fuel is started to be fed into the combustor. Heating-up period generally takes 3 hours. The temperature profile along the combustor is continuously measured and also observed by a data logger on which thermocouples are connected during fuel feeding. If an over increase in the temperature is seen, the fuel feeding rate can be gradually decreased. When the combustion is self-sustained and the temperature profile along the combustor is in the range of 800 and 850°C, the electrical heaters are shut down.

The system is operated in such a way that the pressure is zero at the exit of the first cyclone. The combustor is operated under positive pressure. However, all the units after the first cyclone are operated under vacuum. In order to sustain the pressure balance and to keep the superficial velocity in the combustor between 3 m/s and 4 m/s, the FD and ID fans are adjusted to 45% and 30% of their capacities, respectively. Under this condition, the total gas flow rate is around 25-30 m^3/h (@ 20°C and 1 atm).

When the system reaches steady-state condition which means that there is no variation in temperature and pressure values measured at a specific location, emission measurements

are started. For a combustion test, it approximately takes 5 hours to reach the steady state condition. After emission measurements are started, it is very important to keep the operating conditions of the system constant in order to have the same hydrodynamics in the system.

Tests are also conducted at different excess air ratios to see the effect of the excess air ratio on flue gas emissions. In these tests the total flow rate in the combustor is not increased not to disturb the hydrodynamics of the system. Air flowrate is kept constant. Instead, fuel feeding rate is changed until the required excess air ratio value is reached. When tests are conducted with secondary air injection, a certain percentage of the total air flow rate is given to the combustor as the secondary air and the rest is given as the primary air. Different percentages of secondary air injection to the combustor are tested in different runs.

After a combustion test is completed, fuel feeding is stopped. The air flow into the system continues until the system cools down. The ash formed during the combustion and long-term co-combustion tests is collected, weighted and stored to be analyzed. Ash samples are burned at 950^{o}C until constant weight is reached to determine the amount of unburned carbon in the sample. The difference in weight gives the unburnt carbon in the ash sample. This result is further used in determining combustion efficiency. Ash samples are also subjected to XRF, XRD, and SEM-EDS analyses to determine their elemental compositions.

4.4. Experimental Matrix

There are 23 experiments in the experimental matrix which includes combustion and co-combustion of two biomasses (olive cake and woodchips) with two Turkish lignites (Bursa/Orhaneli and Denizli/Kale). The experimental matrix consists of four different experimental sets. The goal of each set and the parameters to be considered as “constant, variable and control” parameters for each set are given in Table 4.8.

Table 4.8 Goals; constant, variable and control parameters of the experimental sets

SET #	GOAL	PARAMETERS			OUTPUT
		CONSTANT	VARIABLE	CONTROL	
1	to determine optimum excess air ratio (λ)	superficial velocity in the combustor (U_o) = 3-3.5 m/s Temperature of the dense phase (T_{dp}) = 850°C	Fuel feeding rate	1. flue gas emissions	1. emissions vs. (λ) figures 2. flue gas emissions compared to emission limits
2	to determine optimum secondary air ratio (SAR) for CO and NO emissions and its location	Operational parameters for SET#1 at optimum (λ)	Secondary air ratio	1. flue gas emissions	1. emissions vs. SAR figures 2. flue gas emissions compared to emission limits
3	to determine optimum Ca/S_{total} ratio	Operational parameters for SET#1 at optimum (λ)	Ca/S_{total} ratio	1. SO_2 emissions	1. SO_2 emissions vs. (λ) figures 2. SO_2 emissions compared to emission limits
4	to determine the effect of S on ash composition and the effect of biomass+limestone interaction on ash composition and emissions	Optimum (λ)	S content of fuel mixture	ash composition	1. ash analysis (XRF, XRD, SEM/EDS)

EXPERIMENTAL SET#1

The aim of this set of experiments is to determine the optimum excess air ratio (λ) for each experiment. Excess air ratio is defined as the ratio of air supplied for the combustion in excess of that theoretically required for complete combustion. The optimum λ is decided according to the flue gas emissions. During the experiment, the operational condition at which CO emission is minimum is decided to be optimum condition and λ at this condition is selected as optimum λ. Temperature of the dense phase (average temperature of the two thermocouples (TT110 and TT111 in Figure 4.2) which are located in the first module of the combustor), T_{dp}) and superficial velocity in the combustor (U_o) are the operational parameters which should be kept constant during the experiment. T_{dp} is kept constant at about 850°C and U_o is between 3 and 3.5 m/s. When the system reaches steady state, it is the time to measure emissions. The frequencies of two fans, forced draft (FD) and induced draft (ID), are not changed in order to keep U_o constant. Therefore, flue gas emissions can be measured at different λ values by only changing the fuel feeding rate. The only variable parameter in this set is fuel feeding rate. Flue gas emissions are the control parameters in order to find the optimum λ. Total number of experiments in this set is 8. The experiments include combustion of Bursa/Orhaneli lignite, combustion of olive cake, co-combustion of Bursa/Orhaneli lignite and olive cake fuel mixtures containing olive cake 10, 30, and 50% by weight and co-combustion of Bursa/Orhaneli lignite and woodchips fuel mixtures containing woodchips 10, 30, and 50% by weight. Experiments are listed in Table 4.9 below.

Table 4.9 List of experiments in SET#1

Test #	Test Code	Coal	Biomass	Biomass share in fuel mixture, % by wt.
1-1	C1-1	Bursa/Orhaneli	-	-
1-2	C1-B1-1	Bursa/Orhaneli	Olive Cake	10
1-3	C1-B1-2	Bursa/Orhaneli	Olive Cake	30
1-4	C1-B1-3	Bursa/Orhaneli	Olive Cake	50
1-5	B1-1	-	Olive Cake	100
1-6	C1-B2-1	Bursa/Orhaneli	Woodchips	10
1-7	C1-B2-2	Bursa/Orhaneli	Woodchips	30
1-8	C1-B2-3	Bursa/Orhaneli	Woodchips	50

The figures of emission vs. λ are drawn for each experiment. From these figures, it is aimed to determine the optimum λ at which flue gas emissions especially CO emissions are minimum. The aim of this set was to find the optimum λ. The deposit sampling probe was not used in these experiments.

EXPERIMENTAL SET#2

This set of experiments aims to determine the secondary air ratio (SAR) at which maximum decrease in CO and NO emissions is achieved. SAR is the ratio of the secondary air to total air. It is also important to find the location at which the secondary air to the combustor is given. During combustion experiments, secondary air is given to the combustor at different heights of the combustor (riser) and at pre-defined ratios. Thus, the effect of secondary air ratio on the flue gas emissions, especially on CO and NO emission is investigated. The operational parameters defined in the experiments of SET#1 were used here. They are constant T_{dp} and U_o. The only variable in this set is the flow rate of the secondary air. Secondary air is given to the combustor from four different locations along the combustor at specific heights above the distributor plate. The secondary air injection ports used for the experiments are located at 142 cm (on Module-3), 233 cm (on, Module-4), 324 cm (on Module-5), and 415 cm (on Module-6) above the distributor plate. The locations of the secondary injection ports on the combustor can be in Figure 4.2 and Figure 4.5. For each location, the effect of different secondary air ratios, 10-20-30% on flue gas emissions is investigated. Flue gas emissions are the control parameters in order to find the optimum SAR value. Total number of experiments in this set is 4. The experiments include co-combustion of Bursa/Orhaneli lignite and olive cake fuel mixtures containing olive cake 30 and 50% by weight and co-combustion of Bursa/Orhaneli lignite and woodchips fuel mixtures containing woodchips 30% and 50% by weight. Experiments are listed in Table 4.10 below.

Table 4.10 List of experiments in SET#2

Test #	Test Code	Coal	Biomass	Biomass share in fuel mixture, % by wt.
2-1	C1-B1-4	Bursa/Orhaneli	Olive Cake	30
2-2	C1-B1-5	Bursa/Orhaneli	Olive Cake	50
2-3	C1-B2-4	Bursa/Orhaneli	Woodchips	30
2-4	C1-B2-5	Bursa/Orhaneli	Woodchips	50

The emissions vs. SAR were plotted for each experiment. The goal of these experiments was to find the optimum SAR and to find the location at which it should be given to the combustor to make the flue gas emissions especially CO and NO emissions minimum. The deposit sampling probe was not used for these experiments.

EXPERIMENTAL SET#3

This set of experiments aims to determine the optimum Ca/S_{total} ratio for both lignite coals in order to obtain minimum SO_2 emissions. The operational parameters defined for the experiments in SET#1 were used here. They are constant T_{dp} and U_o. The only variable in this set was the amount of limestone used in the fuel+limetone mixture. Since Çan limestone has the highest reactivity index among the five different limestones, it is selected to be used in the experiments. The reactivity indices of five limestones are given

in Section 0. SO_2 emission is the control parameters in order to find the optimum Ca/S_{total} ratio. Total number of experiments in this set is 7. The experiments include combustion of Bursa/Orhaneli lignite together with Çan limestone with Ca/S_{total} ratio of 2-2.5-3, combustion of Denizli/Kale lignite by itself, combustion of Denizli/Kale lignite together with Çan limestone with Ca/S_{total} ratio of 2-2.5-3. Experiments are listed in Table 4.11 below.

Table 4.11 List of experiments in SET#3

Test #	Test Code	Coal	Limestone	Ca/S_{total} ratio
3-1	C1-2	Bursa/Orhaneli	Çan	2
3-2	C1-3	Bursa/Orhaneli	Çan	2.5
3-3	C1-4	Bursa/Orhaneli	Çan	3
3-4	C2-1	Denizli/Kale	-	-
3-5	C2-2	Denizli/Kale	Çan	2
3-6	C2-3	Denizli/Kale	Çan	2.5
3-7	C2-4	Denizli/Kale	Çan	3

SO_2 emission vs. λ are plotted for each coal. The goal of these experiments was to find the optimum Ca/S_{total} ratio for both types of coal. The deposit sampling probe was not used for these experiments.

EXPERIMENTAL SET#4

This set of experiments aims to investigate the effect of sulfur content of fuel on the ash composition. Second aim is to investigate the effect of biomass and limestone mixtures on ash composition and flue gas emissions. The fuels used in SET#4 are Bursa/Orhaneli and Denizli/Kale lignites and olive cake. Bursa/Orhaneli and Denizli/Kale lignites were chosen for the tests in SET#4 in order to see the effect of sulfur in coal on the ash-related problems. While Bursa/Orhaneli lignite represents the low-sulfur coal (S_{total} < 2.7% in Table 4.1), Denizli/Kale lignite represents the high-sulfur coal (S_{total} > 3.6% in Table 4.1). Since the ash-related problems are mainly sourced by alkalis in the biomass ash (See Section 2.2.2), olive cake was selected as a biomass to be used in in the tests of SET#4 due to its high alkali content in ash.

Based on the fuel used in the experiment, the experiments were conducted at the optimum λ obtained from SET#1 The only variable in this set of experiments was the sulfur content of the fuel mixture. The control parameters were ash composition and flue gas emissions. Total number of experiments in this set was 4. The experiments included co-combustion of Bursa/Orhaneli lignite and olive cake mixture containing 50% by wt. olive cake with and without limestone, co-combustion of Denizli/Kale lignite and olive cake

mixture containing 50% by wt. olive cake with and without limestone. The list of experiments is listed in Table 4.12.

Table 4.12 List of experiments in SET#4

Test #	Test Code	Coal	Biomass	Biomass share in fuel mixture, % by wt.	Ca/S_{total} ratio
4-1	C1-B1-6	Bursa/Orhaneli	Olive Cake	50	-
4-2	C1-B1-7	Bursa/Orhaneli	Olive Cake	50	Optimum
4-3	C2-B1-1	Denizli/Kale	Olive Cake	50	-
4-4	C2-B1-2	Denizli/Kale	Olive Cake	50	Optimum

Unlike the other three sets of experiments, the experiments in this set are long-term experiments. A deposit sampling probe was used in the bed to simulate a heat exchanger tube in the freeboard. During the combustion experiments, fly ash samples were collected on the deposit sampling probe. At the end of the combustion experiments, bottom ash from the combustor, fly ash from the 2nd cyclone and bag filter were also collected. Ash deposition rate was calculated. Ash balance was done. Samples taken from the ashes were analyzed in order to investigate the effect of sulfur on ash composition. XRF, XRD, SEM/EDS analysis of ash samples were carried out. The overall list of experiments is given in Table 4.13.

Table 4.13 Details of experiments in each set

Test #	Test Code	Coal	Biomass	Biomass share in fuel mixture, % by wt.	Limestone	Ca/S_{total} ratio
1-1	C1-1	Bursa/Orhaneli	-	-	-	-
1-2	C1-B1-1	Bursa/Orhaneli	Olive Cake	10	-	-
1-3	C1-B1-2	Bursa/Orhaneli	Olive Cake	30	-	-
1-4	C1-B1-3	Bursa/Orhaneli	Olive Cake	50	-	-
1-5	B1-1	-	Olive Cake	100	-	-
1-6	C1-B2-1	Bursa/Orhaneli	Woodchips	10	-	-
1-7	C1-B2-2	Bursa/Orhaneli	Woodchips	30	-	-
1-8	C1-B2-3	Bursa/Orhaneli	Woodchips	50	-	-
2-1	C1-B1-4	Bursa/Orhaneli	Olive Cake	30	-	-
2-2	C1-B1-5	Bursa/Orhaneli	Olive Cake	50	-	-
2-3	C1-B2-4	Bursa/Orhaneli	Woodchips	30	-	-
2-4	C1-B2-5	Bursa/Orhaneli	Woodchips	50	-	-
3-1	C1-2	Bursa/Orhaneli	-	-	Çan	2
3-2	C1-3	Bursa/Orhaneli	-	-	Çan	2.5
3-3	C1-4	Bursa/Orhaneli	-	-	Çan	3
3-4	C2-1	Denizli/Kale	-	-	-	-
3-5	C2-2	Denizli/Kale	-	-	Çan	2
3-6	C2-3	Denizli/Kale	-	-	Çan	2.5
3-7	C2-4	Denizli/Kale	-	-	Çan	3
4-1	C1-B1-6	Bursa/Orhaneli	Olive Cake	50	-	-
4-2	C1-B1-7	Bursa/Orhaneli	Olive Cake	50	Çan	Optimum
4-3	C2-B1-1	Denizli/Kale	Olive Cake	50	-	-
4-4	C2-B1-2	Denizli/Kale	Olive Cake	50	Çan	Optimum

4.5. Deposit Sampling Probe

A “deposit sampling probe” was designed and manufactured to simulate a heat exchanger tube in the combustor. The surface of the deposit sampling probe is cooled internally down to 550^{o}C with air in order to represent the surface temperature of the superheaters. The deposit sampling probe was used in order to collect fly ash samples during the combustion test in SET#4. The particles accumulated on the surface of the probe were collected at the end of the test. After the probe was taken out of the combustor, the particles collected on the probe were very slowly scraped from the surface into a sampling pot. A drawing of the sampling probe with details is shown in Figure 4.7. Deposit sampling probe was located on Module-107. The probe was made from a stainless steel tube of 26.7 mm outer diameter (OD). The length of the probe was 230 mm. The deposit samples accumulated on the surface of the probe on the detachable ring which has a dimension of 26.7 mm OD and 60 mm length was subjected to XRD and SEM/EDS analysis after the combustion tests.

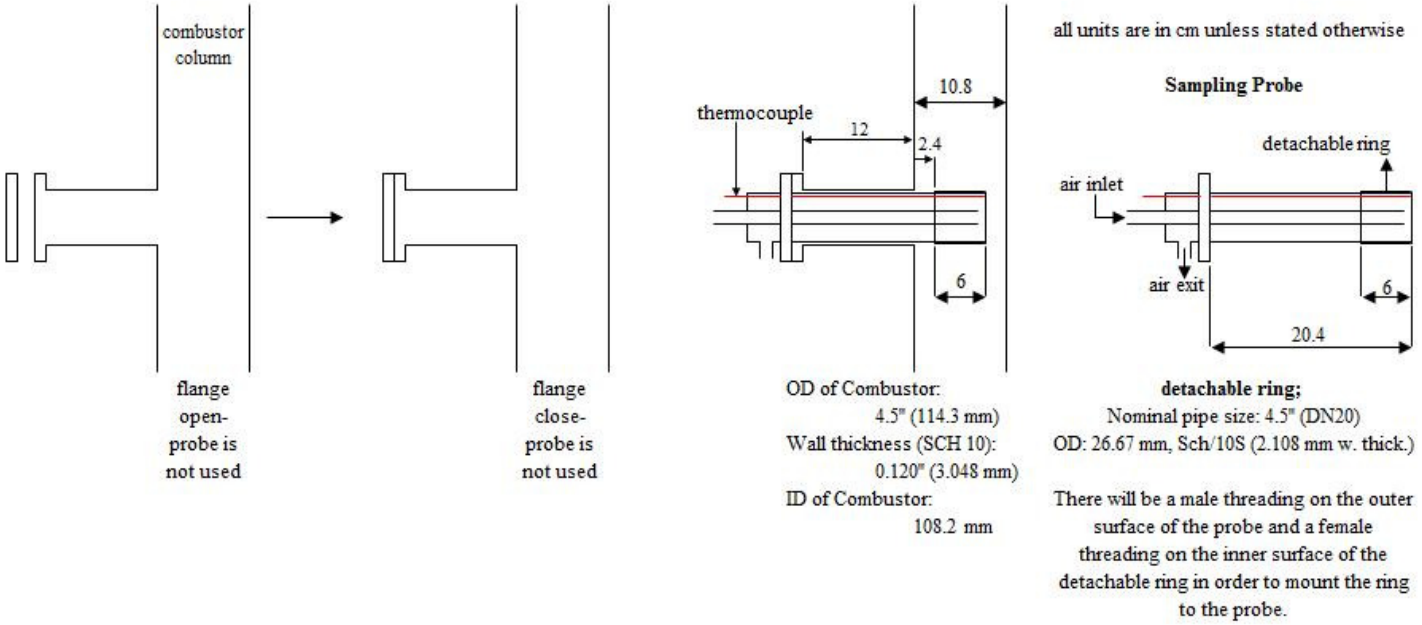

Figure 4.7 Air Cooled Deposit Sampling Probe with a Detachable Ring

4.6. Flue Gas Analyses

ABB-AO 2000 and GASMET-DX 4000 flue gas analyzers were used in order to measure the concentration of pollutants in the flue gas. While CO, NO, SO_2, CO_2, and O_2 concentrations in the flue gas were continuously measured with ABB-AO 2000 flue gas analyzer, gases measured with ABB-AO 2000 flue gas analyzer and additionally N_2O, NO_2, NH_3, CH_4, C_2H_4, C_2H_6, C_3H_8, $C_6H_{14,}$ CHOH, HCl, HF, HCN and H_2O gases were continuously measured in the flue gas with GASMET-DX 4000 flue gas analyzer. The modules in ABB-AO 2000 flue gas analyzer and their measurement ranges are given in Table 4.14. The gases measured by GASMET-DX 4000 flue gas analyzer and their measurement ranges are given in Table 4.15.

Table 4.14 Measurement ranges of ABB-AO 2000 flue gas analyzer

Gas Component	Module	Measurement Range
CO	URAS 26 (IR)	0-10000 ppm
NO	URAS 26 (IR)	0-2000 ppm
SO_2	URAS 26 (IR)	0-3000 ppm
CO_2	URAS 26 (IR)	0-30%
O_2	MAGNOS 106 (PARAMAGNETIC)	0-25%

Table 4.15 Measurement ranges of GASMET-DX 4000 flue gas analyzer

Gas Component	Measurement Range	Gas Component	Measurement Range
CO	0-10000 ppm	C_2H_4	0-100 ppm
NO	0-1000 ppm	C_2H_6	0-100 ppm
SO_2	0-2000 ppm	C_3H_8	0-100 ppm
CO_2	0-30%	C_6H_{14}	0-100 ppm
O_2	0-25%	CHOH	0-140 ppm
N_2O	0-500 ppm	HCl	0-500 ppm
NO_2	0-100 ppm	HF	0-100 ppm
NH_3	0-500 ppm	HCN	0-1000 ppm
CH_4	0-1000 ppm	H_2O	0-30%

4.7. Ash Analyses

Since the high alkali metal content (K and Na) of solid fuel (particularly for olive cake) brings the risk of ash-related problems in the combustor, characterization of ashes of all fuels was done in order to find the metal content (especially alkali metal content) of each ash samples. Two Turkish lignites and two biomass fuels were sampled and ashes from these fuels were obtained by combusting these fuels in a furnace according to the ASTM standards (ASTM D1374-04 Standard Test Method for Ash in the Analysis Sample of Coal and Coke from Coal for coal samples, ASTM E1755-01 Standard Test Method for Ash in Biomass for biomass fuels) for X-ray fluorescence (XRF) analysis in order to characterize the elemental composition of their ashes. XRF analyses were also done for the ashes formed at the end of the co-combustion tests in SET#4. Because the ash-related problems coming from the combustion of olive cake having high-alkali content (K_2O content of olive cake ash was 49% by wt. in Table 4.16) were covered in the SET#4. At the end of the combustion tests in SET#4, bottom ash (BA), fly ash captured in the second cyclone (FA-C), and fly ash captured in the bag filter (FA-BF) were all collected. Samples from each ash material were taken for XRF, X-ray diffraction (XRD) and Scanning Electron microscope-Energy Dispersive X-ray spectroscopy (SEM-EDS) analyses. The results of these analyses and assessment of the results are presented in Section 5.5.

4.7.1. X-ray Fluorescence (XRF)

XRF analyses of fuel sample ashes were presented in Table 4.16. The XRF analyses were done with Philips PW-2404 XRF Spectrometer by an accredited laboratory of Marmara Research Center-Material Institute (MAM-MI) of TUBITAK. The elements between O and Uranium (U) in the periodic table can be determined with the XRF analysis and these analyses give semi-quantitative results. Moreover, the XRF analyses of BA, FA-C, FA-BF and fuel ashes were also conducted for the co-combustion tests in SET#4 and they were given in Section 5.5 for the assessment and discussion of ash analyses.

Table 4.16 Ash composition of fuel samples according to the XRF analysis

Compound	Bursa/Orhaneli	Denizli/Kale	Olive Cake	Woodchips
		% by weight		
Al_2O_3	10.14	10.11	3.04	1.64
CaO	19.73	11.83	20.38	41.53
Cl	0.00		2.19	0.10
Cr_2O_3	0.06	0.16	0.12	0.08
CuO	0.22	0.01	0.08	0.03
Fe_2O_3	9.97	20.25	5.16	0.62
K_2O	0.58	0.62	49.26	25.56
MgO	7.87	8.12	2.95	14.39
MnO_2	0.15	0.07	0.16	2.15
Na_2O	0.27	0.19	0.49	0.19
P_2O_5	0.22	0.13	3.57	6.52
SO_3	29.33	34.94	4.34	4.49
SiO_2	20.82	12.99	7.48	1.64

It can be seen from Table 4.16 that Ca, S, Si, Fe, Mg and Al are the common elements present in the ash of Bursa/Orhaneli and Denizli/Kale lignites. While Denizli/Kale lignite is rich in Fe_2O_3, Bursa/Orhaneli lignite is rich in CaO. For biomasses, K and Ca are the most seen elements in their ashes. Alkali metals, sodium and potassium, of ashes are very important in terms of the ash-related problems. Olive cake with its high K_2O content shows the greatest risk for the ash-related problems among the fuels used in the study. While the ashes of Bursa/Orhaneli and Denizli/Kale lignite have only 0.58% and 0.62% K_2O, respectively, almost half of olive cake ash is K_2O (49.26%). It is 25.56% for the woodchips. Na_2O content is generally low in fuel ashes less than %0.5. Olive cake has the highest content of Na_2O with 0.49%. P_2O_5 is high in biomass ashes when compared to the lignite ashes. Lignites ashes have higher content of Al_2O_3 and SiO_2 than biomass ashes. This is an indication of aluminum silicates contamination from soil. There may be variations in the ash composition, particularly for biomass ashes, due to the changes in the weather conditions, the soil quality. Therefore, the reader should not be surprised to see a wide range of elemental composition for biomass ashes in the literature (Hiltunen et al., 2008).

4.7.2. X-ray Diffraction (XRD)

XRD analyses of BA, FA-C, and FA-BF for the co-combustion tests in SET#4 and fuel ash samples were conducted at MAM-MI. In addition to XRD analyses done by MAM-MI, XRD analyses of the deposit collected on the deposit sampling probe was also performed by METU-Central Laboratory.

4.7.3. Scanning Electron Microscopy

All ash samples taken from bottom ash, fly ashes captured at the 2nd cyclone and bag filter, and also deposits accumulated on the Deposit Sampling Probe at the end of the long-term combustion tests in SET#4 were analyzed by a Scanning Electron Microscope (SEM) (Quanta 400F Field Emission) at METU-Central Laboratory. Energy Dispersive X-ray spectroscopy (EDS) technique was applied to ash samples in order to determine the elemental composition of the ash samples. SEM was equipped with both secondary electron (SE) and back-scattered electron (BSE) detectors. SEM images, SEM-EDS results of the ash samples and the assessment of the results are given in Section 5.5.

4.7.4. Ash Fusion Temperatures

Ash fusion temperatures of fuel samples were determined by the accredited laboratory of in MRC-EI of TUBITAK according to the ASTM D 1857-04. Ashes for fuel samples were prepared according to the ASTM standards in Table 4.1. The ash samples are analyzed in the LECO AF700 Ash Fusion Determinator. The ash of each sample is then mixed with a solution of dextrin to form a stiff plastic mass. The plastic material is pressed with a spatula into a cone mold to form a triangular pyramid. The ash is removed from the cone mold and placed into a furnace. The shape of the cones is observed. The analyzer automatically monitors ash cone deformation temperatures in ash of fuel samples. Ash fusion temperatures, which are mentioned in the ASTM D 1857-04 standard, can automatically be determined with a camera sending images to software in a computer. The ash fusion temperatures (IT, ST, HT, and FT) are explained in detail in Section 2.2.2.3. Ash fusion temperatures for the fuel samples are given in Table 4.17.

Table 4.17 Ash fusion temperatures of fuel used in SET#4

	IT, ^{o}C	ST, ^{o}C	HT, ^{o}C	FT, ^{o}C
Bursa/Orhaneli	1281	1288	1302	1452
Denizli/Kale	1237	1306	1323	>1500
Olive Cake	1121	1323	1330	1349
Woodchips	1457	1490	1492	1497

CHAPTER 5

RESULTS AND DISCUSSION

5.1. Assessment of Experiments for SET#1

Eight experiments were conducted for SET#1 in order to determine the optimum excess air ratio (λ) for each experiment. Excess air ratio was defined as the ratio of air supplied for the combustion in excess of that theoretically required for complete combustion. During the experiment, the operational condition at which CO emission was minimum was decided to be optimum condition and λ at this condition was selected as optimum λ. The experiments included combustion of Bursa/Orhaneli lignite, combustion of olive cake, co-combustion of Bursa/Orhaneli lignite and olive cake fuel mixtures containing olive cake 10, 30, and 50% by weight and co-combustion of Bursa/Orhaneli lignite and woodchips fuel mixtures containing woodchips 10, 30, and 50% by weight. The total duration of each experiment was between 9 and 11 hours which included start-up, steady state period and shut-down. After the system reached the steady-state condition (approximately 5 hours after start-up), the emission measurements were started. The measurements were continuous and lasted until the shut-down period. In this section, only about 40 to 60 mins of emission measurements are presented in the figures to make the figures clear and easily readable.

5.1.1. Combustion of Bursa/Orhaneli Lignite (C1-1)

A combustion test of Bursa/Orhaneli lignite was performed in the Lab-CFBC. Fuel feeding rate was changed between 3.9 and 6.5 kg/h in order to see the effect of different excess air ratios on flue gas emissions. The lignite was fed into the combustor from a fuel hopper which is coded as FH-02. This fuel hopper was decided to be used for coal feeding. As the fuel feeding rate was changed, the thermal power of the system also changed between 13 and 21 kW. From the air given to the combustor and making necessary temperature correction, the superficial velocity was calculated in the range of 3.1-3.3 m/s at operational temperature.

Temperature Profile:
Temperature profiles along the combustor obtained for different excess air ratios (λ) during the experiment are given in Figure 5.1. The highest temperature along the combustor was measured at about 1.25 m above the distributor plate for excess air ratio less than 1.3 in the case of coal combustion. Among the excess air ratios, highest temperature profile was obtained as 860±3°C for excess air ratio of 1.05. As the fuel

feeding rate decreased, less fuel particles were available to meet with air and eventually to react with oxygen, and the excess air caused the combustor to cool down. While there was a 50°C temperature difference between the regions where the highest and the lowest temperatures measured along the combustor for the case of excess air ratio of 1.05, this difference dropped to 25°C by increasing excess air ratio up to 1.66. The highest and lowest temperatures for excess air ratio of 1.66 were 795±7°C and 770±5°C at 1.25 m and 5.8 m above the distributor plate, respectively.

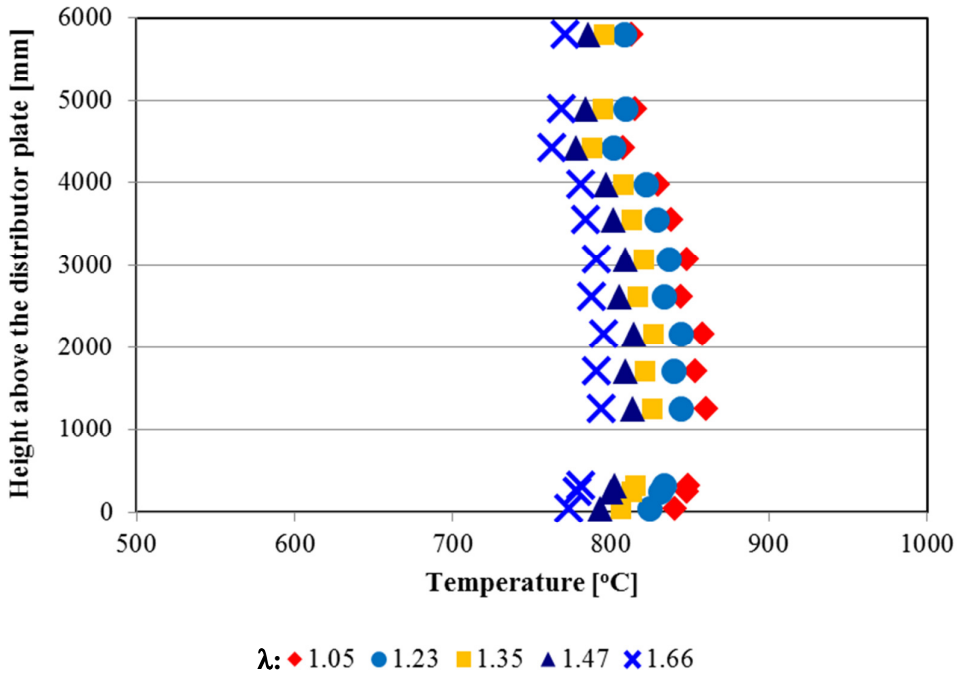

Figure 5.1 Temperature profile along the combustor for the combustion of Bursa/Orhaneli lignite (C1-1)

Temperature profiles along the return leg obtained for different λs are given in Figure 5.2. The highest temperature was measured at the bottom of the first cyclone (TT201 in Figure 4.2, TT201 on the return leg is located 4.7 m above the distributor plate). While it was about 782±1°C for λ = 1.05, it decreased down to 746±5°C for λ = 1.66. The average temperature at TT201 was 768±15°C during the whole test. The average temperature decreased throughout the return leg and reached to about 703±11°C during the whole test at the bottom of the return leg (TT204 in Figure 4.2, TT204 on the return leg is located 0.95 m above the distributor plate). High temperature observed along the return leg was an indicator of good circulation between the combustor and the return leg.

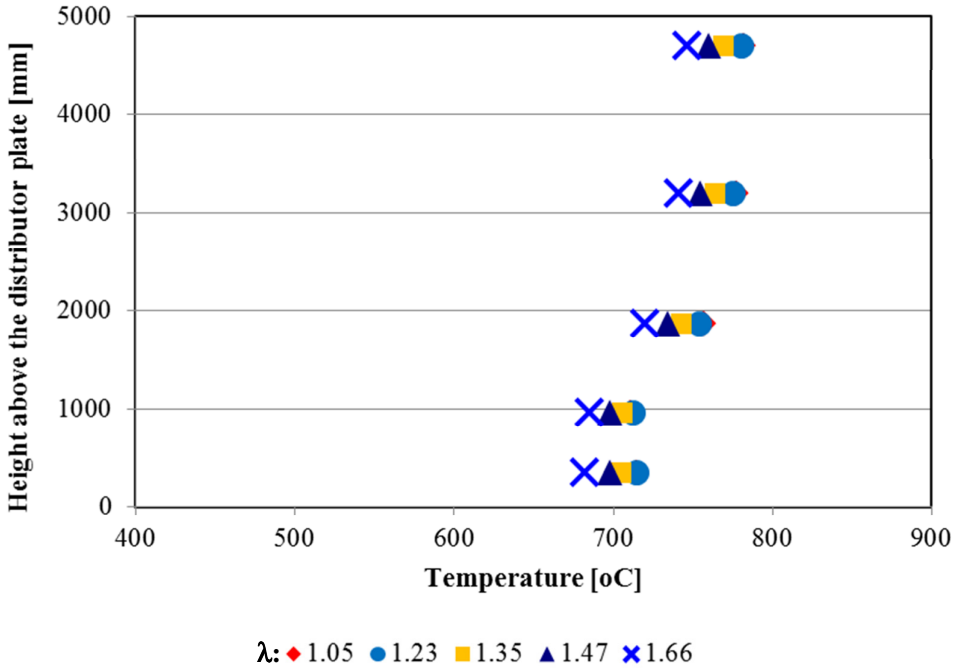

Figure 5.2 Temperature profile along the return leg for the combustion of Bursa/Orhaneli lignite (C1-1)

Emissions:

Effect of excess air ratio on CO, NO, and SO_2 emission in the flue gas is given in Figure 5.3. Concentrations of pollutants in the flue gas are presented in mg/Nm^3(on dry basis) at normal temperature (273 K) and pressure (1 atm) to be consistent with the regulations and they are based on 6 vol% O_2 in the flue gas as required in the Turkish Regulation ("Turkish Regulation for Industrial Air Pollution Control," 2009). Flue gas emissions presented here are 65 minutes of emission measurements during the steady state period of the experiment. The excess air ratio ranges between 1.05 and 1.66. While pollutant concentrations are given in primary y-axis, the average temperature of the dense phase (T_{dp}) is presented in secondary y-axis.

The air flowrate into the combustor was kept constant during the experiments in order not to change hydrodynamics of the combustion system. Therefore, the flue gas measurements at different excess air ratios were done by changing fuel feeding rate.

In Figure 5.3, it can be seen that T_{dp} decreased as the excess air ratio increased. When less fuel was given to the combustor in order to see the effect of higher excess air ratio on the emissions, excess air partly cooled down the combustor. This is why a decrease not only in the T_{dp} but also in the temperature of the whole system was observed. When the T_{dp} was 849±1°C for λ = 1.05, it decreased gradually and reached down to 780±1°C at λ = 1.66.

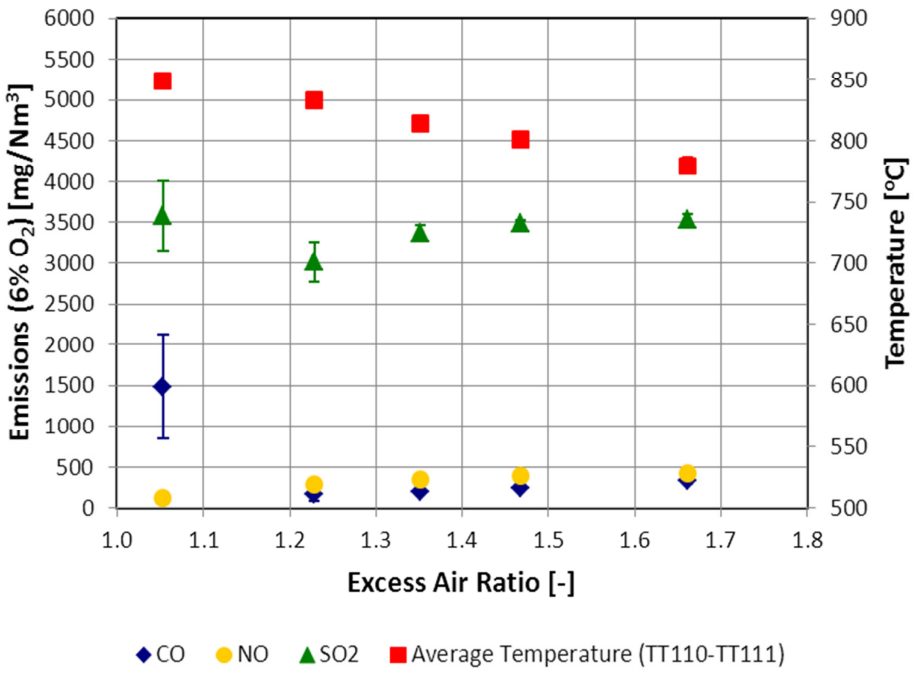

TT110 and TT111 are located 24 cm and 32 cm above the distributor plate, respectively.

Figure 5.3 Effect of excess air ratio on flue gas emissions for the combustion of Bursa/Orhaneli lignite (C1-1)

CO concentration decreased as the excess air ratio increased from 1.05 to 1.23. At λ = 1.23, CO emission reached its minimum value which was 173±80 mg/Nm^3, then, it showed a small increase with increasing excess air ratio. Further increase of excess air ratio leaded to cooling down of the combustor. This decrease on the overall combustor temperature slowed down the conversion of fuel carbon to CO_2 resulting in the formation of incomplete combustion product, CO. Temperature, contact time, and turbulence are very important parameters in order to sustain better combustion. CO is a measure of incomplete combustion. If it is high in concentration, this means that the three parameters mentioned above are not provided sufficiently. Although the maximum temperature was measured in the case of λ = 1.05, CO emission has reached the highest value at this excess air ratio. This may be explained by the lowest excess air ratio measured at that time. If there is not enough oxygen during combustion, a reducing atmosphere in the combustor is formed. Fuel particle cannot be completely burned and CO is formed.

NO emission increased as the excess air ratio increased. There is the general acceptance that volatile nitrogen compounds and nitrogen in char are more likely to be oxidized to NO in the abundance of O_2 (Afacan, 2005). While NO emission was 122±8 mg/Nm^3 at λ = 1.05, it increased up to 427±3 mg/Nm^3 with excess air ratio increasing to 1.66. Depending on the conditions in the combustor, there is a decrease in NO emission when there is less oxygen in the combustor. NO is reduced to N_2 via solid catalytic reactions if

there is reducing agents such as CO in the environment (Afacan, 2005). NO reduction over the char surface under reducing atmosphere was also mention in the study of Desroches-Ducarne et al. (1998). They reported two reactions responsible for NO reduction on the char surface and at high CO concentration. These two reactions are given in Rxn. 5.1 and Rxn. 5.2. The reaction of NO with CO happens on the char surface according to the Rxn. 5.2.

$NO + C \rightarrow 1/2N_2 + CO$ Rxn. 5.1

$NO + CO \rightarrow 1/2N_2 + CO_2$ Rxn. 5.2

The trend observed for CO emission was also valid for SO_2 emission. SO_2 emission was between 3000 and 3600 mg/Nm^3. While it was about 3585±427 mg/Nm^{3}at λ = 1.05, it dropped down to 3022±246 mg/Nm^3 at λ = 1.23, then it showed a slight increase again as the excess air ratio increased. It finally reached 3531±78 mg/Nm^3 at λ = 1.66. These results might be due to some experimental fluctuations.

For the combustion of Bursa/Orhaneli lignite, it can be seen from Figure 5.3 that the optimum operational condition of excess air ratio was around 1.2 in order to get minimum flue gas emissions. In this operational condition, CO emission was 173±80 mg/Nm^3, NO emission was 292±34 mg/Nm^3, and SO_2 emission was 3022±246 mg/Nm^3. According to the emission limits in the Turkish Regulation ("Turkish Regulation for Industrial Air Pollution Control," 2009) given in Table 2.2, CO and NO emissions were under the limits which are 200 mg/Nm^3 for CO emission and 800 mg/Nm^3 for NO emission. SO_2 emission was above the limit which is 2000 mg/Nm^3. In order to decrease SO_2 emission, limestone addition was needed and this was studied in the scope of SET#3.

Addition to the ABB-AO 2000 flue gas analyzer (Gas Analyzer-1), GASMET-DX 4000 flue gas analyzer (Gas Analyzer-2) was also used for the emission measurement of the flue gas in order to double check the emission measurements. The major pollutant (CO, NO, and SO_2) emissions in the flue gas obtained with ABB-AO 2000 and GASMET-DX 4000 flue gas analyzers are given in Figure 5.3 and Figure 5.4, respectively. When these emissions are compared each other, it can be seen that both measurements are quite similar. Therefore, emission data from GASMET-DX 4000 flue gas analyzer have not been used throughout the text to prevent the duplication of the emission data. All the emission data presented in the text are measured by ABB-AO 2000 flue gas analyzer unless otherwise stated.

In addition to NO, CO, and SO_2 emissions; N_2O, NO_2, NH_3, CH_4, C_2H_4, C_2H_6, C_3H_8, $C_6H_{14,}$ CHOH, HCl, HF, and HCN emissions were measured with GASMET-DX 4000 flue gas analyzer and they are given in Figure 5.4 below. There were no NO_2, NH_3, C_2H_6, C_3H_8, $C_6H_{14,}$ CHOH, HCl, and HF emissions in the flue gas during the combustion of Bursa/Orhaneli lignite. While a small amount of CH_4 and C_2H_4 were measured at excess air ratio less than 1.1, they disappeared with a further increase of excess air ratio. N_2O and its precursor, HCN, emissions increased slightly with increasing excess air ratio. Both emissions were also less in concentration when compared to NO emissions. Therefore, all

the other pollutants, except major ones (CO, NO, SO_2), have not be presented in the scope of the thesis. Although N_2O is one of the important greenhouse gases, it is not given in the emission figures due to its low concentration in the flue gas. In addition to that, there is no emission limit for N_2O specified in the Turkish Regulation ("Turkish Regulation for Industrial Air Pollution Control," 2009).

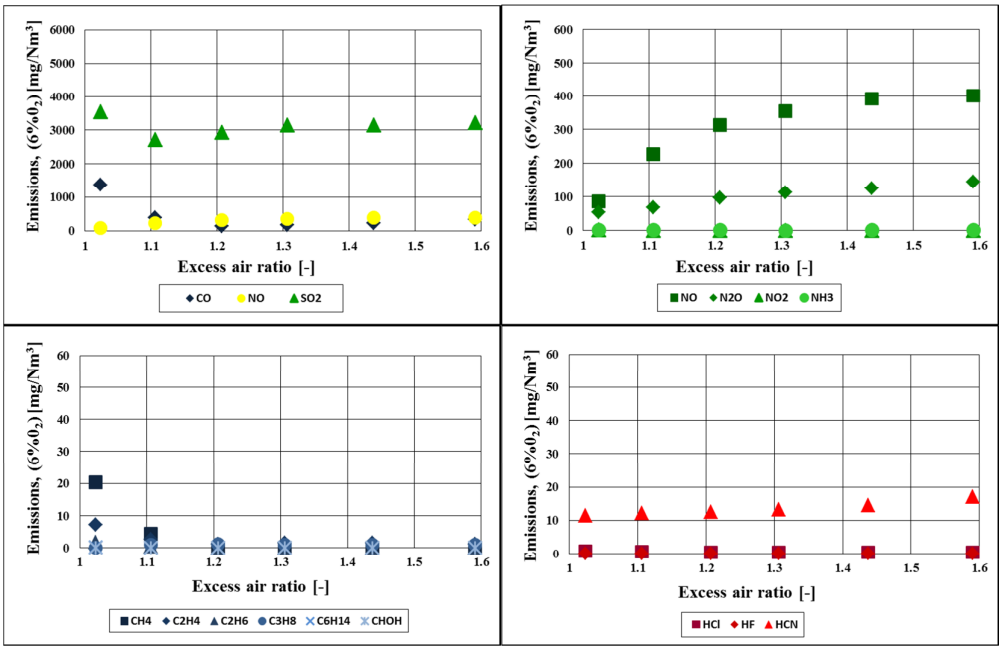

Figure 5.4 Emissions measured by Gas Analyzer-2 with respect to excess air ratio for the combustion of Bursa/Orhaneli lignite (C1-1)

5.1.2. Co-Combustion of Bursa/Orhaneli Lignite with 10% (by wt.) Olive Cake (C1-B1-1)

For the co-combustion experiment of Bursa/Orhaneli lignite with 10% (by wt.) olive cake (OC), fuel feeding rate is changed between 4.2 and 7.6 kg/h. For the co-combustion of Bursa/Orhaneli lignite and olive cake in the tests of SET#1, the Bursa/Orhaneli lignite was fed into the combustor from the fuel hopper (FH-02) and olive cake was fed from the fuel hopper (FH-01). The thermal power of the system was between 14 and 26 kW. The superficial velocity was calculated in the range of 3.2-3.3 m/s.

Temperature Profile:

Temperature profiles along the combustor obtained for λs during the experiment are given in Figure 5.5. While the highest temperature along the combustor was measured at about 1.25 m above the distributor plate for excess air ratios less than 1.4, the highest

temperatures were measured at about 2.16 m above the distributor plate by increasing excess air ratio. Among the excess air ratios, highest temperature profile was obtained for the case of λ = 1.15. While there was a difference of 65°C between the regions where the highest and the lowest temperatures measured along the combustor for the case of λ = 1.04, this difference dropped to 25°C by increasing excess air ratio up to 1.75.

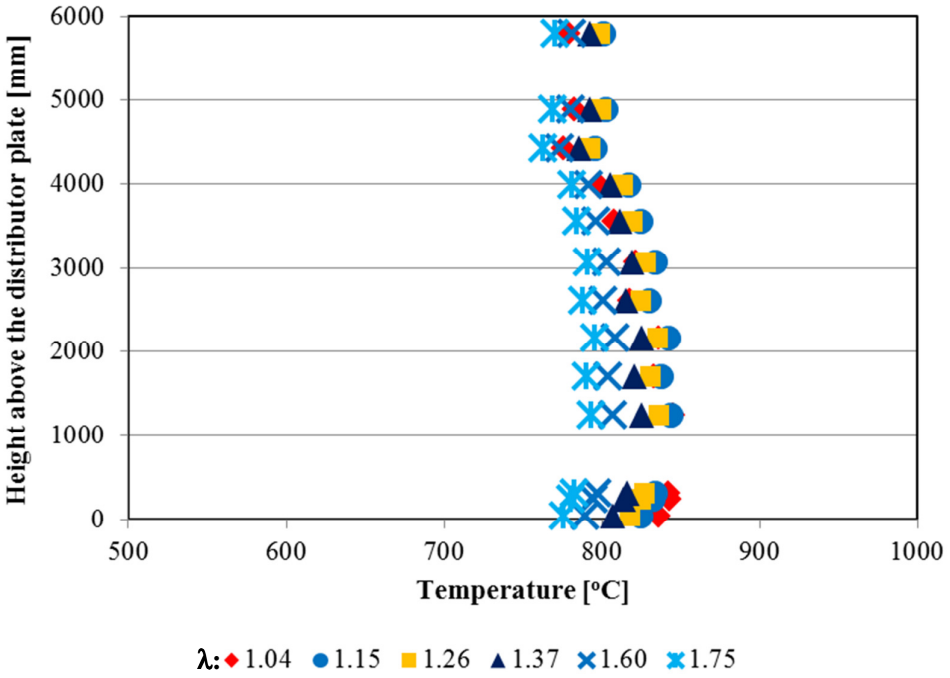

Figure 5.5 Temperature profile along the combustor for the co-combustion of Bursa/Orhaneli lignite with 10% (by wt.) olive cake (C1-B1-1)

Temperature profiles along the return leg obtained for different λs are given in Figure 5.6. While the highest temperature at TT201 was about 779±1°C for λ = 1.15, it decreased down to 751±2°C for λ = 1.75.

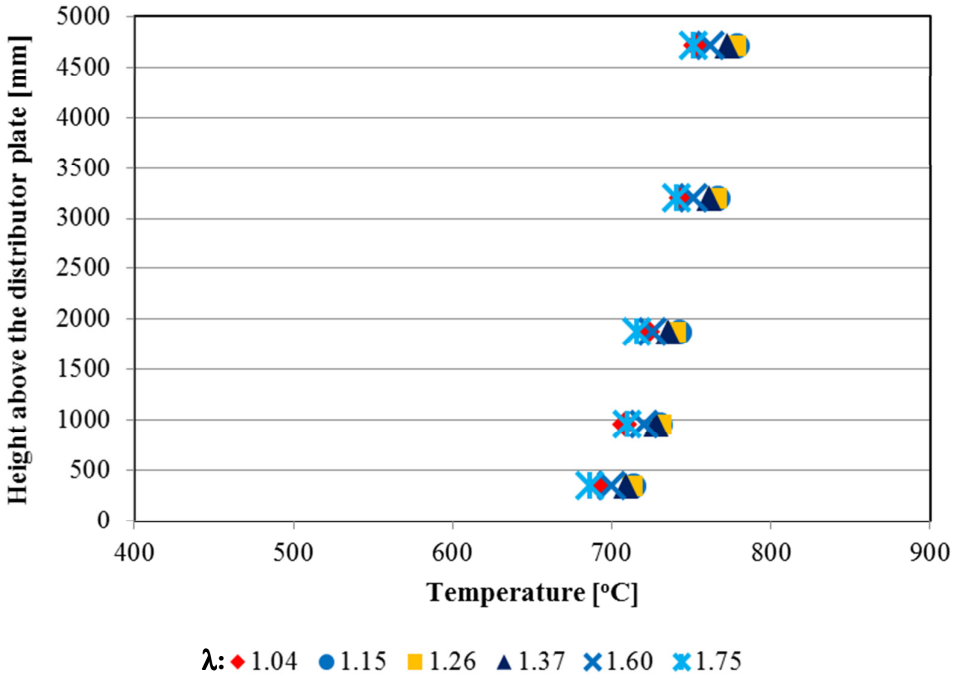

Figure 5.6 Temperature profile along the return leg for the co-combustion of Bursa/Orhaneli lignite with 10% (by wt.) olive cake (C1-B1-1)

Emissions:

Excess air ratio ranged between 1.04 and 1.75. Effect of excess air ratio on CO, NO, and SO_2 emission in the flue gas is given in Figure 5.7. The total duration of emission measurement was 70 minutes. Emissions presented in Figure 5.7, are 45 minutes of emission measurements during the steady state period of the experiment because of the reason stated in the beginning of the section. When dense phase temperature was 843°C for the excess air ratio of 1.04, it decreased gradually and reached down to 782±2°C at λ = 1.75.

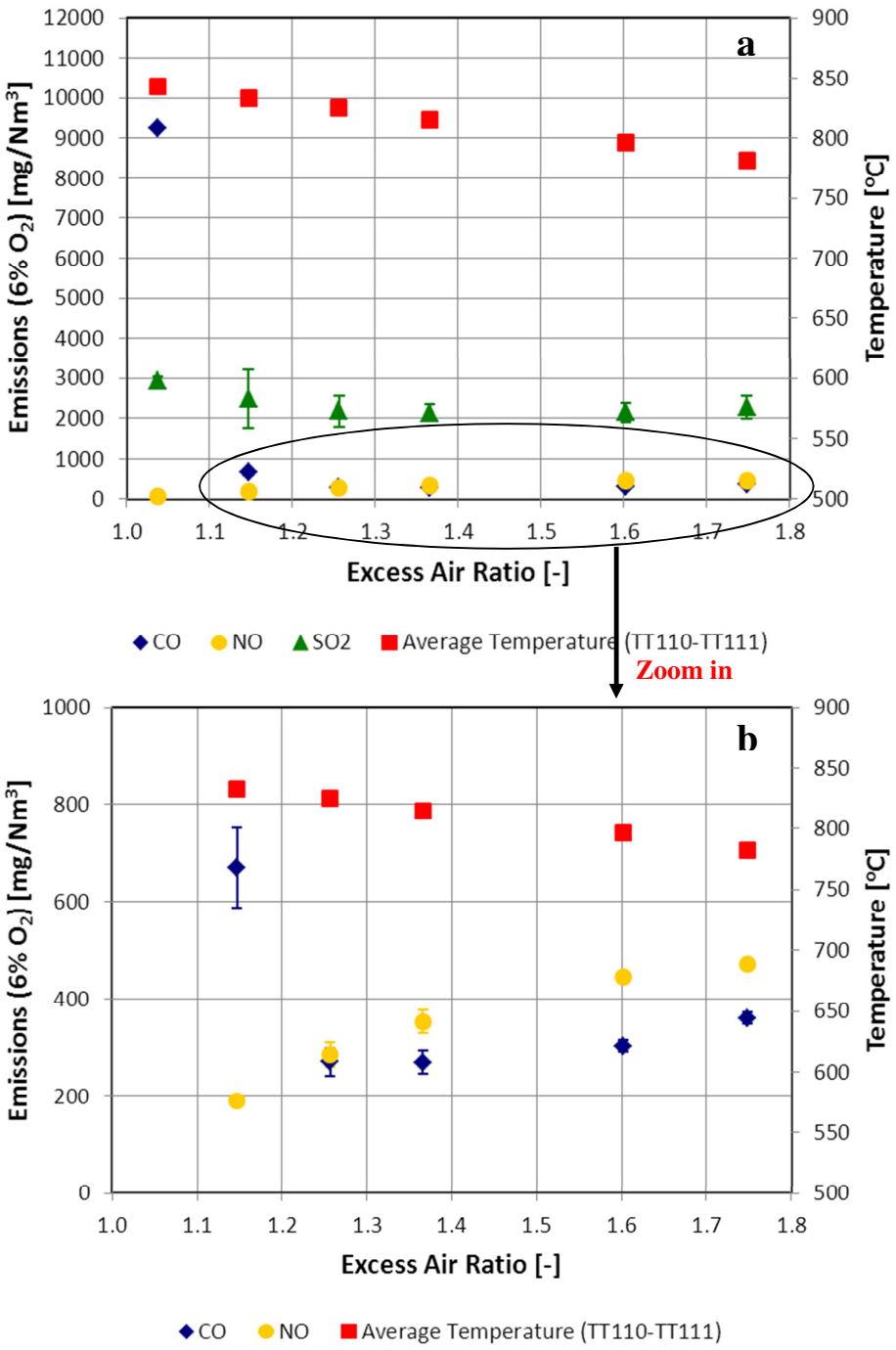

TT110 and TT111 are located 24 cm and 32 cm above the distributor plate, respectively.

Figure 5.7 Effect of excess air ratio on flue gas emissions for the co-combustion of Bursa/Orhaneli lignite with 10% (by wt.) olive cake (C1-B1-1); a-) original figure, b-) enlarged view

With the addition of 10% olive cake (by wt.) to the fuel mixture, CO emission tremendously increased from 1487±642 mg/Nm^3 to 9257±10 mg/Nm^3 at the same excess air ratios of about 1.0. While CO emission was measured as 9257±10 mg/Nm^3 at λ = 1.04, it rapidly decreased as the excess air ratio increased up to 1.37. Since CO and NO emissions are overlapped in Figure 5.7(a), these emissions are redrawn in Figure 5.7(b) excluding the first points. This figure is more useful to see the low emission values. As can be seen from Figure 5.7(b), the lowest CO emission was measured 270±29 mg/Nm^3 at λ = 1.37. Further increase of excess air ratio cooled the combustor and caused CO emission to increase. The cooling effect of excess air on temperature which was followed by high CO emission was also stated by the study of Madhiyanon et al. (2010) investigating combustion of rice-husk.

NO emission increased as the excess air ratio increased. While NO emission was 80±2 mg/Nm^3 at λ = 1.04, it increased up to 471±10 mg/Nm^{3}at λ = 1.75. This increase in NO concentrations is attributed to decrease in the CO concentrations and decrease of the reducing environment for NO. As it was stated in the study of Xie et al. (2007) that NO emission increased with the excess air ratio for the co-combustion of 22% (by wt.) rice husk with coal and it was seen that CO emission decreased with the excess air ratio. The lower NO emission measured at excess air less than 10% was attributed to the presence of char and high CO concentration.

SO_2 emission decreased with excess air ratio until λ equals to 1.37 simply due to dilution effect. When it was 2944±96 mg/Nm^3 at λ = 1.04, it dropped to 2143±220 mg/Nm^3 at λ = 1.37, then, it showed a slight increase with the excess air ratio. It finally reached 2287±281 mg/Nm^3 at λ = 1.75.

For the co-combustion experiment of Bursa/Orhaneli lignite with 10% (by wt.) olive cake, it can be seen from Figure 5.7 that the optimum operational condition of excess air ratio was around 1.37 in order to get minimum CO emission. In this operational condition, CO emission was 270±29 mg/Nm^3, NO emission was 353±24 mg/Nm^3, and SO_2 emission was 2143±220 mg/Nm^3. According to the emission limits in the Turkish Regulation ("Turkish Regulation for Industrial Air Pollution Control," 2009) given in Table 5.4, CO and SO_2 emissions are above the limits which are 230 mg/Nm^3 for CO emission and 1787 mg/Nm^3 for SO_2 emission. NO emission is below the limit which is 505 mg/Nm^3. In order to decrease SO_2 emission, limestone addition is needed and this was studied in the scope of SET#3.

5.1.3. Co-Combustion of Bursa/Orhaneli Lignite with 30% (by wt.) Olive Cake (C1-B1-2)

For the co-combustion experiment of Bursa/Orhaneli lignite with 30% (by wt.) olive cake, fuel feeding rate was changed between 3.6 and 5.7 kg/h. The thermal power of the system was between 13 and 20 kW. The superficial velocity was calculated as 3.2 m/s during the experiment.

Temperature Profile:

Temperature profiles along the combustor obtained for λs during the experiment are given in Figure 5.8. While the highest temperature along the combustor was measured at about 1.25 m above the distributor plate for excess air ratios less than 1.6, the highest temperatures were measured at about 2.16 m above the distributor plate by increasing excess air ratio. Among the excess air ratios, highest temperature profile was obtained for the case of λ = 1.07. While there was a difference of 58°C between the regions where the highest and the lowest temperatures measured along the combustor for the case of λ = 1.07, this difference dropped to 30°C by increasing excess air ratio up to 1.84.

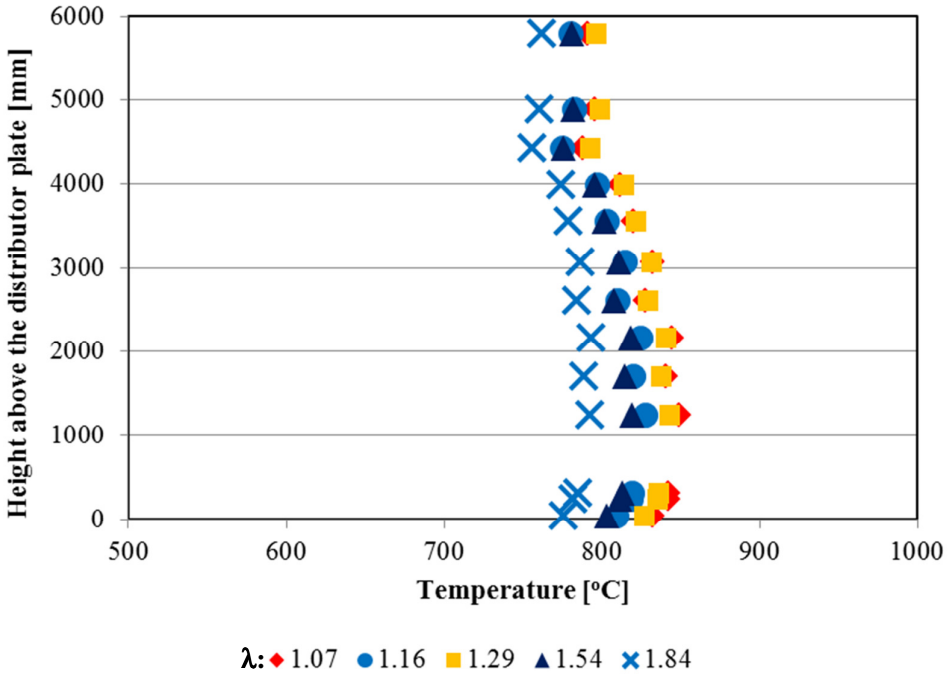

Figure 5.8 Temperature profile along the combustor for the co-combustion of Bursa/Orhaneli lignite with 30% (by wt.) olive cake (C1-B1-2)

Temperature profiles along the return leg obtained for different λs are given in Figure 5.9. While the highest temperature at the bottom of the first cyclone was about 773±3°C for λ = 1.29, it decreased down to 739±6°C for λ = 1.84.

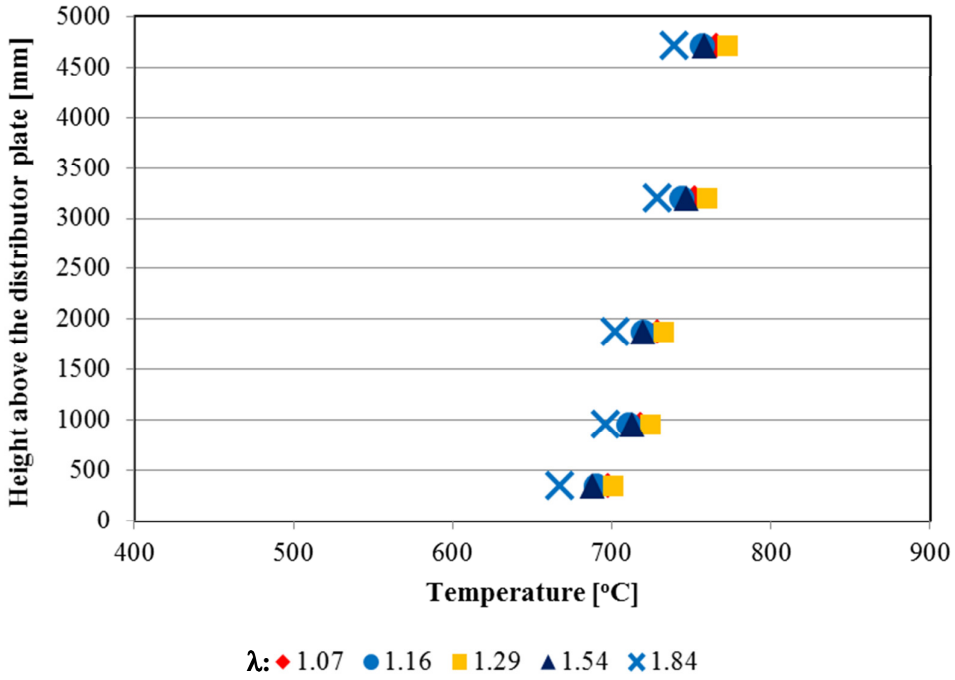

Figure 5.9 Temperature profile along the return leg for the co-combustion of Bursa/Orhaneli lignite with 30% (by wt.) olive cake (C1-B1-2)

Emissions:

Excess air ratio ranged between 1.07 and 1.84. Effect of excess air ratio on CO, NO, and SO_2 emission in the flue gas is given in Figure 5.10. The total duration of emission measurement was 68 minutes. Emissions presented in Figure 5.10 are 54 minutes of emission measurements during the steady state period of the experiment because of the reason stated in the beginning of the section. When dense phase temperature was 842°C for the excess air ratio of 1.07, it decreased gradually and reached down to 783±2°C at λ = 1.84.

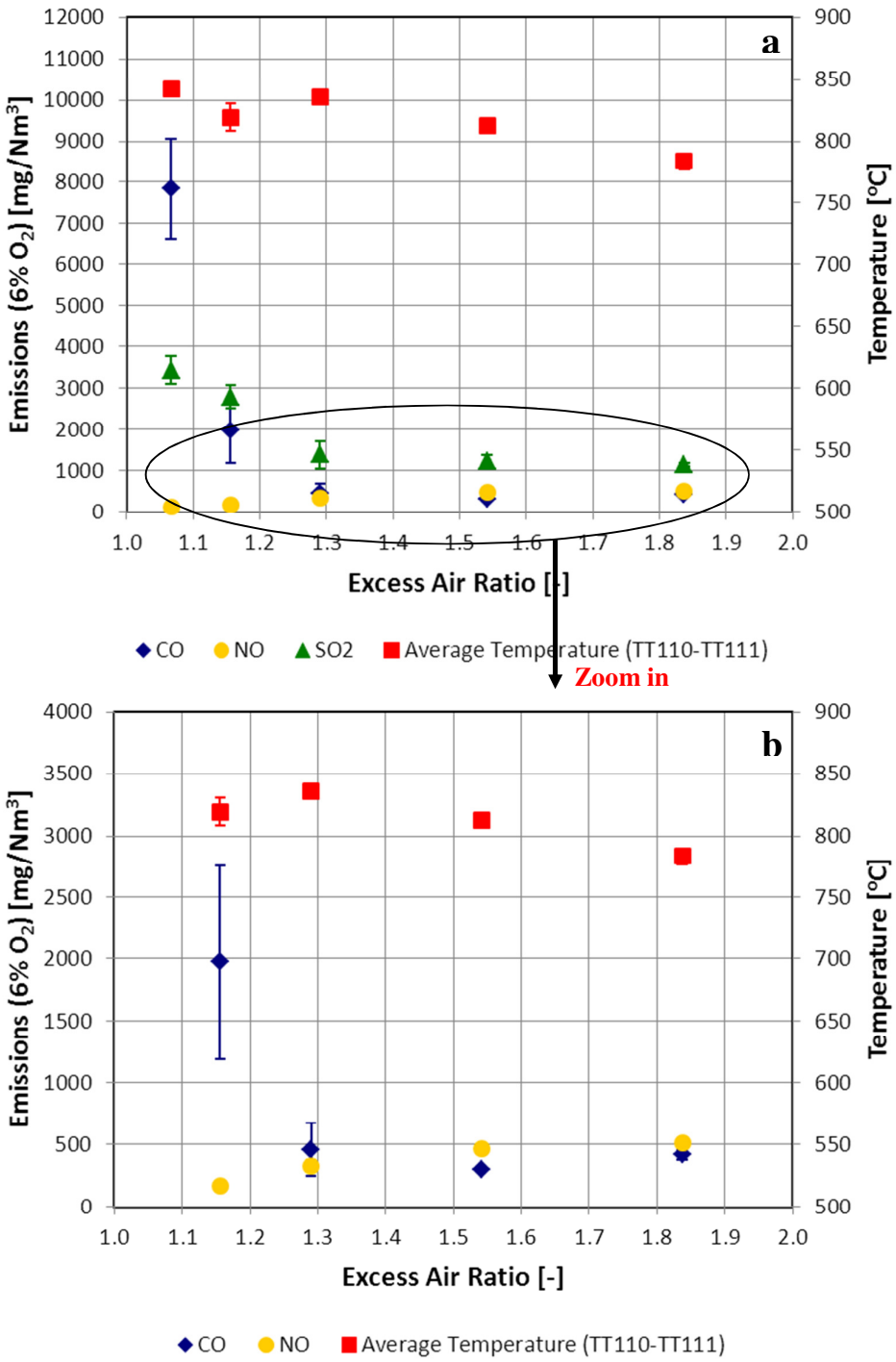

TT110 and TT111 are located 24 cm and 32 cm above the distributor plate, respectively.

Figure 5.10 Effect of excess air ratio on flue gas emissions for the co-combustion of Bursa/Orhaneli lignite with 30% (by wt.) olive cake (C1-B1-2); a-) original figure, b-) enlarged view

The maximum CO emission was measured as 7852±1207 mg/Nm^3 at λ = 1.07. Although the maximum temperatures were measured below excess air ratio of 1.1, CO emission has reached the highest values at these excess air ratios. This may be due to the fact that there was not enough oxygen in the combustor for complete combustion. Increasing excess air ratio up to 1.54 lowered CO emissions. The lowest CO emission was 297±18 mg/Nm^3 and it was obtained when excess air ratio was 1.54. Further increase of excess air ratio cooled the combustor and caused CO emission to increase. "Temperature, contact time, and turbulence (3T's)" are important parameters in order to sustain better combustion. CO is a measure of incomplete combustion. If it is high in concentration, this means that the three parameters mentioned above are not provided sufficiently.

NO emission increased with excess air ratio like in the C1-B1-1. While NO emission was 108±5 mg/Nm^3 at λ = 1.07, it increased up to 508±17 mg/Nm^3 at λ = 1.84. SO_2 emission decreased with excess air ratio. When it was 3435±328 mg/Nm^{3}at λ = 1.07, it dropped to 1145±49 mg/Nm^3 at λ = 1.84.

For the co-combustion experiment of Bursa/Orhaneli lignite with 30% (by wt.) olive cake, it can be seen from Figure 5.10 that the optimum operational condition of excess air ratio was around 1.54 in order to get minimum CO emission. In this operational condition, CO emission was 297±18 mg/Nm^3, NO emission was 464±12 mg/Nm^3, and SO_2 emission was 1226±152 mg/Nm^3. According to the emission limits in the Turkish Regulation ("Turkish Regulation for Industrial Air Pollution Control," 2009) given in Table 5.4, NO and SO_2 emissions are under the limits which are 479 mg/Nm^3 for NO emission and 1386 mg/Nm^3 for SO_2 emission. CO emission is above the limit which is 288 mg/Nm^3.

5.1.4. Co-Combustion of Bursa/Orhaneli Lignite with 50% (by wt.) Olive Cake (C1-B1-3)

For the co-combustion experiment of Bursa/Orhaneli lignite with 50% (by wt.) olive cake, fuel feeding rate was changed between 3.7 and 5.7 kg/h. The thermal power was between 14 and 21 kW. The superficial velocity was calculated in the range of 3.1-3.2 m/s during the experiment.

Temperature Profile:

Temperature profiles along the combustor obtained for different λs during the experiment are given in Figure 5.11. The highest temperature along the combustor was measured at about 1.25 m above the distributor plate for all excess air ratios. Among the excess air ratios, highest temperature profile was obtained for the case of λ = 1.1. While there was a difference of 70^{o}C between the regions where the highest and the lowest temperatures measured along the combustor for the case of λ = 1.06, this difference dropped to 50^{o}C by increasing excess air ratio up to 1.66. As the percentage of olive cake in the fuel mixture increased, the temperature difference along the combustor decreased regardless of excess air ratio. This may be explained with high volatile matter content of olive cake. As the amount of olive cake increased in the fuel mixture, volatile matter of the fuel

mixture also increased. Volatile content of the olive cake mainly burned in the upper part of the combustor increasing the temperature of this part.

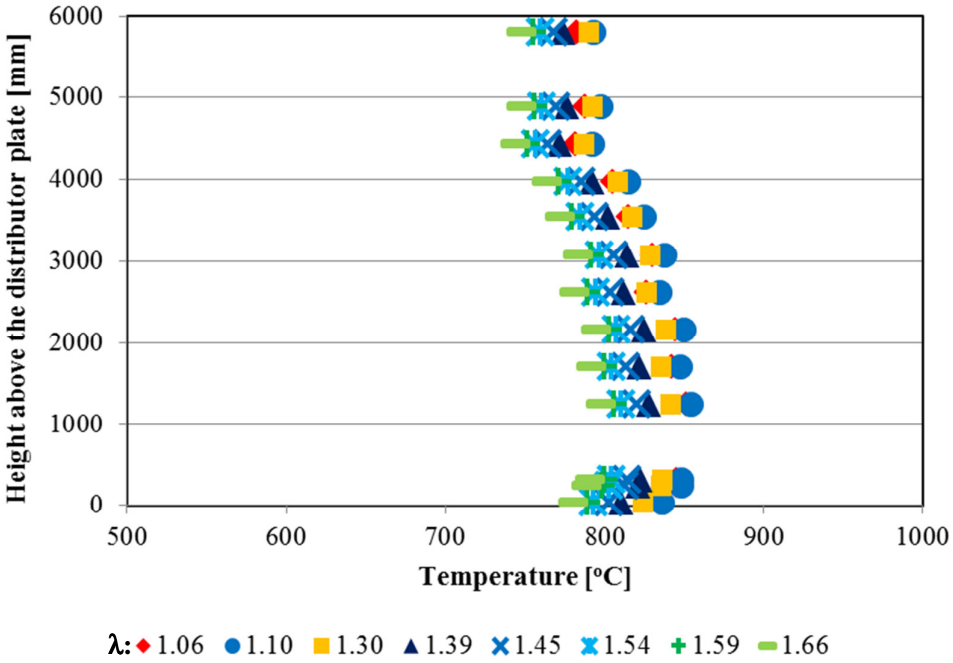

Figure 5.11 Temperature profile along the combustor for the co-combustion of Bursa/Orhaneli lignite with 50% (by wt.) olive cake (C1-B1-3)

Temperature profiles along the return leg obtained for different λs are given in Figure 5.12. While the highest temperature at the bottom of the first cyclone was about 766±2°C for λ = 1.1, it decreased down to 719±3°C for λ = 1.66.

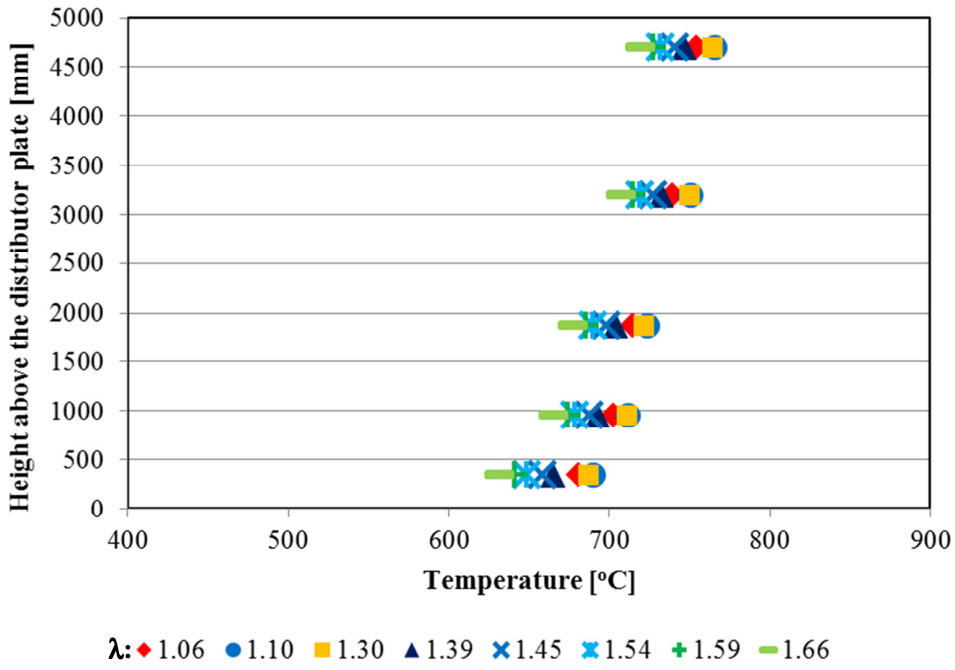

Figure 5.12 Temperature profile along the return leg for the co-combustion of Bursa/Orhaneli lignite with 50% (by wt.) olive cake (C1-B1-3)

Emissions:

Excess air ratio ranged between 1.06 and 1.66. Effect of excess air ratio on CO, NO, and SO_2 emission in the flue gas is given in Figure 5.13. The total duration of emission measurement was 123 minutes. Emissions presented in Figure 5.13 are 62 minutes of emission measurements during the steady state period of the experiment because of the reason stated in the beginning of the section. When dense phase temperature was 848°C for the excess air ratio of 1.1, it decreased gradually and reached down to 790±2°C at λs = 1.66.

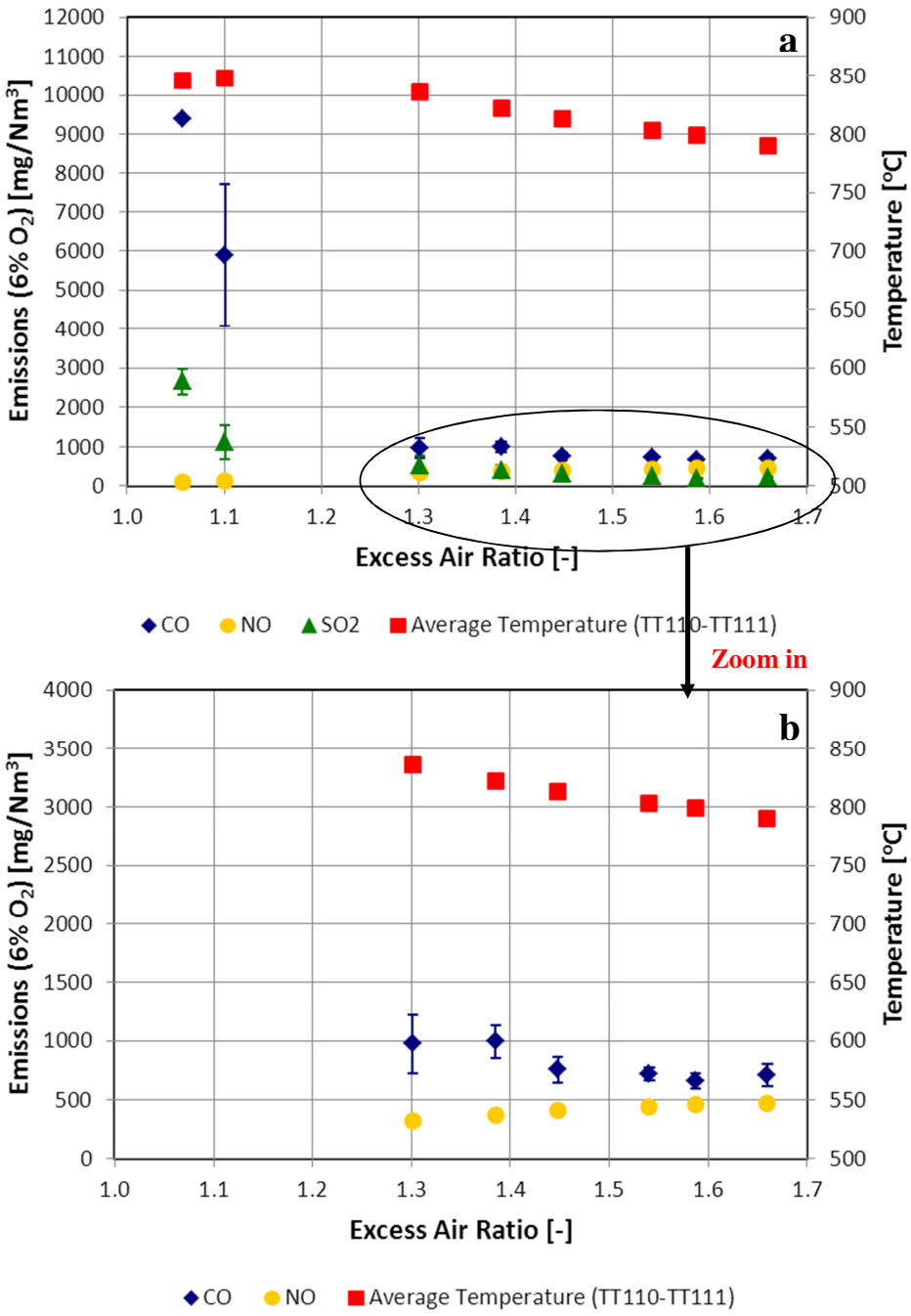

TT110 and TT111 are located 24 cm and 32 cm above the distributor plate, respectively.

Figure 5.13 Effect of excess air ratio on flue gas emissions for the co-combustion of Bursa/Orhaneli lignite with 50% (by wt.) olive cake (C1-B1-3); a-) original figure, b-) enlarged view

While CO emission was measured as 9405±48 mg/Nm^3 at λ = 1.06, it rapidly decreased as the excess air ratio increased up to 1.59. As can be seen from Figure 5.13(b), the lowest CO emission was 660±69 mg/Nm^3 when excess air ratio was 1.59. Further increase of excess air ratio cooled the combustor and caused CO emission to increase. NO emission increased as the excess air ratio increased. While NO emission was 111±2 mg/Nm^3 at λ = 1.06, it increased up to 472±6 mg/Nm^3 at λ = 1.66. SO_2 emission decreased with excess air ratio. When it was 2664±327 mg/Nm^{3}at λ = 1.06, it dropped to 194±8 mg/Nm^3 at λ = 1.59.When excess air ratio increased to 1.66, SO_2 emission increased a little and reached 230±11 mg/Nm^3.

For the co-combustion experiment of Bursa/Orhaneli lignite with 50% (by wt.) olive cake, it can be seen from Figure 5.13 that the optimum operational condition of excess air ratio was around 1.59 in order to get minimum CO emission. In this operational condition, CO emission was 660±69 mg/Nm^3, NO emission was 458±9 mg/Nm^3, and SO_2 emission was 194±8 mg/Nm^3. According to the emission limits in the Turkish Regulation ("Turkish Regulation for Industrial Air Pollution Control," 2009) given in Table 5.4, CO and NO emissions are above the limits which are 342 mg/Nm^3 for CO emission and 454 mg/Nm^3 for NO emission. SO_2 emission is under the limit which is 1015 mg/Nm^3.

5.1.5. Combustion of Olive Cake (B1-1)

A combustion test with olive cake only was performed by changing the fuel feeding rate between 3.5 and 4.7 kg/h. Olive cake was fed into the combustor from a fuel hopper which is coded as FH-01. As the fuel feeding rate is changed, the thermal power of the system also changed between 15 and 19 kW. The superficial velocity was calculated to be 2.7 m/s during the experiment.

Temperature Profile:
Temperature profiles along the combustor obtained for different λs during the experiment are given in Figure 5.14. The highest temperature was measured at about 1.25 m above the distributor plate for all excess air ratios. Temperature decreased after 1.25 m along the combustor. Among the excess air ratios, highest temperature profile was obtained for the case of λ = 1.13. As the fuel feeding rate decreases, less fuel particles were available to meet with air and eventually to react with oxygen, and the excess air caused the combustor to cool down. While temperature difference along the combustor was 70^{o}C for the case of λ = 1.11, it dropped down to 55^{o}C by increasing excess air ratio up to 1.78 due to the better mixing and turbulence. Since the VM content of the olive cake was much higher than the Bursa/Orhaneli lignite (60% vs. 34.4% in Table 4.2), the temperature increase in the upper part of the combustor became more distinct than coal.

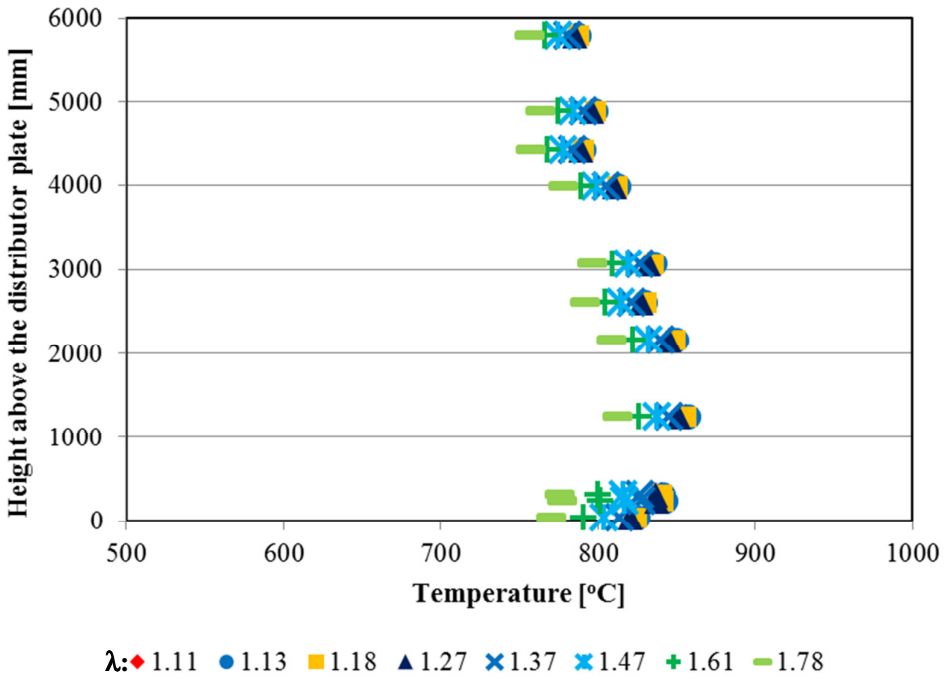

Figure 5.14 Temperature profile along the combustor for the combustion of olive cake (B1-1)

Temperature profiles along the return leg obtained for different λs are given in Figure 5.15. As observed in the experiment C1-1, the highest temperature was measured at TT201. While it was 766°C for λ = 1.11, it decreased down to 717±3°C for λ = 1.78. The temperature at the connection between return leg and the combustor (TT205 in Figure 4.2, TT205 on the return leg is located 35 cm above the distributor plate) was about 566±19°C which was quite less than the temperature for C1-1 test (703±13°C). Lower temperature measured in this region might be a result of doing this experiment at lower superficial velocity. While it was 2.7 m/s for the case of olive cake combustion, it was between 3.1 and 3.2 m/s for the case of Bursa/Orhaneli lignite combustion. Operating the system at lower velocity might cause lower circulation rate. It was tried many times to operate the system at higher velocities but it could not be accomplished probably due to lower density of olive cake than the lignite.

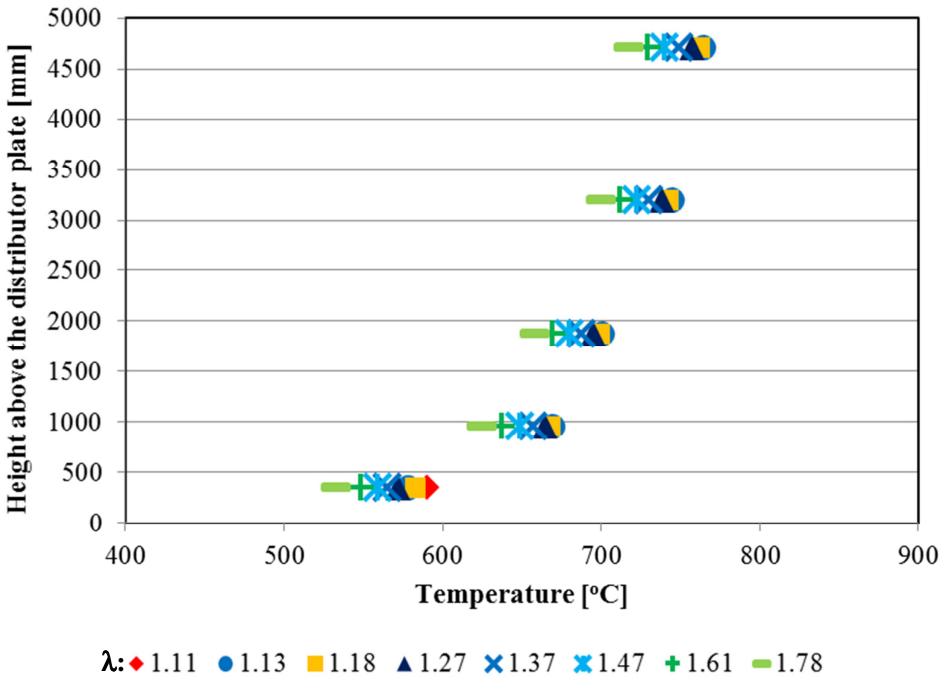

Figure 5.15 Temperature profile along the return leg for the combustion of olive cake (B1-1)

Emissions:

Excess air ratio ranged between 1.11 and 1.78. Effect of excess air ratio on CO, NO, and SO_2 emission is given in Figure 5.16. The total duration of experiments during emission measurement was 43 minutes. Emissions presented in Figure 5.16 are 39 minutes of emission measurements during the steady state period of the experiment because of the reason stated in the beginning of the section. It can be seen that the temperature of the dense phase decreased as the excess air ratio increased. This is a general trend observed in the combustion system. When dense phase temperature was 841±1°C for the excess air ratio of 1.11, it decreased gradually and reached down to 777±1°C at $\lambda = 1.78$.

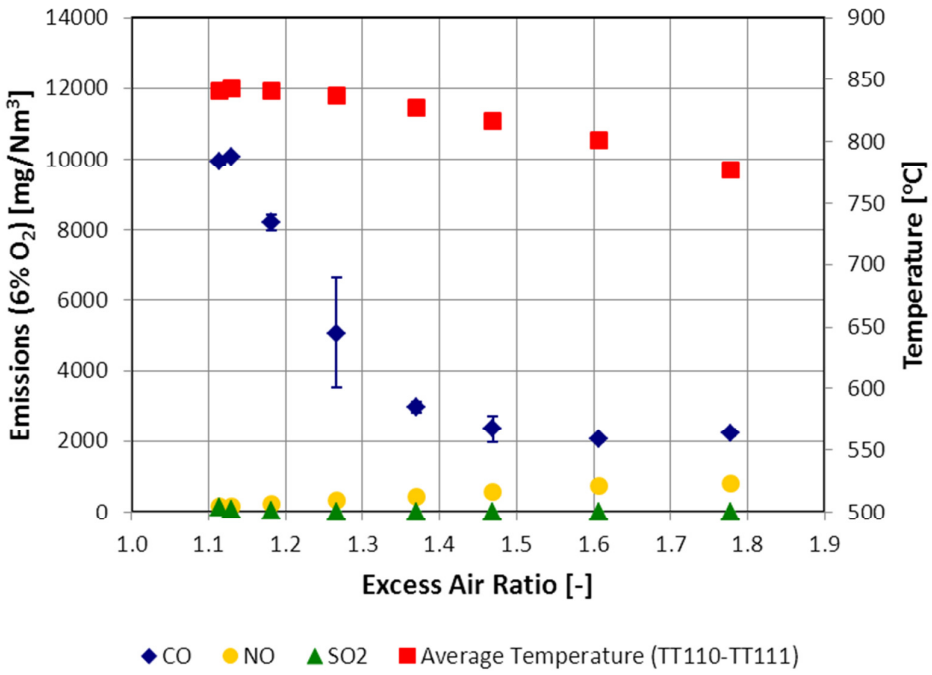

TT110 and TT111 are located 24 cm and 32 cm above the distributor plate, respectively.

Figure 5.16 Effect of excess air ratio on flue gas emissions for the combustion of olive cake (B1-1)

While the highest CO emission was around 1500 mg/Nm^3 for the combustion of Bursa/Orhaneli lignite at λ = 1.1, it rose up 10 000 mg/Nm^3 in the case of olive cake combustion. Moreover, it did not drop below 2000 mg/Nm^3 for all excess air ratios. The high concentration of CO was due to the higher volatile matter content of olive cake (60% by wt.) than Bursa/Orhaneli lignite (34.4% by wt.) and escape of some organic material without complete combustion (oxidation) from the combustion column. When the olive cake particles entered into the combustor, volatiles were quickly released due to the fast heating of the particles and they escaped from the combustor as incomplete combustion products like CO or hydrocarbons. The residence time of an olive cake particle in the combustor was about 2 sec and it was not enough to contact and to react with sufficient oxygen. This might be the reason of high CO emission. CO emission decreased as excess air ratio increased. The lowest CO emission was 2059±94 mg/Nm^3 at λ = 1.61. Further increase of excess air ratio caused CO emission to increase because of the cooling effect of the excess air. Therefore, the combustion of biomass and biomass-coal mixtures in CFBC should be done carefully.

NO emission showed a continuously increasing trend. While NO emission was 159±2 mg/Nm^3 at λ = 1.11, it increased up to 804±40 mg/Nm^3 in the case of λ = 1.78 because of the sudden decrease of the CO concentration with the excess air ratio. With olive cake combustion, less char are formed due to the different structure of olive cake than lignite

coal. Therefore, NO reduction in the presence of char particles in this case is definitely low and NO emissions are more in olive cake combustion.

Olive cake did not contain sulfur. Therefore, zero SO_2 emission was measured during the experiment.

For the combustion of olive cake, the optimum operational condition of excess air ratio was around 1.6 according to the CO emission. CO emission was 2065±94 mg/Nm^3, at this excess air ratio. NO emission was 725±62 mg/Nm^3, and SO_2 emission was zero. According to the emission limits in the Turkish Regulation ("Turkish Regulation for Industrial Air Pollution Control," 2009) given in Table 5.4, SO_2 emission is below the limit which is 200 mg/Nm^3.NO and CO emission are above the limits which are 400 mg/Nm^3 for NO emission and 460 mg/$Nm^3$for CO emission.

The major pollutant concentrations (CO, NO, and SO_2) in the flue gas measured by the Gas Analyzer-2 were given before for the combustion of Bursa/Orhaneli lignite in Section 5.1.1 to compare them with the ones measured by the Gas Analyzer-1. The comparison was repeated for the combustion of olive cake in this section. CO, NO, and SO_2 emissions were measured by GASMET-DX 4000 flue gas analyzer and they are given in Figure 5.17. When CO, NO, and SO_2 emissions presented in Figure 5.16 are compared to the emissions measured by the GASMET-DX 4000 flue gas analyzer in Figure 5.17, it can be seen that they have same emission profiles and emission values are similar each other.

Other pollutants were also presented in Figure 5.17. All the emissions except CO and NO measured by GASMET- DX 4000 flue gas analyzer were less than 35 mg/Nm^3 at excess air ratio above 1.2 for the combustion of olive cake as can be seen in Figure 5.17. It is practical to operate the combustor at excess air ratio less than 1.2 for a long time due to the high CO formation. Therefore, as can be stated in the case of Bursa/Orhaneli lignite combustion in Section 5.1.1, all the pollutants except CO, NO, and SO_2 can be ignored. That is why only major emissions are discussed throughout the text.

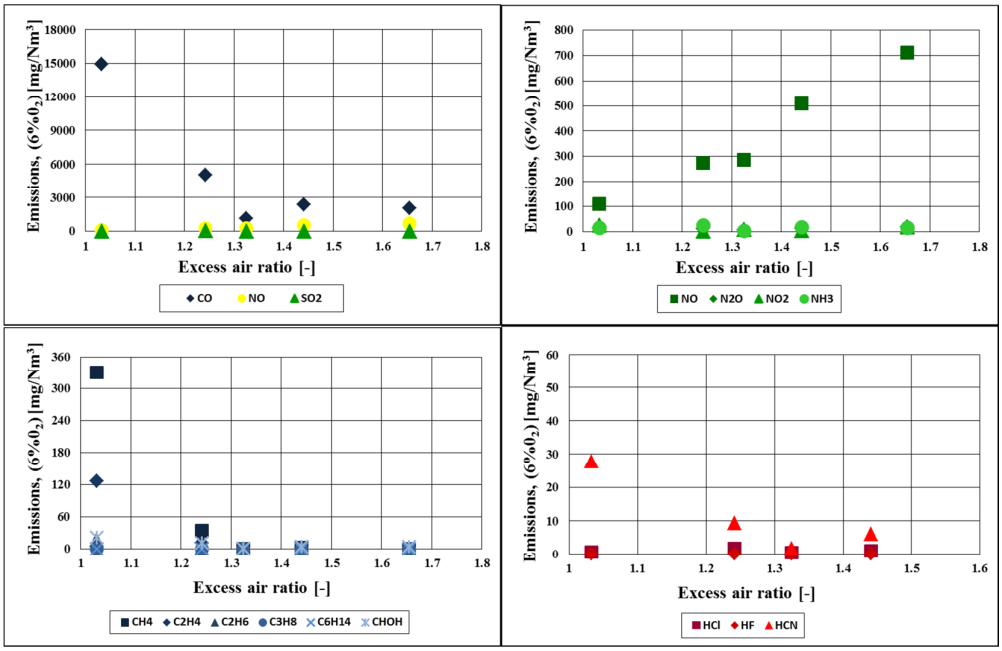

Figure 5.17 Emissions measured by Gas Analyzer-2 with respect to excess air ratio for the combustion of olive cake (B1-1)

5.1.6. Co-Combustion of Bursa/Orhaneli Lignite with 10% (by wt.) Woodchips (C1-B2-1)

For the co-combustion experiment of Bursa/Orhaneli lignite with 10% (by wt.) woodchips (WC), fuel feeding rate was changed between 3.7 and 6.5 kg/h. The lignite and woodchips mixture was fed into the combustor from the fuel hopper (FH-01) for the co-combustion tests of Bursa/Orhaneli lignite and woodchips in SET#1. The thermal power was between 13 and 22 kW. The superficial velocity was calculated in the range of 3.0-3.2 m/s.

Temperature Profile:

Temperature profiles along the combustor obtained for λs during the experiment are given in Figure 5.18. 10% woodchips addition did not lower the temperature profiles too much compared to the Bursa/Orhaneli lignite combustion in Section 5.1.1. The highest temperature was obtained as 861±1°C at 1.25 m above the distributor plate when the excess air ratio was 1.05. While there was a difference of 55°C between the regions where the highest and the lowest temperatures measured along the combustor for the case of λ = 1.05, this difference dropped to 27°C by increasing excess air ratio up to 1.86.

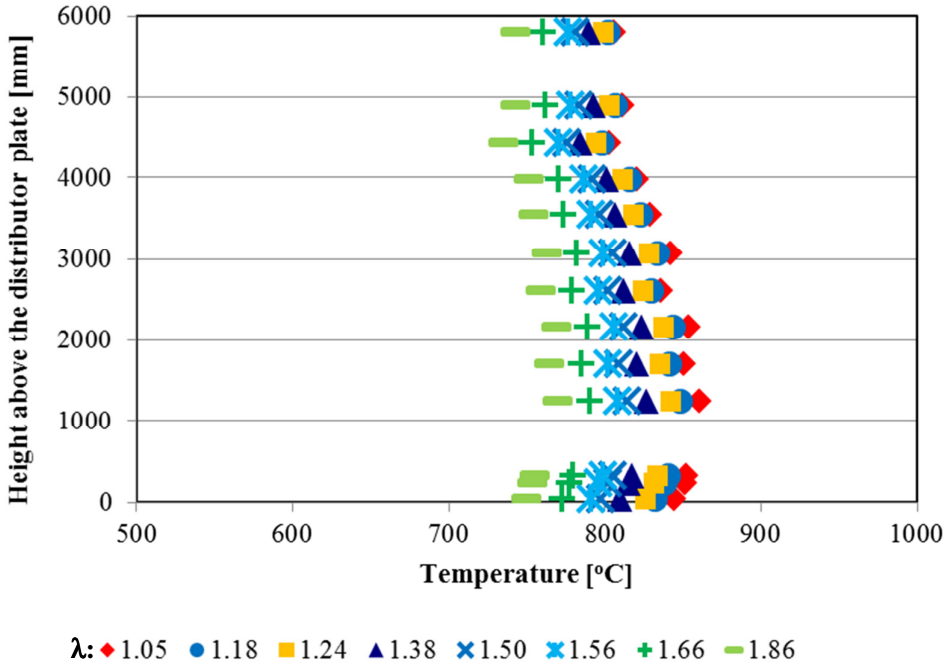

Figure 5.18 Temperature profile along the combustor for the co-combustion of Bursa/Orhaneli lignite with 10% (by wt.) woodchips (C1-B2-1)

Temperature profiles along the return leg obtained for different λs are given in Figure 5.19. While the highest temperature at TT201 was 775°C for λ = 1.05, it decreased down to 719±5°C for λ = 1.86. High temperature observed in the return leg was an indication of good circulation.

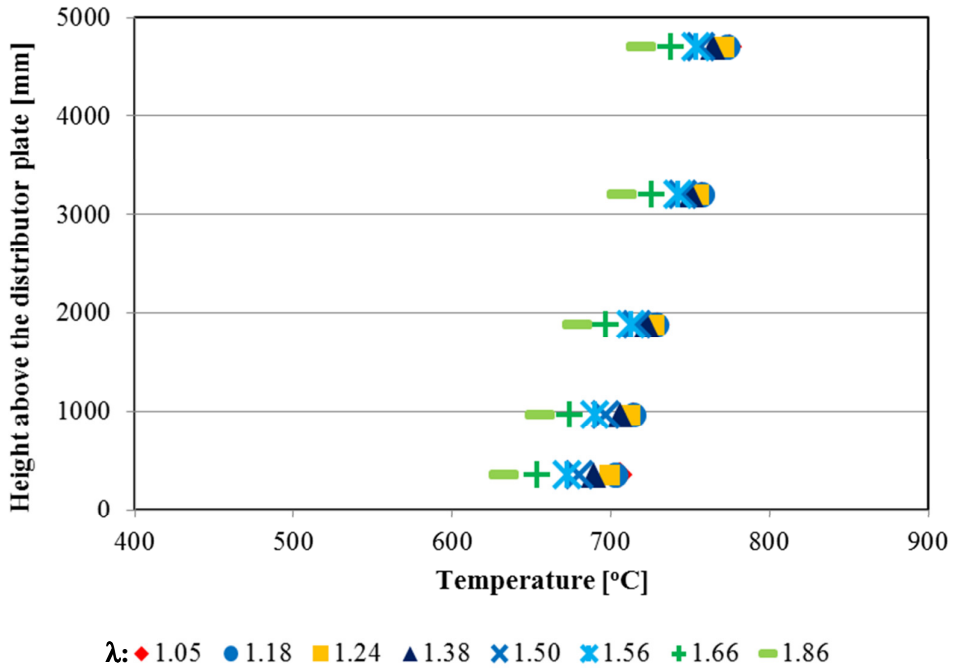

Figure 5.19 Temperature profile along the return leg for the co-combustion of Bursa/Orhaneli lignite with 10% (by wt.) woodchips (C1-B2-1)

Emissions:

Excess air ratio ranged between 1.04 and 1.86. Effect of excess air ratio on CO, NO, and SO_2 emission is given in Figure 5.20. The total duration of emission measurements was 101 minutes. Emissions presented in Figure 5.20 are 57 minutes of emission measurements during the steady state period of the experiment because of the reason stated in the beginning of the section. When the dense phase temperature was 852±1°C for the excess air ratio of 1.05, it decreased gradually and reached down to 754±1°C at λ = 1.86.

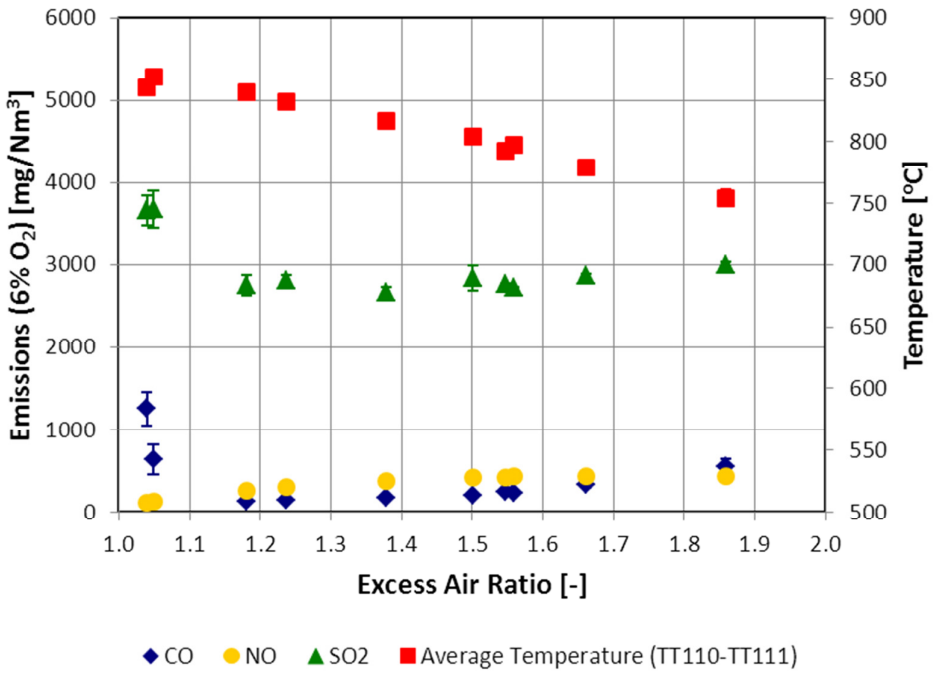

TT110 and TT111 are located 24 cm and 32 cm above the distributor plate, respectively.

Figure 5.20 Effect of excess air ratio on flue gas emissions for the co-combustion of Bursa/Orhaneli lignite with 10% (by wt.) woodchips (C1-B2-1)

While CO emission was measured as 636±174 mg/Nm^3 at λ = 1.05, it decreased as the excess air ratio increased up to 1.18. As can be seen from Figure 5.20, the lowest CO emission was 136±7 mg/Nm^3 and it was obtained when excess air ratio was 1.18. Further increase of excess air ratio cooled the combustor and caused CO emission to increase. When excess air ratio was 1.86, CO emission was measured as 552±84 mg/Nm^3.

NO emission increased as the excess air ratio increased and as the CO concentration decreased because of the reducing effect of CO on NO. While NO emission was 134±7 mg/Nm^3 at λ = 1.05, it increased up to 437±10 mg/Nm^3 at λ = 1.86. SO_2 emission decreased from 3676±222 mg/Nm^3 to 2752±128 mg/Nm^{3}when excess air ratio was increased from 1.05 to 1.18. Further increase on excess air ratio up to 1.56, did not change SO_2 emission too much. After excess air ratio of 1.56, SO_2 emission started to increase and reached to 2997±38 mg/Nm^3 at λ = 1.86.

For the co-combustion experiment of Bursa/Orhaneli lignite with 10% (by wt.) woodchips, it can be seen from Figure 5.20 that the optimum operational condition of excess air ratio was around 1.18 in order to get minimum CO emission. In this operational condition, CO emission was 136±7 mg/Nm^3, NO emission was 262±34 mg/Nm^3, and SO_2 emission was 2752±128 mg/Nm^3. According to the emission limits in the Turkish Regulation ("Turkish Regulation for Industrial Air Pollution Control," 2009) given in

Table 5.4, CO and NO emissions are below the limits which are 235 mg/Nm^3 for CO emission and 503 mg/Nm^3 for NO emission. SO_2 emission is above the limit which is 1753 mg/Nm^3. In order to decrease SO_2 emission, limestone addition was needed and this was studied in the scope of SET#3.

5.1.7. Co-Combustion of Bursa/Orhaneli Lignite with 30% (by wt.) Woodchips (C1-B2-2)

For the co-combustion experiment of Bursa/Orhaneli lignite with 30% (by wt.) woodchips, fuel feeding rate was changed between 3.7 and 6.0 kg/h. The thermal power was between 14 and 22 kW. The superficial velocity was calculated in the range of 3.0-3.2 m/s.

Temperature Profile:

Temperature profiles along the combustor obtained for different λs during the experiment are given in Figure 5.21. The highest temperature along the combustor was measured at about 1.25 m above the distributor plate for different excess air ratios. Among the excess air ratios, highest temperature profile was obtained for the case of λ = 1.04. While there was a difference of 70°C between the regions where the highest and the lowest temperatures measured along the combustor for the case of λ = 1.04, this difference dropped to 55°C by increasing excess air ratio up to 1.80 due to the better mixing.

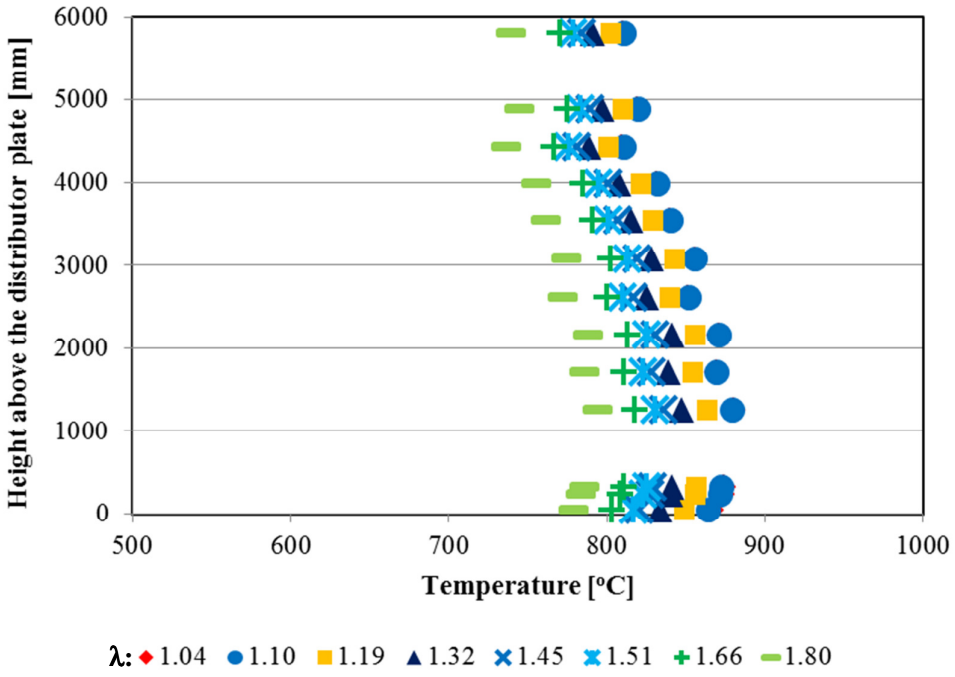

Figure 5.21 Temperature profile along the combustor for the co-combustion of Bursa/Orhaneli lignite with 30% (by wt.) woodchips (C1-B2-2)

Temperature profiles along the return leg obtained for different λs are given in Figure 5.22. While the highest temperature at TT201 was about 772±1°C for λ = 1.04, it decreased down to 703±3°C for λ = 1.80.

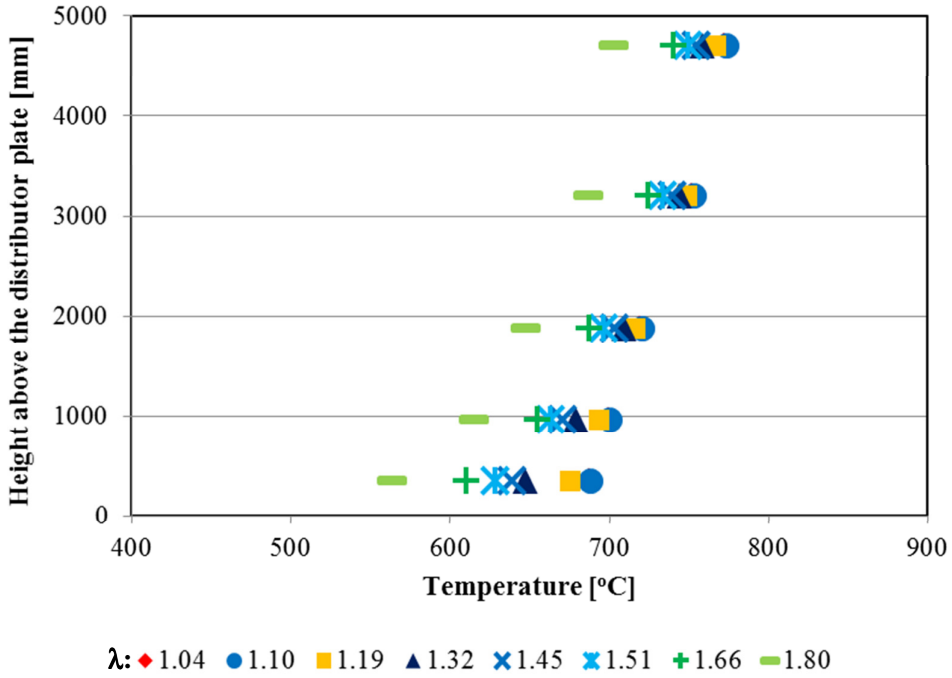

Figure 5.22 Temperature profile along the return leg for the co-combustion of Bursa/Orhaneli lignite with 30% (by wt.) woodchips (C1-B2-2)

Emissions:

Excess air ratio ranged between 1.04 and 1.80. Effect of excess air ratio on CO, NO, and SO_2 emission is given in Figure 5.23. The total duration of emission measurements was 96 minutes. Emissions presented in Figure 5.23 are 50 minutes of emission measurements during the steady state period of the experiment because of the reason stated in the beginning of the section. When the dense phase temperature was 874°C for the excess air ratio of 1.04, it decreased gradually and reached down to 785±2°C at λ = 1.80.

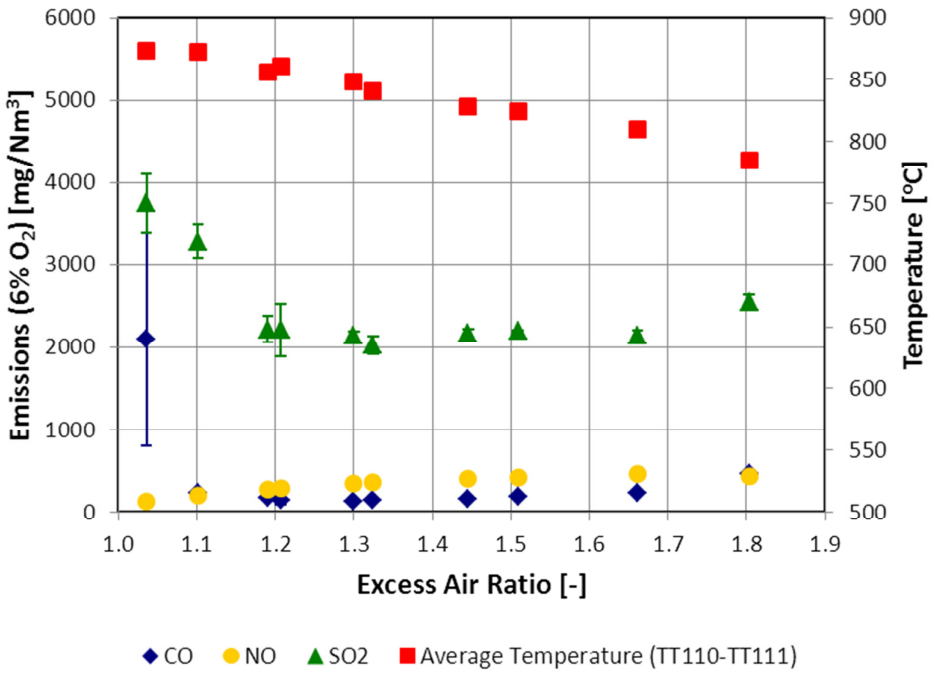

TT110 and TT111 are located 24 cm and 32 cm above the distributor plate, respectively.

Figure 5.23 Effect of excess air ratio on flue gas emissions for the co-combustion of Bursa/Orhaneli lignite with 30% (by wt.) woodchips (C1-B2-2)

As can be seen from Figure 5.23, CO emission showed a sharp decrease from 2099±1301 mg/Nm^3 to 149±11 mg/Nm^3 when the excess air ratio increased from 1.04 to 1.32. Further increase of excess air ratio cooled the combustor and caused CO emission to increase. When excess air ratio was 1.80, CO emission was measured as 460±34 mg/Nm^3.

It can be seen from the Figure 5.23 that NO emission slightly increased with the excess air ratio. NO emission was 131±18 mg/Nm^3 at excess air ratio of 1.04 and it increased to 356±29 mg/Nm^3 at about excess air ratio of 1.32 for the co-combustion of 30% woodchips. It was measured as 429±8 mg/Nm^3 at λ = 1.80. SO_2 emission decreased from 3752±355 mg/Nm^3 to 2023±106 mg/Nm^3 when excess air ratio was increased from 1.04 to 1.32. Further increase on excess air ratio up to 1.66, did not change SO_2 emission too much. After excess air ratio of 1.66, SO_2 emission started to increase and reached to 2549±87 mg/Nm^3 at λ = 1.80 due to the cooling of the combustor.

For the co-combustion experiment of Bursa/Orhaneli lignite with 30% (by wt.) woodchips, it can be seen from Figure 5.23 that the optimum operational condition of excess air ratio was around 1.32 in order to get minimum CO emission. In this operational condition, CO emission was 149±11 mg/Nm^3, NO emission was 356±29 mg/Nm^3, and SO_2 emission was 2023±106 mg/Nm^3. According to the emission limits in the Turkish Regulation ("Turkish Regulation for Industrial Air Pollution Control," 2009) given in

Table 5.4, CO and NO emissions are under the limits which are 217 mg/Nm^3 for CO emission and 465 mg/Nm^3 for NO emission. SO_2 emission is above the limit which is 1619 mg/Nm^3. In order to decrease SO_2 emission, limestone addition was needed and this was studied in the scope of SET#3.

5.1.8. Co-Combustion of Bursa/Orhaneli Lignite with 50% (by wt.) Woodchips (C1-B2-3)

For the co-combustion experiment of Bursa/Orhaneli lignite with 50% (by wt.) woodchips, fuel feeding rate was changed between 4.2 and 6.8 kg/h. The thermal power was between 17 and 27 kW, and the superficial velocity was calculated in the range of 3.3-3.5 m/s.

Temperature Profile:

Temperature profiles along the combustor obtained for different λs during the experiment are given in Figure 5.24. The highest temperature along the combustor was measured at about 1.25 m above the distributor plate for different excess air ratios. Among the excess air ratios, highest temperature profile was obtained for the case of λ = 1.41. While there was a difference of 145°C between the regions where the highest and the lowest temperatures measured along the combustor for the case of λ = 1.26, this difference dropped to 85°C by increasing excess air ratio up to 2.43.

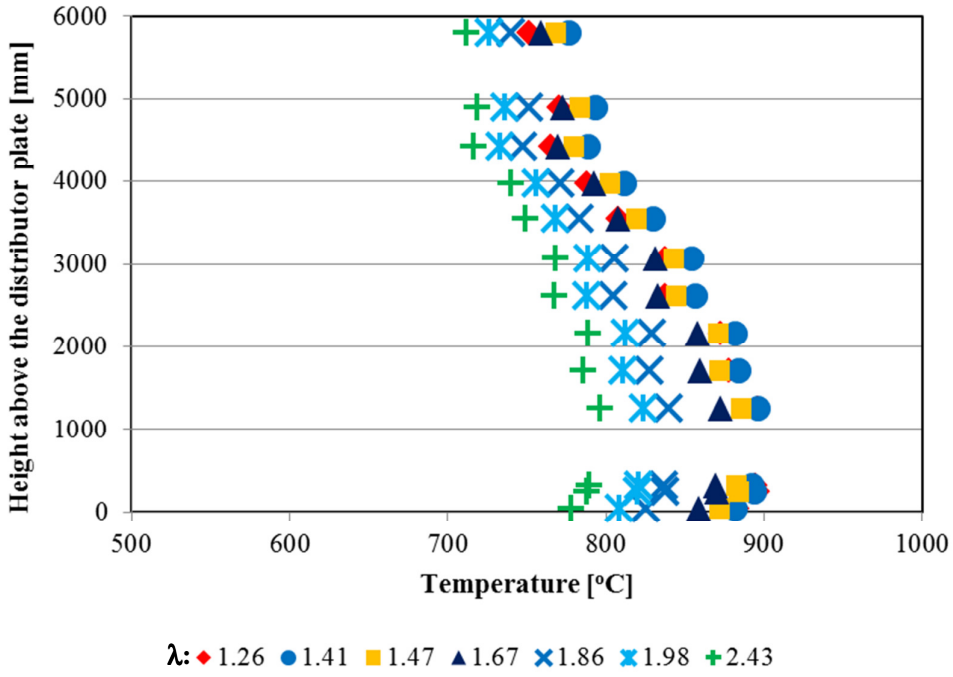

Figure 5.24 Temperature profile along the combustor for the co-combustion of Bursa/Orhaneli lignite with 50% (by wt.) woodchips (C1-B2-3)

Temperature profiles along the return leg obtained for different λs are given in Figure 5.25. While the highest temperature at TT201 was about 730±3°C for λ = 1.41, it decreased down to 657±4°C for λ = 2.43. Although temperature of dense bed and the superficial velocity in the combustor for 50% woodchips co-combustion are higher than the temperature and superficial velocity for combustion of Bursa/Orhaneli lignite, the temperature in the return leg was less than that for combustion of Bursa/Orhaneli lignite. Average temperature between the return leg and the combustor was about 493±4°C for 50% woodchips co-combustion which was less than the temperature for Bursa/Orhaneli lignite combustion (703±13°C). As the woodchips share in the fuel mixture increased, less amount of ash formed during the combustion because of the low the ash content of woodchips. Therefore, a lower temperature profile was observed in the return leg.

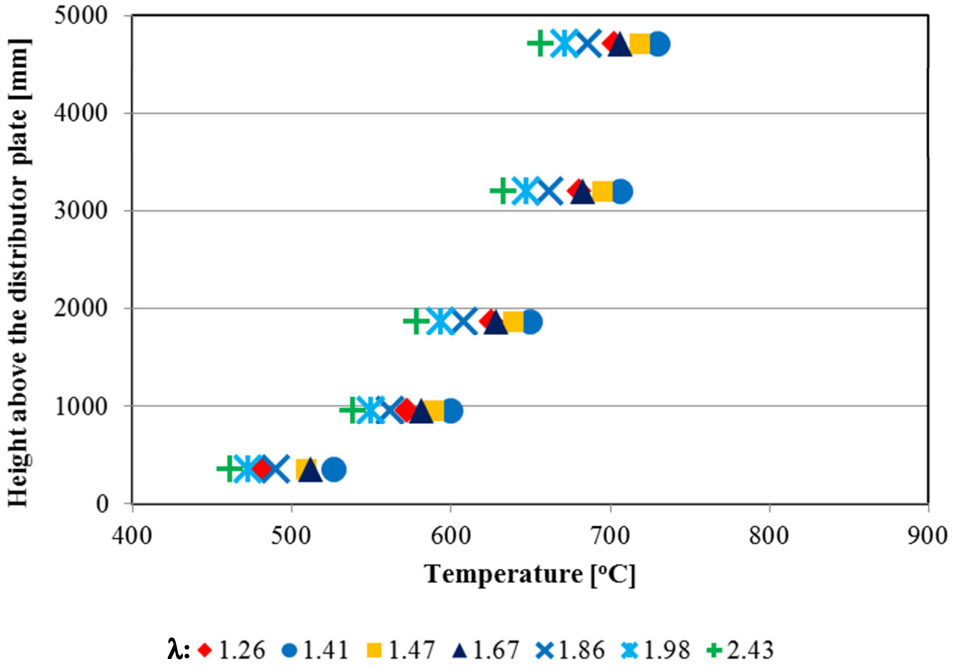

Figure 5.25 Temperature profile along the return leg for the co-combustion of Bursa/Orhaneli lignite with 50% (by wt.) woodchips (C1-B2-3)

Emissions:

Excess air ratio ranged between 1.26 and 2.43. Effect of excess air ratio on CO, NO, and SO_2 emission in the flue gas is given in Figure 5.26. The total duration of emission measurement was 128 minutes. Emissions presented in Figure 5.26 are 65 minutes of emission measurements during the steady state period of the experiment because of the reason stated in the beginning of the section. As the share of woodchips in the fuel mixture was increased, the temperature of the dense phase was also increased. While it was 852±1°C at λ = 1.05 for C1-B2-1 test, it increased to 874°C at λ = 1.04 for C1-B2-2

test. With the increase of woodchips share in the fuel mixture up to 50% by wt., the dense phase temperature was measured as 895±1°C for the excess air ratio of 1.26. When excess air ratio was increased to 2.43, it decreased down to 789±1°C.

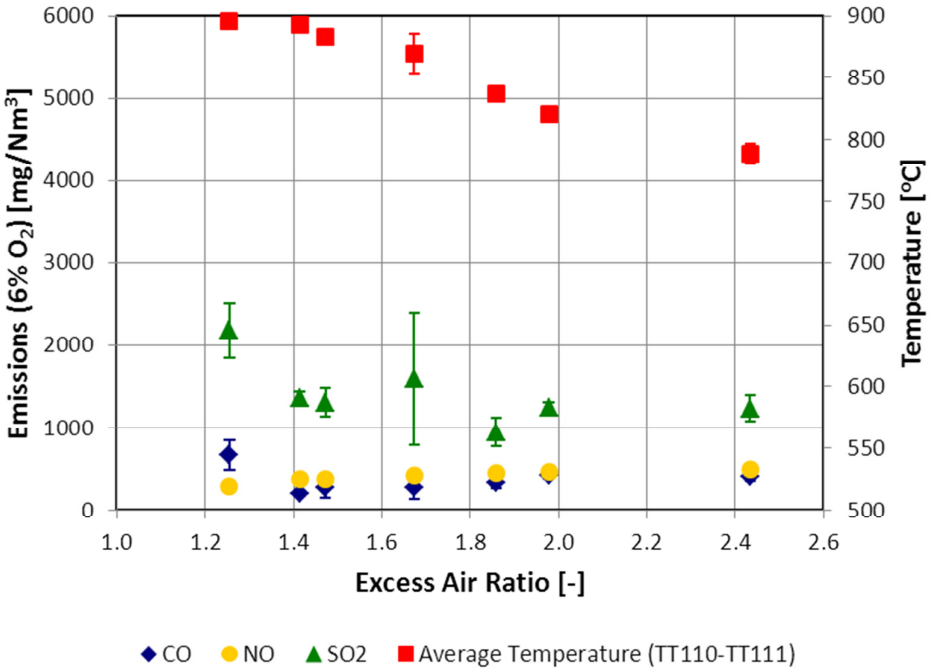

TT110 and TT111 are located 24 cm and 32 cm above the distributor plate, respectively.

Figure 5.26 Effect of excess air ratio on flue gas emissions for the co-combustion of Bursa/Orhaneli lignite with 50% (by wt.) woodchips (C1-B2-3)

CO emission measurement at λ = 1.05 was not obtained in this set of experiments. However, if it were obtained it could be around 3000 mg/Nm^3 which is larger than 2100 mg/Nm^3 for the case of 30% by weight woodchips addition. As the woodchips addition to coal increased, CO emissions also increased at lower λs because of higher VM content of the woodchips (75.2% by wt. in Table 4.2) than Bursa/Orhaneli lignite (34.4% by wt. in Table 4.2). While CO emission was measured as 667±185 mg/Nm^3 at λ = 1.26, it decreased as the excess air ratio increased up to 1.41. As can be seen from Figure 5.26, the lowest CO emission was measured as 206±13 mg/Nm^3 at λ = 1.41. Further increase of excess air ratio cooled the combustor and caused CO emission to increase. When excess air ratio was 2.43, CO emission was measured as 407±60 mg/Nm^3.

NO emission increased as the excess air ratio increased. While it was 285±26 mg/Nm^3 at λ = 1.26, it increased up to 489±17 mg/Nm^3 at λ = 2.43 because of decrease of the CO concentration which forms a reducing medium for NO. The increase in NO emission can be also explained by the increased oxygen concentration which was also given as a reason

for high NO emission with increasing excess air ratio as stated in the study of Madhiyanon et al. (2010). SO_2 emission decreased from 2179±337 mg/Nm^3 to 1307±86 mg/Nm^3 when excess air ratio was increased from 1.26 to 1.47. After excess air ratio of 1.47, SO_2 emission changed between 950 mg/Nm^3 and 1600 mg/Nm^3.

For the co-combustion experiment of Bursa/Orhaneli lignite with 50% (by wt.) woodchips, it can be seen from Figure 5.26 that the optimum operational condition of excess air ratio was around 1.41. In this operational condition, CO emission was 206±13 mg/Nm^3, NO emission was 374±12 mg/Nm^3, and SO_2 emission was 1356±86 mg/Nm^3. According to the emission limits in the Turkish Regulation ("Turkish Regulation for Industrial Air Pollution Control," 2009) given in Table 5.4, SO_2 and NO emissions are under the limits which are 1504 mg/Nm^3 for SO_2 emission and 432 mg/Nm^3 for NO emission. CO emission is a little above the limit which is 202 mg/Nm^3.

5.1.9. Discussion on the Effect of Excess Air Ratio on Emissions in SET#1

A summary of the operational parameters such as excess air ratio, superficial velocity in the combustor during the experiments are given in Table 5.1 for each combustion test. The fuel feeding rates and thermal power gained for these feeding rates are also given in Table 5.1.

Table 5.1 Operational conditions for the combustion and co-combustion tests in SET#1

TEST #	TEST CODE	Fuel Feeding rate kg/h	λ -	P_{th}[a] kW	U_o[b] m/s
1-1	C1-1	3.9-6.5	1.05-1.66	13-21	3.1-3.3
1-2	C1-B1-1	4.2-7.6	1.04-1.75	14-26	3.2-3.3
1-3	C1-B1-2	3.6-5.7	1.07-1.84	13-20	3.2
1-4	C1-B1-3	3.7-5.7	1.06-1.66	14-21	3.1-3.2
1-5	B1-1	3.5-4.7	1.11-1.78	15-19	2.7
1-6	C1-B2-1	3.7-6.5	1.04-1.86	13-22	3.0-3.2
1-7	C1-B2-2	3.7-6.0	1.04-1.80	14-22	3.0-3.2
1-8	C1-B2-3	4.2-6.8	1.26-2.43	17-27	3.3-3.5

[a] P_{th}: Thermal power
[b] U_o: Superficial velocity in the combustor (calculated based on TT112 and flue gas flow rate)

During the emission measurements, CO, NO, and SO_2 emissions were investigated in order to determine the optimum excess air ratio. For the excess air ratios, optimum values were determined according to minimum CO, NO, and SO_2 emissions. Optimum values of excess air ratio and corresponding flue gas emissions are listed in Table 5.2.

Table 5.2 Optimum excess air ratios, corresponding thermal power, superficial velocity and flue gas emissions for the combustion and co-combustion experiments in SET#1

TEST #	TEST CODE	Optimum λ	P_{th} kW	U_o m/s	CO[a] mg/Nm^3	NO[a] mg/Nm^3	SO_2[a] mg/Nm^3
1-1	C1-1	1.23	17	3.2	173±80	292±34	3022±246
1-2	C1-B1-1	1.37	17	3.2	270±29	353±24	2143±220
1-3	C1-B1-2	1.54	14	3.2	297±18	464±12	1226±152
1-4	C1-B1-3	1.59	14	3.2	660±69	458±9	194±8
1-5	B1-1	1.61	15	2.7	2059±94	725±62	0
1-6	C1-B2-1	1.18	19	3.2	136±7	262±34	2752±128
1-7	C1-B2-2	1.32	18	3.2	149±11	356±29	2023±106
1-8	C1-B2-3	1.41	22	3.5	206±13	374±12	1356±86

[a]Emissions are given on dry basis as a reference of 6% O_2.

In Table 5.3, flue gas emission limits specified in the Turkish Regulation for Industrial Air Pollution Control ("Turkish Regulation for Industrial Air Pollution Control," 2009) are listed.

Table 5.3 Flue gas emission limits according to the Turkish Regulation ("Turkish Regulation for Industrial Air Pollution Control," 2009)

Fuel	CO (mg/Nm^3)	NO (mg/Nm^3)	SO_xasSO_2 (mg/Nm^3)
Coal	200	520[b]	2000[d]
Biomass	460[a]	400[c]	200[a]

[a]≥0.5 MW; [b]≥50 MW(emission limit is 800 mg/Nm^3 NO_x as NO_2); [c]≥50 MW; [d]<100 MW_{th}; the limit is 1300 mg/Nm^3 for the plants 100-300 MW_{th} and 1000 mg/Nm^3 for the plants ≥300 MW_{th}

Effect of olive cake (OC) addition to Bursa/Orhaneli lignite on CO, NO, and SO_2 emissions are given in Figure 5.27, Figure 5.28, and Figure 5.29, respectively. Effect of olive cake addition to Bursa/Orhaneli lignite on **CO emissions** with respect to excess air ratio is given in Figure 5.27. As can be seen from Figure 5.27(a) and (b), olive cake addition to Bursa/Orhaneli lignite made the CO emission worse. The trendlines for CO emissions are given in Figure 5.27(c). When the trendlines are examined, it is seen that optimum excess air ratio for CO emission increased as the olive cake share in the fuel mixture increased. While it was estimated to be in the range of 1.2-1.3 for the coal combustion itself, it rises up to the range of 1.3-1.4 for the co-combustion of coal with 10% olive cake and 1.40-1.55 for the mixture containing 30% olive cake. In the case of 50% olive cake, optimum excess air ratio was estimated in the range of 1.55-1.60. This may be explained by the increasing VM content of the fuel mixture with the addition of olive cake. This was also observed in the study of Atimtay and Varol (2009). When olive

cake share in the fuel mixture increased, this shifted the combustion characteristic of the fuel mixture from char combustion to volatile combustion which needed more oxygen for the fuel particles to be completely burned out. The increase in CO emission with an increasing share of biomass in fuel mixture was also attributed to the cooling of the upper part of the combustor as described in the study of Cliffe and Patumsawad (2001). Temperature profile along the combustor for optimum excess air ratio was given in Figure 5.27(d) in order to see the cooling of the upper part of the combustor as the olive cake share in the fuel mixture was increase to 50% by wt.

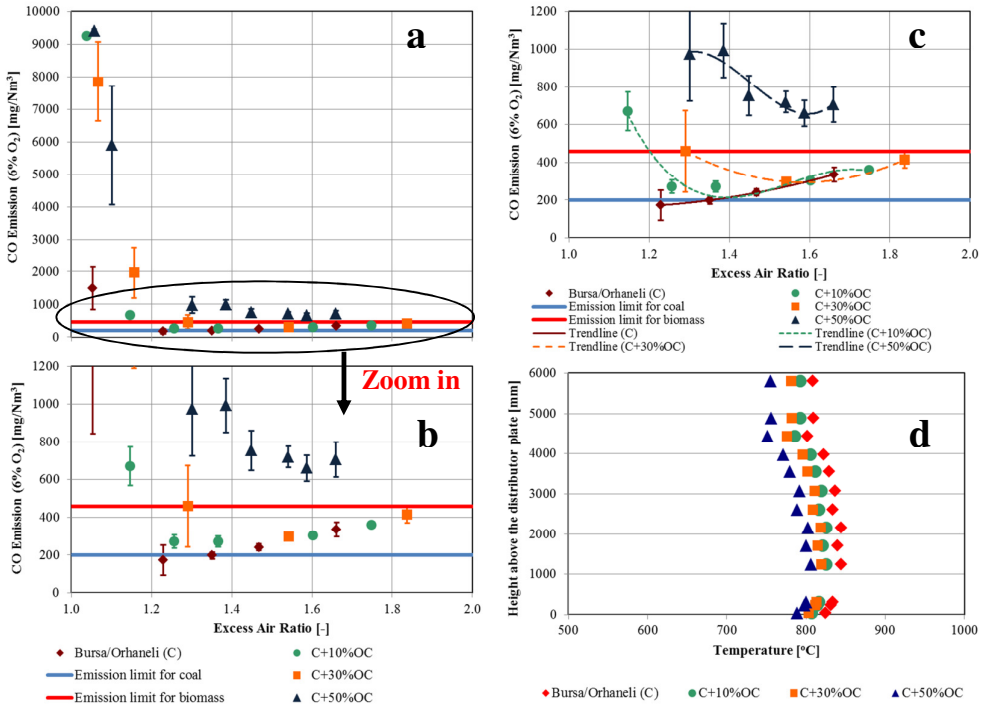

Figure 5.27 Effect of olive cake addition on CO emissions with respect to excess air ratio and comparison of emissions to the limits in the Turkish Regulation ("Turkish Regulation for Industrial Air Pollution Control," 2009) for co-combustion of Bursa/Orhaneli lignite and olive cake fuel mixtures; a-) original figure, b-) enlarged view, c-) emission trendlines, d-) temperature profile at optimum λ

Effects of olive cake addition to Bursa/Orhaneli lignite on **NO emission** can be seen in Figure 5.28. Co-combustion tests of Bursa/Orhaneli lignite and olive cake mixtures resulted in more or less the same emission value and the same emission trend. NO emission was found to increase gradually as excess air ratio increased for all cases as can be seen in Figure 5.28. There is this general acceptance that volatile nitrogen compounds in the fuel and nitrogen in the char are firstly oxidized to NO when more O_2 is available as stated in the study of Afacan et al. (2007). Increase of NO_x emission with excess air ratio was also mentioned in the study of Gungor (2010) in which the predictions of the

model were compared to the results of the study of Topal et al. (2003). Gungor (2010) stated that increasing excess air enhanced the oxidation rate of char causing the amount of char to reduce and following NO_x emissions to increase. An increase in NO emission with respect to excess air ratio was also observed by an earlier study (Vamvuka et al., 2012). Li et al. (1998) also mentioned that in the case where there was less oxygen in the combustor, NO might be reduced to N_2 over char. *Therefore, in a situation where char content becomes less (e.g. high percentage of biomass in the fuel mix fed to the combustor), the conversion of NO to N_2 becomes less and the NO emission increases in the flue gas. Increase in char loading means also not complete combustion and probably formation of more CO. Therefore. NO reduction appears when CO is formed. This might be reason why less NO emissions were obtained at excess air ratio below 1.1.*

In order to ensure NO emission limit for each combustion test, it is obvious from Figure 5.28 that it is needed to operate the system at excess air ratio below 1.4. However, when the system is operated on these conditions, on the other hand, there is no doubt that more CO emission is produced if Figure 5.27 is examined. Therefore, it is necessary to make an optimization on excess air ratio according to CO and NO emissions. In this set of experiments, CO emission has the priority in order to determine the optimum excess air ratio because it is possible to reduce NO emission by giving secondary air to the combustor in the experiments of SET#2.

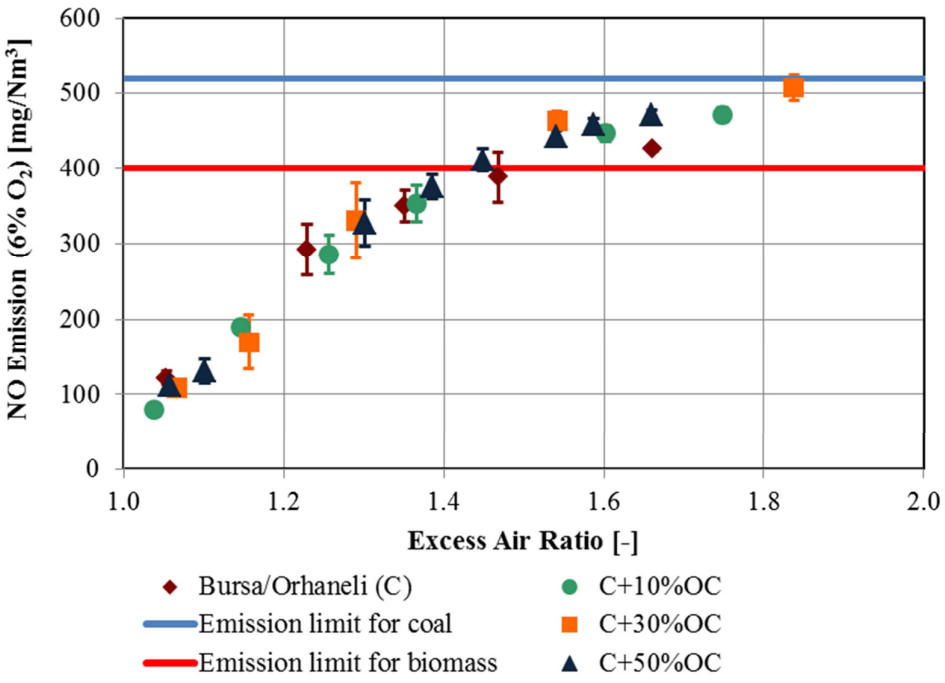

Figure 5.28 Effect of olive cake addition on NO emissions with respect to excess air ratio and comparison of emissions to the limits in the Turkish Regulation ("Turkish Regulation for Industrial Air Pollution Control," 2009) for the co-combustion of Bursa/Orhaneli lignite and olive cake fuel mixtures

Effect of olive cake addition to Bursa/Orhaneli lignite on **SO_2 emission** can be seen in Figure 5.29. When the olive cake percentage on fuel mixture was increased, SO_2 emission was decreased as it was expected. For the case of Bursa/Orhaneli lignite combustion, SO_2 emission was measured above the emission limit (2000 mg/Nm^3) for all excess air ratios. It is necessary to add limestone in order to reduce SO_2 emission. This was studied in SET#3. When the fuel mixture containing olive cake 10% by weight was burned, SO_2 emission was also above the emission limit for all excess air ratios. For other mixtures and for olive cake combustion, SO_2 emissions were under limits at the optimum excess air ratios determined for each test. The optimum excess air ratio for each fuel mixture and corresponding SO_2 emissions are given in Table 5.4.

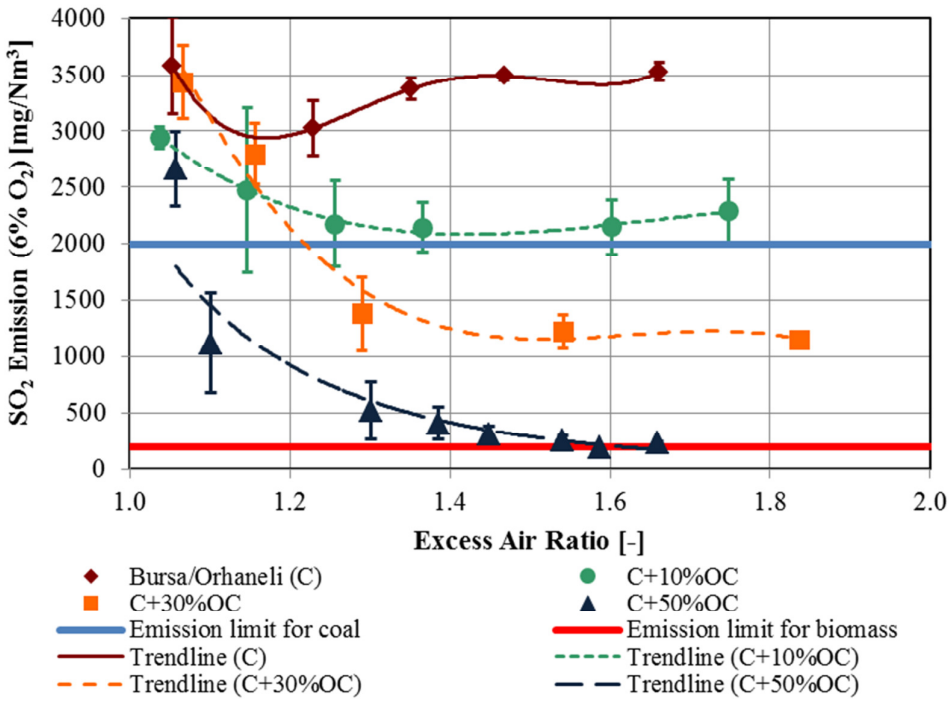

Figure 5.29 Effect of olive cake addition on SO_2 emissions with respect to excess air ratio and comparison of emissions to the limits in the Turkish Regulation ("Turkish Regulation for Industrial Air Pollution Control," 2009) for the co-combustion of Bursa/Orhaneli lignite and olive cake fuel mixtures

Effect of woodchips addition to Bursa/Orhaneli lignite on **CO emissions** with respect to excess air ratio is given in Figure 5.30. As can be seen from Figure 5.30(b), CO emissions for the co-combustion of Bursa/Orhaneli lignite with 10% and 30% woodchips were less than CO emission for the combustion of Bursa/Orhaneli lignite in the excess air ratio range of 1.1-1.7. The trendlines for CO emissions are given in Figure 5.30(c). When the trendlines are examined, it is seen that optimum excess air ratio for CO emission increases as the woodchips share in the fuel mixture increases. While it was estimated to be in the range of 1.2-1.3 for the coal combustion and the co-combustion of coal with 10% woodchips, it rises up to the range of 1.25-1.35 and 1.4-1.5 for the mixture containing 30% and 50% woodchips, respectively. It can be also seen from the trendlines in Figure 5.30(c) that increasing woodchips share in the fuel mixture from 0% to 30% makes CO emission better. Further increase on the share (50%) of woodchips in fuel mixture makes CO emissions worse. This may be because of the lower temperature observed in the upper part of the combustor for the co-combustion tests of 50% woodchips as can be seen in Figure 5.30(d).

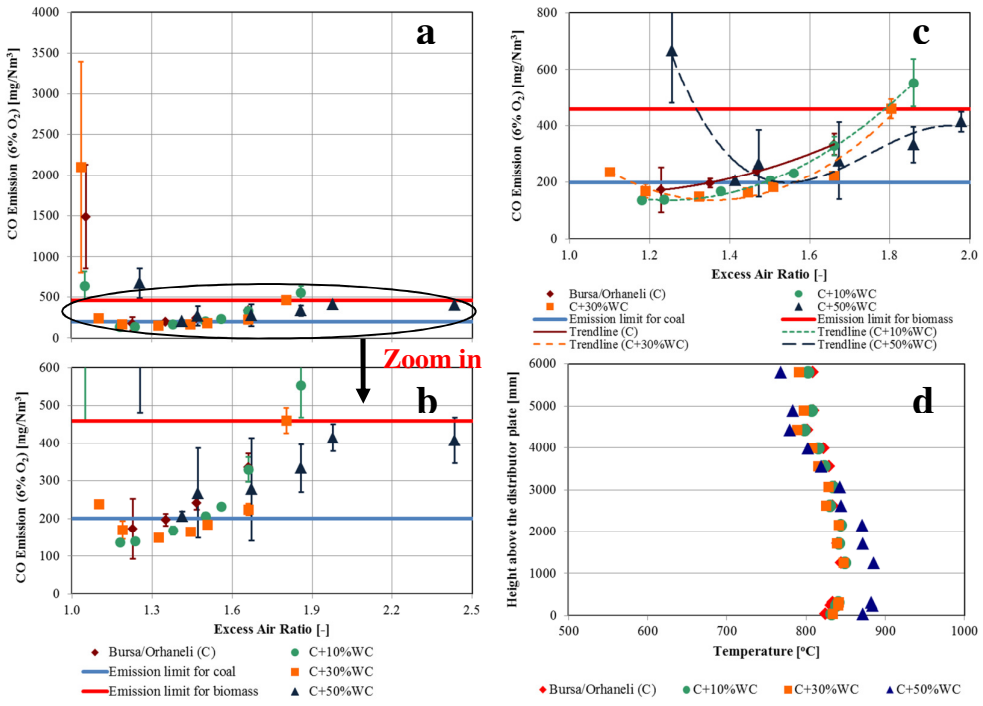

Figure 5.30 Effect of woodchips addition on CO emissions with respect to excess air ratio and comparison of emissions to the limits in the Turkish Regulation ("Turkish Regulation for Industrial Air Pollution Control," 2009) for co-combustion of Bursa/Orhaneli lignite and woodchips fuel mixtures; a-) original figure, b-) enlarged view, c-) emission trendlines, d-) temperature profile at optimum λ

Effect of woodchips addition to Bursa/Orhaneli lignite on **NO emission** is given in Figure 5.31. It was expected that NO emission will decrease as the woodchips share in the fuel mixture increased due to the lowering N-content of fuel mixture. While N-content of Bursa/Orhaneli lignite was 0.54% by wt. on dry basis (see Table 4.3), it decreased to 0.42% by wt. for the 50% woodchips fuel mixture. However, it is seen from Figure 5.31 that woodchips addition to Bursa/Orhaneli lignite did not change NO emission. This might be due to the decrease in amount of the char formed with increasing woodchips percentage in the fuel mixture. As it was discussed above for the effect of olive cake addition on NO emission, the presence of char is important because of its catalytic effect on NO reduction by CO and carbon (Glarborg et al., 2003; Permchart and Kouprianov, 2004; Khan et al., 2009). The decrease in the char concentration could cause heterogeneous NO reduction mechanism to be ceased. These two affects, decrease in N-content and char content of the fuel mixture might compensate each other and resulted in NO emission to be constant. There might be another mechanism responsible preventing NO emission to increase with the increase of woodchips share in the fuel mixture. This might be gas phase oxidation of nitrogen compounds. NH_3 release from fuel particles during devolatilization may react with NO forming nitrogen (Permchart and Kouprianov, 2004). NO emission increased as excess air ratio increased. The general trend has been

stated in the literature (Li et al., 1998; Lyngfelt and Leckner, 1999; Afacan et al., 2007; Xie et al., 2007) that CO gas being a reducing gas, helps to reduce NO over char surfaces when less amount of oxygen is present in the combustor. Increase of NO with respect to excess air ratio was also stated in the study of Suksankraisorn et al. (2004). Mahmoudi et al. (2010) were also mentioned in their review study that deNO_x technique was one of the control methods used for NO reduction giving less amount of air into the combustor. However, CO emissions produced due to the less amount of air were the limitation of this method.

In order to ensure NO emissions to be below the limits, it is necessary to operate the system at excess air ratio below 1.4. However, when the system is operated under these conditions more CO is produced as can be seen from Figure 5.30. Therefore, it is necessary to make an optimization on excess air ratio according to CO and NO emissions.

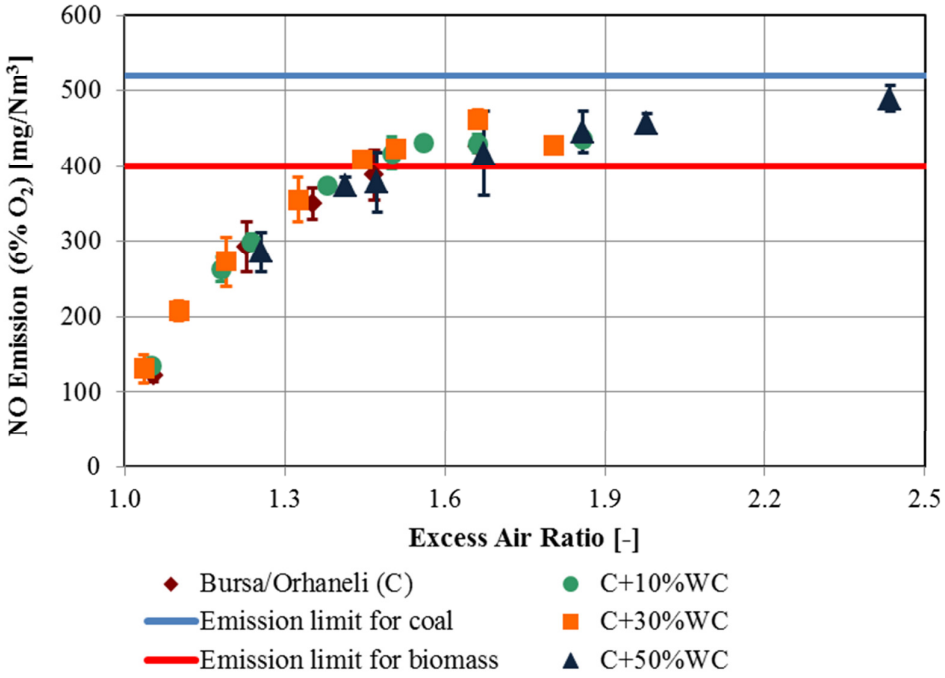

Figure 5.31 Effect of woodchips addition on NO emissions with respect to excess air ratio and comparison of emissions to the limits in the Turkish Regulation ("Turkish Regulation for Industrial Air Pollution Control," 2009) for the co-combustion of Bursa/Orhaneli lignite and woodchips fuel mixtures

Effect of woodchips addition to Bursa/Orhaneli lignite on **SO_2 emission** can be seen in Figure 5.32. When the woodchips percentage in fuel mixture was increased, SO_2 emission was decreased as it was expected since woodchips did not have any sulfur in its composition. For the case of Bursa/Orhaneli lignite combustion, SO_2 emission was

measured above the emission limit (2000 mg/Nm^3) for all excess air ratios. It seems that CaO content in coal ash (19.7% in Table 4.16) is not enough to capture S in coal and in-situ limestone addition is required in order to keep SO_2 emission below the limit. It is necessary to add limestone in order to reduce SO_2 emission. This was studied in SET#3. While the average SO_2 emission was 2914±88 mg/Nm^3 for the co-combustion of 10% woodchips, it was 2542±132 mg/Nm^3 for the 30% woodchips. In both cases, SO_2 emission was above the limit for all excess air ratios. Combustion of coal with 50% woodchips was the only case that limestone was not needed. In that case, average SO_2 emission was 1407±257 mg/Nm^3.

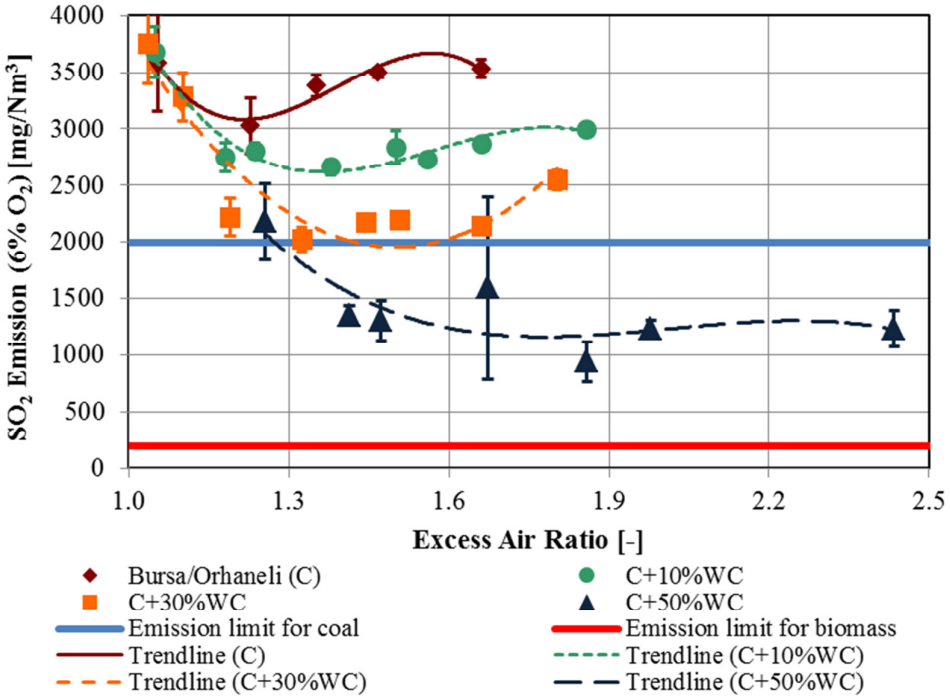

Figure 5.32 Effect of woodchips addition on SO_2 emissions with respect to excess air ratio and comparison of emissions to the limits in the Turkish Regulation ("Turkish Regulation for Industrial Air Pollution Control," 2009) for the co-combustion of Bursa/Orhaneli lignite and woodchips fuel mixtures

The flue gas emissions resulted in the combustion and co-combustion experiments at the optimum excess air ratios were compared to the emission limits specified by the Turkish Regulation ("Turkish Regulation for Industrial Air Pollution Control," 2009) in Table 5.4. If the measured emission value is below the emission limit, it is light gray in color. If it is above the emission limit, it is dark gray in color. NO_x (as NO_2) emission limit for coals in the Turkish Regulation is 800 mg/Nm^3. Since ABB-AO 2000 flue gas analyzer measures NO concentration but not NO_2 and from the fact that NO accounts for the most (95% by

volume) of NO_x emission, the emission limit for NO_x (as NO_2) was converted to NO and it was recalculated to be 520 mg/Nm^3 (NO emission limit).

When Table 5.4 is examined, it can be seen that CO emission was measured under the limit for the combustion of Bursa/Orhaneli lignite. However, olive cake addition to Bursa/Orhaneli lignite caused CO emission to exceed the limit. In the case of olive cake combustion, CO emission was highly above the limit. The addition of woodchips to Bursa/Orhaneli lignite 10% and 30% by wt. did not cause to exceed limit. The 50% woodchips case was the only one that exceeded the limit in terms of CO emission.

NO emissions were under the limits for all cases except for the case of co-combustion of Bursa/Orhaneli lignite and olive cake (50% by wt.) and combustion of olive cake by itself. This result was attributed to less char formation as the amount of biomass in the fuel mixture is increased. NO emission can be reduced by giving secondary air to the combustor. This was studied in the experiments done for SET#2.

SO_2 emissions were above the limits in the cases where Bursa/Orhaneli lignite was combusted by itself and with 10% olive cake by wt. SO_2 emissions were below the limit in the case of 50% woodchips combustion because of a very low S content in the biomass. For the Bursa/Orhaneli lignite and woodchips mixtures having less than 50% woodchips by wt., limestone addition is necessary to keep SO_2 emissions below the limit. SO_2 emission can be reduced by introducing of limestone into the combustor. This was studied in the experiments conducted for SET#3.

Table 5.4 Comparison of flue gas emissions at the optimum excess air ratio for combustion experiments in SET#1 with the limits in the Turkish Regulation ("Turkish Regulation for Industrial Air Pollution Control," 2009)

Test #	Test Code	CO (mg/Nm^3)		NO (mg/Nm^3)		SO_x as SO_2 (mg/Nm^3)	
		measured	Limit	measured	Limit	measured	Limit
1-1	C1-1	173±80	200	292±34	520[b]	3022±246	2000[d]
1-2	C1-B1-1	270±29	230	353±24	505	2143±220	1787
1-3	C1-B1-2	297±18	288	464±12	479	1226±152	1386
1-4	C1-B1-3	660±69	342	458±9	454	194±8	1015
1-5	B1-1	2059±94	460[a]	725±62	400[c]	0	200[a]
1-6	C1-B2-1	136±7	235	262±34	503	2752±128	1753
1-7	C1-B2-2	149±11	217	356±29	465	2023±106	1619
1-8	C1-B2-3	206±13	202	374±12	432	1356±86	1504

[a]≥0.5 MW; [b]≥50 MW(emission limit is 800 mg/Nm^3 NO_x as NO_2); [c]≥50 MW; [d]<100 MW_{th}; the limit is 1300 mg/Nm^3 for the plants 100-300 MW_{th} and 1000 mg/Nm^3 for the plants ≥300 MW_{th}

5.2. Assessment of Experiments for SET#2

Four experiments were conducted in SET#2 in order to investigate the effect of secondary air ratio (SAR) and its location along the combustor on the major emissions (CO, NO, and SO_2) in the flue gas. SAR is the ratio of secondary air to total air. Total air given into the combustor was kept constant during the combustion experiments. For example, 20% SAR means 20% by volume of the total air is given as secondary air and the rest is introduced to the combustor throughout the distributor plate as primary air. If SAR is increased to 30%, this indicates a 10% by volume more decrease in the primary air. Secondary air was given to the combustor from four different locations along the combustor at 142 cm, 233 cm, 324 cm, and 415 cm above the distributor plate. The experiments included co-combustion of Bursa/Orhaneli lignite and olive cake fuel mixtures containing olive cake 30 and 50% by weight and co-combustion of Bursa/Orhaneli lignite and woodchips fuel mixtures containing woodchips 30% and 50% by weight.

5.2.1. Co-Combustion of Bursa/Orhaneli Lignite with 30% (by wt.) Olive Cake (C1-B1-4)

The effect of secondary air (SA) and its location on temperature profile along the combustor and return leg for the co-combustion of Bursa/Orhaneli lignite with 30% by wt. olive cake is given in Figure 5.33 and Figure 5.34, respectively. When Figure 5.33 is examined, it can be seen that secondary air ratio (SAR) had a heating effect on dense phase (<1.25 m) and a cooling effect on upper part of the combustor (>1.25 m). As SA was introduced into the combustor from higher levels, this effect became clearer. It seems that SA caused the combustor to have two different phases in terms of hydrodynamics. This finding can also be supported by the study of Ersoy et al. (2004). Secondary air acted like a barrier for the primary air coming from the bottom of the combustor and it created two parts in the combustor; namely, a hot and dense part below the point where secondary air injected and a cool and dilute part above the point where secondary air injected. As the SAR was increased, the primary air given into the combustor through the distributor plate was decreased as much as the increase in SAR because the total air given to the combustor was kept constant. The decrease in the primary air caused the temperature of the dense phase to increase. Increasing SAR decreased the temperature of the upper part of the combustor and also lowered the recirculation rate because most of the solids were trapped in the dense phase of the combustor.

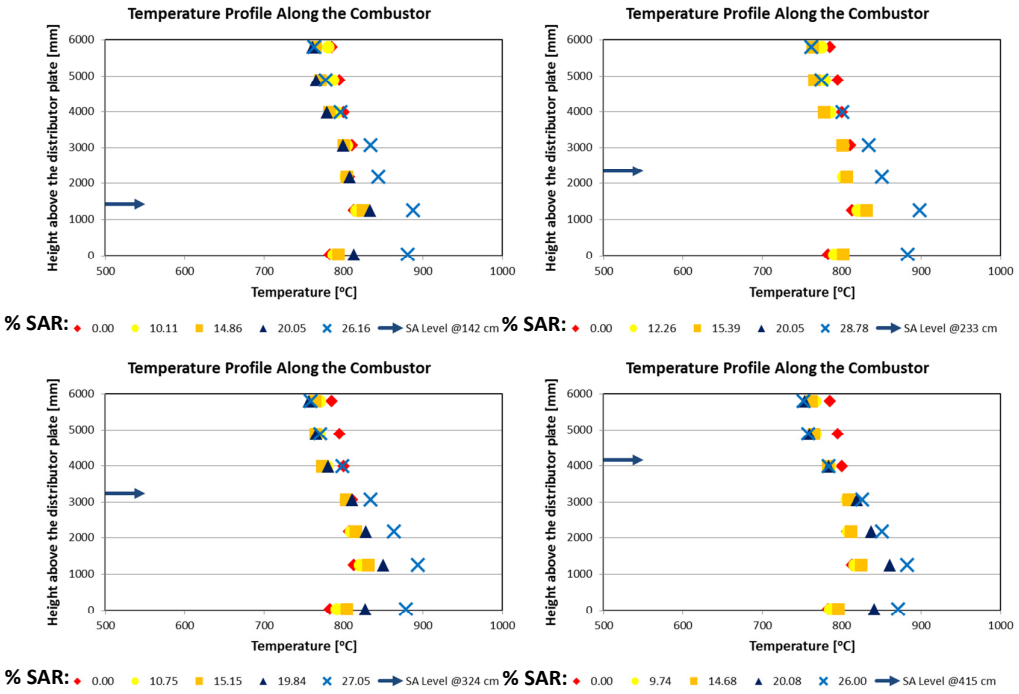

Figure 5.33 Effect of secondary air ratio and its location on temperature profile along the combustor for co-combustion of Bursa/Orhaneli lignite with 30% (by wt.) olive cake (C1-B1-4)

The effect of SAR and its location on the temperature profile along the return leg can be seen in Figure 5.34. While SA was given into the combustor at 142 cm above the distributor plate, temperature profiles in the case of SAR less than 15% were almost the same with the temperature profile at SAR=0. However, lower temperature profiles were obtained with SAR less than 15% when SA was introduced to the combustor at 415 cm above the distributor plate.

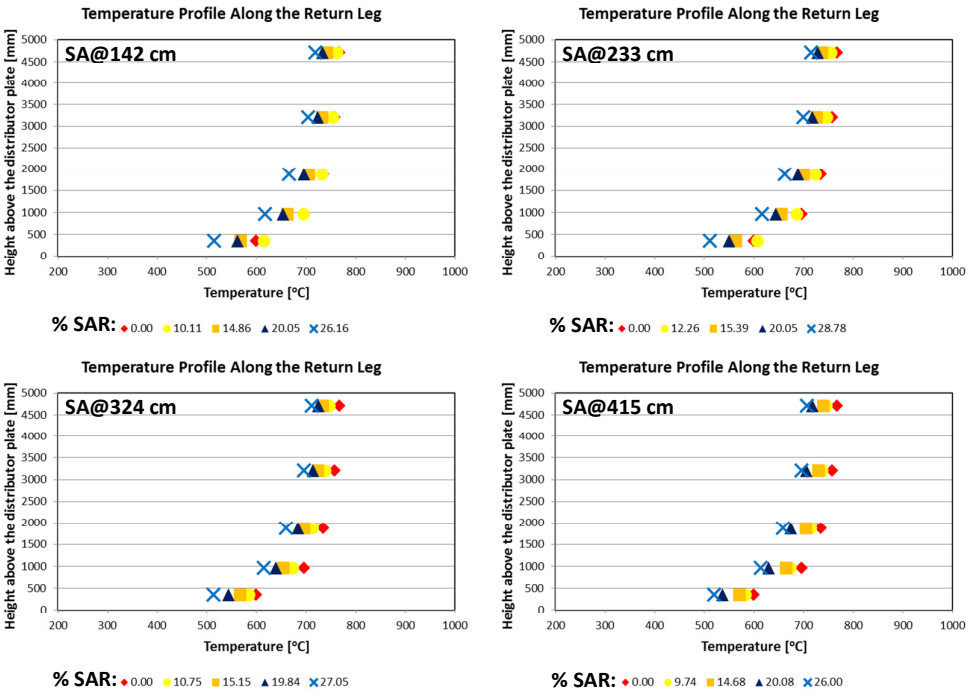

Figure 5.34 Effect of secondary air ratio and its location on temperature profile along the return leg for co-combustion of Bursa/Orhaneli lignite with 30% (by wt.) olive cake (C1-B1-4)

5.2.2. Co-Combustion of Bursa/Orhaneli Lignite with 50% (by wt.) Olive Cake (C1-B1-5)

The effect of SA and its location on temperature profile along the combustor and return leg for the co-combustion of Bursa/Orhaneli lignite with 50% by wt. olive cake is given in Figure 5.35 and Figure 5.36, respectively. As can be seen in Figure 5.35, the temperature of the dense phase was increased with the secondary air ratio. However, the temperature profiles for all cases of SAR was more compact than the temperature profiles obtained in the case of co-combustion with 30% olive cake in Figure 5.33.

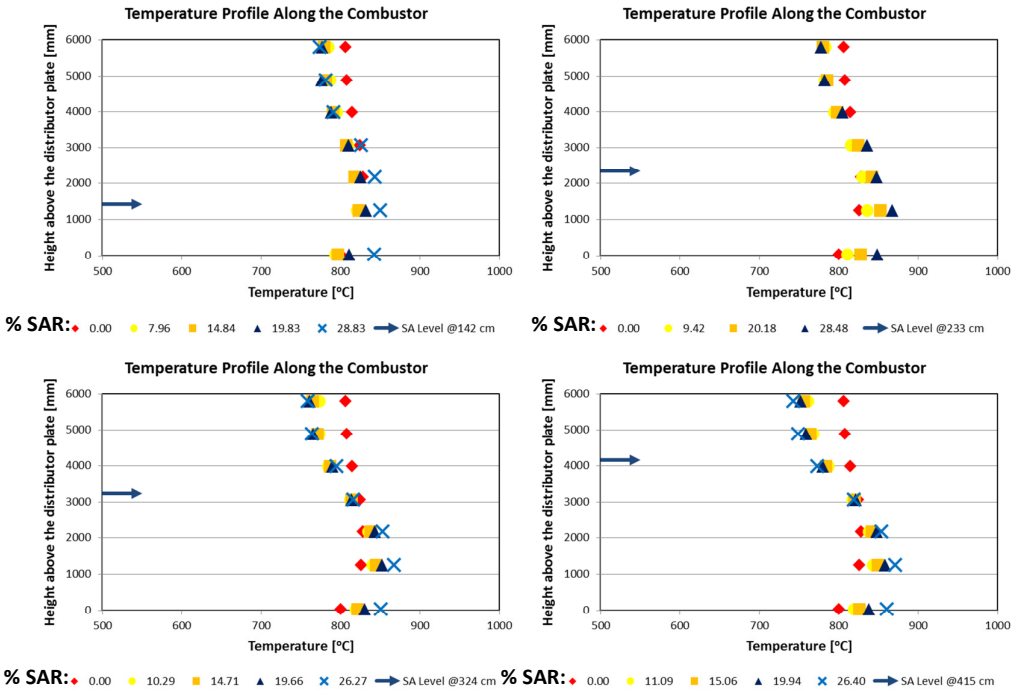

Figure 5.35 Effect of secondary air ratio and its location on temperature profile of combustor for co-combustion of Bursa/Orhaneli lignite with 50% (by wt.) olive cake (C1-B1-5)

With the increase of olive cake in the fuel mixture from 30% to 50% increased the total volatile matter of the fuel mixture as well. Burning of volatile matters mainly in the dilute phase (>1.25 m) caused temperatures measured in that region to be close to each other for different SARs. The more compact temperature distribution at the top of the combustor resulted in smooth temperature profiles along the return leg for C1-B1-5 as can be seen in Figure 5.36.

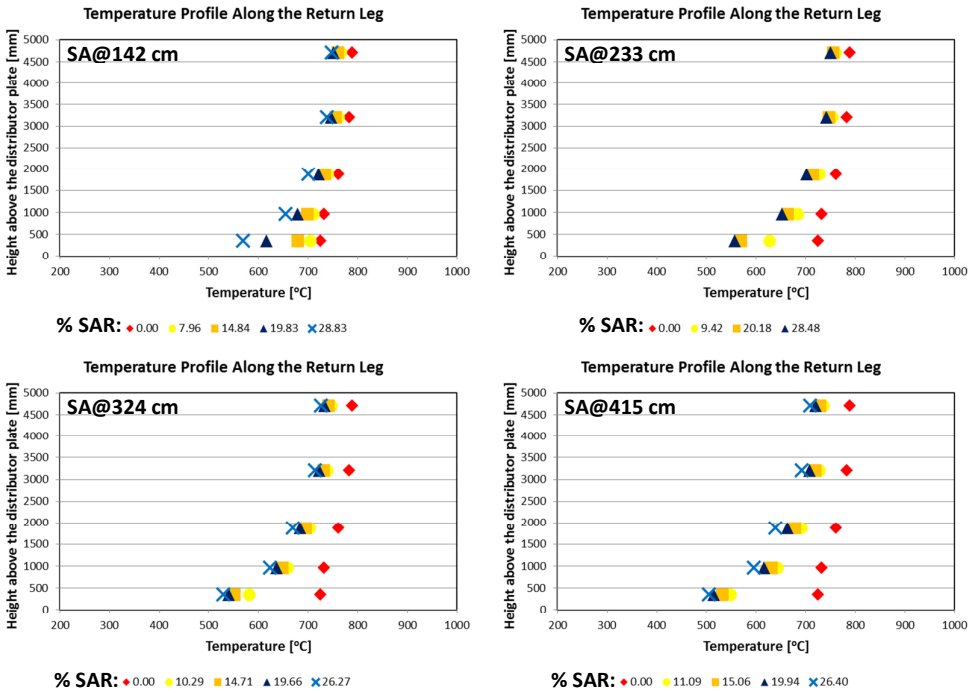

Figure 5.36 Effect of secondary air ratio and its location on temperature profile of return leg for co-combustion of Bursa/Orhaneli lignite with 50% (by wt.) olive cake (C1-B1-5)

5.2.3. Co-Combustion of Bursa/Orhaneli Lignite with 30% (by wt.) Woodchips (C1-B2-4)

The effect of secondary air SA and its location on temperature profile along the combustor and return leg for the co-combustion of Bursa/Orhaneli lignite with 30% by wt. woodchips is given in Figure 5.37 and Figure 5.38, respectively. When Figure 5.37 is examined, it can be seen that SAR had a heating effect on dense phase (<1.25 m) and a cooling effect on dilute phase (>1.25 m). As SA was introduced into the combustor from higher levels, this effect became clearer. Increasing SAR lowers the recirculation rate which is followed by an increase in temperature of the dense phase and a decrease in the temperature of the upper part of the combustor as it was depicted in Section 5.2.1.

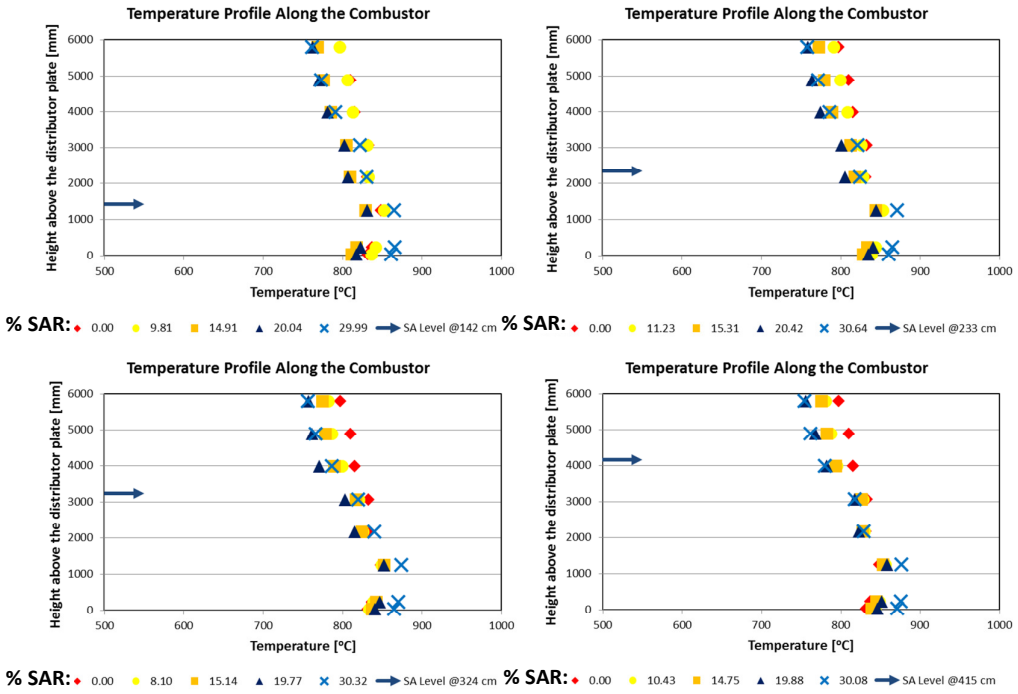

Figure 5.37 Effect of secondary air ratio and its location on temperature profile along the combustor for co-combustion of Bursa/Orhaneli lignite with 30% (by wt.) woodchips (C1-B2-4)

When Figure 5.38 is examined in order to see the effect of SAR and its location on the temperature profile of the return leg, the effect of SAR on the recirculation is more apparent. While it created denser phase than usual below the SA injection port, it caused the upper part above the injection port to cool down and to be more dilute. It is also important to note that while SAR of 30% adversely affected the recirculation rate due to the change of the hydrodynamics in the combustor in the case of SA injection@142 cm, 20% SAR was enough for the other SA ports to have the same effect on temperature profile of the return leg.

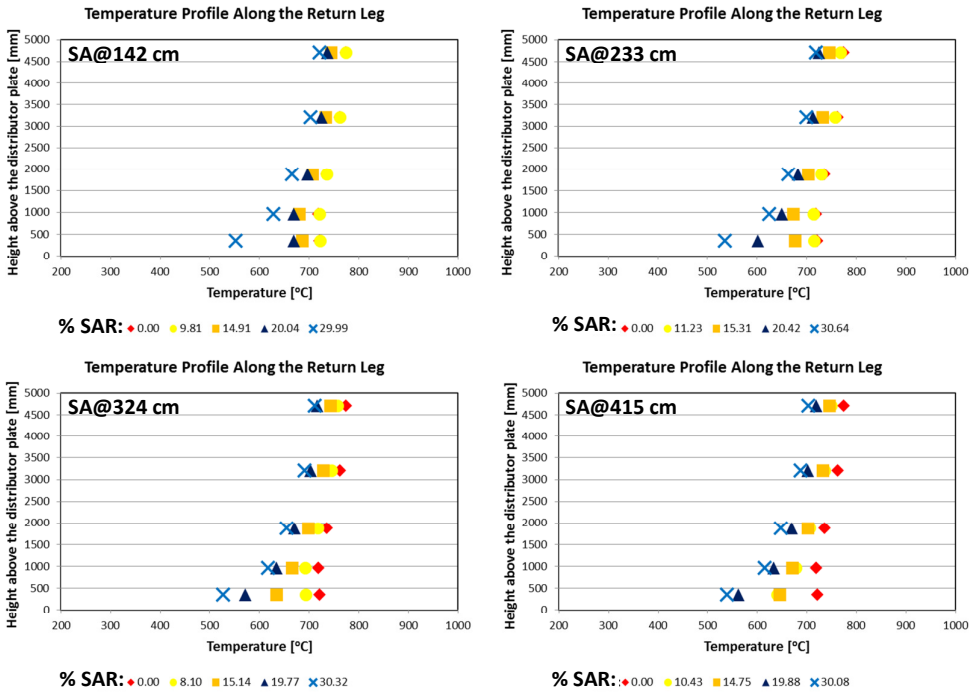

Figure 5.38 Effect of secondary air ratio and its location on temperature profile along the return leg for co-combustion of Bursa/Orhaneli lignite with 30% (by wt.) woodchips (C1-B2-4)

5.2.4. Co-Combustion of Bursa/Orhaneli Lignite with 50% (by wt.) Woodchips (C1-B2-5)

The effect of SA and its location on temperature profile along the combustor and return leg for the co-combustion of Bursa/Orhaneli lignite with 50% by wt. woodchips is given in Figure 5.39 and Figure 5.40, respectively. When the temperature profiles of the combustor in Figure 5.39 are compared to that for the case of co-combustion of 30% woodchips in Figure 5.37, it can be seen that the effect of SAR on the temperature of dense phase is more significant in the case of co-combustion of 50% woodchips than 30% woodchips case. While the temperature difference of the average dense phase for different SAR (ranging from 0 to 30%) was between 30 and 45°C for C1-B2-4, it became larger and ranged between 55 and 90°C for C1-B2-5. This might be explained by the decreasing char amount in the combustor with the increasing share of woodchips in the fuel mixture. From the point of thermal inertia, the ash material mainly coming from the coal helps the thermal stability of the combustor to be kept constant. However, when the amount of the woodchips increases, the amount of the ash formation decreases. Less amount of ash formation for the co-combustion of 50% woodchips and 50% coal, might be the reason why more separate temperature profiles are obtained in the dense phase.

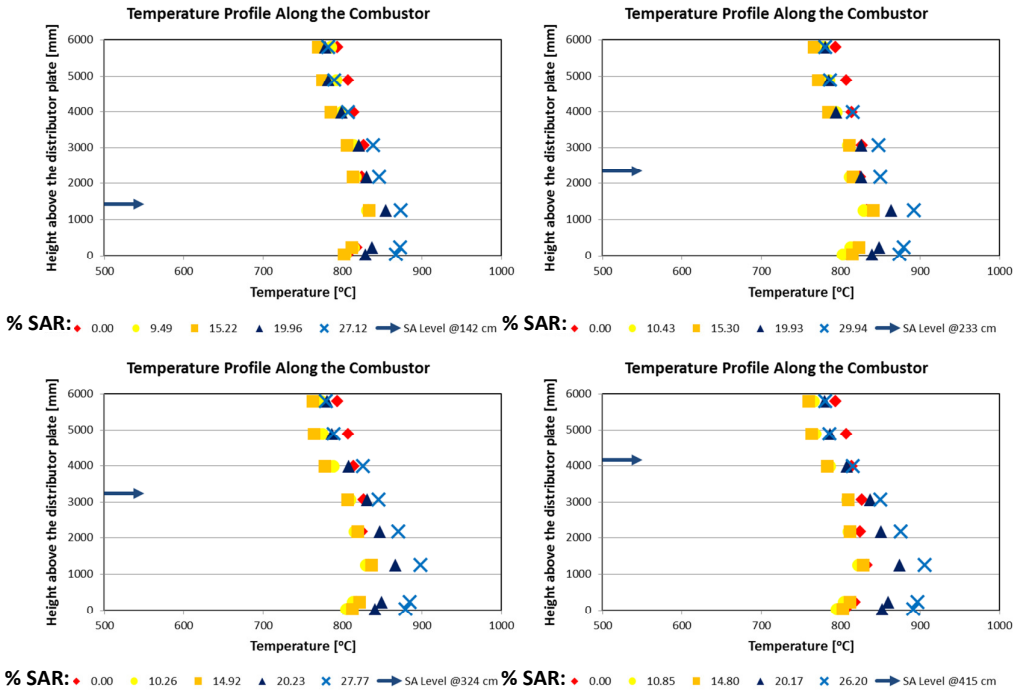

Figure 5.39 Effect of secondary air ratio and its location on temperature profile of combustor for co-combustion of Bursa/Orhaneli lignite with 50% (by wt.) woodchips (C1-B2-5)

The volatile matter content of fuel mixture rose up to 55.1% from 46.1% with an increase in the share of woodchips in fuel mixture from 30% to 50%. Burning of volatile matters mainly in the dilute phase (>1.25 m) caused temperatures measured in that region to be close to each other for different SARs. While the difference between the highest and the lowest temperature of the gas leaving the combustor ranges between 36 and 43°C for C1-B2-4, it was more close and ranging between 25 and 34°C for C1-B2-5. The more compact and smoother temperature distribution at the top of the combustor resulted in smoother temperature profile along the return leg for C1-B2-5 as can be seen in Figure 5.40. Therefore, it can be said that the temperature profile along the return leg is more dependent on the temperature of the dilute phase of the combustor rather than that of the dense phase.

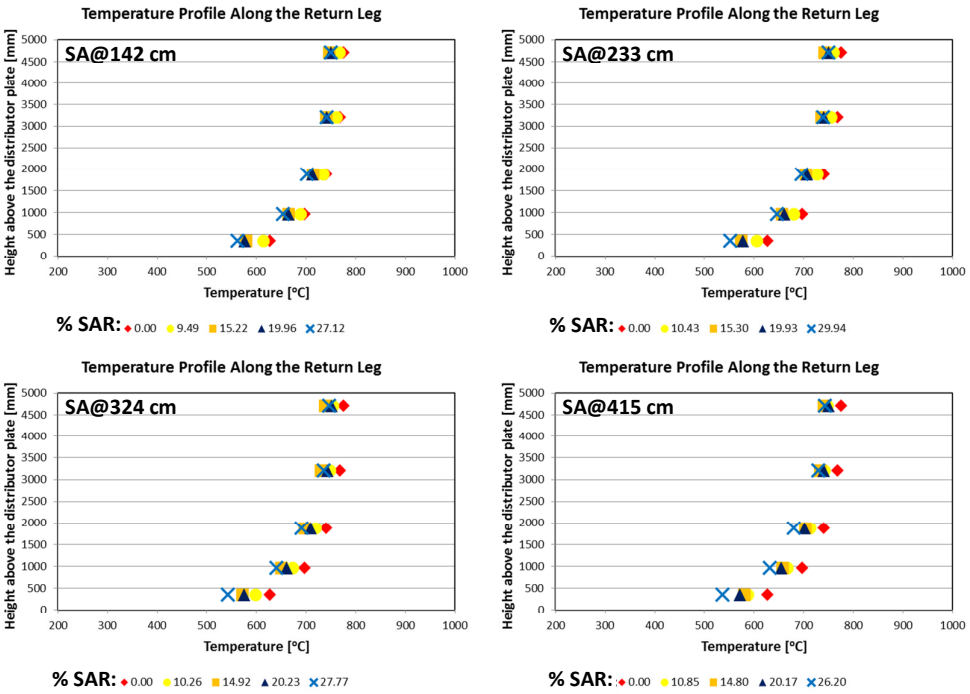

Figure 5.40 Effect of secondary air ratio and its location on temperature profile of return leg for co-combustion of Bursa/Orhaneli lignite with 50% (by wt.) woodchips (C1-B2-5)

5.2.5. Discussion on the Effect of Secondary Air Ratio on Emissions in SET#2

CO, NO, and SO_2 emissions and average temperature of dense phase with corresponding secondary air ratios during the co-combustion of **Bursa/Orhaneli lignite with 30% olive cake** are given in Table 5.5. The effect of secondary air ratio (SAR) and its location on the CO, NO, and SO_2 emissions resulting from the co-combustion of Bursa/Orhaneli lignite with 30% olive cake and also comparison of CO, NO, and SO_2 emissions with the emission limits given in the Turkish Regulation ("Turkish Regulation for Industrial Air Pollution Control," 2009) is given in Figure 5.41, Figure 5.42, and Figure 5.43, respectively.

Table 5.5 Secondary air ratios and corresponding CO, NO, and SO_2 emissions and T_{dp} for the co-combustion of Bursa/Orhaneli lignite with 30% olive cake (by wt.) (C1-B1-4)

SAR [%]	CO	NO (6% O_2) [mg/Nm^3]	SO_2	T_{dp}* [^oC]
Location of SA Injection: 142 cm above distributor plate				
0.00	390.12	400.65	2057.45	785.93
10.11	440.19	386.50	2119.92	788.13
14.86	556.56	393.00	2092.63	793.37
20.05	581.13	378.23	2184.60	812.54
26.16	573.45	361.87	2999.31	878.30
Location of SA Injection: 233 cm above distributor plate				
0.00	390.12	400.65	2057.45	785.93
12.26	498.20	381.89	2159.43	790.27
15.39	542.73	387.77	2179.06	801.81
20.05	561.53	389.12	2236.43	821.38
28.78	457.67	347.45	3295.27	880.54
Location of SA Injection: 324 cm above distributor plate				
0.00	390.12	400.65	2057.45	785.93
10.75	575.27	381.21	2156.99	791.61
15.15	606.40	368.91	2213.01	803.63
19.84	513.01	387.80	2270.71	826.00
27.05	502.10	312.04	3296.53	875.63
Location of SA Injection: 415 cm above distributor plate				
0.00	390.12	400.65	2057.45	785.93
9.74	508.50	391.63	2120.68	785.01
14.68	543.42	368.54	2148.32	795.60
20.08	527.92	364.45	2398.16	839.53
26.00	555.56	307.48	3164.85	868.22

*Average of (TT109-TT110-TT112)

The effect of SAR and its location on **CO emission** is given in Figure 5.41. CO emission was about 400 mg/Nm^3 in the case of where secondary air was not used. After the introduction of secondary air into the combustor, CO emission started to increase regardless of the location of the secondary air injection. When secondary air was given into the combustor at 142 cm above distributor plate, CO emission increased as SAR was increased. When it was given into the combustor at 233 cm above the distributor plate, it increased with SAR up to 20%. After that ratio, a further increase in SAR caused a little decrease in CO emission. This trend was also valid for the secondary air injections at 324 cm and 415 cm above the distributor plate. In these cases, CO emissions were maximum at SAR=15%, and then, they started to decrease with an increase in SAR. Among the SARs, range of 10-15% was seen to be best for CO emission. With further increases in SAR, CO emission got worse. In all other cases of secondary air injection, CO emission increased with secondary air ratio. Minimum CO emission was measured in the case of

where secondary air was given into the combustor at 142 cm above the distributor plate at SAR=10%. It was about 440 mg/Nm^3, however; it is still above the emission limit (285 mg/Nm^3) specified by the Turkish Regulation ("Turkish Regulation for Industrial Air Pollution Control," 2009). This limit was calculated as the weighted-average of thermal power obtained from each fuel according to the Turkish Regulation ("Turkish Regulation for Industrial Air Pollution Control," 2009). In Figure 5.41, emission limits for coal (200 mg/Nm^3) and for biomass (460 mg/Nm^3) were also shown.

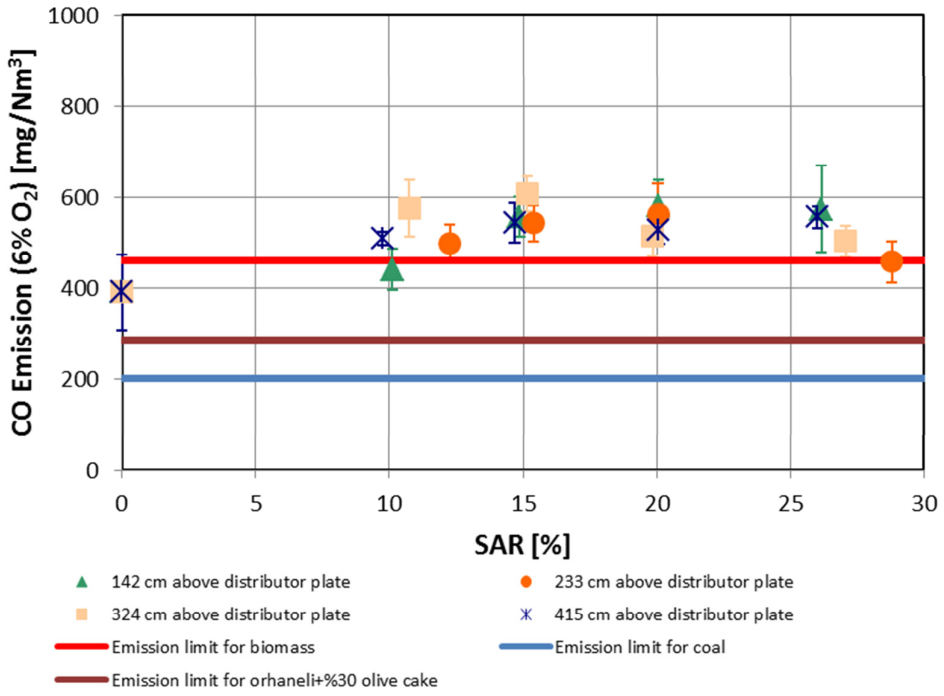

Figure 5.41 Effect of secondary air ratio and its location on CO emission and comparison of CO emission to emission limits for co-combustion of Bursa/Orhaneli lignite with 30% (by wt.) olive cake (C1-B1-4)

The effect of secondary air ratio and its location on **NO emission** is given in Figure 5.42. As can be seen from Figure 5.42, NO emission decreased with increasing secondary air ratio. The decrease observed in NO emission might be explained by the formation of reducing atmosphere at the lower parts of the combustor with the introduction of secondary air to the combustor. It was observed that the location of secondary air given into the combustor did not have distinctive effect on NO emission. In all cases of secondary air injection, NO emission was under emission limit (480 mg/Nm^3) for the fuel mixture.

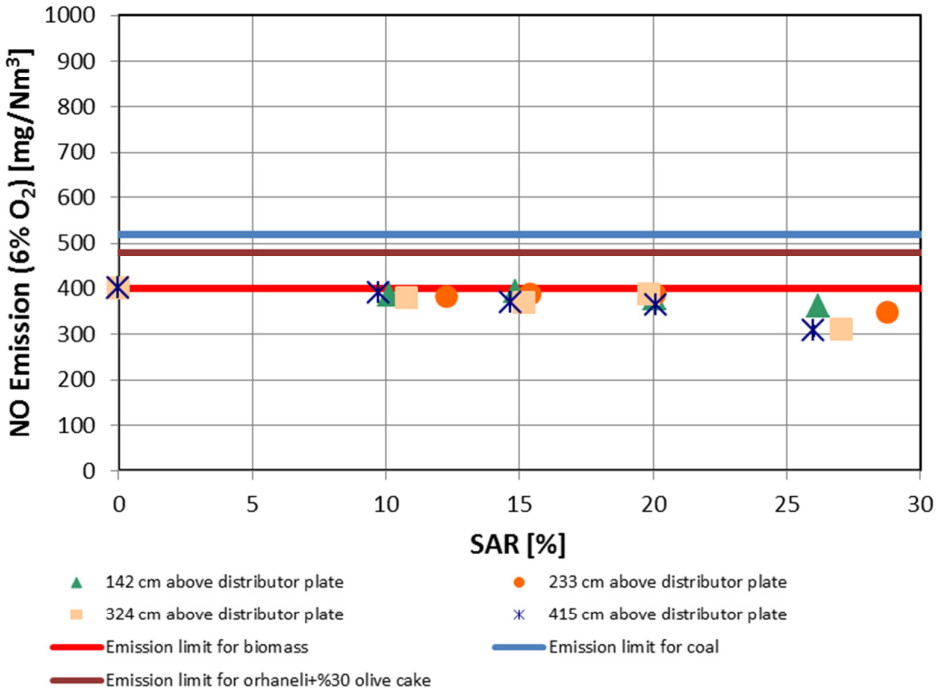

Figure 5.42 Effect of secondary air ratio and its location on NO emission and comparison of NO emission to emission limits for co-combustion of Bursa/Orhaneli lignite with 30% (by wt.) olive cake (C1-B1-1)

Effect of secondary air ratio and its location on **SO_2 emission** is given in Figure 5.43. As can be seen from Figure 5.43, SO_2 emission increased with secondary air ratio in all cases of injection of secondary air to combustor at different locations. In all cases of secondary air injection, SO_2 emission was above emission limit (1405 mg/Nm^3) for the fuel mixture. SO_2 emission also increases by increasing the height at which the secondary air given to the combustor. When some portion of combustion air is given into the combustor as secondary air, the amount of secondary air injected to combustor at specific location might create an extra resistance on the primary air coming through the distributor plate. This resistance might affect the hydrodynamic of all system, particularly the hydrodynamic of the dense phase. The dense phase of the combustor might become denser in term of particulates with the secondary air injection into the combustor. The reduction in the amount of air given in dense phase and the increase in the particulate concentration in the same region might be a reason for the temperature increase observed in dense phase. This temperature increase probably triggered conversion of fuel-S to SO_2 emission. Limestone addition was suggested for the co-combustion of Bursa/Orhaneli lignite with 30% olive cake.

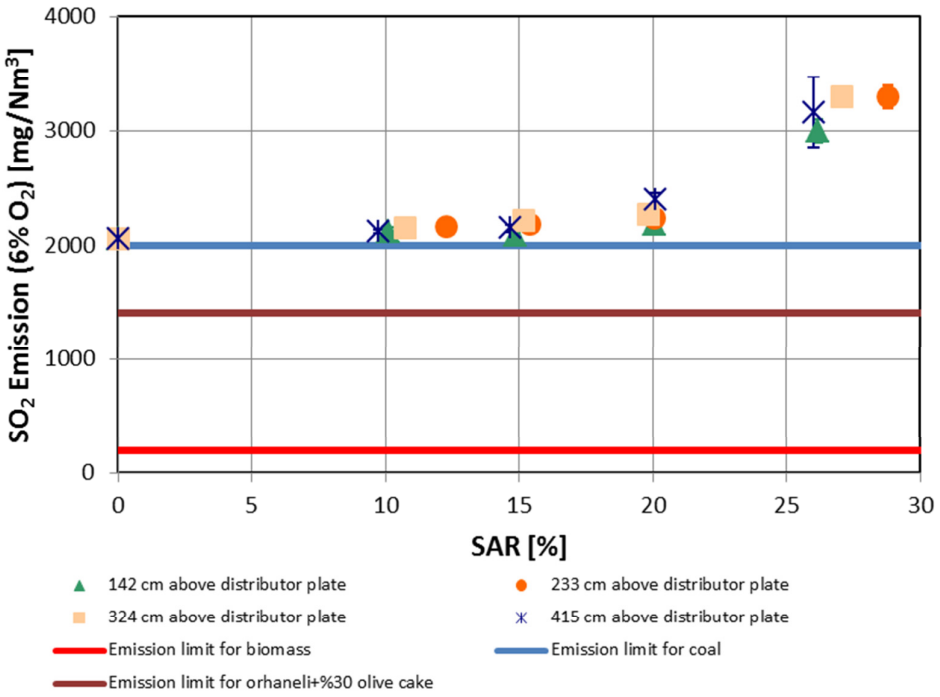

Figure 5.43 Effect of secondary air ratio and its location on SO_2 emission and comparison of SO_2 emission to emission limits for co-combustion of Bursa/Orhaneli lignite with 30% (by wt.) olive cake (C1-B1-4)

CO, NO, and SO_2 emissions and average temperature of dense phase corresponding to secondary air ratios during the co-combustion of **Bursa/Orhaneli lignite with 50% olive cake** are given in Table 5.6. Comparison of CO, NO, and SO_2 emissions resulting from the combustion of Bursa/Orhaneli lignite with 50% olive cake by using secondary air, with the emission limits given in the Turkish Regulation ("Turkish Regulation for Industrial Air Pollution Control," 2009) is given in Figure 5.44, Figure 5.45, and Figure 5.46, respectively.

Table 5.6 Secondary air ratios and corresponding CO, NO, and SO_2 emissions and T_{dp} for the co-combustion of Bursa/Orhaneli lignite with 50% olive cake (by wt.) (C1-B1-5)

SAR [%]	CO	NO (6% O_2) [mg/Nm^3]	SO_2	T_{dp}* [^{o}C]
Location of SA Injection: 142 cm above distributor plate				
0.00	1381.82	361.46	852.06	812.99
7.96	971.72	353.44	905.05	807.17
14.84	762.69	348.36	966.74	809.60
19.83	1074.96	314.09	1200.93	821.32
Location of SA Injection: 233 cm above distributor plate				
0.00	1381.82	361.46	852.06	812.99
9.42	1215.03	340.34	1068.81	823.33
20.18	899.54	339.84	1162.86	839.94
28.48	958.21	308.44	1659.51	857.75
Location of SA Injection: 324 cm above distributor plate				
0.00	1381.82	361.46	852.06	812.99
10.29	569.23	380.69	1376.57	829.80
14.71	571.23	384.17	1392.22	832.86
19.66	568.40	369.28	1516.80	841.26
26.27	547.24	319.67	1944.42	859.18
Location of SA Injection: 415 cm above distributor plate				
0.00	1381.82	361.46	852.06	812.99
11.09	546.94	357.20	1328.24	831.13
15.06	597.28	354.89	1380.53	837.54
19.94	693.45	333.70	1571.23	848.07
26.40	1345.11	276.40	1948.37	866.14

*Average of (TT109-TT110-TT112)

The effect of secondary air ratio and its location on **CO emission** is given in Figure 5.44. When secondary air was introduced to the combustor column at 142 cm above the distributor plate, CO emission started to decrease at low secondary air ratios. When it was about 1380 mg/Nm^3 without secondary air injection, it decreased down to 760 mg/Nm^3 at SAR=15%. Among the SARs, range of 10-15% was seen to be best for CO emission. Further increases of SAR made CO emission worse. In all other cases of secondary air injection, CO emission increased with secondary air ratio. Minimum CO emissions were measured when secondary air was given at 324 cm and 415 cm above the distributor plate and SAR was between 10-15%. CO emission was measured in the range of 550-600 mg/Nm^3 in those operational conditions. However, it was still above the limit (333 mg/Nm^3) specified by the Turkish Regulation ("Turkish Regulation for Industrial Air Pollution Control," 2009).

As the percentage of olive cake in the fuel mixture was increased, CO emissions increased. This increase on CO emissions might be explained by the high volatile content

of olive cake (64.3% by wt.) compared to that of Bursa/Orhaneli lignite (36.6% by wt.) as can be seen in Table 4.2. If these volatiles cannot find enough oxygen to burn, they leave the combustor as partially oxidized species. That is why CO emissions become high in the flue gas. This phenomenon was also observed and explained in the previous studies of authors (Varol and Atimtay, 2007; Atimtay and Varol, 2009).

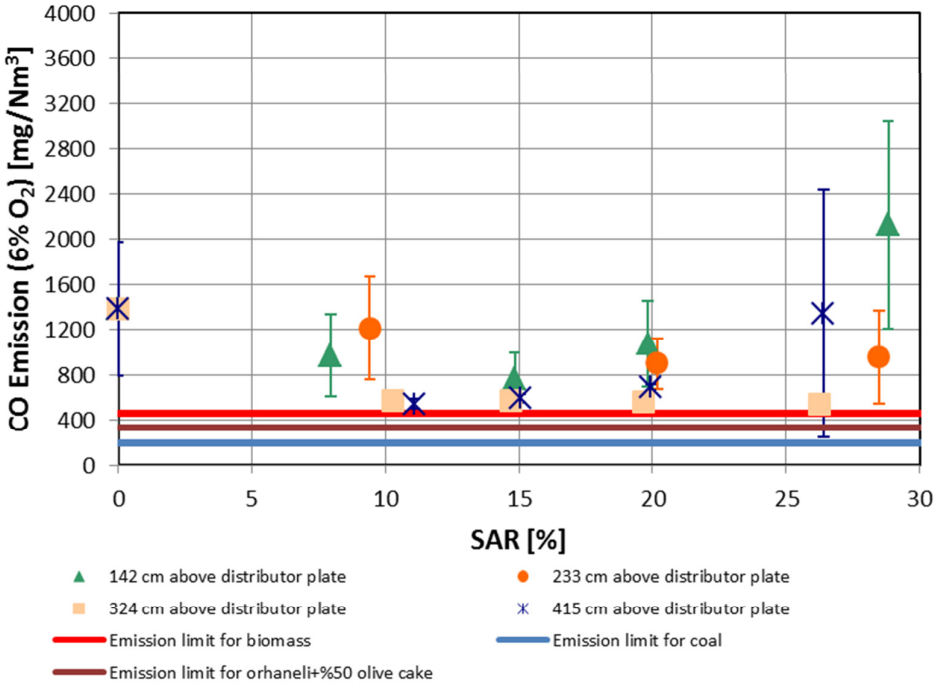

Figure 5.44 Effect of secondary air ratio and its location on CO emission and comparison of CO emission to emission limits for co-combustion of Bursa/Orhaneli lignite with 50% (by wt.) olive cake (C1-B1-5)

Effect of secondary air ratio and its location on **NO emission** is given in Figure 5.45. As can be seen from Figure 5.45, NO emission decreased with increasing secondary air ratio as a general trend. In all cases of secondary air injection, NO emission was under emission limit (458 mg/Nm^3) for the fuel mixture.

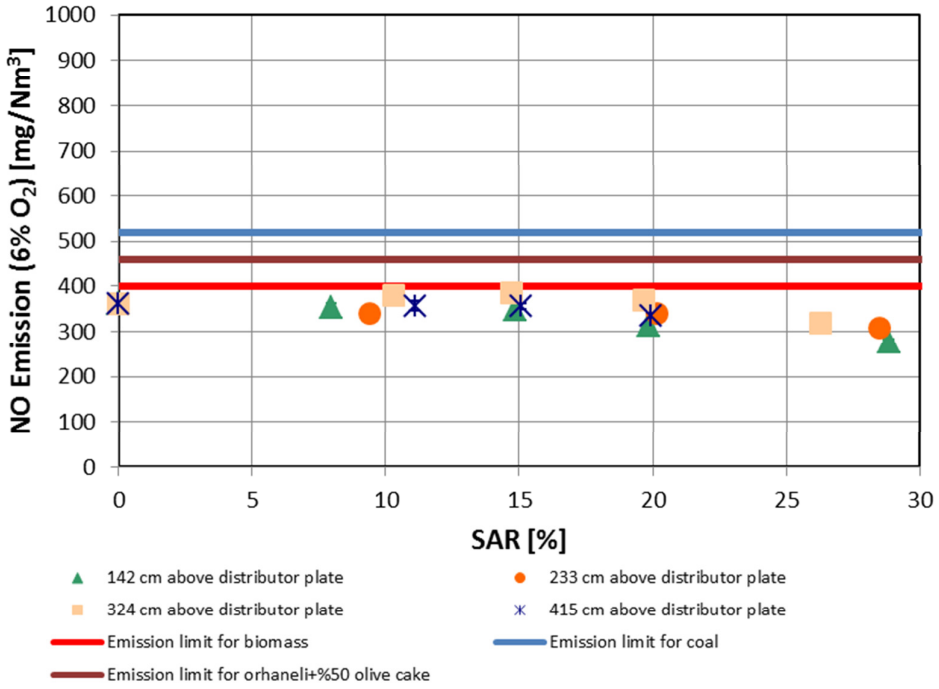

Figure 5.45 Effect of secondary air ratio and its location on NO emission and comparison of NO emission to emission limits for co-combustion of Bursa/Orhaneli lignite with 50% (by wt.) olive cake (C1-B1-5)

Effect of SAR and its location on **SO_2 emission** is given in Figure 5.46. SO_2 emission increased with secondary air injection as can be seen in the co-combustion of Bursa/Orhaneli lignite with 30% olive cake. The increase of SO_2 emission can be explained with the temperature increase in the dense phase. While SO_2 emission was under emission limit (1075 mg/Nm^3) without secondary air, it exceeded the limit with the introduction of secondary air into the combustor. Secondary air can be given to the combustor from 142 cm above the distributor plate at a rate less than 15% in order to be under the emission limits.

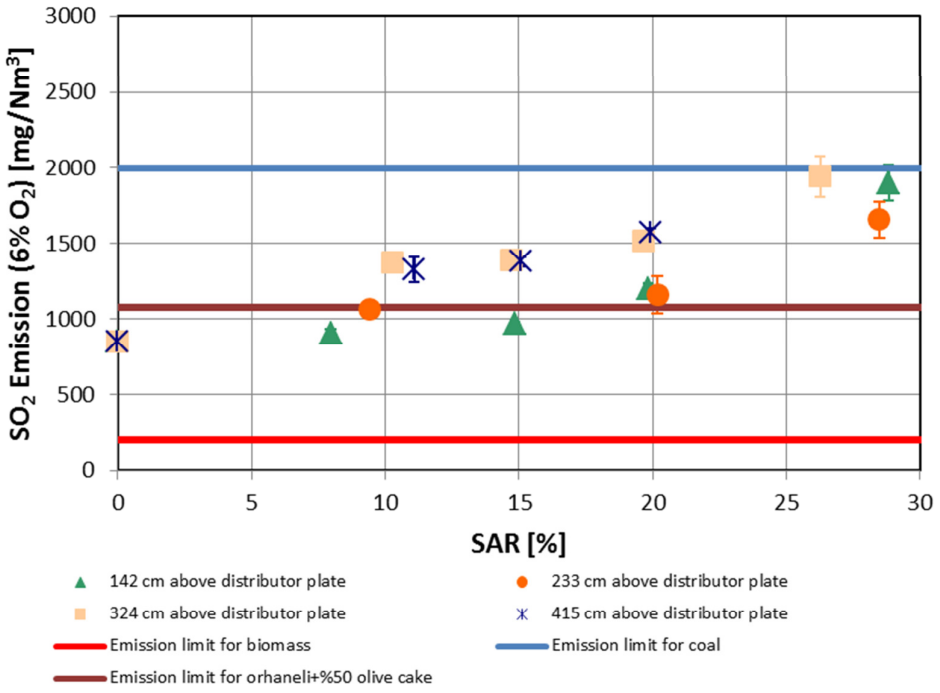

Figure 5.46 Effect of secondary air ratio and its location on SO_2 emission and comparison of SO_2 emission to emission limits for co-combustion of Bursa/Orhaneli lignite with 50% (by wt.) olive cake (C1-B1-5)

CO, NO, and SO_2 emissions and T_{dp} to corresponding SARs during the co-combustion of **Bursa/Orhaneli lignite with 30% woodchips** are given in Table 5.7. The effect of SAR and its location on the CO, NO, and SO_2 emissions resulting from the co-combustion of Bursa/Orhaneli lignite with 30% woodchips and also comparison of CO, NO, and SO_2 emissions with the emission limits of the Turkish Regulation ("Turkish Regulation for Industrial Air Pollution Control," 2009) is given in Figure 5.47, Figure 5.49, and Figure 5.50, respectively.

Table 5.7 Secondary air ratios and corresponding CO, NO, and SO_2 emissions and T_{dp} for the co-combustion of Bursa/Orhaneli lignite with 30% woodchips (by wt.) (C1-B2-4)

SAR	CO	NO	SO_2	T_{dp}*	Cyclone Outlet Temperature
[%]		(6% O_2) [mg/Nm^3]		[^oC]	[^oC]
Location of SA Injection: 142 cm above distributor plate					
0.00	303.94	278.89	2429.73	839.11	728.39
9.81	276.06	277.12	2747.53	843.47	729.93
14.91	313.35	353.17	2391.52	819.42	704.37
20.04	336.84	302.31	2466.61	824.00	698.81
29.99	561.82	225.92	2995.85	864.32	690.41
Location of SA Injection: 233 cm above distributor plate					
0.00	303.94	278.89	2429.73	839.11	728.39
11.23	340.11	280.79	2731.12	845.27	726.14
15.31	399.12	315.88	2503.25	835.46	706.58
20.42	467.10	267.18	2709.65	840.36	692.90
30.64	660.40	221.37	3154.73	865.75	688.80
Location of SA Injection: 324 cm above distributor plate					
0.00	303.94	278.89	2429.73	839.11	728.39
8.10	287.26	309.80	2655.26	840.62	717.51
15.14	307.00	287.03	2581.80	844.10	707.39
19.77	429.78	253.51	2727.04	846.95	688.75
30.32	586.40	194.51	3744.56	869.97	686.08
Location of SA Injection: 415 cm above distributor plate					
0.00	303.94	278.89	2429.73	839.11	728.39
10.43	289.67	261.03	2646.06	849.34	713.40
14.75	289.29	281.51	2561.77	845.51	709.61
19.88	502.81	206.83	2763.23	852.18	689.25
30.08	506.68	181.55	4117.07	874.35	684.50

*Average of (TT109-TT110-TT112)

The effect of SAR and its location on **CO emission** is given in Figure 5.47. CO emission was about 300 mg/Nm^3 in the case of where SA was not used. With the introduction of 10% SA into the combustor, CO emissions decreased a little for all location of SA injection except at 233 cm above the distributor plate, and then they started to increase with further increase in SAR. While minimum CO emission was obtained at 10% SAR for the locations 142 cm and 324 cm, it was minimum at 15% for the location of 415 cm. Among the SARs, range of 10-15% was seen to be best for CO emission. Further increases in SAR made the CO emission worse. Minimum CO emission was measured in the case of where SA was given into the combustor at 142 cm above the distributor plate at SAR=9.8%. It was about 276 mg/Nm^3, which is slightly above the emission limit (273 mg/Nm^3) specified by the Turkish Regulation, ("Turkish Regulation for Industrial Air Pollution Control," 2009).

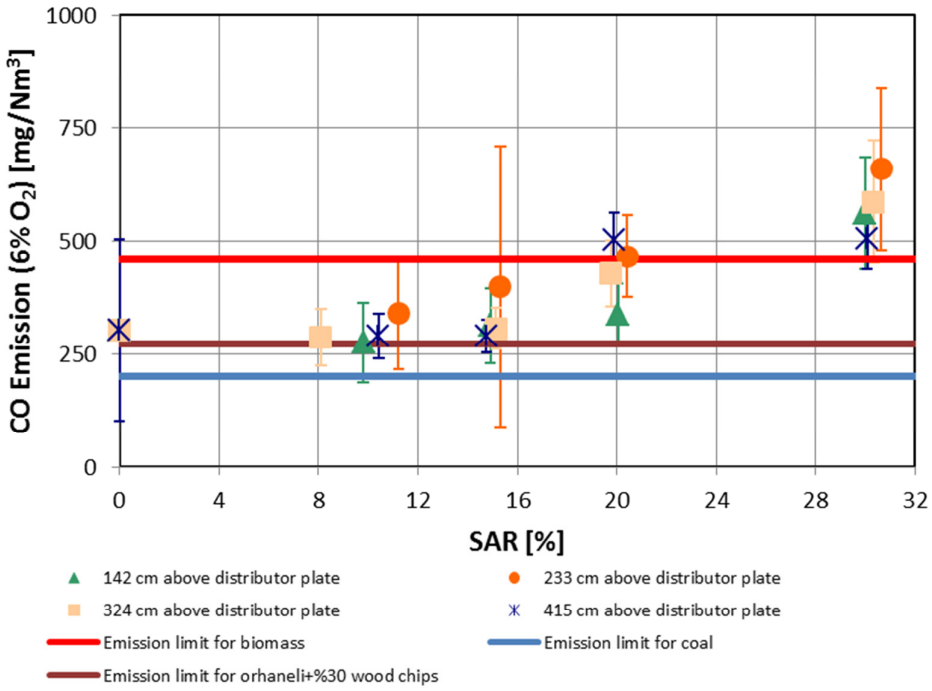

Figure 5.47 Effect of secondary air ratio and its location on CO emission and comparison of CO emission to emission limits for co-combustion of Bursa/Orhaneli lignite with 30% (by wt.) woodchips (C1-B2-4)

It is said that CO emissions are influenced by SAR and they increase by increasing SAR. In order to check that statement, CO emissions and cyclone outlet temperature were plotted with respect to SAR in Figure 5.48 for the case of SA injection@142 cm above the distributor plate. It was drawn for only SA@142 cm since CO emissions and cyclone outlet temperature profiles were all the same for other levels of SA. As can be seen in Figure 5.48, CO emission increases with SAR but at the same time, cyclone outlet temperature, which has a decreasing effect on CO emissions according to the study of Lyngfelt and Leckner (1999), also decreases with SAR. Increasing SAR by causing cyclone outlet temperature to decrease may indirectly result in CO emissions to increase.

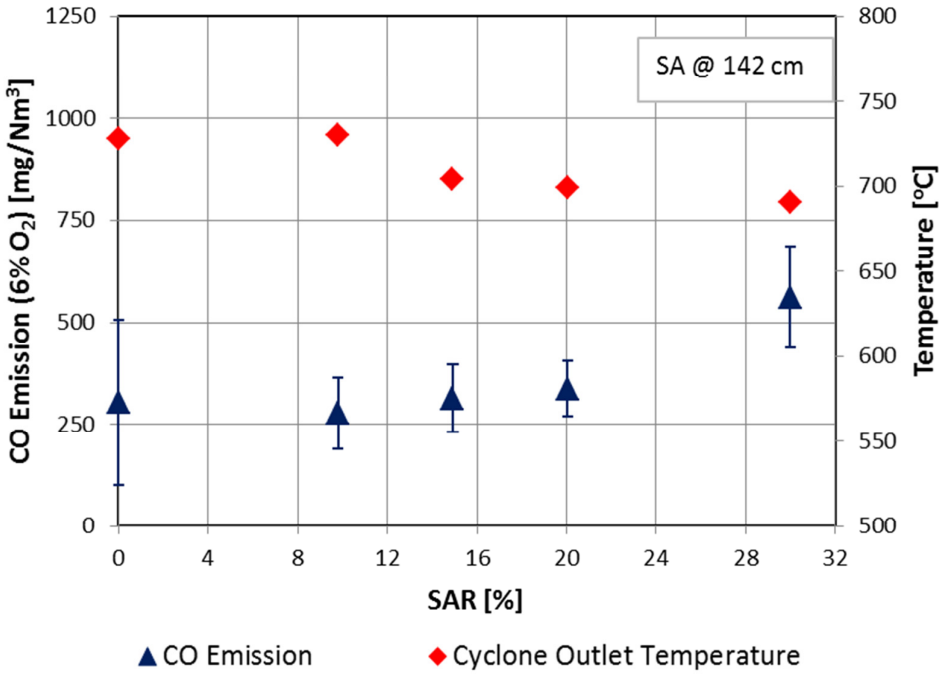

Figure 5.48 Effect of secondary air ratio on CO emission with respect to cyclone outlet temperature for co-combustion of Bursa/Orhaneli lignite with 30% (by wt.) woodchips (C1-B2-4)

The effect of SAR and its location on **NO emission** is given in Figure 5.49. As can be seen from Figure 5.49, NO emission decreased with increasing SAR. As the SA was introduced into the combustor, the primary air was reduced as much as the amount of air which was given as SA, keeping the total amount of air constant. Thus, the more SA was given into the combustor, the more reducing atmosphere was established in the dense phase. Therefore, the decrease observed in NO emission might be explained by the formation of reducing atmosphere at the lower parts of the combustor with the introduction of SA to the combustor. This was also explained by the study of Suksankraisorn et al. (2004) stating that NO might be reduced by CO, CH_4 and char in the bed in the dense phase which was become the reduction zone with the increase in SAR. It was observed that the location of SA given into the combustor had a distinctive effect on NO emission especially for SA higher than 15%. In all cases of SA injection, NO emissions were below the emission limit (486 mg/Nm^3) for the fuel mixture.

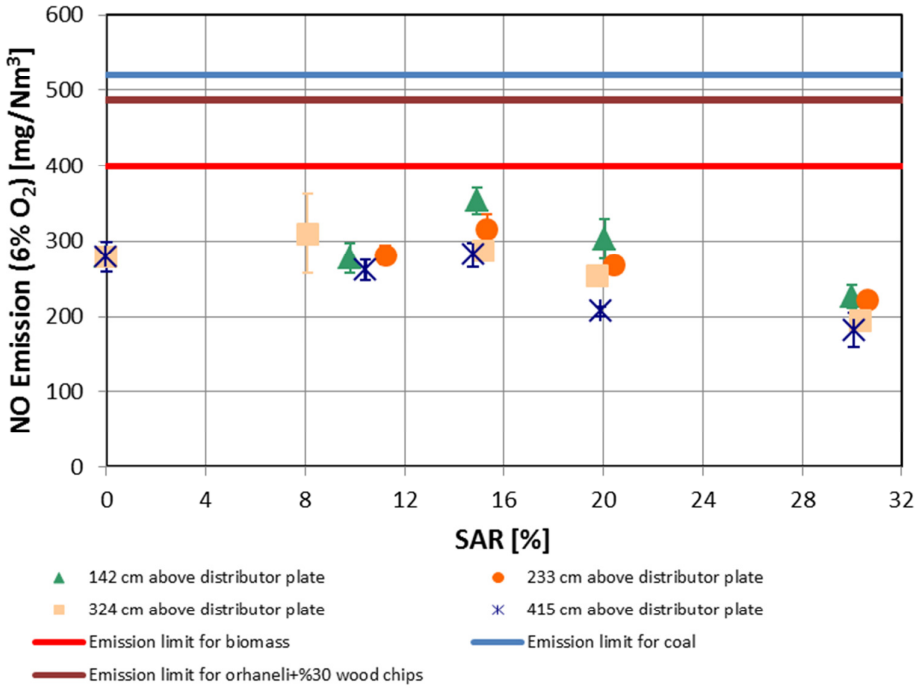

Figure 5.49 Effect of secondary air ratio and its location on NO emission and comparison of NO emission to emission limits for co-combustion of Bursa/Orhaneli lignite with 30% (by wt.) woodchips (C1-B2-4)

Effect of SAR and its location on **SO_2 emission** is given in Figure 5.50. As can be seen from Figure 5.50, SO_2 emission increased with SAR in all cases. In all cases of SA injection, SO_2 emission was above emission limit (1496 mg/Nm^3) for the fuel mixture. SO_2 emission increased with increasing the height of SA injection especially after 20%. When some portion of combustion air is given into the combustor as SA, the amount of SA injected to combustor at specific location might create an extra resistance on the primary air coming through the distributor plate. This resistance might affect the hydrodynamic of all system, particularly the hydrodynamic of the dense phase. The dense phase of the combustor might become denser in term of particulates with SA injection into the combustor. The reduction in the amount of air given in dense phase and the increase in the particulate concentration in the same region might be a reason for the temperature increase observed in that region. This temperature increase probably triggered conversion of fuel-S to SO_2 emission.

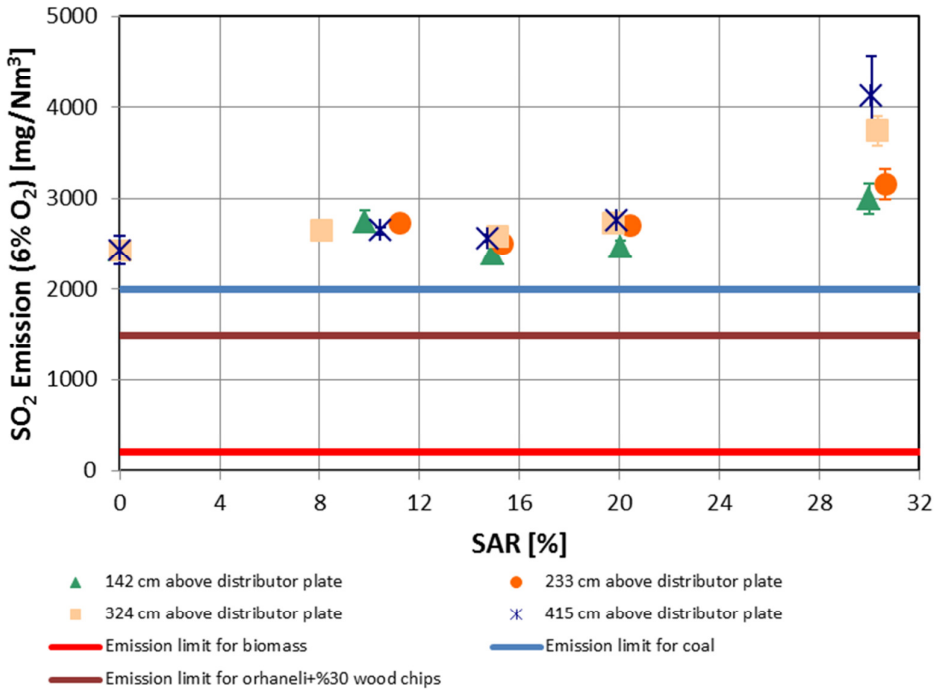

Figure 5.50 Effect of secondary air ratio and its location on SO_2 emission and comparison of SO_2 emission to emission limits for co-combustion of Bursa/Orhaneli lignite with 30% (by wt.) woodchips (C1-B2-4)

CO, NO, and SO_2 emissions and T_{dp} to corresponding SARs during the co-combustion of **Bursa/Orhaneli lignite with 50% woodchips** are given in Table 5.8. Comparison of CO, NO, and SO_2 emissions resulting from the combustion of Bursa/Orhaneli lignite with 50% woodchips by using SA, with the emission limits of the Turkish Regulation ("Turkish Regulation for Industrial Air Pollution Control," 2009) is given in Figure 5.51, Figure 5.52, and Figure 5.53, respectively.

Table 5.8 Secondary air ratios and corresponding CO, NO, and SO_2 emissions and T_{dp} for the co-combustion of Bursa/Orhaneli lignite with 50% woodchips (by wt.) (C1-B2-5)

SAR	CO	NO	SO_2	T_{dp}*	Cyclone Outlet Temperature
[%]		(6% O_2) [mg/Nm^3]		[^oC]	[^oC]
Location of SA Injection: 142 cm above distributor plate					
0.00	228.51	332.02	1878.25	819.01	729.64
9.49	257.16	341.54	1993.33	816.03	723.30
15.22	343.33	318.33	1887.84	815.54	706.89
19.96	475.74	271.93	1874.59	840.36	713.02
27.12	342.60	284.32	2215.76	871.12	716.29
Location of SA Injection: 233 cm above distributor plate					
0.00	228.51	332.02	1878.25	819.01	729.64
10.43	275.74	347.18	1966.25	814.80	717.74
15.30	327.65	301.91	1877.69	826.06	703.02
19.93	315.78	281.13	1892.28	850.76	714.01
29.94	219.61	317.13	2354.65	882.19	714.40
Location of SA Injection: 324 cm above distributor plate					
0.00	228.51	332.02	1878.25	819.01	729.64
10.26	308.16	335.34	1992.16	815.79	712.61
14.92	355.88	305.59	1985.52	823.54	699.73
20.23	259.06	290.65	1905.41	852.29	714.95
27.77	223.94	286.44	2369.10	887.74	712.72
Location of SA Injection: 415 cm above distributor plate					
0.00	228.51	332.02	1878.25	819.01	729.64
10.85	348.12	353.49	2007.10	807.23	706.92
14.80	359.24	326.90	1979.08	814.16	701.09
20.17	239.41	275.72	1993.79	862.30	713.82
26.20	238.26	261.83	2554.01	897.89	711.16

*Average of (TT109-TT110-TT112)

The effect of SAR and its location on **CO emission** is given in Figure 5.51. In the case of without SA, CO emissions were about 230 mg/Nm^3. With the introduction of SA, CO emissions started to increase, reaching their maximum value at 15% SAR for all SA injection levels except the level of 142 cm. In this case, CO emission was at the highest value for 25% SAR. After then, they showed a decreasing trend with a further increase in SAR. The increase observed in CO emissions with the increase of SAR up to 15% for all levels of SA injection can attributed to the temperature decrease seen in the cyclone outlet. In the case of C1-B2-4, CO emissions were at maximum in the range of 510-660 mg/Nm^3 for 30% SAR. In this case, the temperatures of cyclone outlet were in the range of 685-690^{o}C. When the woodchips share in fuel mixture increased up to 50%, CO emissions dropped down to the levels of 220 and 340 mg/Nm^3 for 30% SAR because of the increase in the temperatures of cyclone outlet which were in the range of 711-716^{o}C.

The increase of woodchips share in the fuel mixture from 30% to 50% increased the total amount of volatile matter content of fuel mixture and also increased the number of particles which were lighter than the coal particles. Because of the increased volatile matter of the fuel mixture from 46.1% up to 55.1%, the more woodchips particles started to burn in the upper part of the combustor and consequently the temperature of the this region climbed up after the introduction of SAR more than 15% when compared to the temperature in the upper part of the combustor of the test C1-B2-4. The decrease in CO emissions with SAR after 15% can also be explained by the temperature increase in dense phase. Increasing the amount of SA, particularly more than 15%, in total air reduced the amount of primary air leading the temperature of the dense phase region to increase. The increase in the dense phase temperature can also increase all the temperature within the system finally having a reducing effect on CO emissions. CO emissions were all below the limit (337 mg/Nm^3) specified by the Turkish Regulation ("Turkish Regulation for Industrial Air Pollution Control," 2009) in the case of all SA injection from 233 cm high above the distributor plate. They were also below the limit in the case of SA@324 cm except 15% SAR. In the case of SA@415 cm, SAR should be higher that 20% to keep CO emission below the limit.

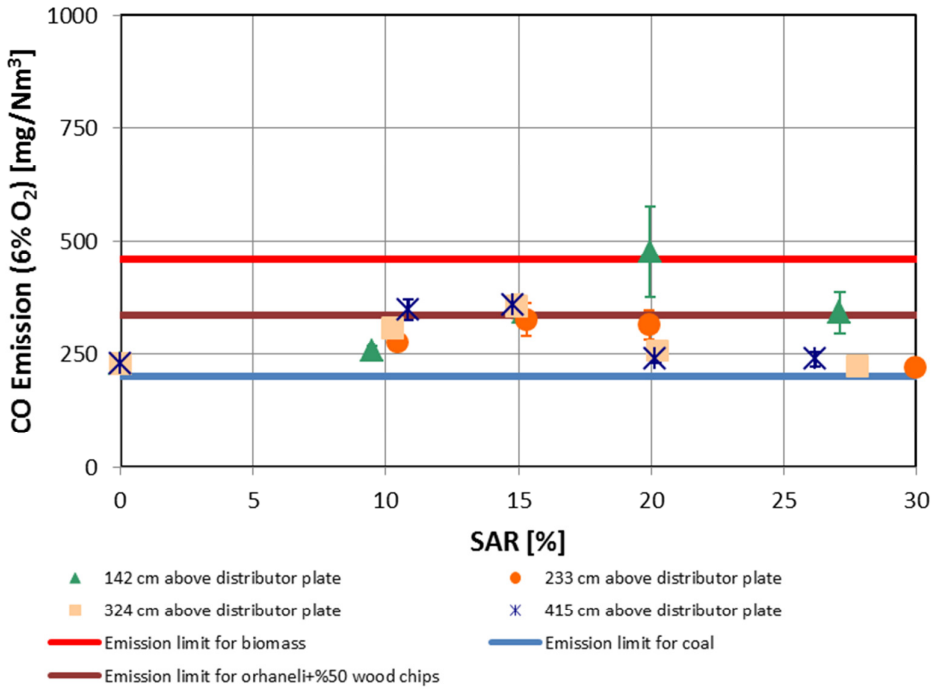

Figure 5.51 Effect of secondary air ratio and its location on CO emission and comparison of CO emission to emission limits for co-combustion of Bursa/Orhaneli lignite with 50% (by wt.) woodchips (C1-B2-5)

Effect of SAR and its location on **NO emission** is shown in Figure 5.52. As can be seen from Figure 5.52, NO emission decreased with increasing SAR as a general trend as seen in C1-B2-4. While NO emissions were in the range of 182-353 mg/Nm^3 for C1-B2-4 (30% woodchips), they increased a little up and measured in the range of 262-353 mg/Nm^3 for C1-B2-5 (50% woodchips). Although N content of the fuel mixture decreased down to 0.44% from 0.69% on dry basis by weight with the increase woodchips share in the fuel mixture from 30% to 50%, NO emissions were dropped down. While a reduction between 19-35% on NO emission was seen for C1-B2-4, it was only between 5 and 21% for C1-B2-5. This can be explained by the less amount of char formed which has a reducing effect on the fuel-N conversion to NO as stated in the study of Suksankraisorn et al. (2004). This was also mentioned in the study of Leckner et al. (2004). In all cases of SA injection, NO emissions were under emission limit (457 mg/Nm^3) for the fuel mixture.

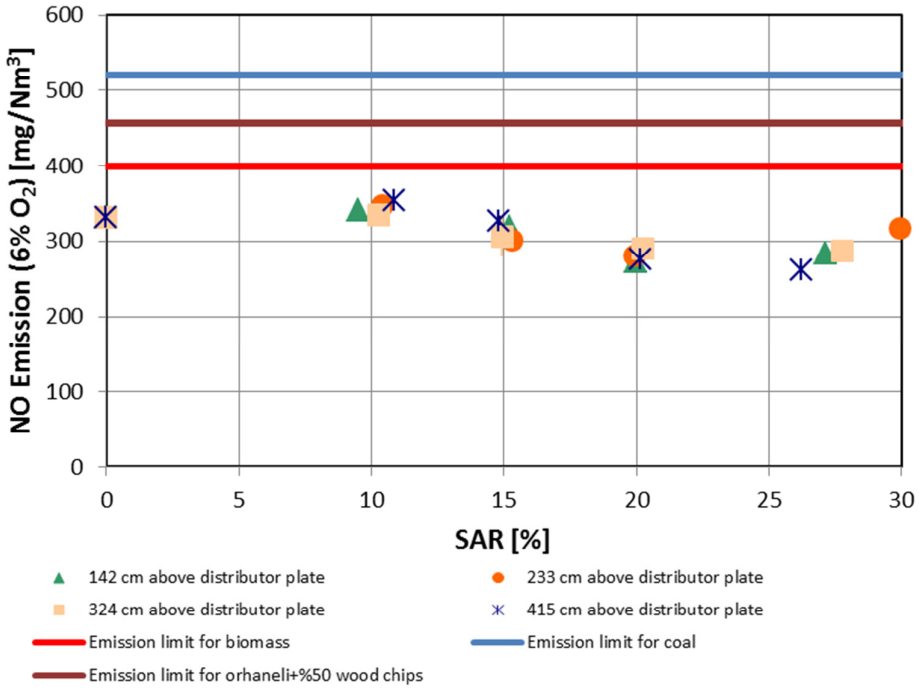

Figure 5.52 Effect of secondary air ratio and its location on NO emission and comparison of NO emission to emission limits for co-combustion of Bursa/Orhaneli lignite with 50% (by wt.) woodchips (C1-B2-5)

Effect of SAR and its location on **SO_2 emission** is given in Figure 5.53. SO_2 emission did not change too much with SAR up to 20%. It was in the range of 1990 and 2000 mg/Nm^3. A further increase in SAR (25-30%) also increased SO_2 emission up to 2400 mg/Nm^3. As the location of SA increased, T_{dp} also increased. While it was 870 ^oC for the case of SA@142 cm, it went up 900^oC for the case of SA@415 cm. All other T_{dp} temperatures

for the cases of SA less than 25% were lower than 865°C. Therefore, the increase of SO_2 emission for SA higher than 25% can be explained with the temperature increase in dense phase. SO_2 emissions were above the emission limit (1049 mg/Nm^3) for all cases. Limestone addition is required to lower SO_2 emission below the limit. As the woodchips share in fuel mixture was increased from 30% up to 50%, SO_2 emissions decreased down to the range of 1900 mg/Nm^3 (SAR=0%) and 2400 mg/Nm^3 (SAR=25-30%). It was in the range of 2400 mg/Nm^3 (SAR=0%) and 3500 mg/Nm^3 (SAR=25-30%) for 30% woodchips share in C1-B2-4.

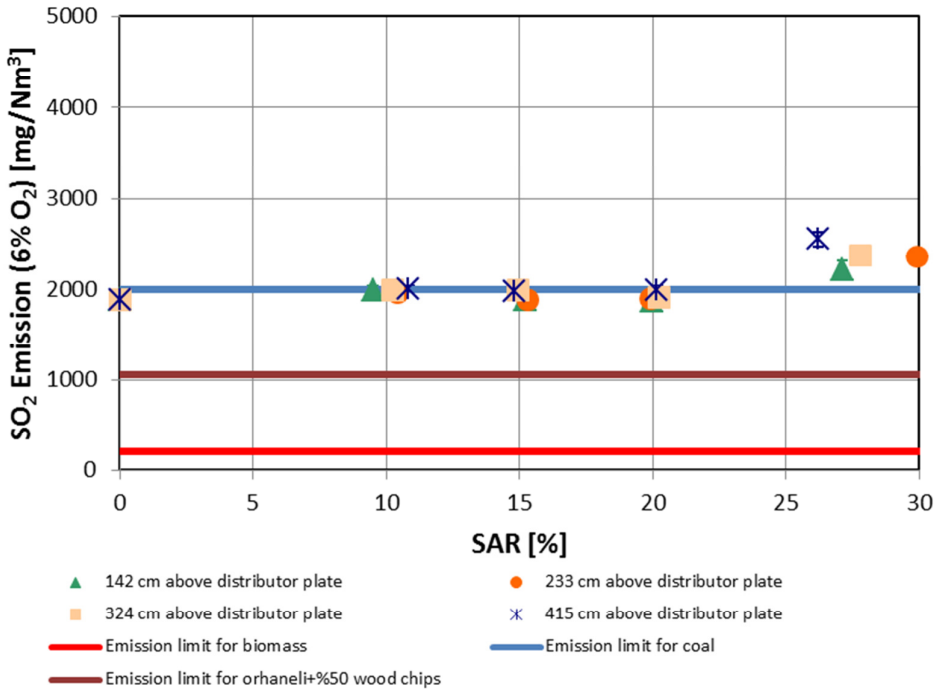

Figure 5.53 Effect of secondary air ratio and its location on SO_2 emission and comparison of SO_2 emission to emission limits for co-combustion of Bursa/Orhaneli lignite with 50% (by wt.) woodchips (C1-B2-5)

5.3. Assessment of Experiments for SET#3

5.3.1. Combustion of Bursa/Orhaneli Lignite with Addition of Çan Limestone (Ca/S = 2.0) (C1-2)

Bursa/Orhaneli lignite was combusted with Çan limestone in order to see the effect of limestone on SO_2 emission. In this experiment, Ca/S molar ratio was 2. Excess air ratio was 1.16±0.01 for C1-2. Superficial velocity for C1-2 was calculated as 3.38±0.03 m/s

corresponding average dense phase temperature of 826±2°C. Thermal power of the combustion system for C1-2 was 23 kW. With these operational conditions, emission measurement was done. CO, NO, and SO_2 emissions in flue gas were measured to be 130±7 mg/Nm^3, 280±10 mg/Nm^3, and 1575±135 mg/Nm^3, respectively. SO_2 emission measured in C1-2 was compared with SO_2 emission obtained from the combustion of Bursa/Orhaneli lignite. SO_2 emission was measured as 2828±102 mg/Nm^3 at excess air ratio of 1.14 for the combustion of Bursa/Orhaneli lignite. This was the reference case for determining the optimum Ca/S molar ratio which was enough to keep SO_2 emission below the limit value (2000 mg/Nm^3). SO_2 emissions can be seen in Figure 5.54.

5.3.2. Combustion of Bursa/Orhaneli Lignite with Addition of Çan Limestone (Ca/S = 2.5) (C1-3)

Bursa/Orhaneli lignite was also combusted with addition of Çan limestone when Ca/S molar ratio was 2.5. Excess air ratio was 1.13±0.01 for C1-3 experiment. Superficial velocity for C1-3 was calculated as 3.42±0.02 m/s at average dense phase temperature of 850±1°C. Thermal power of the combustion system for C1-3 experiment was 24 kW. CO, NO, and SO_2 emissions in the flue gas were measured as 189±26 mg/Nm^3, 272±8 mg/Nm^3, and 1016±77 mg/Nm^3, respectively. SO_2 emission measured in C1-3 is given in Figure 5.54.

5.3.3. Combustion of Bursa/Orhaneli Lignite with Addition of Çan Limestone (Ca/S = 3.0) (C1-4)

In this experiment, Ca/S molar ratio was increased to 3. Excess air ratio was 1.14±0.01 for C1-4 experiment. Superficial velocity for C1-4 was calculated as 3.43±0.02 m/s at average dense phase temperature of 878±2°C. Thermal power of the combustion system for C1-4 experiment was 23 kW. CO, NO, and SO_2 emissions in the flue gas were measured as 258±53 mg/Nm^3, 281±9 mg/Nm^3, and 759±102 mg/Nm^3, respectively. SO_2 emission measured in the experiment C1-4 can be seen in Figure 5.54.

5.3.4. Combustion of Denizli/Kale Lignite (C2-1)

Denizli/Kale lignite was first combusted without the addition of Çan limestone to see SO_2 emissions and to compare them with other experimental results where there was no limestone addition. Excess air ratio was 1.13±0.02 for the experiment C2-1. Superficial velocity was calculated as 3.23±0.00 m/s at average dense phase temperature of 834±2°C. Thermal power of the combustion system was 31 kW. With these operating conditions, emission measurements were done, and CO, NO and SO_2 concentrations in the flue gas were measured as 209±61 mg/Nm^3, 178±18 mg/Nm^3, and 6924±106 mg/Nm^3, respectively. SO_2 emission in this experiment was taken as a reference for determining the optimum Ca/S molar ratio which was enough to keep SO_2 emission below the limit value (2000 mg/Nm^3). SO_2 emissions can be seen in Figure 5.55.

5.3.5. Combustion of Denizli/Kale Lignite with Addition of Çan Limestone (Ca/S = 2.0) (C2-2)

Denizli/Kale lignite was combusted with the addition of Çan limestone when Ca/S molar ratio was 2. Excess air ratio was 1.12±0.02. Superficial velocity was calculated as 3.13±0.01 m/s at average dense phase temperature of 825±3°C. Thermal power of the combustion system for C2-2 experiment was 34 kW. At these operating conditions, CO, NO, and SO_2 emissions in the flue gas were measured as 156±51 mg/Nm^3, 192±24 mg/Nm^3, and 1134±130 mg/Nm^3, respectively. SO_2 emissions can be seen in Figure 5.55.

5.3.6. Combustion of Denizli/Kale Lignite with Addition of Çan Limestone (Ca/S = 2.5) (C2-3)

Denizli/Kale lignite was also combusted with the addition of Çan limestone when Ca/S molar ratio was 2.5. Excess air ratio was 1.10±0.02. Superficial velocity was calculated as 2.89±0.02 m/s at average dense phase temperature of 807±2°C. Thermal power of the combustion system for C2-3 experiment was 32 kW. CO, NO, and SO_2 emissions in the flue gas were measured as 461±258 mg/Nm^3, 141±21 mg/Nm^3, and 438±80 mg/Nm^3, respectively. SO_2 emission measured in C2-3 is given in Figure 5.55.

5.3.7. Combustion of Denizli/Kale Lignite with Addition of Çan Limestone (Ca/S = 3.0) (C2-4)

In this case, Ca/S molar ratio was increased to 3. Excess air ratio was 1.12±0.02. Superficial velocity was calculated as 3.05±0.01 m/s at average dense phase temperature of 814±1°C. Thermal power of the combustion system was 34 kW. CO, NO, and SO_2 emissions in the flue gas were measured as 874±273 mg/Nm^3, 176±24 mg/Nm^3, and 376±29 mg/Nm^3, respectively. SO_2 emissions measured in C2-4 experiment can be seen in Figure 5.55.

5.3.8. Discussion on the Effect of Ca/S Ratio on SO_2 Emissions in SET#3

For C1-1 combustion test conducted in SET#1, it is decided that optimum excess air ratio is about 1.23 in order to obtain minimum CO emission. In SET#3, combustion of Bursa/Orhaneli lignite was repeated under the same operating conditions as in C1-1. Operating conditions in this experiment could not be provided exactly the same as in the experiment C1-1 because of difficulties due to nature of combustion processes. However, the conditions were adjusted almost to be the same as in C1-1. In order to investigate the effect of Ca/S molar ratio on SO_2 emission, SO_2 emission obtained from combustion of Bursa/Orhaneli lignite were used as a reference. SO_2 emission was 2828±102 mg/Nm^3.

In the replica experiments, optimum excess air ratio was determined as 1.14. Superficial velocity in the combustor was 3.37±0.01 m/s, average dense phase temperature was 827±0.4°C, and thermal power gained was 22 kW. CO and NO emissions were measured as 129±5 mg/Nm^3 and 248±3 mg/Nm^3, respectively.

In Figure 5.54, the point where Ca/S is zero shows SO_2 emission resulting from combustion of Bursa/Orhaneli lignite alone. With the addition of limestone, SO_2 emission starts to decrease. When limestone is added to Bursa/Orhaneli lignite at a Ca/S ratio of 2, SO_2 emission decreased down to 1575±135 mg/Nm^3 which is under the SO_2 emission limit (2000 mg/Nm^3) given in the Turkish Regulation ("Turkish Regulation for Industrial Air Pollution Control," 2009). Further increase of limestone addition to the fuel mixture caused SO_2 emission to decrease.

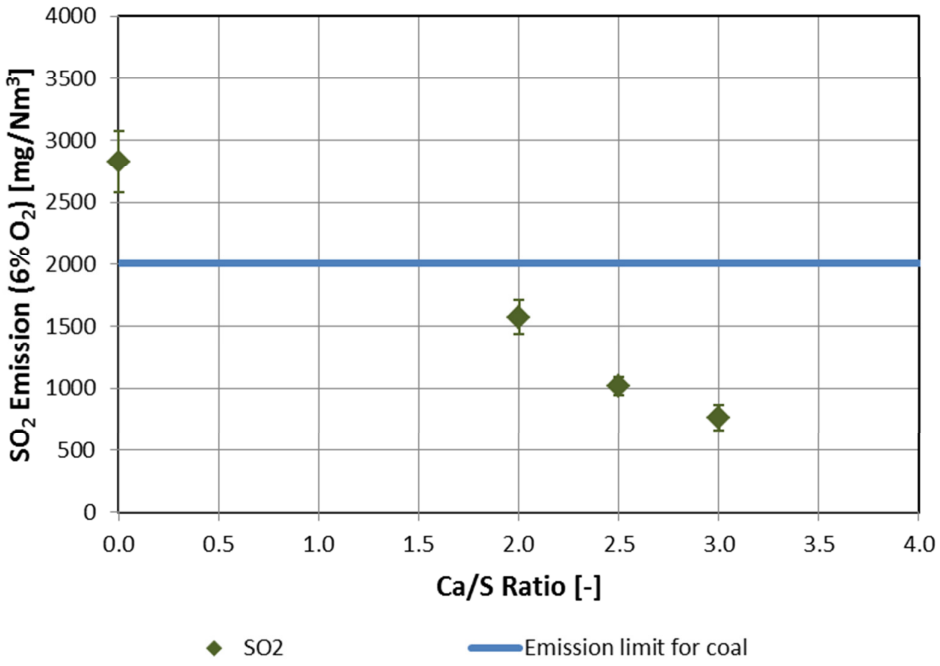

Figure 5.54 Effect of Ca/S ratio on SO_2 emission for the combustion of Bursa/Orhaneli lignite in SET#3

The effect of Ca/S ratio on SO_2 emission is given in Figure 5.55. When Denizli/Kale lignite was combusted alone, SO_2 emission was measured as 6924±106 mg/Nm^3 at excess air ratio of 1.13±0.02 because sulfur content of Denizli/Kale lignite were higher than Bursa/ Orhaneli lignite.

With the addition of limestone at a Ca/S ratio of 2 to the combustor, SO_2 emission decreased down to 1134±130 mg/Nm^3 which is under the SO_2 emission limit (2000 mg/Nm^3) given in the Turkish Regulation ("Turkish Regulation for Industrial Air Pollution Control," 2009). Almost 85% SO_2 capture was achieved at this Ca/S ratio.

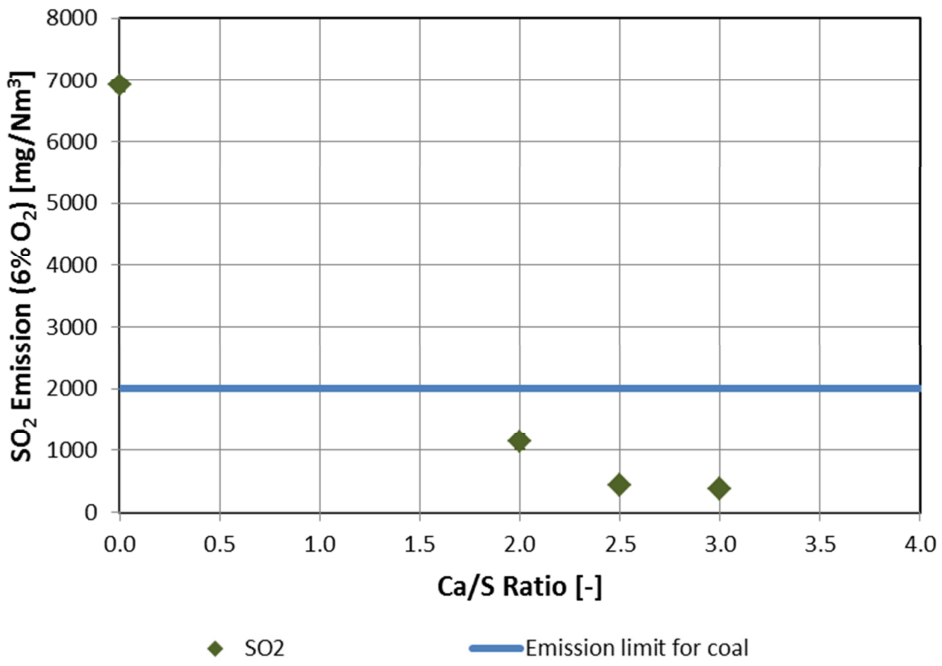

Figure 5.55 Effect of Ca/S ratio on SO_2 emission for the combustion of Denizli/Kale lignite in SET#3

Limestone addition to reduce SO_2 emission increases the formation of $CaSO_4$. $CaSO_4$ is a solid product and stays in the combustor mixed with ash increasing the amount of the solid product that has to be removed from the combustor. On the other hand, using high Ca/S ratio, which means high feeding rate of limestone, increases the operational cost of the process. Therefore, it is necessary to use the lowest Ca/S ratio which is capable to reduce SO_2 emission just below the emission limit. It can be seen from Figure 5.54 that addition of limestone with Ca/S ratio of 1.5 to Bursa/Orhaneli lignite seems good enough to reduce SO_2 emission under the emission limit. For the case of Denizli/Kale lignite as can be seen in Figure 5.55, Ca/S ratio of 1.7 is necessary to reduce SO_2 emission below the limit value.

5.4. Assessment of Experiments for SET#4

5.4.1. Co-Combustion of Bursa/Orhaneli Lignite and Olive Cake (50% by wt.) – Long Term Test (C1-B1-6)

For the long term co-combustion experiment of Bursa/Orhaneli lignite and olive cake (50% by wt.), fuel feeding rate was changed between 4.6 and 6.1 kg/h. The lignite was fed into the combustor from the fuel hopper (FH-02) and olive cake was fed from the fuel hopper (FH-01). The thermal power of the system changed between 23 and 31 kW. From

the air given to the combustor, flue gas generated and making necessary temperature correction, the superficial velocity was calculated between 3.6 m/s and 4.1 m/s during the experiment. The superficial velocity was calculated at 1.25 m above the distributor plate. This was the region where the lean phase started. The temperature correlation was done with the temperature data coming from TT112 thermocouple.

Total duration of the experiment was 29 hours and 3 minutes. The duration for fuel feeding was 25 hours and 3 minutes. This test was repetition of the test C1-B1-3. The only difference is that C1-B1-6 was long-term experiment. Proximate and ultimate analyses of coals and biomasses are given in Table 5.9.

Table 5.9 Proximate and ultimate analyses of fuels used in the co-combustion test (C1-B1-6)

Proximate analysis	**FC**	**VM**	**Ash**	**Moisture**	**HHV**	**LHV**
	%, by weight (as fired)				**kcal/kg (as fired)**	
C1-B1-6 (Bursa/Orhaneli)	32.62	35.50	11.45	20.43	4503	4210
C1-B1-6 (Olive Cake)	15.26	70.93	5.67	8.14	4788	4456

Ultimate analysis	**C**	**H**	**N**	**O**	**$S_{combustible}$**	**S_{total}**	**Ash**
	%, by weight (dry basis)						
C1-B1-6 (Bursa/Orhaneli)	66.35	4.47	1.35	12.34	1.10	2.43	14.39
C1-B1-6 (Olive Cake)	55.57	5.68	1.32	30.71	0.54	0.65	6.17

Operational parameters for the test (C1-B1-6) are given in Table 5.10.

Table 5.10 Operational Parameters for the co-combustion test (C1-B1-6)

Test Code	C1-B1-6
Coal	Bursa/Orhaneli
Biomass (% by wt.)	Olive Cake (50% by wt.)
Limestone	-
Molar Ca/S_{total} ratio	-
Duration of Test, hh:mm	29:03
Duration of Fuel Feeding, hh:mm	25:03
Coal Feeding Rate, kg/h	2.3 – 3.0
Biomass Feeding Rate, kg/h	2.3 – 3.1
Thermal Power, kW	23 – 31
Air Flowrate, Sm^3/h (@20°C, 1 atm)	28 – 34
u_o, superficial velocity, m/s	3.6 – 4.1
Excess Air Ratio (λ), -	1.16 – 1.49
Temperature of Dense Phase (T_{dp}), °C	824±11
Temperature of Freeboard (T_{fb}), °C	831±14
Temperature of Return Leg (T_{rl}), °C	726±39

Secondary Air Ratio (SAR): Secondary Air Flowrate/Total Air Flowrate
T_{dp}: Average of TT110 and TT111
T_{fb}: Average of TT112, TT114, TT116, TT118, and TT120
T_{rl}: Average of TT201, TT202, TT203, and TT204

Temperature Profile:

Temperature profiles along the combustor obtained for different excess air ratios (λ) during the experiment are given in Figure 5.56. Temperature measured along the combustor by thermocouples TT109 (40 mm), TT110 (240 mm), TT111 (320 mm), TT112 (1250 mm), TT114 (2160 mm), TT116 (3070 mm), TT118 (3980 mm), TT120 (4890 mm) and TT121 (5800 mm) are given in Figure 5.56. The values in parentheses are the distance of the thermocouples from the distributor plate. Within the 1 m of the combustor, average temperature of dense phase was between 800°C and 820°C for λ of 1.16-1.30. A little increase in air volume given into the system increases the dense phase temperature. For λ of 1.30-1.44, average temperature of dense phase was between 820°C and 830°C. Corresponding freeboard temperatures were between 820°C and 825°C for λ of 1.16-1.30 and between 845°C and 850°C for λ of 1.30-1.44. Higher temperature profile observed for λ of 1.30-1.44 was also the reason of lower CO and NO emissions measured throughout the experiment. While the highest temperature of dense phase was measured at about 837°C for λ of 1.49, average temperature of freeboard (818°C) and return leg (645°C) for this λ were lower than the other λ values. This might be the reason why higher CO and NO emissions were measured at λ of 1.49.

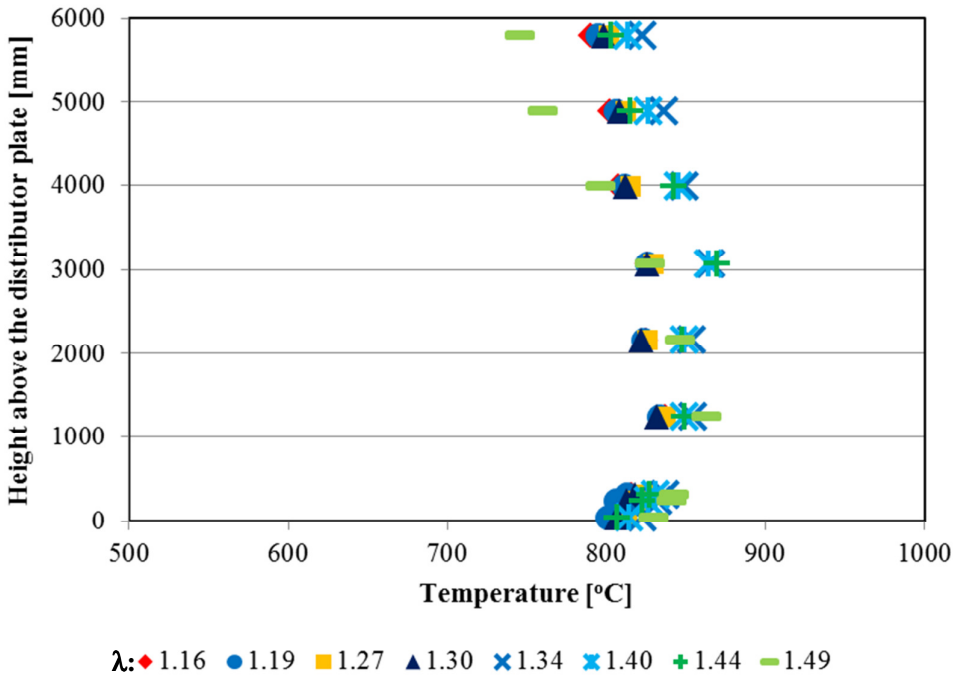

Figure 5.56 Temperature profile along the combustor for the co-combustion of Bursa/Orhaneli lignite and 50% olive cake (by wt.) - Long Term Test (C1-B1-6)

Temperature profiles along the return leg obtained for different λs are given in Figure 5.57. Temperatures at each location along the return leg were very close to each other for each λ, except λ=1.49. In the case of λ=1.49, the experiment was about to be ended. The ash formed during the experiment was taken out of the system in order to keep the mass load within the system to be constant. The mass load within the system increased in time causing the circulation of particles to be deteriorated at the end of 29-hour test. The excess air given into the system might also have an impact on the cooling of the freeboard and also return leg. The average temperature measured at the exit of the first cyclone was about 770°C for λ range of 1.16-1.49, it decreased down to 680°C at the end of the return leg. High temperature observed along the return leg is an indication of good circulation between the combustor and the return leg.

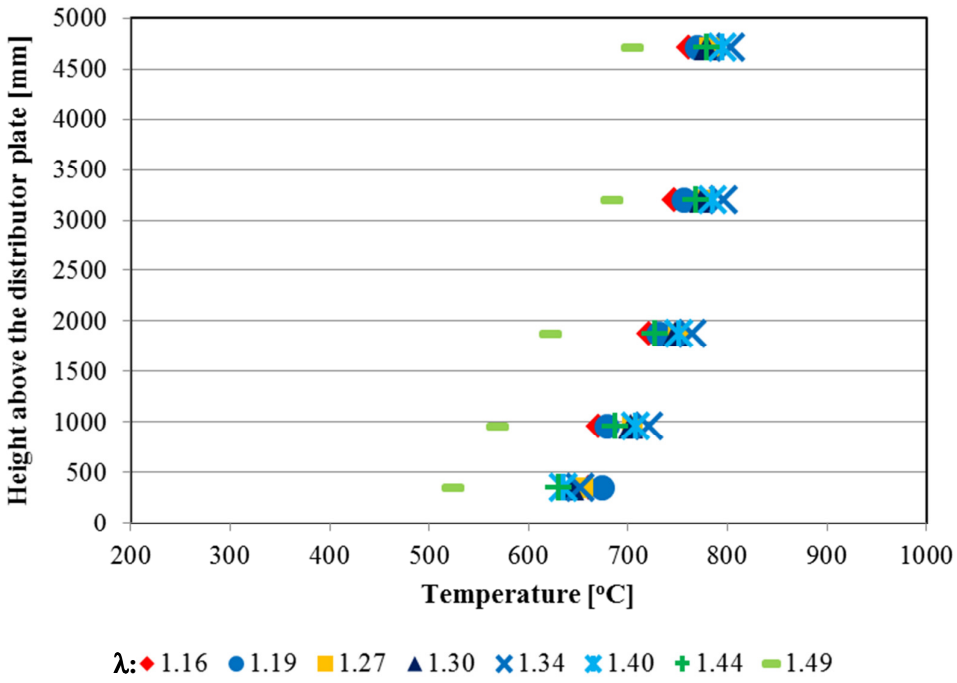

Figure 5.57 Temperature profile along the return leg for the co-combustion of Bursa/Orhaneli lignite and 50% olive cake (by wt.) - Long Term Test (C1-B1-6)

Emissions:

Total duration of flue gas measurement was 23 hours and 18 minutes. 17 hours and 15 minutes of it was found suitable to be used for drawing of emission graphics. The number of data used in the emission graphics was reduced without disturbing the trend in emissions in order to minimize the data clutter in the emission graphics. 2 hours and 54 minutes part of 17 hours and 15 minutes emission measurement is presented in Figure 5.58.

Flue gas emission limits according to the Turkish Regulation for the co-combustion of Bursa/Orhaneli lignite with 50% olive cake (by wt.) are given in Table 5.11.

Table 5.11 Flue gas emission limits for the co-combustion test (C1-B1-6) according to the Turkish Regulation ("Turkish Regulation for Industrial Air Pollution Control," 2009)

Test #	Test Code	CO (mg/Nm^3)	NO (mg/Nm^3)	SO_xasSO_2 (mg/Nm^3)
4-1	C1-B1-6	334	458	1070

It is determined from the emission data presented in Figure 5.58 for C1-B1-6 combustion test that CO and NO emissions, which are corresponding to the emissions measurements at λ=1.34 and λ=1.40, are under emission limits of the Turkish Regulation ("Turkish Regulation for Industrial Air Pollution Control," 2009). As can be seen from Table 5.11, the emission limits for CO and NO are 334 mg/Nm^3 and 458 mg/Nm^3, respectively. It is suitable to burn these fuel mixtures at these operational conditions (Table 5.12). Since limestone was not used in the experiment, SO_2 emission was above the emission limit (1070 mg/Nm^3). As can be seen from Figure 5.58, λ should be between 1.34 and 1.44 in order to keep CO emission under emission limit (334 mg/Nm^3). For NO emission to be lower than emission limit (458 mg/Nm^3), λ is needed to be kept less than 1.34.

Table 5.12 Measurement duration, optimum excess air ratios, corresponding thermal power, superficial velocity and flue gas emissions for the co-combustion test (C1-B1-6)

Measurement Duration min	λ	P_{th} kW	U_o m/s	CO[a] mg/Nm^3	NO[a] mg/Nm^3	SO_2[a] mg/Nm^3
68	1.34	30	4.05	298±53	399±7	1507±24
56	1.40	30	4.06	271±21	421±5	1526±13

[a]Emissions are given on dry basis as a reference of 6% O_2.

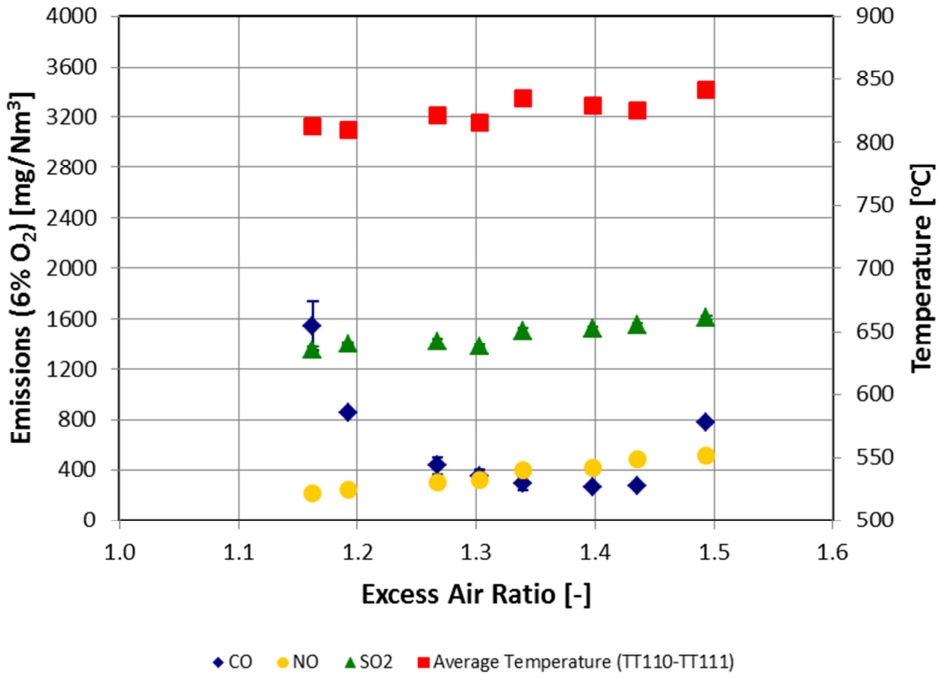

TT110 and TT111 are located 24 cm and 32 cm above the distributor plate, respectively.

Figure 5.58 Effect of excess air ratio on flue gas emissions for the co-combustion of Bursa/Orhaneli lignite and 50% olive cake (by wt.) - Long Term Test (C1-B1-6)

5.4.2. Co-Combustion of Bursa/Orhaneli Lignite and Olive Cake (50% by wt.) with Çan Limestone (Ca/S_{total} = 2.0) – Long Term Test (C1-B1-7)

For the long term co-combustion experiment of Bursa/Orhaneli lignite and olive cake (50% by wt.) with Çan limestone, fuel feeding rate was changed between 4.9 and 6.1 kg/h. The lignite was fed into the combustor from the fuel hopper (FH-02) and olive cake was fed from the fuel hopper (FH-01). The thermal power of the system changed between 25 and 31 kW. The superficial velocity was calculated between 3.4 and 3.6 m/s during the experiment by using the amount of air given to the combustor, flue gas generated and making necessary temperature corrections. The superficial velocity was calculated at 1.25 m above the distributor plate. This was the region where the lean phase started. The temperature correction was done with the temperature data coming from TT112 thermocouple.

Total duration of the experiment was 42 hours and 57 minutes. The duration for fuel feeding was 40 hours and 24 minutes. Proximate and ultimate analyses of coals and biomasses are given in Table 5.13.

Table 5.13 Proximate and ultimate analyses of fuels used in the co-combustion test (C1-B1-7)

Proximate analysis	**FC**	**VM**	**Ash**	**Moisture**	**HHV**	**LHV**
	%, by weight (as fired)				**kcal/kg (as fired)**	
C1-B1-7 (Bursa/Orhaneli)	31.73	33.49	7.94	26.84	4435	4112
C1-B1-7 (Olive Cake)	16.07	69.18	5.64	9.11	4867	4533

Ultimate analysis	**C**	**H**	**N**	**O**	**$S_{combustible}$**	**S_{total}**	**Ash**
	%, by weight (dry basis)						
C1-B1-7 (Bursa/Orhaneli)	70.62	4.66	1.66	10.85	1.36	2.61	10.85
C1-B1-7 (Olive Cake)	57.31	5.79	1.19	28.84	0.67	0.84	6.21

Operational parameters for the test (C1-B1-7) are given in Table 5.14.

Table 5.14 Operational Parameters for the co-combustion test (C1-B1-7)

Test Code	C1-B1-7
Coal	Bursa/Orhaneli
Biomass (% by wt.)	Olive Cake (50% by wt.)
Limestone	Çan
Molar Ca/S_{total} ratio	2
Duration of Test, hh:mm	42:57
Duration of Fuel Feeding, hh:mm	40:24
Coal Feeding Rate, kg/h	2.5 – 3.0
Biomass Feeding Rate, kg/h	2.5 – 3.1
Thermal Power, kW	25 – 31
Air Flowrate, Sm^3/h (@20^oC, 1 atm)	27 – 30
u_o, superficial velocity, m/s	3.4 – 3.6
Excess Air Ratio (λ), -	1.12 – 1.48
Temperature of Dense Phase (T_{dp}), °C	798±6
Temperature of Freeboard (T_{fb}), °C	800±7
Temperature of Return Leg (T_{rl}), °C	710±20

Secondary Air Ratio (SAR): Secondary Air Flowrate/Total Air Flowrate
T_{dp}: Average of TT110 and TT111
T_{fb}: Average of TT112, TT114, TT116, TT118, and TT120
T_{rl}: Average of TT201, TT202, TT203, and TT204

Temperature Profile:

Temperature profiles along the combustor obtained for different excess air ratios (λ) during the experiment are given in Figure 5.59. Temperature measured along the combustor by thermocouples TT109 (40 mm), TT110 (240 mm), TT111 (320 mm),

TT112 (1250 mm), TT114 (2160 mm), TT116 (3070 mm), TT118 (3980 mm), TT120 (4890 mm) and TT121 (5800 mm) are given in Figure 5.59. The excess air ratio was changed between 1.12 and 1.48 during the experiment. Average temperature of dense phase was 798°C with a standard deviation of 6°C for λ range of 1.12-1.48. If the average temperatures of dense phase for co-combustion tests C1-B1-6 and C1-B1-7 from Table 5.10 and Table 5.14 are compared, it can be seen that limestone addition to fuel mixture decreases the dense phase temperature about 25°C. While it was 824±11°C for C1-B1-6, it was 798±6°C for C1-B1-7. The difference between co-combustion tests C1-B1-6 and C1-B1-7 was only addition of limestone. Limestone addition was done in C1-B1-7. Limestone addition did not only affect the dense phase temperature, it also decreased the freeboard temperature. While freeboard temperature was 831±14°C for C1-B1-6, it was 800±7 for C1-B1-7. This might be explained by the calcination of limestone. When limestone is fed into the combustor, calcination of limestone is an endothermic reaction and extracts heat from the surrounding. This was the reason for the decrease in temperature. In all cases of λ, maximum temperature was observed at the location where TT112 thermocouple was located. It was 1.25 m above the distributor plate.

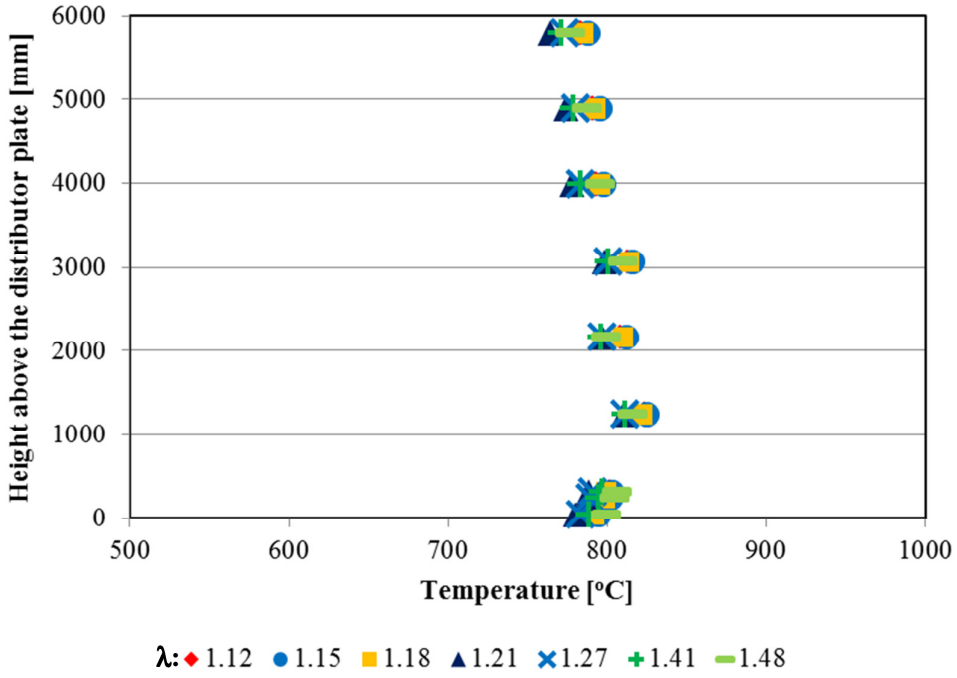

Figure 5.59 Temperature profile along the combustor for the co-combustion of Bursa/Orhaneli lignite and 50% olive cake (by wt.) with Çan Limestone (Ca/S_{total} = 2.0) - Long Term Test (C1-B1-7)

Temperature profiles along the return leg obtained for different λs are given in Figure 5.60. Temperatures at each location along the return leg were very close to each other for

each λ. The average temperature measured at the exit of the first cyclone was about 750°C for λ range of 1.12-1.4, it decreased down to 670°C at the end of the return leg. High temperature observed along the return leg is an indication of good circulation between the combustor and the return leg.

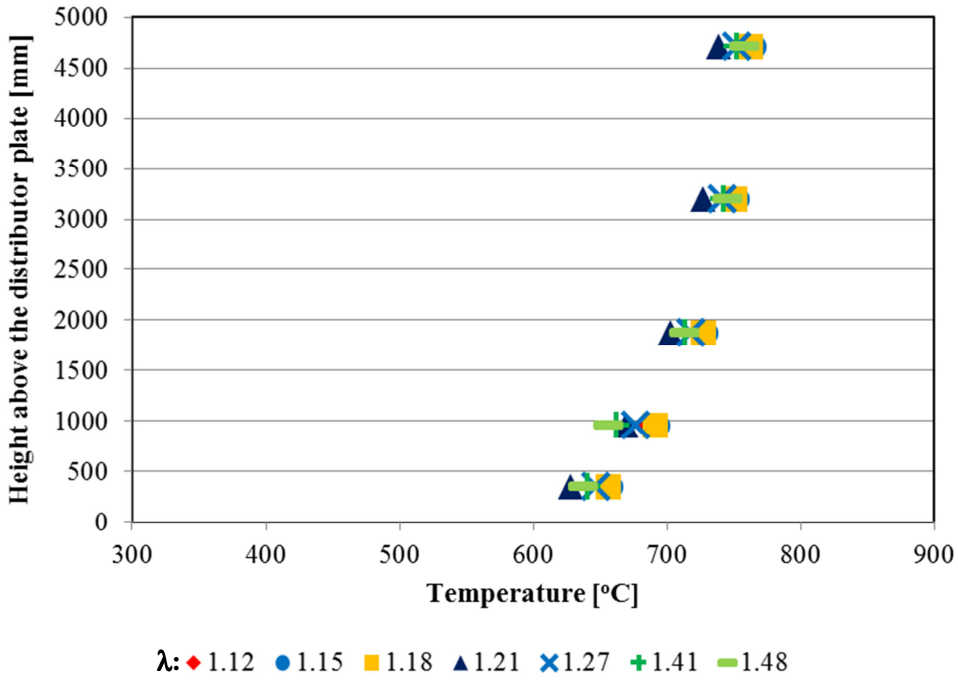

Figure 5.60 Temperature profile along the return leg for the co-combustion of Bursa/Orhaneli lignite and 50% olive cake (by wt.) with Çan Limestone (Ca/S_{total} = 2.0) - Long Term Test (C1-B1-7)

Emissions:

Total duration of flue gas measurement was 38 hours and 27 minutes. 37 hours and 27 minutes of it was found suitable to be used for drawing of emission graphics. The number of data used in the emission graphics was reduced without disturbing the trend in emissions in order to minimize the data clutter in the emission graphics. 5 hours and 59 minutes part of 37 hours and 27 minutes emission measurement is presented in Figure 5.61.

Flue gas emission limits according to the Turkish Regulation for the co-combustion of Bursa/Orhaneli lignite with Olive cake (50% by wt.) and with Çan limestone are given in Table 5.15.

Table 5.15 Flue gas emission limits for the co-combustion test (C1-B1-7) according to the Turkish Regulation ("Turkish Regulation for Industrial Air Pollution Control," 2009)

Test #	Test Code	CO (mg/Nm^3)	NO (mg/Nm^3)	SO_xasSO_2 (mg/Nm^3)
4-2	C1-B1-7	337	457	1051

As can be seen from Figure 5.61, λ should be higher than 1.45 so that CO emission is under the limit (337 mg/Nm^3). Addition of limestone into the fuel mixture caused temperatures in all system to be decreased. While the average temperature of dense phase, freeboard, and return leg were 824°C, 831°C, and 726°C, respectively for C1-B1-6 test, they were 798°C, 800°C, and 710°C for C1-B1-7 test. Decreasing of temperature in whole system because of limestone addition might be accepted to be the reason for CO emissions to increase. In contrast to CO emission, λ should be less than 1.4 so that NO emission is under limits (457 mg/Nm^3). When CO and NO emissions are examined, there is no λ range in where CO and NO emissions are below the limits. For CO emission to be under limit, λ should be greater than 1.45. On the other hand, λ should be less than 1.4 for NO emission to be under limit. SO_2 emission was measured very close to zero with the addition of limestone, as it was expected.

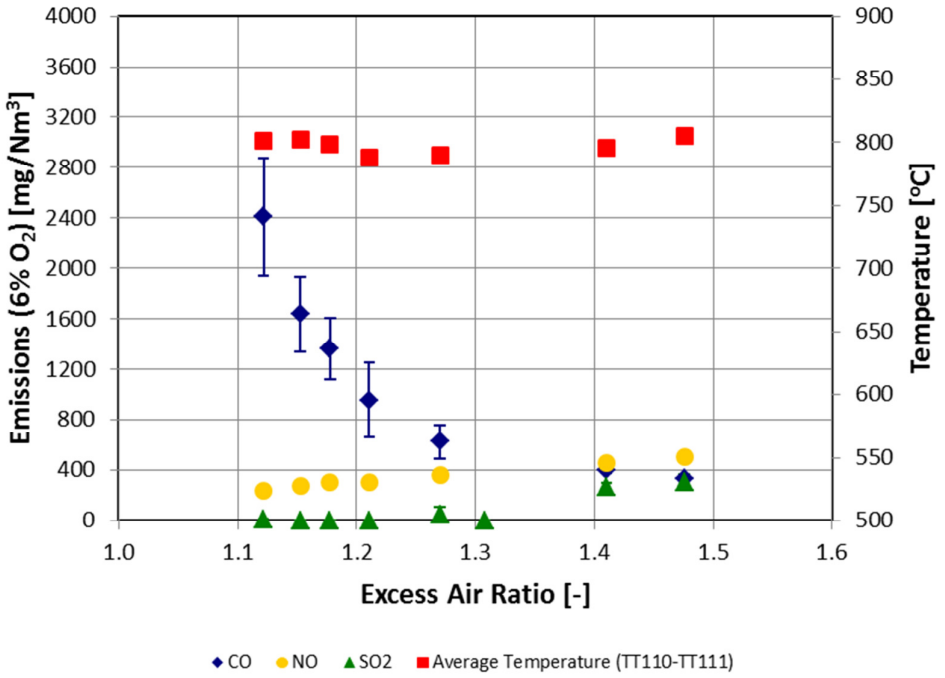

TT110 and TT111 are located 24 cm and 32 cm above the distributor plate, respectively.

Figure 5.61 Effect of excess air ratio on flue gas emissions for the co-combustion of Bursa/Orhaneli lignite and 50% olive cake (by wt.) with Çan Limestone (Ca/S_{total} = 2.0) - Long Term Test (C1-B1-7)

5.4.3. Co-Combustion of Denizli/Kale Lignite and Olive Cake (50% by wt.) – Long Term Test (C2-B1-1)

For the long term co-combustion experiment of Denizli/Kale lignite and olive cake (50% by wt.), fuel feeding rate was changed between 6.4 and 6.9 kg/h. The lignite was fed into the combustor from the fuel hopper (FH-02) and olive cake was fed from the fuel hopper (FH-01). The thermal power of the system changed between 29 and 31 kW. The superficial velocity was calculated between 3.4 and 3.6 m/s during the experiment by using the amount of air given to the combustor, flue gas generated and making necessary temperature corrections. The superficial velocity was calculated at 1.25 m above the distributor plate. This was the region where the lean phase was started. The temperature correlation was done with the temperature data coming from TT112 thermocouple.

Total duration of the experiment was 63 hours and 9 minutes. The duration for fuel feeding was 49 hours and 50 minutes. Proximate and ultimate analyses of coals and biomasses are given in Table 5.16.

Table 5.16 Proximate and ultimate analyses of fuels used in the co-combustion test (C2-B1-1)

Proximate analysis	**FC**	**VM**	**Ash**	**Moisture**	**HHV**	**LHV**
	%, by weight (as fired)				**kcal/kg (as fired)**	
C2-B1-1 (Denizli/Kale)	28.66	37.71	17.19	16.44	4137	3867
C2-B1-1/2 (Olive Cake)	17.59	61.64	9.69	11.08	4120	3818

Ultimate analysis	**C**	**H**	**N**	**O**	**$S_{combustible}$**	**S_{total}**	**Ash**
	%, by weight (dry basis)						
C2-B1-1 (Denizli/Kale)	56.26	3.48	1.47	16.75	1.47	3.69	20.57
C2-B1-1/2 (Olive Cake)	49.80	4.90	1.64	32.13	0.63	0.84	10.90

Operational parameters for the test (C2-B1-1) are given in Table 5.17.

Table 5.17 Operational Parameters for the co-combustion test (C2-B1-1)

Test Code	C2-B1-1
Coal	Denizli/Kale
Biomass (% by wt.)	Olive Cake (50% by wt.)
Limestone	-
Molar Ca/S_{total} ratio	-
Duration of Test, hh:mm	63:09
Duration of Fuel Feeding, hh:mm	49:50
Coal Feeding Rate, kg/h	3.2 – 3.5
Biomass Feeding Rate, kg/h	3.2 – 3.4
Thermal Power, kW	29 – 31
Air Flowrate, Sm^3/h (@20°C, 1 atm)	27 – 28
u_o, superficial velocity, m/s	3.4 – 3.6
Excess Air Ratio (λ), -	1.11 – 1.35
Temperature of Dense Phase (T_{dp}), °C	804±23
Temperature of Freeboard (T_{fb}), °C	798±18
Temperature of Return Leg (T_{rl}), °C	695±10

Secondary Air Ratio (SAR): Secondary Air Flowrate/Total Air Flowrate
T_{dp}: Average of TT110 and TT111
T_{fb}: Average of TT112, TT114, TT116, TT118, and TT120
T_{rl}: Average of TT201, TT202, TT203, and TT204

Temperature Profile:

Temperature profiles along the combustor obtained for different excess air ratios (λ) during the experiment are given in Figure 5.62. Temperature measured along the combustor by thermocouples TT109 (40 mm), TT110 (240 mm), TT111 (320 mm),

TT112 (1250 mm), TT114 (2160 mm), TT116 (3070 mm), TT118 (3980 mm), TT120 (4890 mm) and TT121 (5800 mm) are given in Figure 5.62. Temperature at each measurement point along the combustor decreased as the excess air ratio was increased. Maximum temperature along the combustor was measured at 1.25 m above the distributor plate for each λ. Within the 1 m of the combustor, average temperature of dense phase was between 800°C and 830°C for λ less than 1.20. A little increase in air volume given into the system decreased the dense phase temperature. For λ of 1.20-1.35, average temperature of dense phase was between 770°C and 800°C.

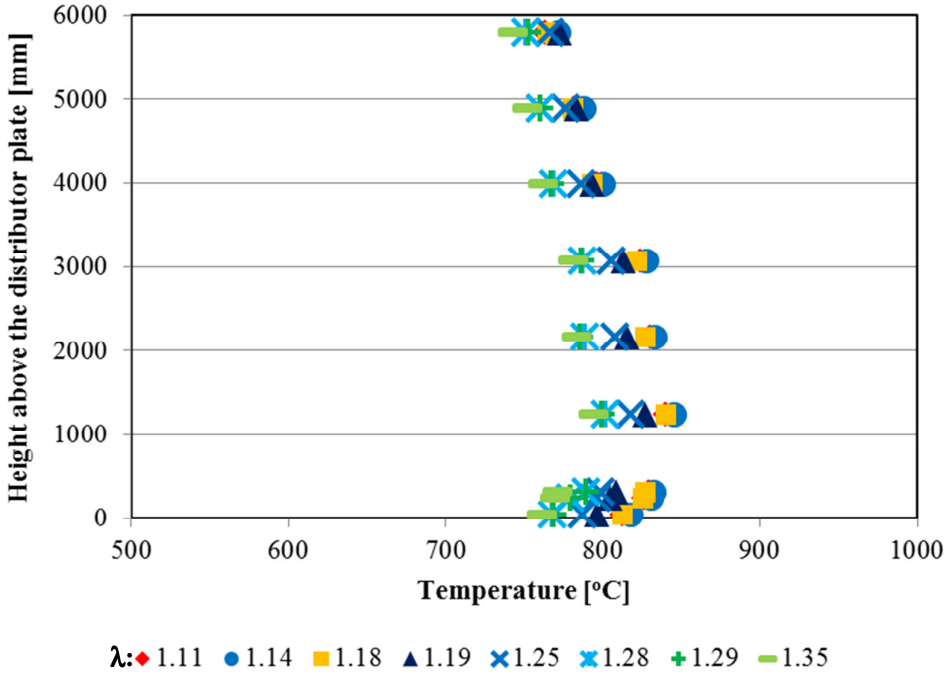

Figure 5.62 Temperature profile along the combustor for the co-combustion of Denizli/Kale lignite and 50% olive cake (by wt.) - Long Term Test (C2-B1-1)

Temperature profiles along the return leg obtained for different λs are given in Figure 5.63. The highest temperatures along the return leg were measured for λ=1.19. Average temperature of the return leg was 711°C for this case. This operational condition, at the same time, corresponds to the conditions at minimum CO emission measured. When excess air ratio was 1.19 the average of 1185 minute-CO emission measurement was about 320 mg/Nm^3 which was below the limit for CO emission (327 mg/Nm^3). If a good circulation within the circulating fluidized bed combustor is achieved, it may also improve the flue gas emissions mainly CO emission. The temperatures measured by TT205 which was located at 350 mm above the distributor plate on the connection pipe between combustor and return leg were lower than the temperatures measured by TT201,

TT202, TT203, and TT204 along the return leg. This is because more air is given to the connection pipe in order to provide a good circulation.

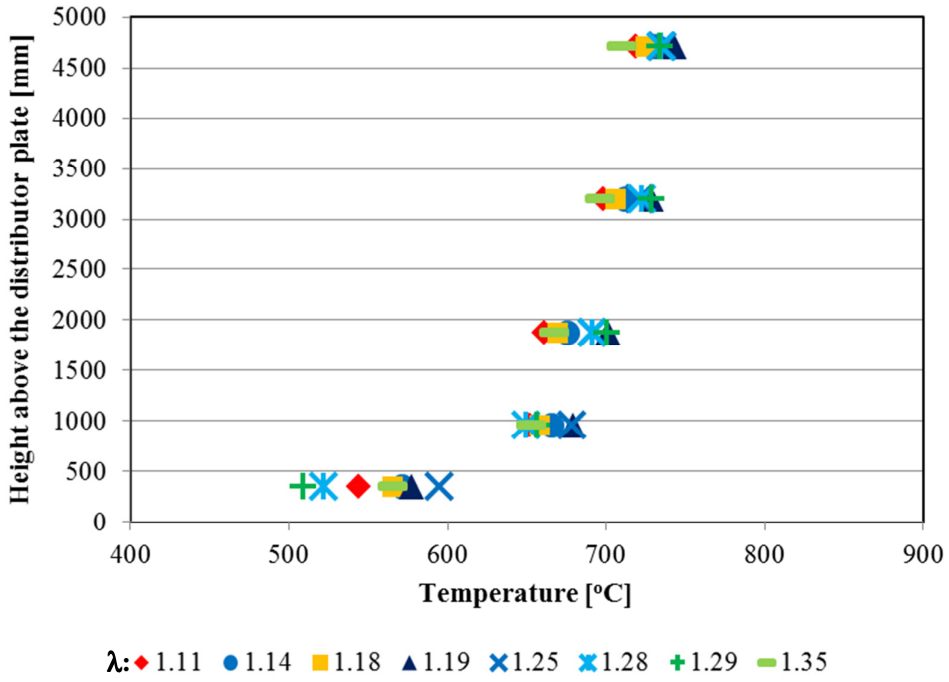

Figure 5.63 Temperature profile along the return leg for the co-combustion of Denizli/Kale lignite and 50% olive cake (by wt.) - Long Term Test (C2-B1-1)

Emissions:

Total duration of flue gas measurement was 48 hours and 27 minutes. 47 hours and 45 minutes of it was found suitable to be used for drawing of emission graphics. The number of data used in the emission graphics was reduced without disturbing the trend in emissions in order to minimize the data clutter in the emission graphics. 23 hours and 45 minutes part of 47 hours and 45 minutes emission measurement is presented in Figure 5.64.

Flue gas emission limits according to the Turkish Regulation for the co-combustion of Bursa/Orhaneli lignite with Olive cake (50% by wt.) are given in Table 5.18.

Table 5.18 Flue gas emission limits for the co-combustion test (C2-B1-1) according to the Turkish Regulation ("Turkish Regulation for Industrial Air Pollution Control," 2009)

Test #	Test Code	CO (mg/Nm^3)	NO (mg/Nm^3)	SO_xasSO_2 (mg/Nm^3)
4-3	C2-B1-1	327	461	1118

As can be seen from Figure 5.64, λ should be at about 1.20 in order to keep CO emission under the emission limit (327 mg/Nm^3). NO emissions are below the limit (457 mg/Nm^3) for λ range of 1.11-1.35. Since limestone was not used in the experiment, SO_2 emission was above the emission limit (1118 mg/Nm^3).

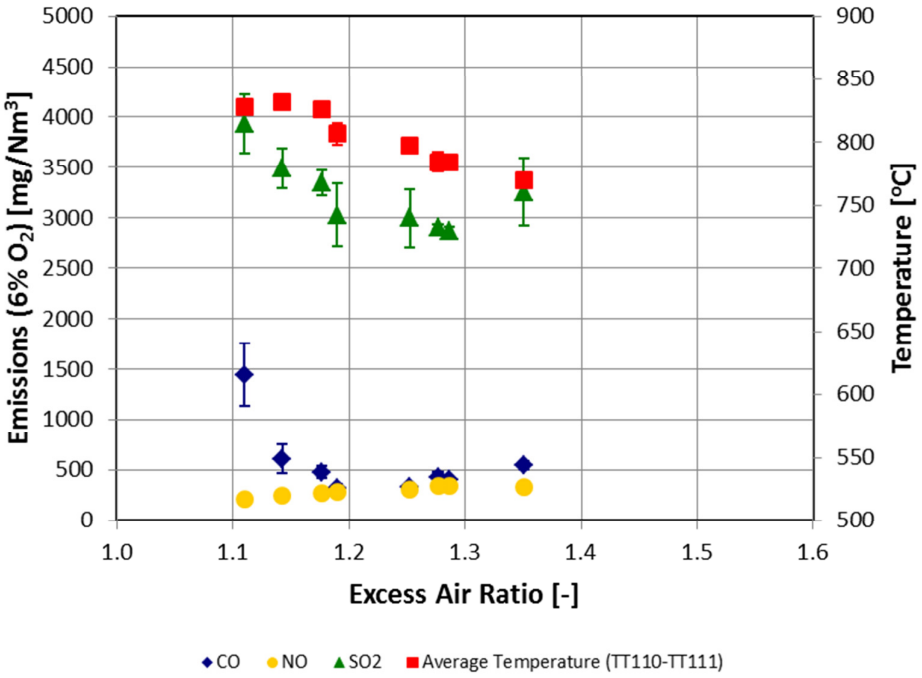

TT110 and TT111 are located 24 cm and 32 cm above the distributor plate, respectively.

Figure 5.64 Effect of excess air ratio on flue gas emissions for the co-combustion of Denizli/Kale lignite and 50% olive cake (by wt.) - Long Term Test (C2-B1-1)

5.4.4. Co-Combustion of Denizli/Kale Lignite and Olive Cake (50% by wt.) with Çan Limestone (Ca/S_{total} = 2.0) – Long Term Test (C2-B1-2)

For the long term co-combustion experiment of Denizli/Kale lignite and olive cake (50% by wt.) with Çan limestone, fuel feeding rate was changed between 6.3 and 7.0 kg/h. The

lignite was fed into the combustor from the fuel hopper (FH-02) and olive cake was fed from the fuel hopper (FH-01). The thermal power of the system changed between 28 and 31 kW. The superficial velocity was calculated between 3.4-3.6 m/s during the experiment by using the amount of air given to the combustor, flue gas generated and making necessary temperature corrections. The superficial velocity was calculated at 1.25 m above the distributor plate. This was the region where the lean phase was started. The temperature correction was done with the temperature data coming from TT112 thermocouple.

Total duration of the experiment was 71 hours and 55 minutes. The duration for fuel feeding was 51 hours and 25 minutes. Proximate and ultimate analyses of coals and biomasses are given in Table 5.19.

Table 5.19 Proximate and ultimate analyses of fuels used in the co-combustion test (C2-B1-2)

Proximate analysis	**FC**	**VM**	**Ash**	**Moisture**	**HHV**	**LHV**
	%, by weight (as fired)				**kcal/kg (as fired)**	
C2-B1-2 (Denizli/Kale)	28.49	37.46	17.13	16.92	4125	3854
C2-B1-1/2 (Olive Cake)	17.59	61.64	9.69	11.08	4120	3818

Ultimate analysis	**C**	**H**	**N**	**O**	**$S_{combustible}$**	**S_{total}**	**Ash**
	%, by weight (dry basis)						
C2-B1-2 (Denizli/Kale)	55.23	3.36	1.45	17.41	1.94	3.79	20.62
C2-B1-1/2 (Olive Cake)	49.80	4.90	1.64	32.13	0.63	0.84	10.90

Operational parameters for the test (C2-B1-2) are given in Table 5.20.

Table 5.20 Operational Parameters for the co-combustion test (C2-B1-2)

Test Code	C2-B1-2
Coal	Denizli/Kale
Biomass (% by wt.)	Olive Cake (50% by wt.)
Limestone	Çan
Molar Ca/S_{total} ratio	2
Duration of Test, hh:mm	71:55
Duration of Fuel Feeding, hh:mm	51:25
Coal Feeding Rate, kg/h	3.2 – 3.5
Biomass Feeding Rate, kg/h	3.1 – 3.4
Thermal Power, kW	24 – 27
Air Flowrate, Sm^3/h (@20^oC, 1 atm)	24 – 27
u_o, superficial velocity, m/s	3.4 – 3.6
Excess Air Ratio (λ), -	1.09 – 1.42
Temperature of Dense Phase (T_{dp}), °C	806±11
Temperature of Freeboard (T_{fb}), °C	787±8
Temperature of Return Leg (T_{rl}), °C	698±29

Secondary Air Ratio (SAR): Secondary Air Flowrate/Total Air Flowrate
T_{dp}: Average of TT110 and TT111
T_{fb}: Average of TT114, TT118, and TT120 (TT12 and TT116 failed to work in the experiment)
T_{rl}: Average of TT201, TT202, TT203, and TT204

Temperature Profile:

Temperature profiles along the combustor obtained for different excess air ratios (λ) during the experiment are given in Figure 5.65. Temperature measured along the combustor by thermocouples TT109 (40 mm), TT110 (240 mm), TT111 (320 mm), TT112 (1250 mm), TT114 (2160 mm), TT116 (3070 mm), TT118 (3980 mm), TT120 (4890 mm) and TT121 (5800 mm) are given in Figure 5.65. Thermocouples TT112 (1250 mm) and TT116 (3070 mm) did not properly operate in the experiment. Because of that, they were not shown in Figure 5.65. Within the 1 m of the combustor, average temperature of dense phase was between 810^{o}C and 820^{o}C for λ higher than 1.30. For λ less than 1.30, average temperature of dense phase was between 785^{o}C and 805^{o}C. The decrease in average temperature of dense phase for λ<1.30 might be an indication of good circulation of solid particles. The heat within the combustor might be dispersed throughout the whole system. Thus, the temperature difference between the combustor and the return leg decreased.

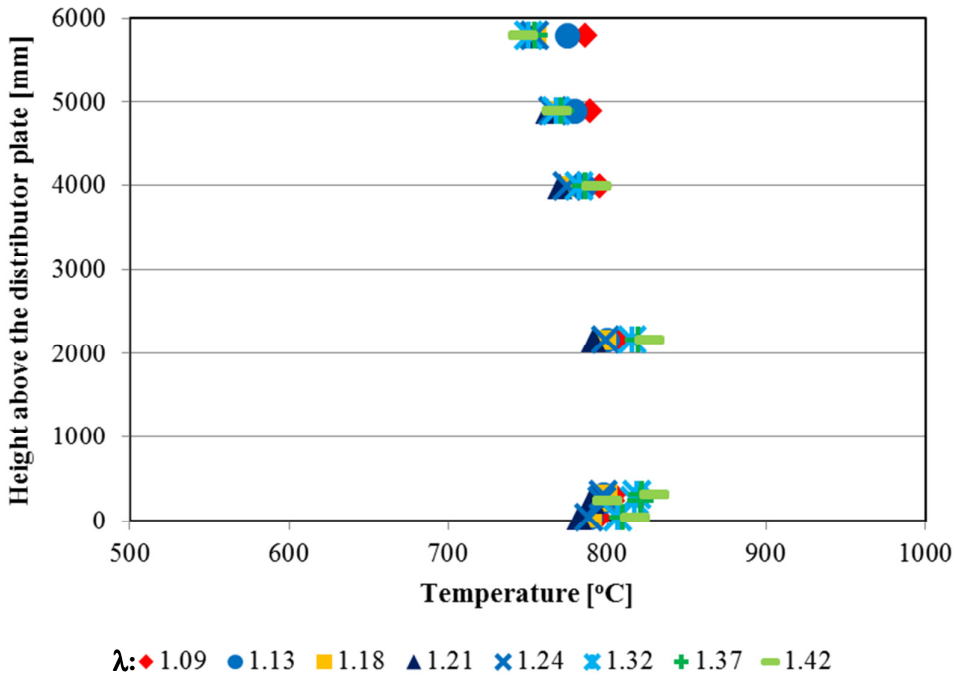

Figure 5.65 Temperature profile along the combustor for the co-combustion of Denizli/Kale lignite and 50% olive cake (by wt.) with Çan Limestone (Ca/S_{total} = 2.0) - Long Term Test (C2-B1-2)

Temperature profiles along the return leg obtained for different λs are given in Figure 5.66. The highest temperatures along the return leg were measured for λ= 1.09. Average temperature of the return leg was 744°C for this case. The average temperature of the return leg decreased with an increase on excess air given to the system during the test. In the case of λ=1.42, it decreased down to 650°C. When limestone was fed into the combustor, the average temperatures in the combustion system were decreased and also the circulation got worse. As a result, high level of CO emission in the flue gas was measured during the experiment. The temperatures measured by TT205 which was located at 350 mm above the distributor plate on the connection pipe between combustor and return leg were lower than the temperatures measured by TT201, TT202, TT203, and TT204 along the return leg. This was because more air is given to the connection pipe in order to provide a good circulation.

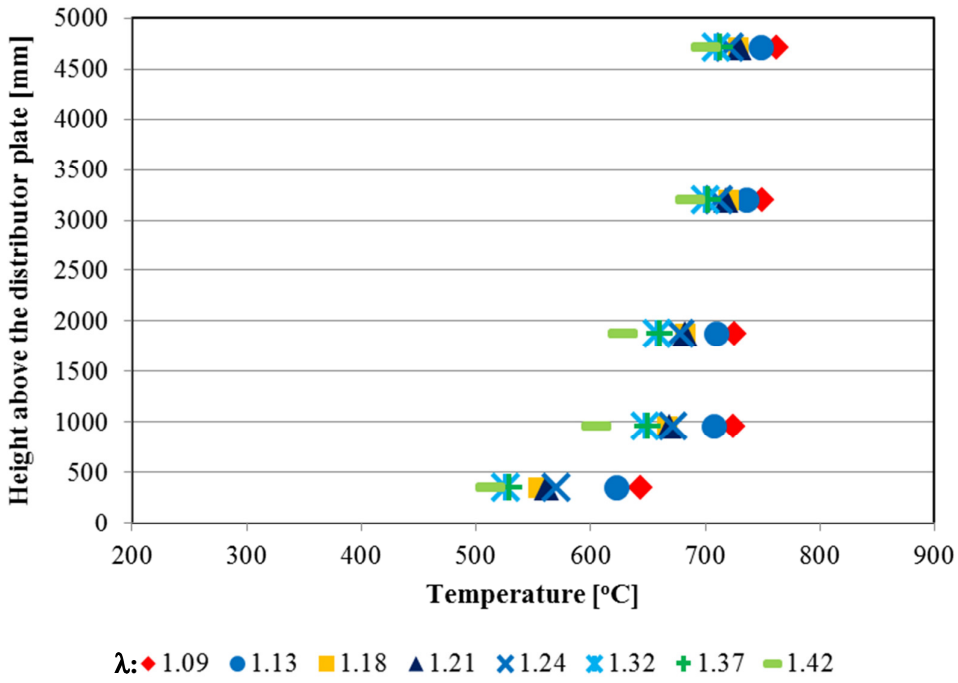

Figure 5.66 Temperature profile along the return leg for the co-combustion of Denizli/Kale lignite and 50% olive cake (by wt.) with Çan Limestone (Ca/S_{total} = 2.0) - Long Term Test (C2-B1-2)

Emissions:

Total duration of flue gas measurement was 49 hours and 11 minutes. 44 hours and 45 minutes of it was found suitable to be used for drawing of emission graphics. The number of data used in the emission graphics was reduced without disturbing the trend in emissions in order to minimize the data clutter in the emission graphics. 13 hours and 20 minutes part of 44 hours and 45 minutes emission measurement is presented in Figure 5.67.

Flue gas emission limits according to the Turkish Regulation for the co-combustion of Bursa/Orhaneli lignite with Olive cake (50% by wt.) are given in Table 5.21.

Table 5.21 Flue gas emission limits for the co-combustion test (C2-B1-2) according to the Turkish Regulation ("Turkish Regulation for Industrial Air Pollution Control," 2009)

Test #	Test Code	CO (mg/Nm^3)	NO (mg/Nm^3)	SO_xasSO_2 (mg/Nm^3)
4-4	C2-B1-2	328	461	1117

As can be seen from Figure 5.67, CO emissions are all above the emission limit (328 mg/Nm^3) for all λ values. This might be explained by limestone addition into the combustor in order to decrease SO_2 emission. When limestone was given into the combustor, it locally decreased the temperature leading to produce high CO emission. NO emissions were below the limit (461 mg/Nm^3) for λ range of 1.09-1.42. Since limestone was used in the experiment, SO_2 emission was under the emission limit (1117 mg/Nm^3).

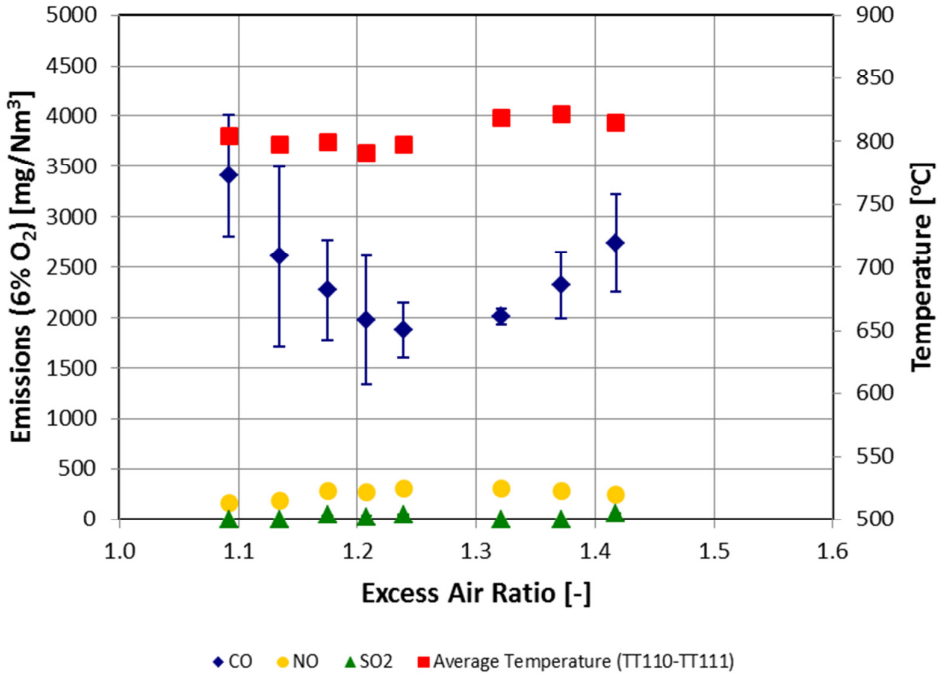

TT110 and TT111 are located 24 cm and 32 cm above the distributor plate, respectively.

Figure 5.67 Effect of excess air ratio on flue gas emissions for the co-combustion of Denizli/Kale lignite and 50% olive cake (by wt.) with Çan Limestone (Ca/S_{total} = 2.0) - Long Term Test (C2-B1-1)

5.4.5. Combustion of Olive Cake – Long Term Test (B1-2)

Combustion of olive cake was tried many times. It was possible to burn olive cake for a short time as can be seen from Section 5.1.5. However, the sustainability of the experiment for a long time was complicated and problematic. In each trial, a problem has occurred on the return leg. Olive cake was easily burnt in the combustor for a certain time. After a while, the temperature in the return leg started to decrease. The decrease in the temperature was a sign of a blockage in the return leg. The blockage in the return leg resulted in shutdown of the system. The inside diameter of the return leg was 42.16 mm (DN 32/SCH 10). There were many holes on the pipe of the return leg in order to locate

thermocouples, pressure transmitters and to inject air from the critical points such as bends. These holes might be the reason of blockage encountered during the tests.

When olive cake was used as a fuel for a combustion test, the alkali metal content of olive cake ash might result the formation of alkali silicates which had low melting point. In the long-term experiments, the ash particles containing alkali silicates might stick on the surface of the thermocouples which were located perpendicular to the flow. These ash particles might also accumulate on the holes which were opened for air purge. The holes were located on the connection line between the return leg and combustor. The accumulation of the ash particles on holes might cause total blockage of that region in a long run. The accumulation within this region prevented the circulation of the bed material. The temperature profiles both along the combustor and return leg were failed. While high temperature profile within the dense bed was observed, the temperatures in the return leg decreased. In order to solve this problem, the diameter of the return leg might be increased. This might provide easy flow of particles in the return leg and extend the operating time for a while. However, it was possible to face with the same operational problems. For this reason, the experiment of olive cake combustion was extracted from the SET#4 of experimental matrix. Olive cake, such as other biomass resources, is generally used as supplementary fuel in the combustion plants. It is not feasible to use only olive cake in the energy production because it is a seasonal product and there are many difficulties about the storage and continuous supply of the olive cake. These types of constraints have been a valid basis for removal of tests of olive cake combustion from the experimental matrix.

5.4.6. Comparison of Emissions in SET#4 with the Limits in Turkish Regulation

A summary of the operational parameters such as excess air ratio, superficial velocity in the combustor during the experiments are given in Table 5.22 for each combustion test. The fuel feeding rates and thermal power gained for these feeding rates are also given in Table 5.22.

Table 5.22 Operational conditions for the co-combustion tests in SET#4

Test #	Test Code	Fuel Feeding rate kg/h	λ -	P_{th}[a] kW	U_o[b] m/s
4-1	C1-B1-6	4.6-6.1	1.16-1.49	23-31	3.6-4.1
4-2	C1-B1-7	4.9-6.1	1.12-1.48	25-31	3.4-3.6
4-3	C2-B1-1	6.4-6.9	1.11-1.35	29-31	3.4-3.6
4-4	C2-B1-2	6.3-7.0	1.09-1.42	28-31	3.4-3.6

[a] P_{th}: Thermal power

[b] U_o: Superficial velocity in the combustor (calculated based on TT112 and flue gas flow rate) (Average temperature of TT110 and TT111 was considered in the calculation of superficial velocity because TT112 was out of order for the test#4.4.)

During emission measurements, CO, NO, and SO_2 emissions were investigated in order to determine the optimum excess air ratio. For the excess air ratios, optimum values were determined according to minimum CO, NO, and SO_2 emissions. Optimum values of excess air ratio and corresponding flue gas emissions are listed in Table 5.23.

Table 5.23 Optimum excess air ratios, corresponding thermal power, superficial velocity and flue gas emissions for the co-combustion tests in SET#4

Test #	Test Code	Optimum λ	P_{th} kW	U_o m/s	CO[a] mg/Nm^3	NO[a] mg/Nm^3	SO_2[a] mg/Nm^3
4-1	C1-B1-6	1.34	30	4.0	298±53	399±7	1507±24
4-1	C1-B1-6	1.40	30	4.0	271±21	421±5	1526±13
4-2	C1-B1-7	1.48	25	3.4	331±8	508±9	307±56
4-2	C1-B1-7	1.41	26	3.4	398±25	456±9	269±27
4-3	C2-B1-1	1.19	31	3.5	320±43	291±29	3031±310
4-4	C2-B1-2	1.24	28	3.6	1878±272	306±21	46±3

[a]Emissions are given on dry basis as a reference of 6% O_2.

The flue gas emission limits specified in the Turkish Regulation for Industrial Air Pollution Control ("Turkish Regulation for Industrial Air Pollution Control," 2009) are listed in Table 5.3 in Section 5.1.9. Flue gas emission limits for co-combustion of coal and biomass are calculated according to the Turkish Regulation ("Turkish Regulation for Industrial Air Pollution Control," 2009). In order to find the emission limit for a facility using more than one fuel, emission limit of each fuel is multiplied by its thermal power. Then, they are summed up and divided by the total thermal power of the fuels. Emission limits resulting from co-firing carried out in this study are calculated according to the formula mentioned and they are given in Table 5.24 for each test.

The flue gas emissions resulted in the co-combustion experiments of SET#4 at the optimum excess air ratios were compared to the emission limits specified by the Turkish Regulation ("Turkish Regulation for Industrial Air Pollution Control," 2009) in Table 5.24. If the measured emission value is below the emission limit, it is light gray in color. If it is above the emission limit, it is dark gray in color.

CO emissions measured were under the emission limit (334 mg/Nm^3) in the operational conditions of λ between 1.34 and 1.40 for the co-combustion of the fuel mixture containing 50% by wt. Bursa/Orhaneli lignite and 50% by wt. olive cake (C1-B1-6). When the co-combustion experiment was repeated by addition of limestone, CO emission got worse. CO emission which was measured for λ=1.48 was the only measurement below the emission limit. However, in that case, NO emission was measured above the emission limit. Therefore, it is not possible to give an optimum excess air ratio for both minimum CO and NO emissions. When CO emission is considered, excess air ratio is suggested to be kept around 1.48. When NO emission is taken into account, excess air

ratio is suggested to be kept around 1.41. When Denizli/Kale lignite was used in the co-combustion experiments (C2-B1-1), CO emissions measured were under the emission limit (327 mg/Nm^3) in the operational conditions of λ=1.19. However, limestone addition to fuel mixture caused CO emission to exceed the emission limit (328 mg/Nm^3). Minimum CO emission was measured as 1878 mg/Nm^3 for the case of λ=1.24. In the case of C2-B1-2, CO emission was highly above the emission limit.

NO emissions were under the limits for all cases except for the case of λ=1.48 in the test C1-B1-7. In this case, NO emission was 508 mg/Nm^3 which is above the emission limit for NO (457 mg/Nm^3). However, at the same time, it was the case where CO emission was measured to be 331 mg/Nm^3 which was under the emission limit for CO (337 mg/Nm^3). As a general trend observed in the combustion and co-combustion experiments, when NO emissions were low CO emissions were high because of the reducing effect of CO on NO.

SO_2 emissions were above the emission limit (1070 mg/Nm^3) when the fuel mixture containing 50% by wt. Bursa/Orhaneli lignite and 50% by wt. olive cake was combusted in the scope of C1-B1-6 test. When the combustion test (C1-B1-7) was repeated by addition of limestone, SO_2 emissions were measured below the emission limit (1051 mg/Nm^3) during the long-term test. SO_2 emission values (269 mg/Nm^3 and 307 mg/Nm^3) given in Table 5.24 are the highest measurements experienced throughout the C1-B1-7 test. When Denizli/Kale lignite, which has higher sulfur content than Bursa/Orhaneli lignite, was used instead of Bursa/Orhaneli lignite in the co-combustion test, SO_2 emission was measured about 3000 mg/Nm^3 which is above the emission limit (1118 mg/Nm^3) for C2-B1-1 test. When the co-combustion test was repeated by addition of limestone, SO_2 emissions were measured below the emission limit (1117 mg/Nm^3) during the long-term test (C2-B1-2).

Table 5.24 Comparison of flue gas emissions at the optimum excess air ratio for the co-combustion tests in SET#4 with the limits in the Turkish Regulation ("Turkish Regulation for Industrial Air Pollution Control," 2009)

Test #	Test Code	CO (mg/Nm^3)		NO (mg/Nm^3)		SO_x as SO_2 (mg/Nm^3)	
		measured	Limit	measured	Limit	measured	Limit
4-1	C1-B1-6	298±53	334	399±7	458	1507±24	1070
4-1	C1-B1-6	271±21	334	421±5	458	1526±13	1070
4-2	C1-B1-7	331±8	337	508±9	457	307±56	1051
4-2	C1-B1-7	398±25	337	456±9	457	269±27	1051
4-3	C2-B1-1	320±43	327	291±29	461	3031±310	1118
4-4	C2-B1-2	1878±272	328	306±21	461	46±3	1117

5.4.7. Combustion Efficiency (Carbon-based)

The carbon-based combustion efficiency (η) was conducted for each co-combustion test. The efficiency was calculated by subtracting combustion losses from 100%. The combustion losses are originated from formation of CO and several hydrocarbons (CH_4, C_2H_4, C_2H_6, C_3H_8, C_6H_{14}) in the flue gas and the unburnt carbon in the bottom ash, fly ash from 2nd cyclone and fly ash from bag filter. The combustion losses due to the formation of CO and unburnt hydrocarbons are defined as L_{CO} and L_{HC}, respectively. The combustion losses due to the unburnt carbon in the bottom ash, fly ash from the 2nd cyclone and from the bag filter are defined as L_{BA}, $L_{FA\text{-}C}$, $L_{FA\text{-}BF}$, respectively.

The combustion loss due to formation of CO in the flue gas was calculated according to Eq. 5.1 as follows:

$$L_{CO} = \frac{[\mathrm{CO}] * Q_{fluegas} * \Delta H^0_{c_{CO}} * 4.18}{\mathrm{P}_{th} * 1000 * 3600} * 100 \qquad \text{Eq. 5.1}$$

where,

L_{CO} : Combustion loss due to formation of CO in the flue gas, %
[CO] : CO concentration measured in the flue gas, mg/Nm^3
$Q_{fluegas}$: Flue gas flowrate, 30-35 Nm^3/h
$\Delta H_c{}^0{}_{CO}$: Heat of combustion for CO, 2.42 kcal/g (Perry, 1973)
P_{th} : Thermal power obtained from the fuel mixture, kW
1 cal = 4.18 J
1 g = 1000 mg
1 h = 3600 s

Combustion losses due to unburnt hydrocarbons in the flue gas were calculated for each hydrocarbon measured by GASMET flue gas analyzer according to Eq. 5.2 and Eq. 5.3 given below:

$$L_{HC} = \sum_{i=1}^{5} L_{HC_i} \qquad \text{Eq. 5.2}$$

$$L_{HC_i} = \frac{[\mathrm{HC}_i] * Q_{fluegas} * \Delta H^0_{c_{HC_i}} * 4.18}{\mathrm{P}_{th} * 1000 * 3600} * 100 \qquad \text{Eq. 5.3}$$

where,

L_{HC} : Total combustion losses due to the formation of hydrocarbons, %
L_{HCi} : The combustion loss for each component (CH_4, C_2H_4, C_2H_6, C_3H_8, C_6H_{14}) of hydrocarbons, %
[HC_i] : Concentration of hydrocarbon measured in flue gas, mg/Nm^3
$\Delta H_c{}^0{}_{HCi}$: Heat of combustion for each component of hydrocarbons, 11.98 kcal/g for CH_4, 11.29 kcal/g for C_2H_4, 11.38 kcal/g for C_2H_6, 11.10 kcal/g for C_3H_8, and 10.80 kcal/g for C_6H_{14} (Perry, 1973)

The combustion loss due to unburnt carbon in the bottom ash was calculated according to Eq. 5.4:

$$L_{BA} = \frac{[C_{BA}] * Q_{BA} * \Delta H_{C_C}^0 * 1000}{P_{th} * 3600} \quad \text{Eq. 5.4}$$

where,

L_{BA} : Combustion loss due to unburnt carbon in the bottom ash, %
$[C_{BA}]$: Unburnt carbon in the bottom ash, % (kg C/kg ash)
Q_{BA} : Discharge rate for the bottom ash, kg/h
$\Delta H_c{}^0{}_C$: Heat of combustion for char, 32.81 kJ/g (Perry, 1973)

The combustion loss due to unburnt carbon in the fly ash from the 2nd cyclone was calculated according to Eq. 5.5:

$$L_{FA-C} = \frac{[C_{FA-C}] * Q_{FA-C} * \Delta H_{C_C}^0 * 1000}{P_{th} * 3600} \quad \text{Eq. 5.5}$$

where,

L_{FA-C}: Combustion loss due to unburnt carbon in the fly ash from the 2nd cyclone, %
$[C_{BA}]$: Unburnt carbon in the fly ash from the 2nd cyclone, % (kg C/kg ash)
Q_{BA} : Discharge rate for the fly ash from the 2nd cyclone, kg/h

The combustion loss due to unburnt carbon in the fly ash from the bag filter was calculated according to Eq. 5.6:

$$L_{FA-BF} = \frac{[C_{FA-BF}] * Q_{FA-BF} * \Delta H_{C_C}^0 * 1000}{P_{th} * 3600} \quad \text{Eq. 5.6}$$

where,

L_{FA-BF} : Combustion loss due to unburnt carbon in the fly ash from the bag filter, %
$[C_{FA-BF}]$: Unburnt carbon in the fly ash from the bag filter, % (kg C/kg ash)
Q_{FA-BF} : Discharge rate for the fly ash from the bag filter, kg/h

At the end of each co-combustion test, bottom ash from the combustor and fly ashes from the 2nd cyclone and the bag filter were collected and weighted. Average ash discharge rates were calculated from the beginning of fuel feeding. Total durations of fuel feeding were 25.1 h, 40.4 h, 49.8 h, and 51.4 h for co-combustion tests C1-B1-6, C1-B1-7, C2-B1-1, and C2-B1-2, respectively. Samples taken from each ash investigated in this study were burnt in an oven at 950°C to the constant weight. The difference in weights before and after combustion gave the amount of unburnt carbon in the ash samples. The

percentages of unburnt carbon in ash samples and the discharge rates for the each co-combustion tests are given in Table 5.25. As can be seen from the table, the largest percentages of unburnt carbon are in the fly ash of the 2nd cyclone and fly ash of the bag filter, especially in tests 4-2, 4-3 and 4-4. However, discharge rates for these ashes are small. Therefore, these unburnt carbons do not affect the combustion efficiency considerably.

Table 5.25 Percentages of unburnt carbon in the ashes and ash discharge rates for co-combustion tests in SET#4

Test #	Test Code	$[C_{BA}]$ %	$[C_{FA\text{-}C}]$ %	$[C_{FA\text{-}BF}]$ %	Q_{BA} kg/h	$Q_{FA\text{-}C}$ kg/h	$Q_{FA\text{-}BF}$ kg/h
4-1	C1-B1-6	0.70	0.61	1.89	0.20	0.21	0.24
4-2	C1-B1-7	1.13	4.41	4.51	0.14	0.21	0.21
4-3	C2-B1-1	1.54	5.59	7.55	0.12	0.41	0.35
4-4	C2-B1-2	0.65	4.04	3.60	0.25	0.44	0.14

Carbon-based combustion efficiency (η) was calculated according to Eq. 5.7 as given below:

$$\eta = 100 - (L_{CO} + L_{HC} + L_{BA} + L_{FA-C} + L_{FA-BF}) \quad \text{Eq. 5.7}$$

Combustion losses and carbon-based combustion efficiencies for the co-combustion tests in SET#4 are given in Table 5.26. As can be seen from Table 5.26, the minimum efficiency was calculated as 98.4% for the co-combustion of Denizli/Kale lignite with 50% by wt. olive cake (C2-B1-1). The maximum efficiency was calculated as 99.7% for the co-combustion of Bursa/Orhaneli lignite with 50% by wt. olive cake (C1-B1-6). The major loss was coming from the unburnt carbon in the fly ash of the 2nd cyclone and fly ash of the bag filter. When limestone was added to the fuel mixture (C2-B1-2), the contribution of cyclone ash to the total combustion loss was higher than that of the bag filter ash. High CO emissions during the test were another major contributor to the combustion loss. However, in general, the combustion efficiency was between 98.4% and 99.7% which were pretty close to each other. This result indicated that the combustion conditions at optimum excess air ratios were quite efficient in terms of carbon conversion.

Table 5.26 Combustion losses and carbon-based combustion efficiencies for the co-combustion tests in SET#4

Test #	Test Code	Optimum λ	L_{CO} %	L_{HC} %	L_{BA} %	L_{FA-C} %	L_{FA-BF} %	η %
4-1	C1-B1-6	1.34	0.10	0.01	0.04	0.04	0.14	99.68
4-1	C1-B1-6	1.40	0.09	0.01	0.04	0.04	0.14	99.68
4-2	C1-B1-7	1.48	0.11	0.01	0.06	0.35	0.35	99.13
4-2	C1-B1-7	1.41	0.13	0.01	0.06	0.35	0.35	99.11
4-3	C2-B1-1	1.19	0.09	0.00	0.01	0.68	0.78	98.43
4-4	C2-B1-2	1.24	0.60	0.07	0.01	0.57	0.16	98.59

The results obtained here have shown that combustion efficiencies in the Circulating Fluidized Bed Combustor used in this study are very good. There is a good mixing in the combustor and sufficient contact time between the fuel particles and air. The efficiency results obtained in this study are quite comparable with the literature data. Co-combustion of coal with biomass brought some inefficiency in the process due to high volatile matter content of the biomass and increase in CO formation. However, decrease in efficiency was less than 1-1.5 % which was mostly due to CO formation, unburnt carbon in the fly ash of the 2nd cyclone and the fly ash from the bag filter. The decrease in efficiency due to unburnt hydrocarbons was quite small and minimal.

5.5. Assessment of Ash Analysis for Experiments in SET#4

The effect of sulfur content of fuel mixture and possible interaction between biomass and limestone on ash composition was investigated for the long-term experiments done in SET#4. Bursa/Orhaneli and Denizli/Kale lignites were used as low-sulfur (S_{total} < 2.7% in Table 4.1) and high-sulfur coals (S_{total} > 3.6% in Table 4.1), respectively. Olive cake was selected as biomass because of its high alkali content in ash (K_2O content of olive cake ash was about 50% by wt. in Table 4.16). Fuels used in the experiments and their percentage in the fuel mixture are given in Table 5.27. Samples taken from the bottom ash (BA), fly ash captured in the second cyclone (FA-C), and fly ash captured in the bag filter (FA-BF) were subjected to XRF and XRD analyses. Bursa/Orhaneli lignite, Denizli/Kale lignite and olive cake used in the tests were sampled before combustion. Ashes from these fuels were obtained by combusting these fuels in a furnace according to the ASTM standards (ASTM D1374-04 Standard Test Method for Ash in the Analysis Sample of Coal and Coke from Coal for coal samples, ASTM E1755-01 Standard Test Method for Ash in Biomass for olive cake). XRF and XRD analyses of the ashes were also performed. The results of fuel ash analyses were compared with the analysis results of ashes obtained from the co-combustion experiments. XRF and XRD give semi-quantitative results. The deposit sampling probe was used during the experiments. The deposit accumulated on the surface of the deposit sampling probe was also subjected to

XRD analysis. SEM-EDS analysis was conducted for the bottom ashes and deposits. The results of these analyses and assessment of the results are presented in this section.

Table 5.27 List of experiments conducted in the scope of SET#4

Test #	Test Code	Coal	Biomass	Biomass share in fuel mixture, % by wt.	Ca/S_{total} ratio
4-1	C1-B1-6	Bursa/Orhaneli	Olive Cake	50	-
4-2	C1-B1-7	Bursa/Orhaneli	Olive Cake	50	Optimum
4-3	C2-B1-1	Denizli/Kale	Olive Cake	50	-
4-4	C2-B1-2	Denizli/Kale	Olive Cake	50	Optimum

5.5.1. Co-Combustion of Bursa/Orhaneli Lignite and Olive Cake (50% by wt.) (C1-B1-6)

Bursa/Orhaneli lignite was used as the coal and olive cake was used as the biomass material in this experiment. The weight percent of olive cake in the fuel mixture was 50. Some of the operational parameters are given in Table 5.28.

Table 5.28 Range of operational parameters for the co-combustion test (C1-B1-6)

Test #	Test Code	Fuel Feeding rate kg/h	λ -	P_{th}[a] kW	U_o[b] m/s
4-1	C1-B1-6	4.6-6.1	1.16-1.49	23-31	3.6-4.1

[a] P_{th}: Thermal power
[b] U_o: Superficial velocity in the combustor (calculated based on TT112 and flue gas flow rate)

The co-combustion test of fuel mixture containing Bursa/Orhaneli lignite and olive cake 50% by weight was performed at the dense phase temperature of 824±11°C. The XRF results of bottom ash (BA) fly ash from the second cyclone (FA-C) and fly ash from the bag filter (FA-BF) are given in Table 5.29. Ashes of both fuels were generated at the operating conditions in the laboratory according to ASTM standards. XRF analyses of these fuel ashes, being a reference for comparison with the CFBC ashes, are also given in Table 5.29. The XRD results of the ashes are presented in Table 5.30.

Table 5.29 XRF results of fuel ashes and ashes formed at the end of the co-combustion test (C1-B1-6)

Compound	Bursa/Orhaneli	Olive Cake	BA	FA-C	FA-BF
	% by wt.				
Al_2O_3	10.14	3.04	2.73	7.33	7.15
CaO	19.73	20.38	10.47	22.63	24.53
Cl	0.00	2.19	0.00	0.13	0.24
Cr_2O_3	0.06	0.12	0.17	0.06	0.02
CuO	0.22	0.08	0.07	0.08	0.09
Fe_2O_3	9.97	5.16	5.88	9.43	10.16
K_2O	0.58	49.26	4.44	5.15	9.72
MgO	7.87	2.95	11.20	4.68	5.28
MnO_2	0.15	0.16	0.10	0.20	0.30
Na_2O	0.27	0.49	0.11	0.18	0.35
P_2O_5	0.22	3.57	0.30	1.75	1.27
SO_3	29.33	4.34	8.12	13.60	24.93
SiO_2	20.82	7.48	55.96	34.21	15.27
Normalized To (%)	100.0	100.0	100.0	100.0	100.0
Sum Before Normaliz. (%)	110.4	54.3	72.2	67.7	73.5

When Table 5.29 is investigated, it can be seen that Al_2O_3, CaO, Fe_2O_3, MgO, and SiO_2 are the major oxides in the Bursa/Orhaneli lignite ash. However, K_2O, CaO, and SiO_2 are the major oxides in the olive cake ash. When these percentages are compared with the ash composition collected from the BA, FA-C, and FA-BF, a considerable change has been observed. First of all, Al_2O_3 content has decreased in the bottom ash to 3% while coal ash has 10% Al_2O_3 content. While both fuel ashes has 20% CaO, CaO content in the bottom ash has decreased to 10%. CaO, MgO, and SiO_2 are the major oxides in the bottom ash. In the ash samples collected from the cyclone and the bag filter, mostly CaO, Fe_2O_3, SiO_2 and partly K_2O are observed. In order to understand in which phase these elements are, XRD analysis of each sample were performed. As can be seen from the XRD results of fuel ashes in Table 5.30, Anhydrite phase was determined in the ash of Bursa/Orhaneli lignite. This may show that Ca and S elements seen in XRF result are probably in the form of $CaSO_4$. Si and Fe elements may be in the form of SiO_2 and Fe_2O_3, respectively. K element which is the major element in the ash of olive cake is most likely in the phase of Potassium Carbonate Hydrate ($K_2CO_3.1,5H_2O$) and Fairchildite ($K_2Ca(CO_3)_2$). A small amount of K element may be in Arcanite (K_2SO_4) phase. 2.2% Cl element in XRF result may appear in Sylvite (KCl) phase in the structure of olive cake ash.

Table 5.30 XRD (Rietveld method) results of fuel ashes and ashes formed at the end of the co-combustion test (C1-B1-6)

Phase	Bursa/Orhaneli	Olive Cake	BA	FA-C	FA-BF
	% by wt.				
Quartz, SiO_2	24.1	2.7	√	73.7	23.6
Calcite, $CaCO_3$	2.2	9.9			
Lime, CaO			√	4.4	5.4
Anhydrite, $CaSO_4$	61.3		√	4	16
Hematite, Fe_2O_3	12.4			17.9	21.9
Arcanite, K_2SO_4		9.3	√		17.5
Potassium Calcium Sulfate, $K_2Ca_2(SO_4)_3$					15.6
Fairchildite, $K_2Ca(CO_3)_2$		35.8			
Potassium Carbonate Hydrate, $K_2CO_3.1{,}5H_2O$		28			
Sylvite, KCl		4.4			
Forsterite, $Mg_2(SiO_4)$			√		

In the XRD analysis, different phases were determined in the bottom ash but these phases could not be quantified according to the Rietveld method. Quartz (SiO_2), Lime (CaO), Anhydrite ($CaSO_4$), Arcanite (K_2SO_4) and Forsterite ($Mg_2(SiO_4)$) phases are encountered in the bottom ash. The Quartz (sand) which is used as bed material is the dominant phase in the bottom ash. In the same way, it is seen in the XRD analysis of fly ash collected in the second cyclone that Quartz is the dominant phase in the fly ash, too. In addition to Quartz, Hematite, Lime and Anhydrite are the phases observed in the fly ash of the second cyclone. Determination of Quartz phase in the fly ash of the 2nd cyclone is an indication that a small amount of sand escapes from the system. The Quartz phase is also determined in the fly ash captured in the bag filter. However, the amount is less than the amount collected in the second cyclone. According to the XRD analysis conducted in MAM-ME, the phases containing K element are encountered in the fly ash sample from the bag filter. These phases are Arcanite and Potassium Calcium Sulfate. Encountering of potassium salts in the bag filter might be an indication that the potassium element which is in the structure of olive cake leaves the system in the gas phase, and then, it turns into potassium salts in the bag filter since the gas temperature is below 200^{o}C in the bag filter.

A **Deposit Probe** was designed to stimulate a heat exchanger tube in the combustor. It is cooled internally with air and wall temperature of the probe is held at 550^{o}C. When combustion gases pass around this probe, the particles hit the probe and some of the particles (especially the sticky ones) are deposited on the probe. This stimulates the heat transfer on a heat exchanger tube on the way of hot combustion gases. The deposit sampling probe was used during the combustion test. The particles accumulated on the surface of the probe were collected at the end of the combustion test. After the probe is

taken out of the combustor, the particles collected on the probe are very slowly scraped from the surface into a sampling pot. Then, they are sent for XRD, and SEM-EDS analysis. When XRD analysis of deposit accumulated on the surface of deposit sampling probe in Table 5.31 is examined, it can be seen that the main phase determined is Potassium Calcium Sulfate ($K_2Ca_2(SO_4)_3$). Since the surface of the deposit sampling probe is cooled to 550^oC, it is likely that the Potassium element in the gas mixture condenses on the surface of the probe, reacts with CaO and SO_2, and transforms into the phase of Potassium Calcium Sulfate. Furthermore, as iron oxides Magnetite and Hematite are encountered on the probe surface.

Table 5.31 XRD (RIR method) results of deposit collected from deposit sampling probe at the end of the co-combustion test (Analyses were done at METU-Central Laboratory) (C1-B1-6)

Phase	**Ash Deposit on the Sampling Probe % by wt.**
Hematite, Fe_2O_3	5
Magnetite, Fe_3O_4	20
Potassium Calcium Sulfate, $K_2Ca_2(SO_4)_3$	70
Arcanite, K_2SO_4	4
Magnesioferrite, $MgFe_2O_4$	1

After the co-combustion test was completed, the combustion system was left to cool down. At the end of the cooling process, all ashes formed during the combustion test were collected and weighted. These ashes are bottom ash, fly ash captured in the second cyclone and fly ash captured in the bag filter. Representative samples were taken from the bottom ash and deposit on the deposit sampling probe and they were investigated on a Scanning Electron Microscope (SEM) in order to observe both the morphology of ash samples and to determine their elemental composition. SEM micrographs, SEM-EDS results of the ash samples and the assessment of the results are given below.

5.5.1.1. SEM-EDS Analysis of Bottom Ash (C1-B1-6)

A general view of the sample taken from the bottom ash is given in Figure 5.68.

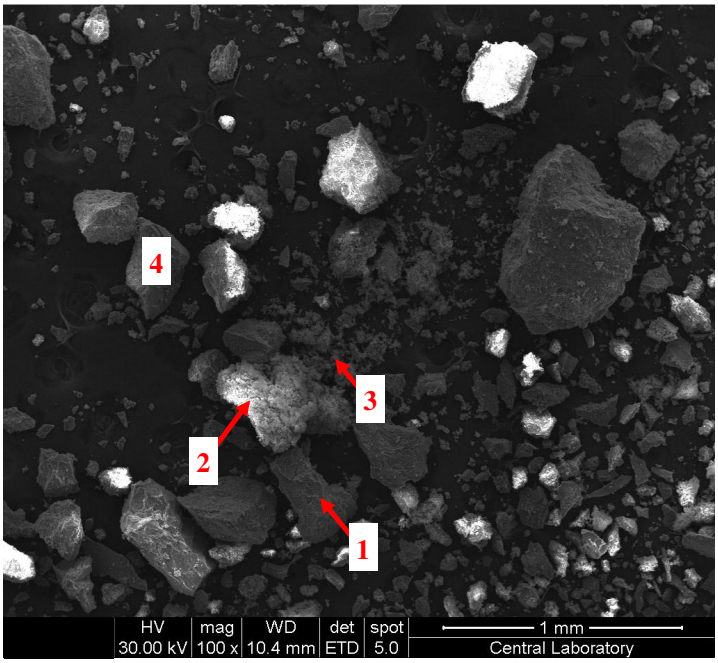

Figure 5.68 General view of sample taken from the bottom ash (C1-B1-6)

Four different hot points in Figure 5.68 were identified and SEM-EDS analysis was applied for these four locations. In the first part, the particle shown as "1" in Figure 5.68 was focused. The view was magnified 700 times and SEM-EDS analysis was applied for the particle. The enlarged view of the particle and also SEM-EDS result was given in Figure 5.69. The particle in Figure 5.69 was about 300 µm in length and 150 µm in width. The whole surface of the particle was rough and there were signs of fractures and breaks on the surface of the particle. The particle mainly consisted of O, Si, C, Mg, K, Fe and S elements. When XRD result of bottom ash in Table 5.30 was investigated, it can be stated that the particle was probably composed of Quartz (SiO_2), Forsterite (Mg_2SiO_4), and Arcanite (K_2SO_4).

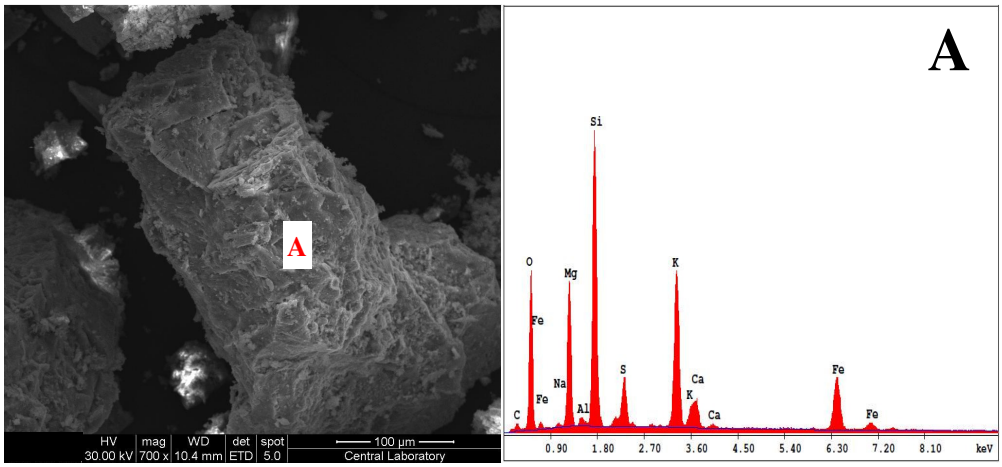

Figure 5.69 SEM micrograph and SEM-EDS result of point A on the particle shown as "1" in Figure 5.68

The particle shown as "2" in Figure 5.68 was magnified 519 times and SEM-EDS analysis was applied for the particle. The enlarged view of the particle and also SEM-EDS result are given in Figure 5.70. The surface of the particle is uneven in shape. According to the SEM-EDS result of point "A" on the surface of the particle, O, C, Ca, K, and S are the main elements present on the surface. As can be seen from XRD result of bottom ash in Table 5.30, these elements may be in the form of Arcanite (K_2SO_4) and Anhydrite ($CaSO_4$) phases.

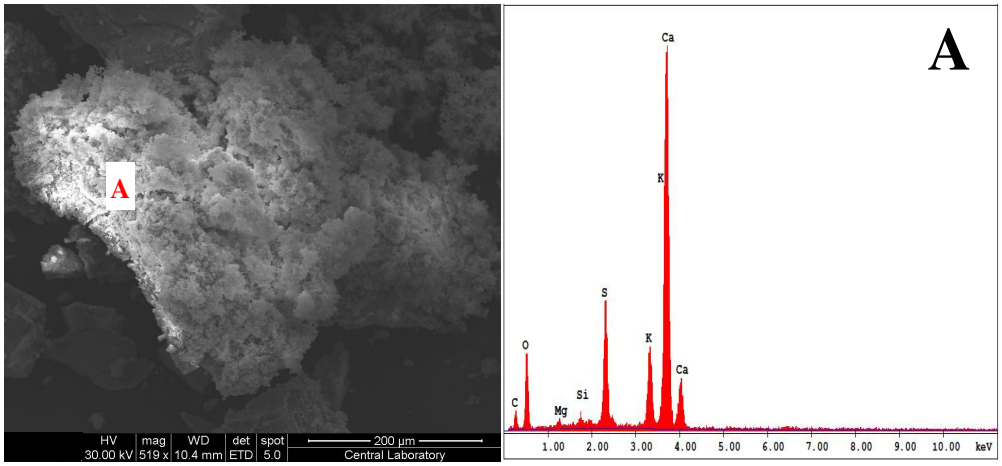

Figure 5.70 SEM micrograph and SEM-EDS result of point A on the particle shown as "2" in Figure 5.68

The enlarged view of the region "3" in Figure 5.68 is given in Figure 5.71. The particle in the middle of the Figure 5.71 was viewed more closely. The image was enlarged 6000 times. Two points on the surface of the particle was investigated by SEM-EDS analysis. The enlarged view of the particle and also SEM-EDS results of two points "A" and "B" on the surface of the particle are given in Figure 5.72.

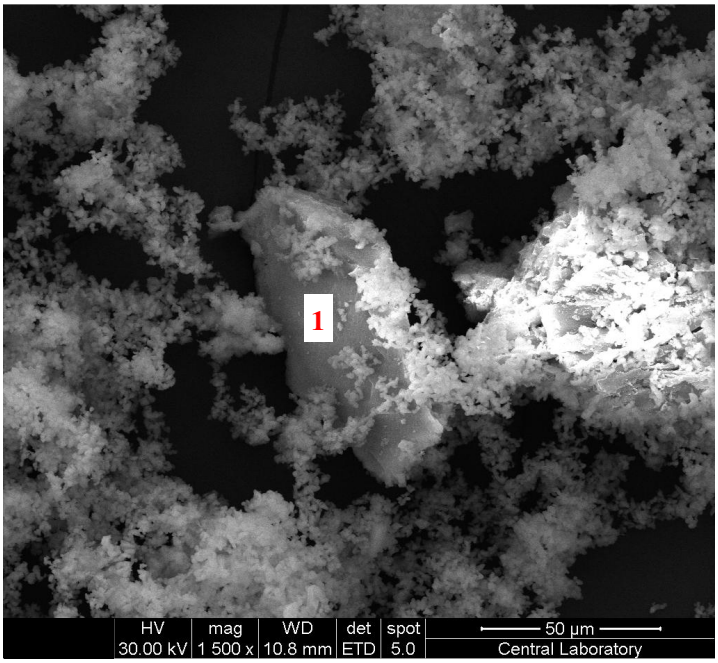

Figure 5.71 Enlarged view of the region shown as "3" in Figure 5.68

As the SEM-EDS result presented in Figure 5.70 studied, the main elements determined on the surface of the particle were O, C, and Ca. Unlike the SEM-EDS result in Figure 5.70, Fe element was detected on the particle surface. Fe element might be in the Hematite (Fe_2O_3) phase.

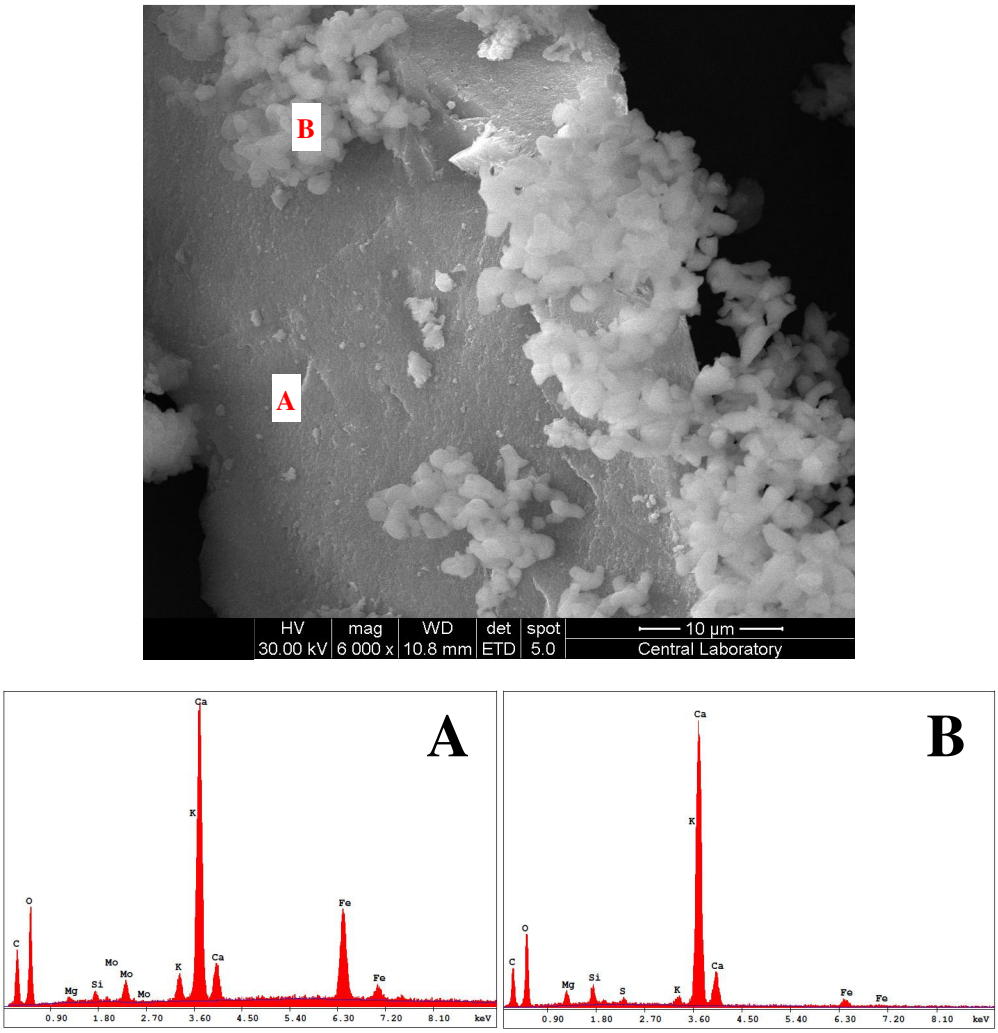

Figure 5.72 Enlarged view of the particle in Figure 5.71 and SEM-EDS results of points A and B on the particle

The view of the particle shown as "4" in Figure 5.68 was magnified 1500 times and SEM-EDS analysis was applied for the particle. The enlarged view of the particle and also SEM-EDS results of two points on the particle are given in Figure 5.73. When the SEM micrograph is observed, it is noticed that the particle has a smooth shape and there is an accumulation on the surface of the particle. The point "A" was selected to represent the particle itself and the point "B" was selected to represent the accumulation on the surface of the particle. When the SEM-EDS result of the point "A" is investigated, it is possible that the particle is mainly composed of Quartz (SiO_2), Forsterite (Mg_2SiO_4). Gold (Au) element is coming from coating because the ash sample was coated by Gold/Palladium (Au/Pd) alloy for SEM analysis.

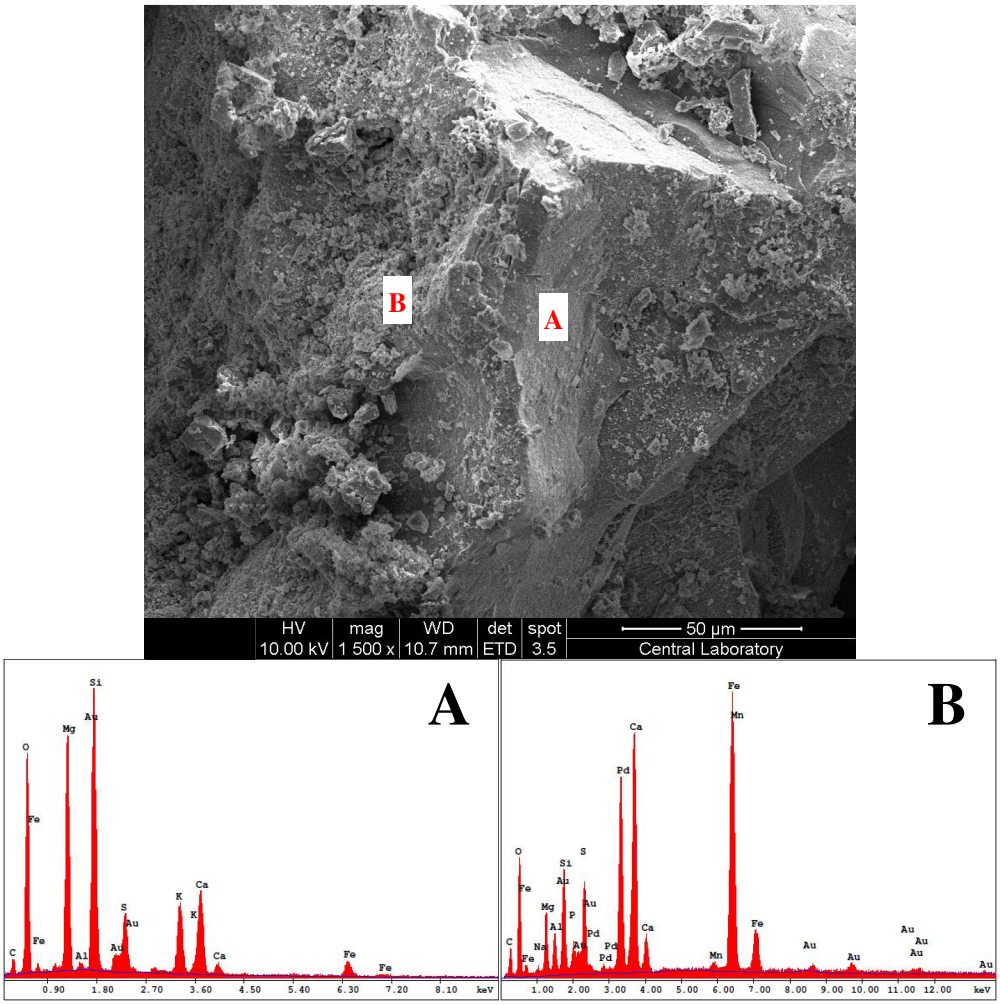

Figure 5.73 SEM micrograph and SEM-EDS results of points A and B on the particle shown as "4" in Figure 5.68

5.5.1.2. SEM-EDS Analysis of Deposit on the Deposit Sampling Probe (C1-B1-6)

The deposit sampling probe was used during the combustion test. At the end of 29 hour and 3 minute-test, the deposit sampling probe was carefully removed from the combustor. The images of the deposit sampling probe taken from four different sides are given in Figure 5.74. Part (a) in Figure 5.74 shows the upper part of the deposit sampling probe. When an observer looks down the probe from the top of the combustor, this is the view in part a. This is called as leeward view. The probe is rotated by 90^o counter-clockwise and then a picture of it is taken. This is right-side view and it is given in part (b) in Figure 5.74. The probe is rotated by 90^o counter-clockwise and then a picture of it is taken. This is windward view and it is given in part (c) in Figure 5.74. This part of the deposit

sampling probe is the part which is mostly exposed to particles within the combustor. The probe is again rotated by 90^{o} counter-clockwise and then a picture of it is taken. This is left-side view and it is given in part (d) in Figure 5.74.

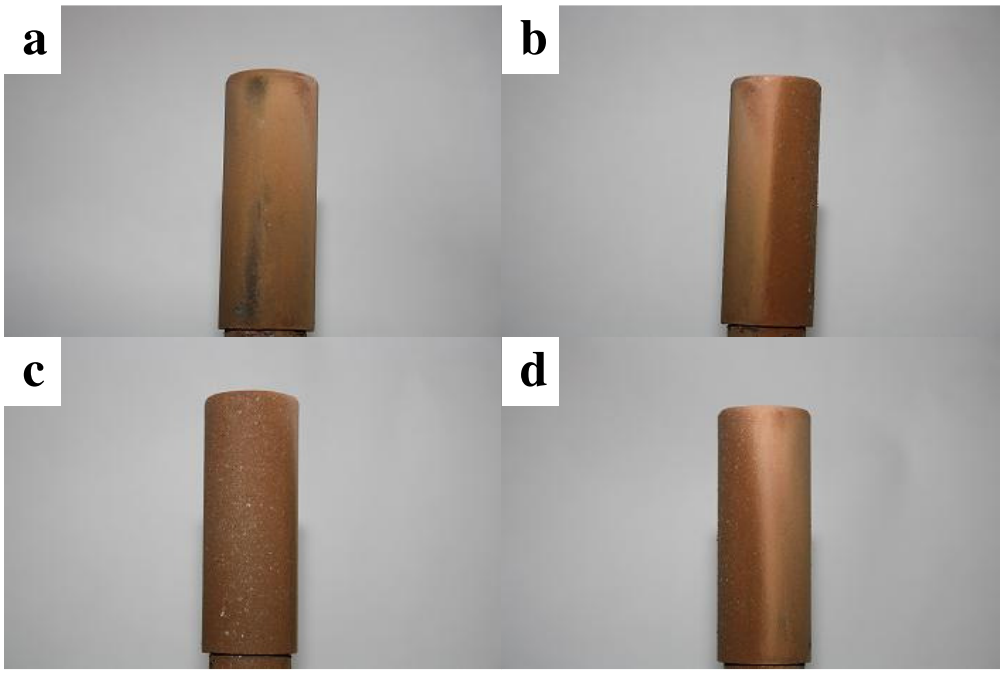

Figure 5.74 Images of the deposit sampling probe a) top view b) right-side view c) bottom view d) left-side view (C1-B1-6)

The deposit accumulated on the surface of the probe was collected at the end of the combustion test. The total amount of the deposit accumulated on the probe surface was about 1 g. The outside diameter of the probe was 26.7 mm and the length of the probe was 60 mm. The projected surface area where deposit can accumulate was 16.02 cm^2 (OD=26.7 mm; L=60 mm). Total duration for fuel feeding was 25 hours. Thus, the deposition rate was calculated as 25 g/m^2-h. The deposition rate is defined as mass of deposits per square meter of projected surface area of the probe per hour (Theis et al, 2006). If the deposition rate exceeds 20 g/m^2-h, this can be used as a sign of slagging and fouling problems in the measured area of the boiler (Göğebakan, 2007). Since the deposition rate calculated as 25 g/m^2-h for the co-combustion test C1-B1-6, it is higher than the limit (20 g/m^2-h) value, it is possible to face with a fouling problem in case of co-combustion of olive cake and Bursa/Orhaneli lignite (50% by wt.).

A general view of the sample taken from the deposit sampling probe is given in Figure 5.75.

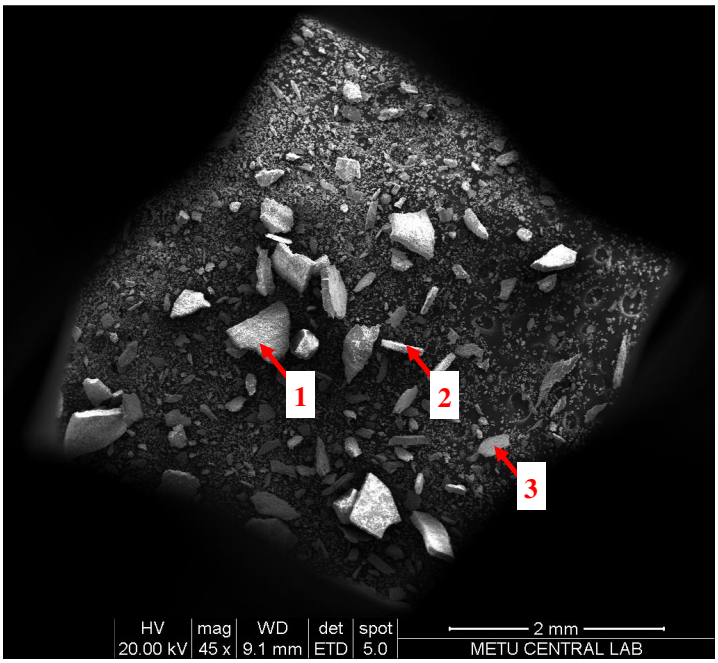

Figure 5.75 General view of sample taken from deposit sampling probe (C1-B1-6)

Three different hot points in Figure 5.75 were identified and SEM-EDS analysis was applied to these three locations. In the first part, the particle shown as "1" in Figure 5.75 was focused. The view was magnified 400 times and SEM micrograph was taken and it is given in Figure 5.76. The particle in Figure 5.76 was about 600 µm in length and 450 µm in width.

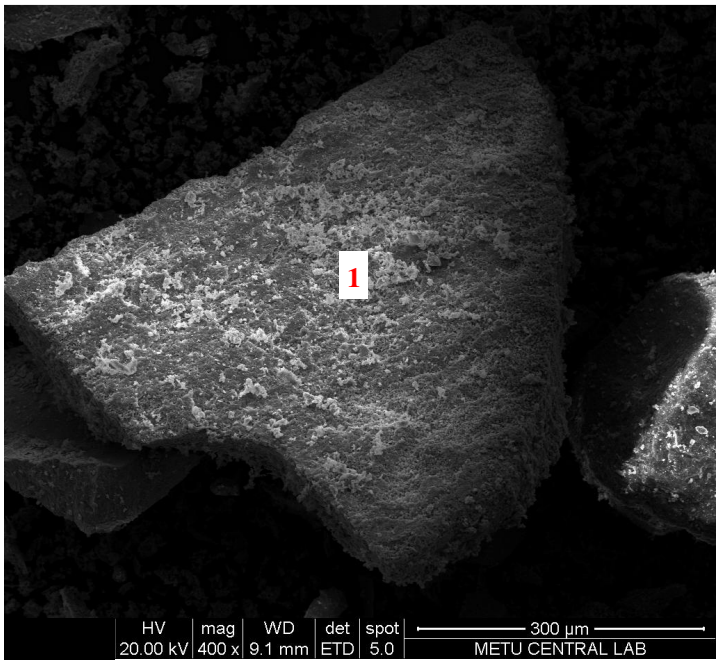

Figure 5.76 Enlarged view of particle shown as "1" in Figure 5.75

The view of the location numbered as "1" on the surface of the particle shown in Figure 5.76 was focused. The view was magnified 3000 times and SEM micrograph of it is taken and it is given in Figure 5.77. Two points on the surface of the particle was investigated by SEM-EDS analysis. The enlarged view of the particle and also SEM-EDS results of two points "A" and "B" on the surface of the particle are given in Figure 5.77. The surface of the particle is uneven in shape. According to the SEM-EDS result of point "A" on the surface of the particle in Figure 5.77, O, K, S, and C are the main elements existing on the surface. As can be seen from XRD result of the bottom ash in Table 5.31, these elements may be in the form of Arcanite (K_2SO_4) and Potassium Calcium Sulfate, $K_2Ca_2(SO_4)_3$ phases. When the SEM-EDS result of point "B" is investigated, it can be seen that same elements encountered on point "A" are the dominant ones on this surface. But, the amounts of S and K elements on point "B" are less than that of on point "A".

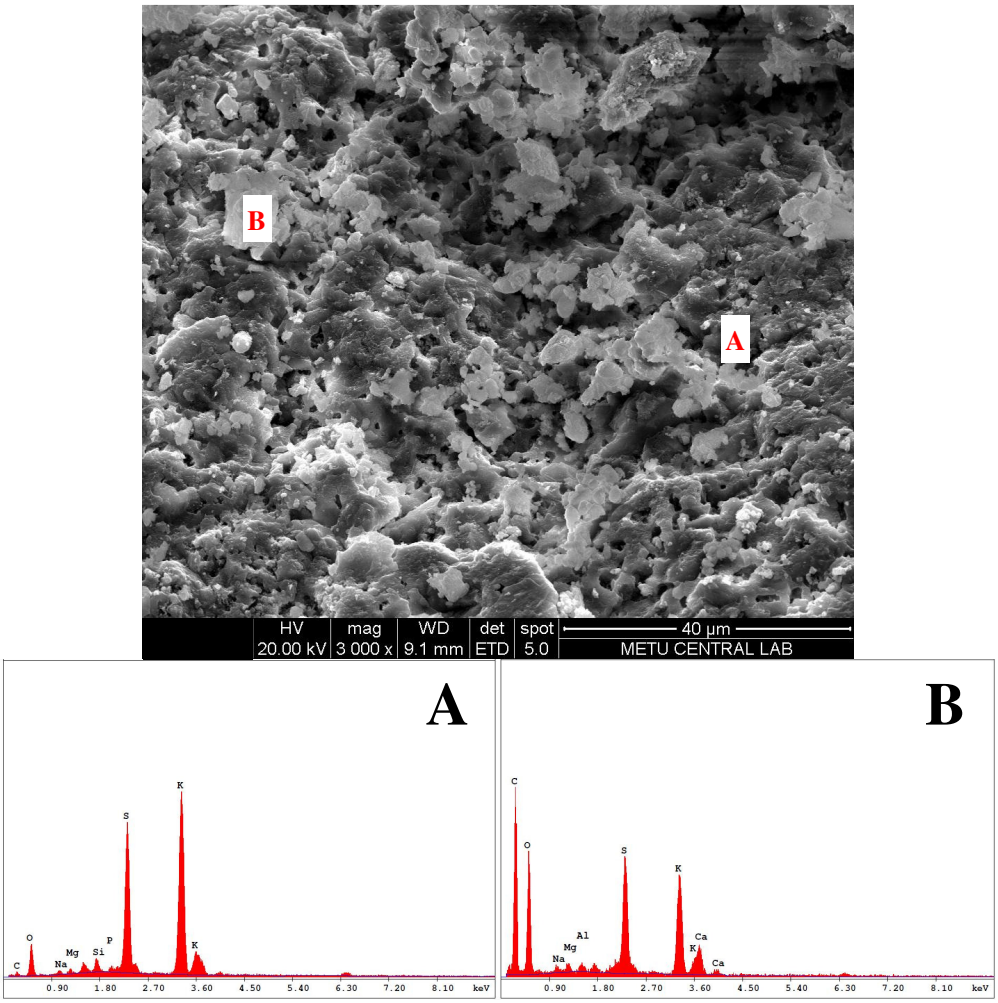

Figure 5.77 Enlarged view of the surface of the particle shown as "1" in Figure 5.76 and SEM-EDS results of points A and B

The view of the particle shown as “2” in Figure 5.75 was magnified 566 times and SEM micrograph of it is taken and it is given in Figure 5.78.

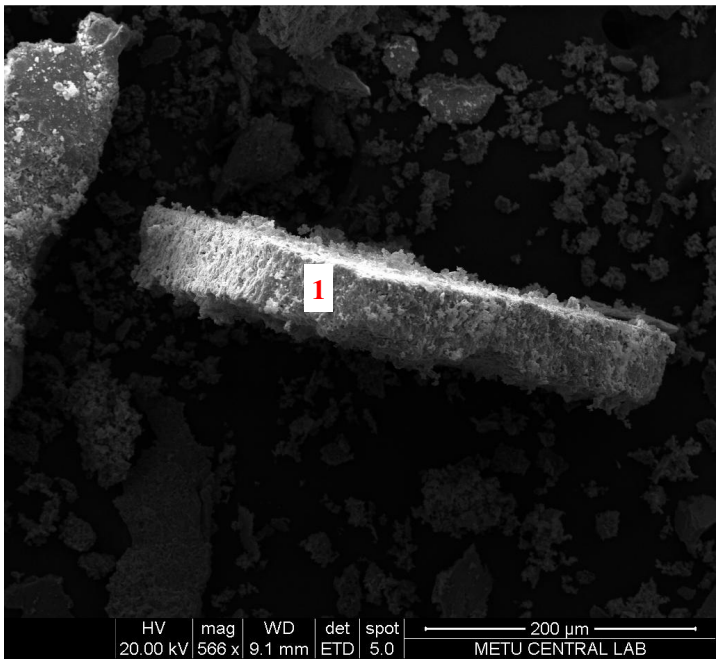

Figure 5.78 Enlarged view of the particle shown as “2” in Figure 5.75

The view of the particle shown as “1” in Figure 5.78 was magnified 3000 times and SEM-EDS analysis was applied for the particle. The enlarged view of the particle and also SEM-EDS results of two points on the particle are given in Figure 5.79. When the SEM-EDS result of both point “A” and “B” is investigated, it can be seen that main elements on the surface are O, K, C, S, Fe, and Ca. These elements might be in the phase of Potassium Calcium Sulfate ($K_2Ca_2(SO_4)_3$), Arcanite (K_2SO_4), Magnetite (Fe_3O_4), or Hematite (Fe_2O_3). These phases are the main phases that were determined by XRD analysis given in Table 5.31.

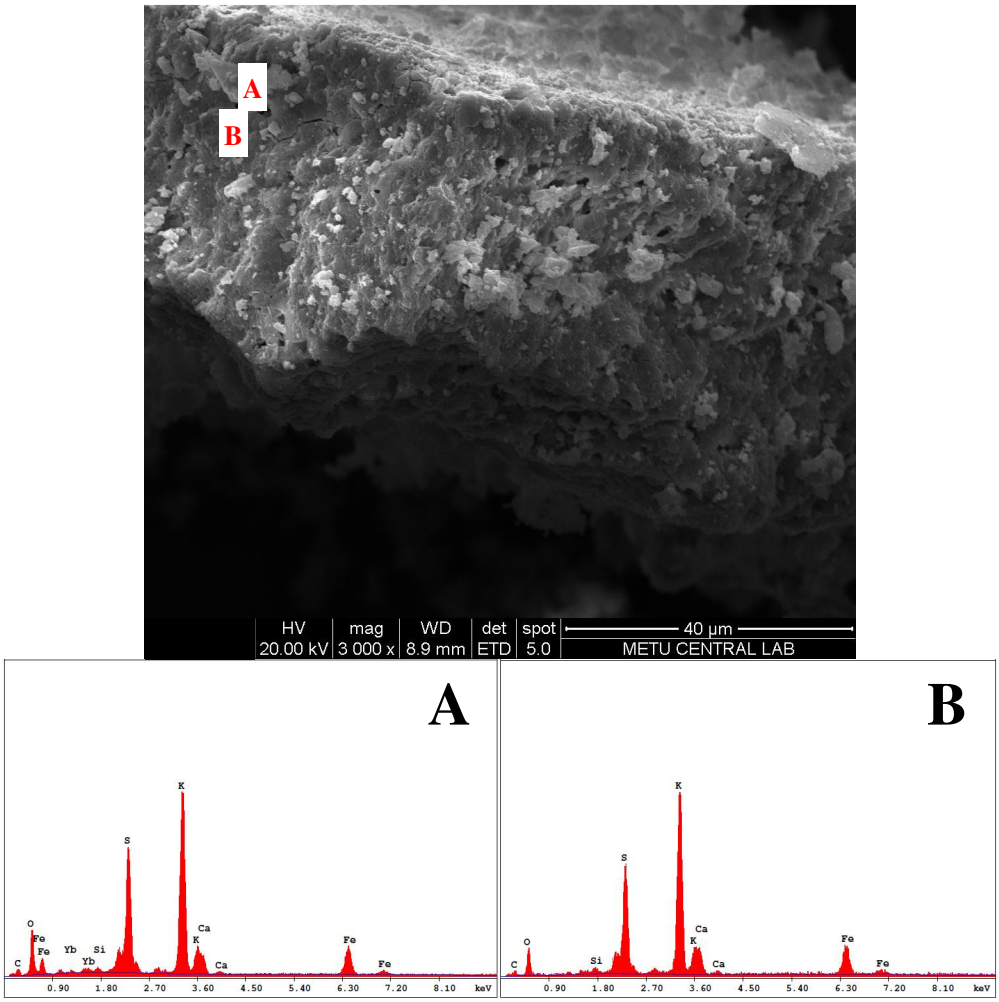

Figure 5.79 Enlarged view of the area shown as "1" in Figure 5.78 and SEM-EDS results of points A and B

The view of the particle shown as “3” in Figure 5.75 was magnified 800 times and SEM micrograph of it is taken and it is given in Figure 5.80.

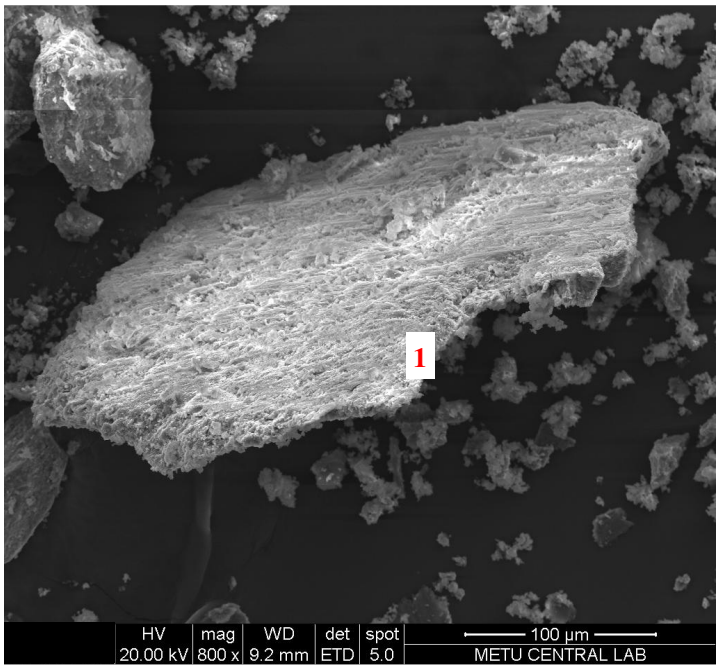

Figure 5.80 Enlarged view of particle shown as “3” in Figure 5.75

The view of the particle shown as “1” in Figure 5.80 was magnified 6000 times and SEM-EDS analysis was applied for the particle. The enlarged view of the particle and also SEM-EDS results of four points on the particle are given in Figure 5.81.

When the SEM-EDS results presented in Figure 5.81 are examined, the main elements determined on the surface of the particle are O, C, K, and S. These are the common elements encountered in four points on the particle surface. According to the SEM-EDS results of four points, it might be stated that the particle has the same elemental composition on its surface. Fe element was also detected on the particle surface. Fe element might be in phase of Magnetite (Fe_3O_4), or Hematite (Fe_2O_3) in accordance with the result in Table 5.31. Fe element might be coming from the surface of the deposit sampling probe because it is strongly possible that when the ash accumulated on the probe surface was scratch out from the probe surface, ash might also remove the upper layer of the probe which is 304 type of stainless steel.

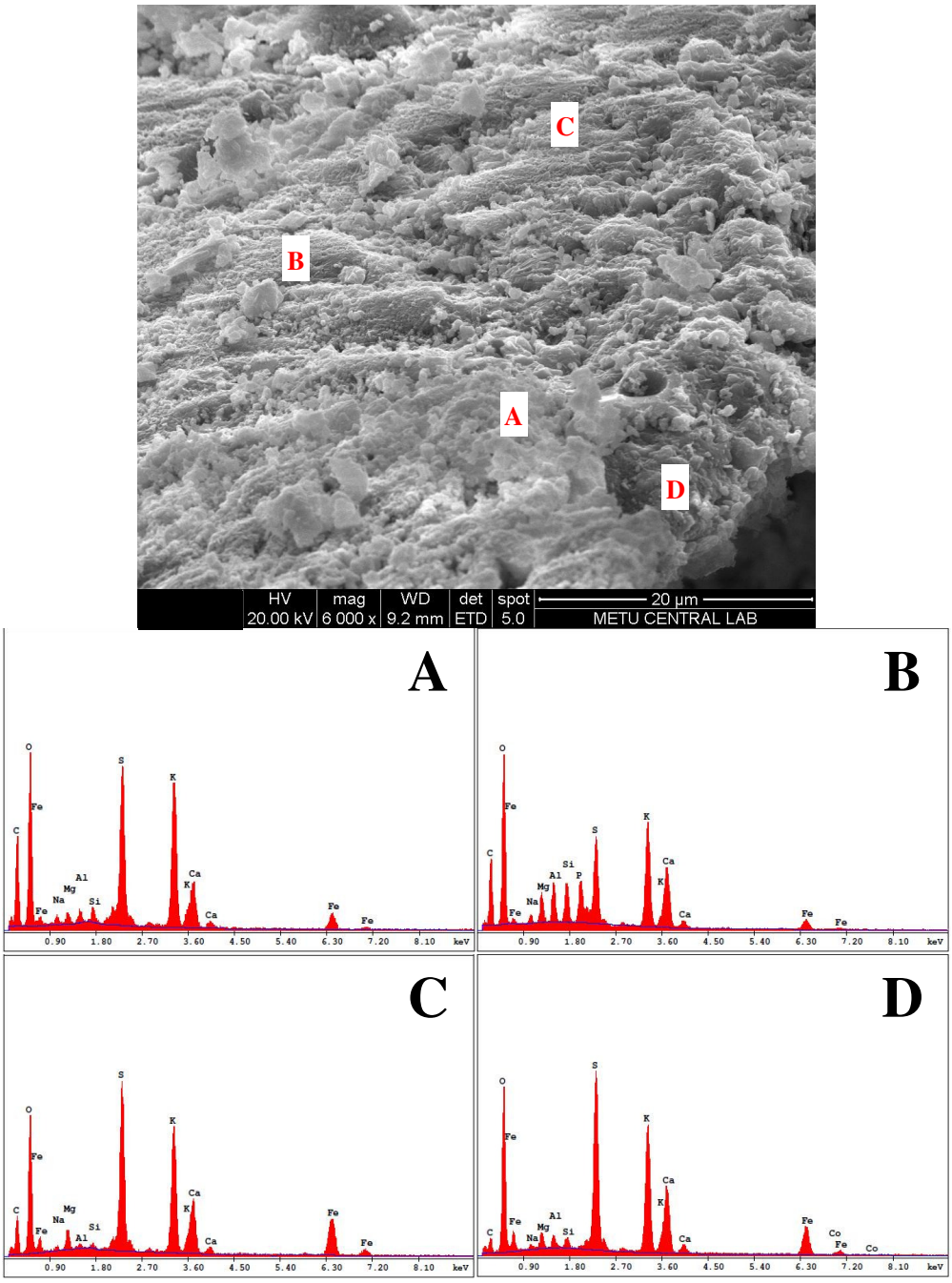

Figure 5.81 Enlarged view of the area shown as "1" in Figure 5.80 and SEM-EDS results of points A, B, C, and D

5.5.2. Co-Combustion of Bursa/Orhaneli Lignite and Olive Cake (50% by wt.) with Çan Limestone (Ca/S_{total} = 2.0) (C1-B1-7)

Bursa/Orhaneli lignite was used as the coal and olive cake was used as the biomass in this experiment. The weight percent of olive cake in the fuel mixture was 50. Çan limestone was added into the fuel mixture and Ca/S_{total} ratio was kept at 2. Some of the operational parameters are summarized in Table 5.32.

Table 5.32 Range of operational parameters for the co-combustion test (C1-B1-7)

Test #	Test Code	Fuel Feeding rate kg/h	λ -	P_{th}[a] kW	U_o[b] m/s
4-2	C1-B1-7	4.9-6.1	1.12-1.48	25-31	3.4-3.6

[a] P_{th}: Thermal power
[b] U_o: Superficial velocity in the combustor (calculated based on TT112 and flue gas flow rate)

The co-combustion test of fuel mixture containing Bursa/Orhaneli lignite and olive cake 50% by weight was performed at the dense phase temperature of 798±6°C. Unlike C1-B1-6 test, limestone was fed into the combustor with Bursa/Orhaneli lignite in this experiment. The XRF and XRD results of BA, FA-C, and FA-BF are given in Table 5.33 and Table 5.34, respectively.

Table 5.33 XRF results of fuel ashes and ashes formed at the end of the co-combustion test (C1-B1-7)

Compound	Bursa/Orhaneli	Olive Cake	BA	FA-C	FA-BF
	% by wt.				
Al_2O_3	6.80	3.04	1.73	6.51	6.05
CaO	16.83	20.38	35.48	29.99	31.95
Cl	0.00	2.19	0.02	0.28	0.88
Cr_2O_3	0.11	0.12	0.18	0.04	0.02
CuO	0.01	0.08	0.05	0.11	0.09
Fe_2O_3	10.11	5.16	3.43	10.56	9.60
K_2O	0.28	49.26	4.23	5.86	9.89
MgO	9.72	2.95	5.46	4.84	4.81
MnO_2	0.15	0.16	0.08	0.16	0.24
Na_2O	0.13	0.49	0.07	0.15	0.36
P_2O_5	0.16	3.57	0.30	1.53	1.33
SO_3	29.59	4.34	26.37	17.99	23.33
SiO_2	25.66	7.48	22.35	21.37	10.89
Normalized To (%)	99.9	100.0	100.0	100.0	100.0
Sum Before Normaliz. (%)	98.8	54.3	73.9	71.3	75.0

When Table 5.33 is investigated, it can be seen that Al_2O_3, CaO, Fe_2O_3, MgO, and SiO_2 are the major oxides in the coal ash. However, K_2O, CaO, and SiO_2 are the major oxides in the olive cake ash. Al_2O_3 content has decreased in the bottom ash to 2% while coal ash has 7% Al_2O_3 content. While both fuel ashes has 20% CaO, CaO content in the bottom ash has increased to 35%. This is mainly due to limestone addition. CaO, MgO, and SiO_2 are the major oxides in the bottom ash. In the ash samples collected from the cyclone and the bag filter, mostly CaO, Fe_2O_3, SiO_2 and partly K_2O are observed. As can be seen from the XRD results of fuel ashes in Table 5.34, Anhydrite phase was determined in the ash of Bursa/Orhaneli lignite. This may show that Ca and S elements seen in XRF result are probably in the form of $CaSO_4$. Si and Fe elements may be in the form of SiO_2 and Fe_2O_3, respectively. Since limestone was used in the experiment, Lime (CaO) phase was detected in both bottom and fly ashes. Compared to XRD analysis of ashes for C1-B1-6, amount of Lime is higher in these ashes which indicate that calcination of limestone occurred but lime could not fully react with sulfur in the combustor. K element which is the major element in the ash of olive cake is most likely in the phase of Potassium Calcium Sulfate ($K_2Ca_2(SO_4)_3$). A small amount of K element may be in Arcanite (K_2SO_4) phase. Arcanite phase was only determined in the fly ash collected from the bag filter. This may be explained by the lower temperature in the bag filter compared to the combustor and cyclone. K oxides may condense on cool surfaces of bag filter and may form Arcanite. 2.2% Cl element in XRF result may appear in Sylvite (KCl) phase in the structure of olive cake ash.

Table 5.34 XRD (Rietveld method) results of fuel ashes and ashes formed at the end of the co-combustion test (C1-B1-7)

Phase	Bursa/Orhaneli	Olive Cake	BA	FA-C	FA-BF
	% by wt.				
Quartz, SiO_2	24.1	2.7	24.5	47.6	8.1
Calcite, $CaCO_3$	2.2	9.9	3.3	9.1	6.2
Lime, CaO			18.4	7.9	12.1
Anhydrite, $CaSO_4$	61.3		18.7	10.6	17.3
Hematite, Fe_2O_3	12.4			12.4	21.2
Arcanite, K_2SO_4		9.3			12.1
Potassium Calcium Sulfate, $K_2Ca_2(SO_4)_3$			21.8	12.4	23
Fairchildite, $K_2Ca(CO_3)_2$		35.8			
Potassium Carbonate Hydrate, $K_2CO_3.1{,}5H_2O$		28			
Sylvite, KCl		4.4			
Forsterite, $Mg_2(SiO_4)$			13.4		

Quartz (SiO_2), Calcite ($CaCO_3$), Lime (CaO), Anhydrite ($CaSO_4$), Potassium Calcium Sulfate ($K_2Ca_2(SO_4)_3$) and Forsterite $Mg_2(SiO_4)$ phases were determined in the bottom ash. Calcite in the limestone reacts with sulfur in coal and forms Anhydrite and Potassium Calcium Sulfate phases. Another phase determined in bottom ash is Lime. There was no SO_2 emission during the experiment because of limestone usage. CaO forms at the end of calcination of $CaCO_3$ in limestone make a reaction with SO_2 gas molecules and forms $CaSO_4$ as a solid product. Since no SO_2 emission occurred, Lime phase observed in the bottom ash is CaO which did not react with SO_2 and left in the ash. This may be an indication that limestone was fed into the combustor more than the required.

The Quartz (sand) which is used as a bed material is the dominant phase in the fly ash of the second cyclone. In addition to Quartz, Potassium Calcium Sulfate, Hematite, Anhydrite, Calcite and Lime are the phases observed in the fly ash of the second cyclone. Determination of Quartz phase in the fly ash of the 2nd cyclone is an indication that a small amount of sand escapes from the system. The Quartz phase is also determined in the fly ash captured in the bag filter. However, the amount of it is less than the amount collected in the second cyclone. According to the XRD analysis conducted in MAM-ME, the phases containing K element are encountered in the fly ash sample from the bag filter. These phases are Arcanite and Potassium Calcium Sulfate. Encountering of potassium salts in the bag filter might be an indication that the potassium element which is in the structure of olive cake leaves the system on the gas phase, and then, it turns into potassium salts in the bag filter since the gas temperature decreases below 200^{o}C in the bag filter.

When XRD analysis of deposit accumulated on the surface of deposit sampling probe in Table 5.35 is examined, it can be seen that the main phase determined is Potassium Calcium Sulfate ($K_2Ca_2(SO_4)_3$). Since the surface of the deposit sampling probe was internally cooled down to 550^oC, it was likely that the Potassium element in the fuel mixture condensed on the surface of the probe and transformed into the phase of Potassium Calcium Sulfate. Furthermore, Magnetite and Quartz were the other two dominant phases in the deposit.

Table 5.35 XRD (RIR method) results of deposit collected from deposit sampling probe at the end of the co-combustion test (Analyses were done at METU-Central Laboratory) (C1-B1-7)

Phase	**Ash Deposit on the Sampling Probe % by wt.**
Quartz, SiO_2	18
Lime, CaO	4.7
Anhydrite, $CaSO_4$	2
Potassium Calcium Sulfate, $K_2Ca_2(SO_4)_3$	62
Magnetite, Fe_3O_4	13

5.5.2.1. SEM-EDS Analysis of Bottom Ash (C1-B1-7)

A general view of the sample taken from bottom ash is given in Figure 5.82.

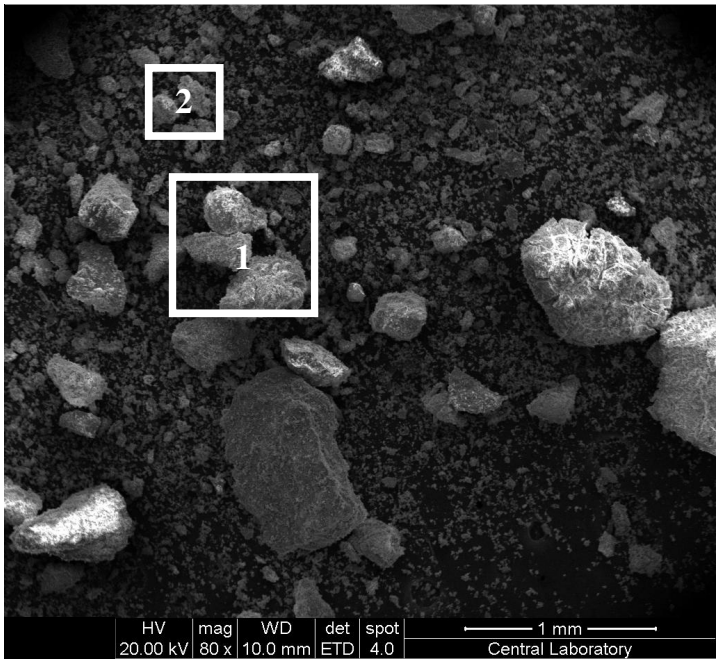

Figure 5.82 General view of sample taken from bottom ash (C1-B1-7)

Two locations were selected in Figure 5.82. The first one represents bigger particles with a size of around 300 µm. The second one represents smaller particles. In the first part, the particle shown as "1" in Figure 5.82 was focused. The view was magnified 400 times and the enlarged view of the region is given in Figure 5.83.

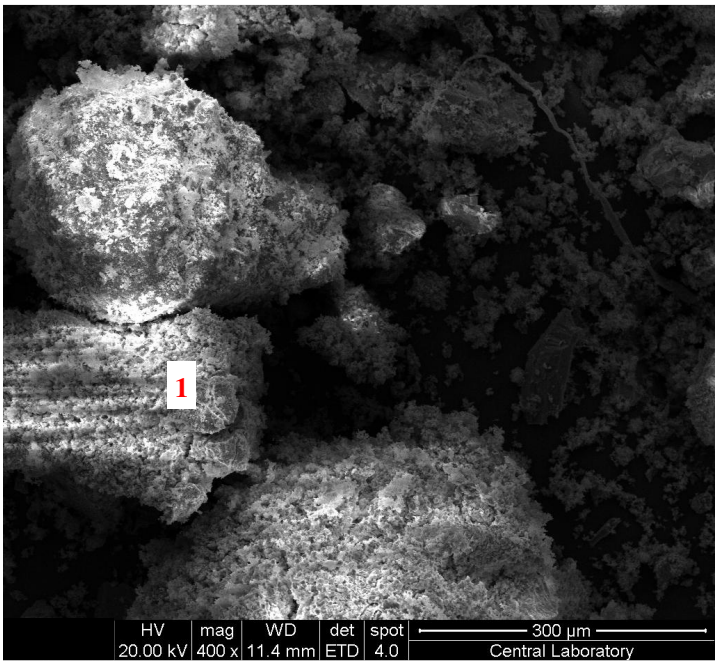

Figure 5.83 Enlarged view of the region shown as "1" in Figure 5.82

The enlarged view of the particle shown as "1" in Figure 5.83 and also SEM-EDS results of two spot points "A" and "B" was given in Figure 5.84. The particle in Figure 5.83 was about 300 µm in length and 150 µm in width.

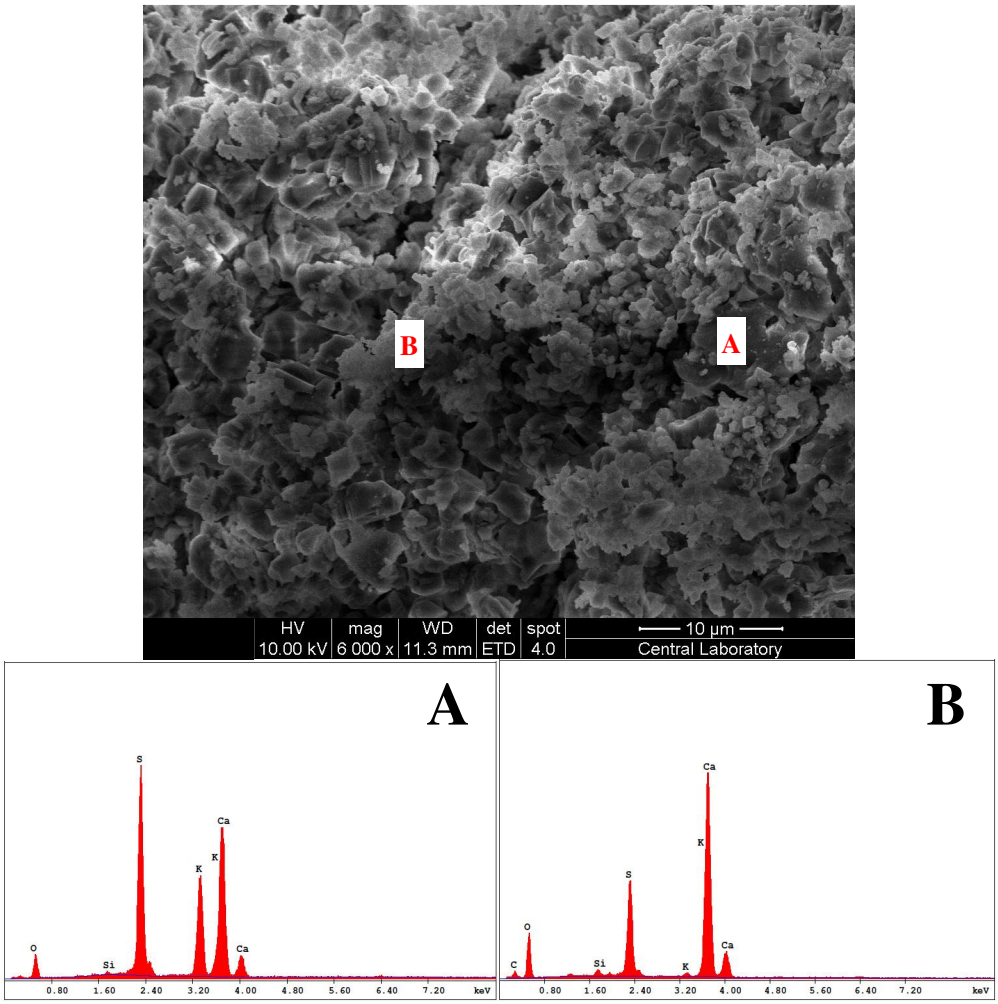

Figure 5.84 SEM micrograph and SEM-EDS results of points A and B on the particle shown as "1" in Figure 5.83

The main elements determined in points "A" and "B" are Ca, K, and S. When XRD result of bottom ash in Table 5.34 was investigated, it can be stated that the particle was probably composed of Anhydrite ($CaSO_4$) and Potassium Calcium Sulfate ($K_2Ca_2(SO_4)_3$) phases.

The enlarged view of the region shown as “2” in Figure 5.82 is given in Figure 5.85.

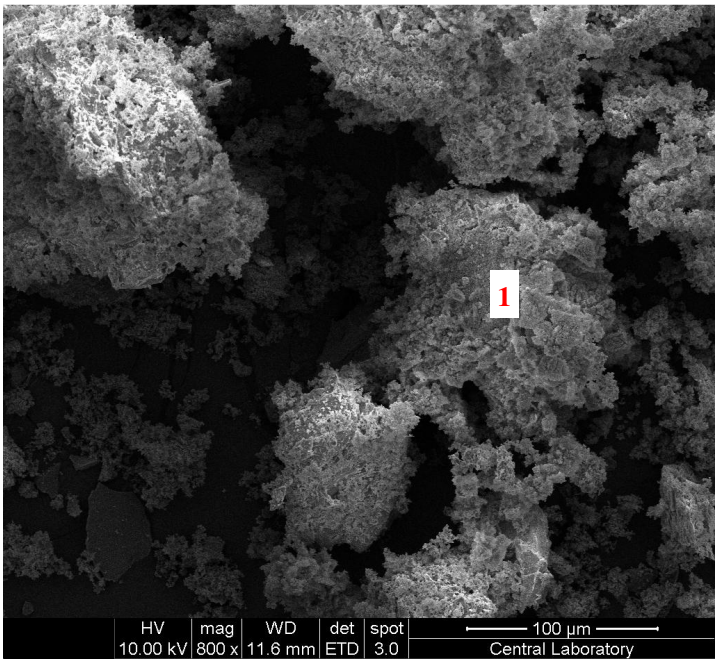

Figure 5.85 Enlarged view of the region shown as “2” in Figure 5.82

The enlarged view of the particle shown as “1” in Figure 5.85 and also SEM-EDS results of two spot points “A” and “B” is given in Figure 5.86. The main elements are Ca, K, and S for points “A” and “B”. This particle might also be composed of Anhydrite ($CaSO_4$) and Potassium Calcium Sulfate ($K_2Ca_2(SO_4)_3$) phases like the particle in Figure 5.83.

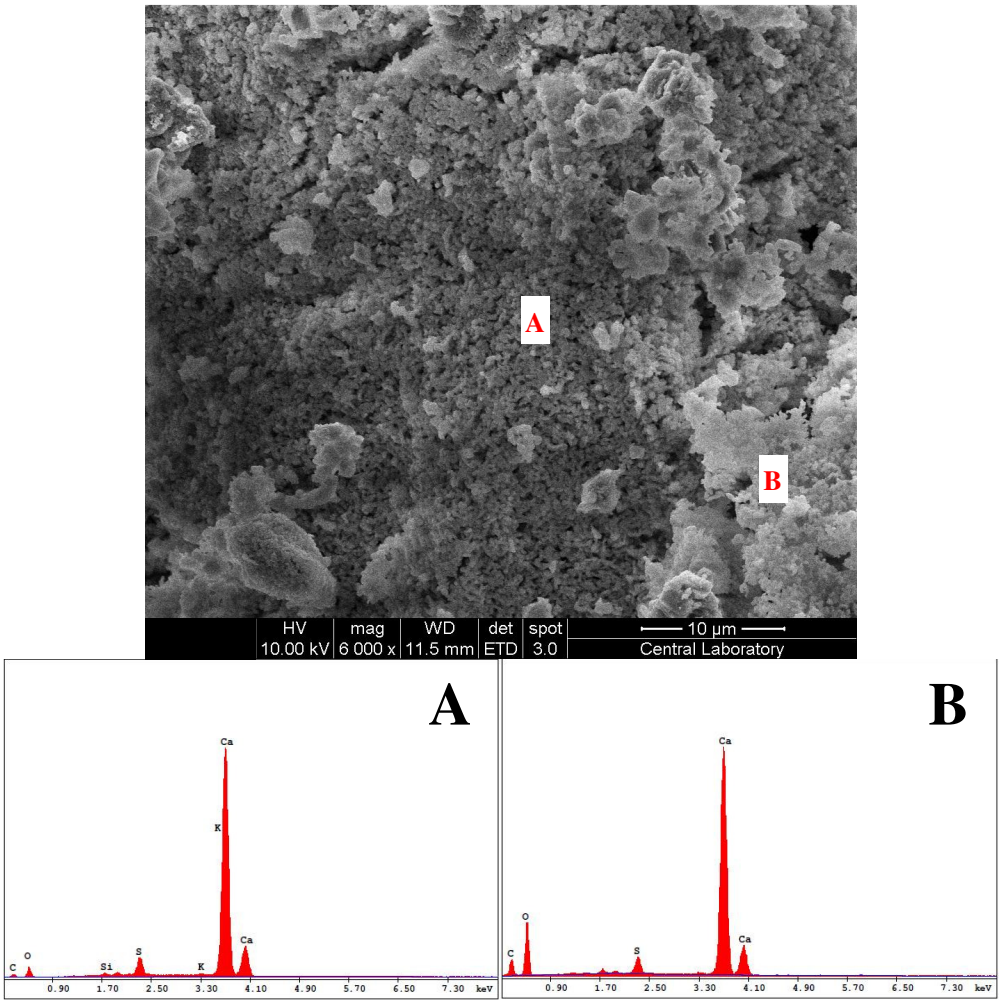

Figure 5.86 SEM micrograph and SEM-EDS results of points A and B on the particle shown as "1" in Figure 5.85

5.5.2.2. SEM-EDS Analysis of Deposit on the Deposit Sampling Probe (C1-B1-7)

The deposit sampling probe was used during the combustion test. At the end of 42 hour and 57 minute-test, the deposit sampling probe was carefully removed from the combustor. The images of the deposit sampling probe taken from four different sides are given in Figure 5.87. The images from four different directions in Figure 5.87 were taken as described in Section 5.5.1.2.

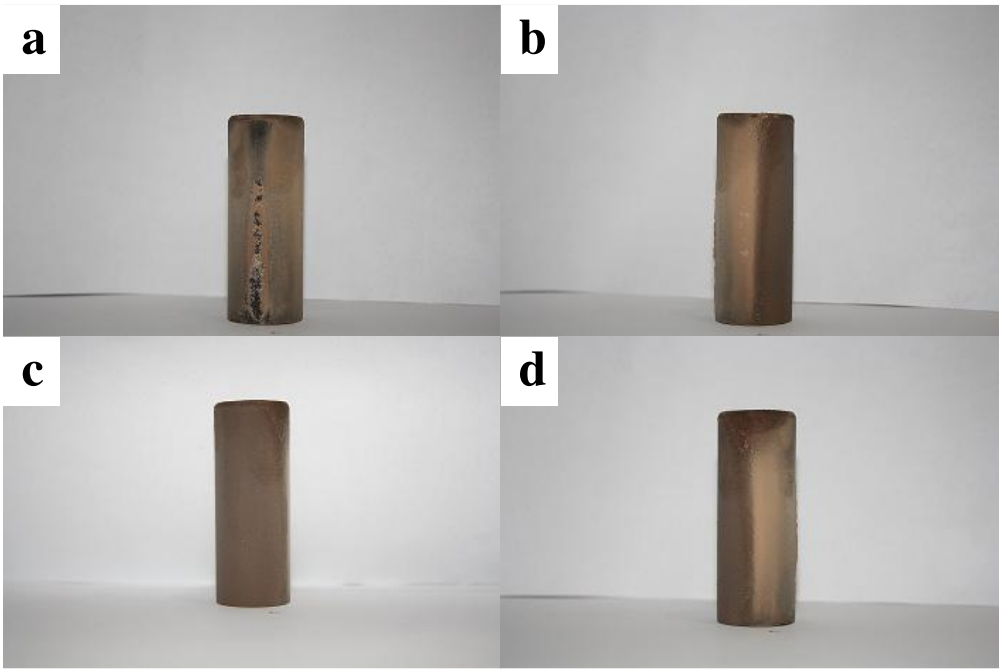

Figure 5.87 Image of the deposit sampling probe a) top b) right-side c) bottom d) left-side (C1-B1-7)

The total amount of the deposit accumulated on the probe surface was 1.74 g. The outside diameter of the probe was 26.7 mm and the length of the probe was 60 mm. The projected surface area where deposit can accumulate was 16.02 cm^2 (OD=26.7 mm; L=60 mm). Total duration for fuel feeding was 40.5 hours. Thus, the deposition rate was calculated as 27 g/m^2-h which is above the index value (20 g/m^2-h in Section 5.5.1.2).

A general view of the sample taken from deposit sampling probe is given in Figure 5.88.

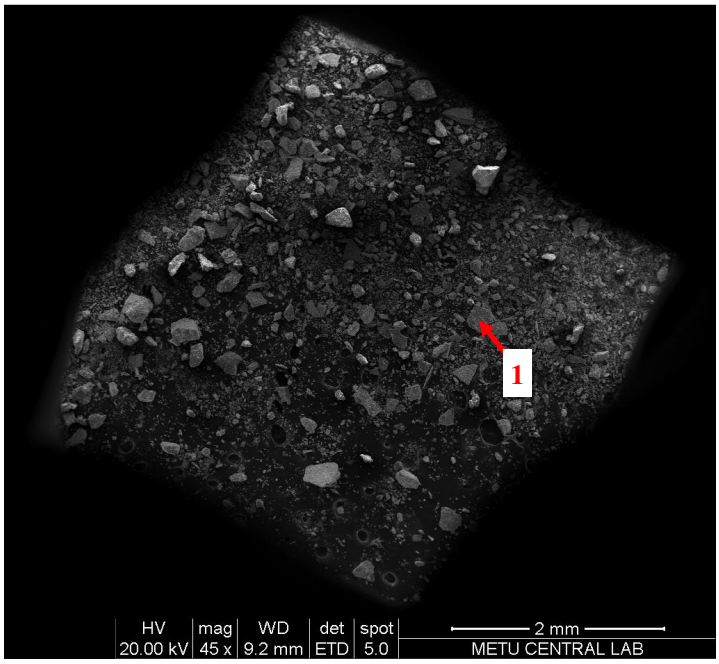

Figure 5.88 General view of sample taken from deposit sampling probe (C1-B1-7)

In Figure 5.88, the region shown as “1” was focused. The view was magnified 400 times and enlarged view of the region is given in Figure 5.89.

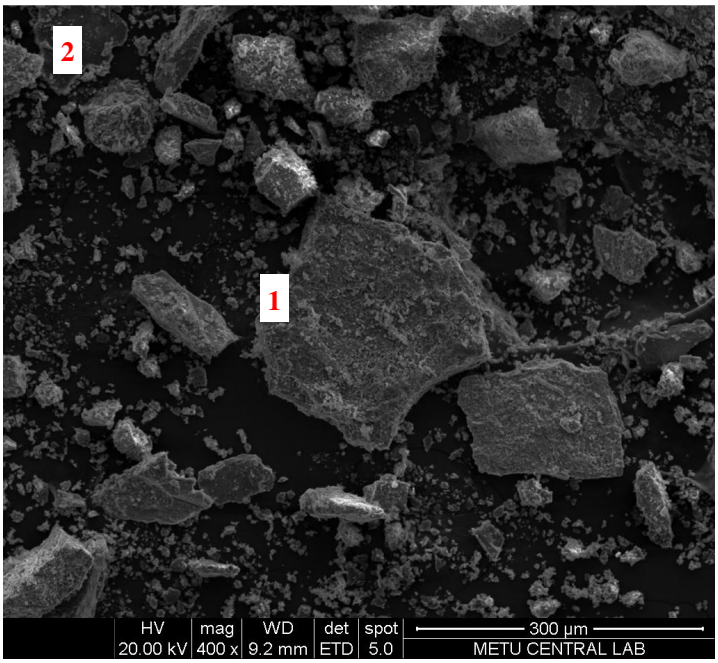

Figure 5.89 Enlarged view of region shown as “1” in Figure 5.88

Two different particles in Figure 5.89 were selected to be investigated. The location “1” on the particle was examined and SEM-EDS analysis was applied for this part of the particle. SEM micrograph of the location shown as “1” in Figure 5.89 and SEM-EDS results of points “A”, “B”, and “C” on the particle are given in Figure 5.90. When SEM-EDS results of three points are examined in Figure 5.90, it is clearly seen that Ca, K, and S are the main elements on the particle excluding C and O elements. These elements might be in the phase of Potassium Calcium Sulfate. These results are consistent with the XRD result of deposit of the deposit sampling probe in Table 5.35. Fe element detected in the particle might be in the phase of Magnetite.

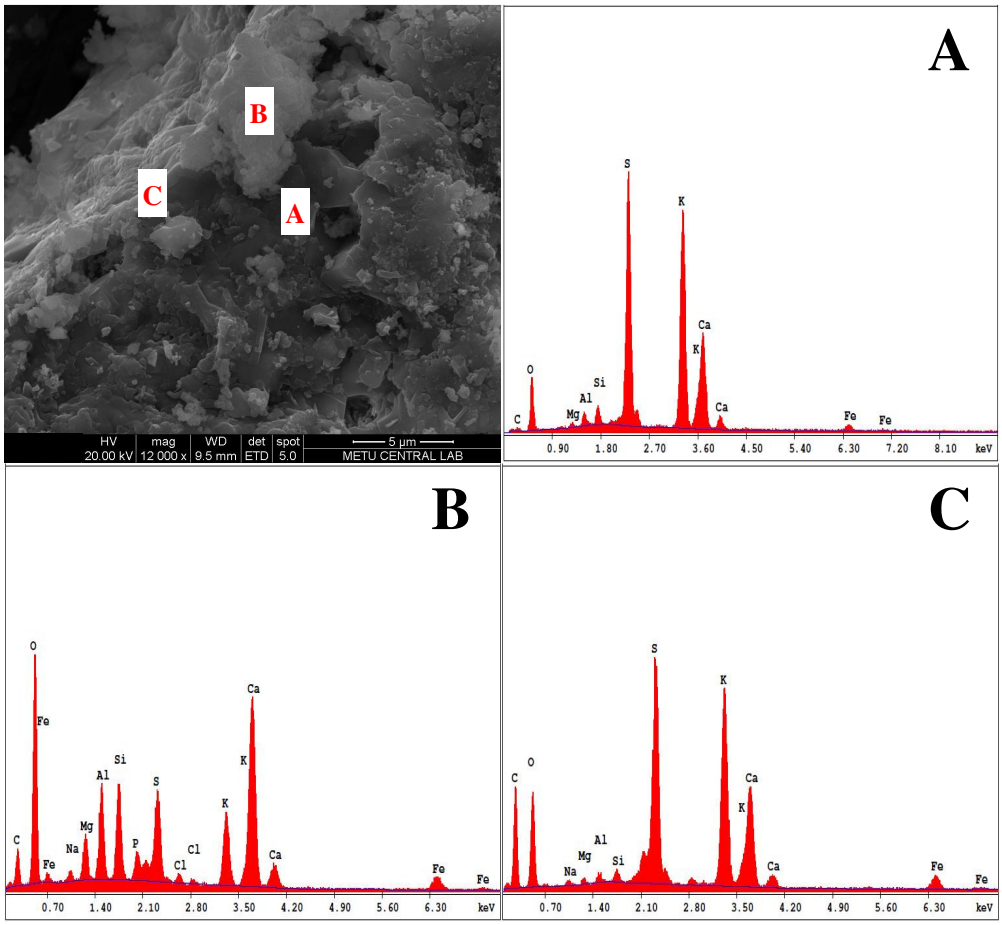

Figure 5.90 SEM micrograph and SEM-EDS results of points A, B and C on the particle shown as "1" in Figure 5.89

The particle shown as “2” in Figure 5.89 was focused. The view was magnified 1500 times. Enlarged view of the particle is given in Figure 5.91.

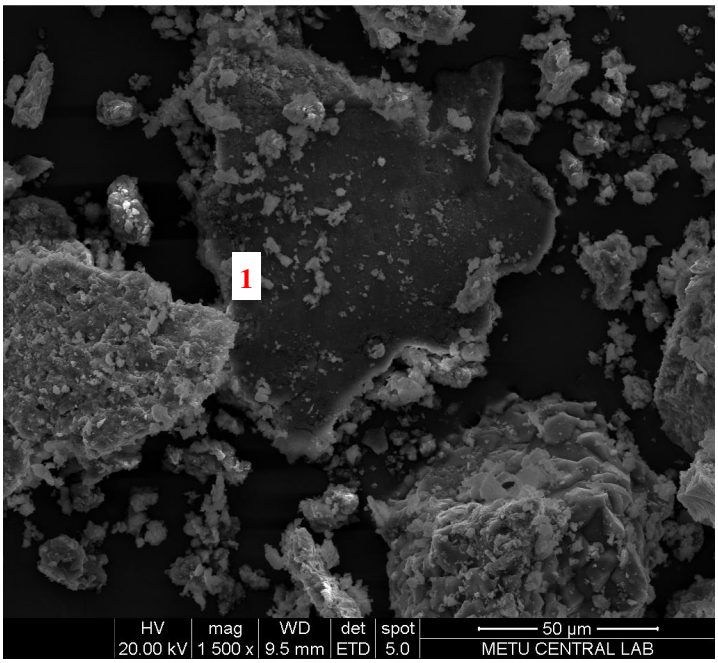

Figure 5.91 Enlarged view of region shown as “2” in Figure 5.89

The location “1” on the particle in Figure 5.91 was examined and SEM-EDS analysis was applied for this part of the particle. SEM micrograph of the location shown as “1” in Figure 5.91 and SEM-EDS results of points “A”, “B”, “C”, and “D” on the particle are given in Figure 5.92. When SEM-EDS results of four points are examined in Figure 5.92, the results are more or less same with the SEM-EDS results presented in Figure 5.90. The particle is mainly composed of C, O, Ca, K, and S elements. These elements might be in the phase of Potassium Calcium Sulfate. These results are consistent with the XRD result of deposit of the deposit sampling probe in Table 5.35. Fe element detected in the particle might be in the phase of Magnetite.

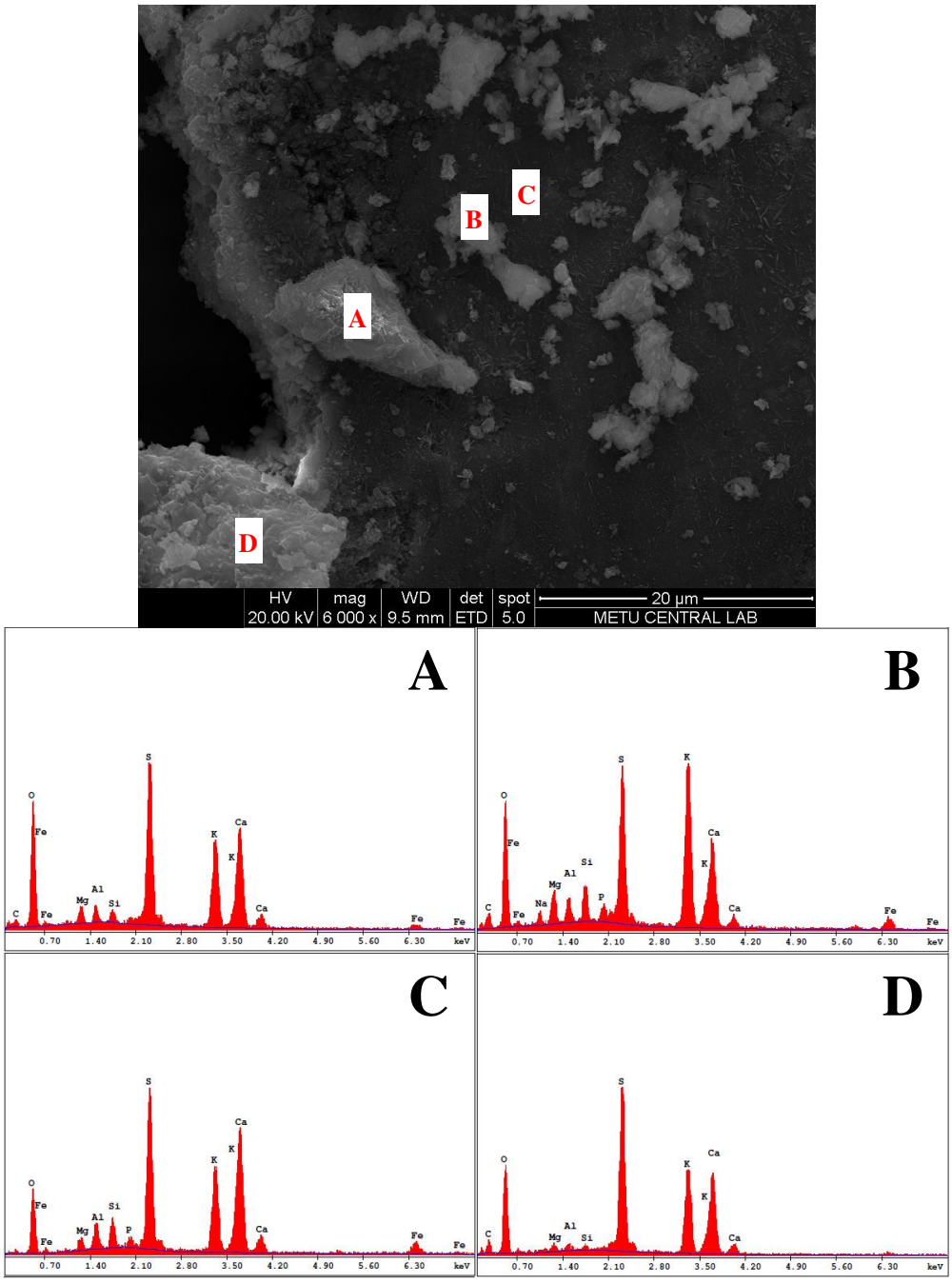

Figure 5.92 SEM micrograph and SEM-EDS results of four points (A, B, C and D) on the particle shown as "1" in Figure 5.91

5.5.3. Co-Combustion of Denizli/Kale Lignite and Olive Cake (50% by wt.) (C2-B1-1)

In this experiment, Denizli/Kale lignite was used instead of Bursa/Orhaneli in order to see the effect of sulfur content of the coal on ash composition. Olive cake was the biomass used in the experiment. The weight percent of olive cake in the fuel mixture was 50. Some of the operational parameters are given in Table 5.36.

Table 5.36 Range of operational parameters for the co-combustion test (C2-B1-1)

Test #	Test Code	Fuel Feeding rate kg/h	λ -	P_{th}[a] kW	U_o[b] m/s
4-3	C2-B1-1	6.4-6.9	1.11-1.35	29-31	3.4-3.6

[a] P_{th}: Thermal power
[b] U_o: Superficial velocity in the combustor (calculated based on TT112 and flue gas flow rate)

The co-combustion test of fuel mixture containing Denizli/Kale lignite and olive cake 50% by weight was performed at dense phase temperature of 804±23°C. XRF and XRD analyses of BA, FA-C, and FA-BF are presented in Table 5.37 and Table 5.38, respectively.

Table 5.37 XRF results of fuel ashes and ashes formed at the end of the co-combustion test (C2-B1-1)

Compound	Denizli/Kale	Olive Cake	BA	FA-C	FA-BF
	% by wt.				
Al_2O_3	16.12	3.06	14.86	16.36	14.92
CaO	10.75	18.65	13.18	10.59	13.00
Cl		2.30		0.07	0.09
Cr_2O_3	0.08	0.03	0.07	0.07	0.08
CuO	0.01	0.07	0.04	0.05	0.07
Fe_2O_3	13.01	5.09	6.91	12.59	14.09
K_2O	1.90	52.10	5.05	4.86	5.39
MgO	8.06	2.93	4.94	7.77	8.78
MnO_2	0.08	0.13	0.07	0.08	0.10
Na_2O	0.42	0.46	0.36	0.51	0.51
P_2O_5	0.19	3.18	0.18	0.55	0.57
SO_3	19.06	3.93	19.81	11.56	15.30
SiO_2	29.34	7.35	33.66	33.98	26.12
Normalized To (%)	100.0	100.0	100.0	100.0	100.0
Sum Before Normaliz. (%)	77.2	50.3	75.3	73.9	75.9

When Table 5.37 is investigated, it can be seen that SiO_2, Al_2O_3, CaO, Fe_2O_3, and MgO are the major oxides in the Denizli/Kale ash. However, K_2O, CaO, and SiO_2 are the major oxides in the olive cake ash. SiO_2 is the major oxide present in all ash samples. It is followed by SO_3 and Al_2O_3. High level of SO_3 and Al_2O_3 is an indication of ash content of Denizli/Kale lignite is more dominant than olive cake ash. This is because of the higher ash content of Denizli/Kale lignite (17.19% in Table 5.16) compared to olive cake (9.69% in Table 5.16). Although about half of the olive cake ash was K_2O, K_2O in ashes did not exceed 6%. Ca and S elements seen in XRF result are probably in the form of Anhydrite ($CaSO_4$). Anhydrite was determined in all ashes and in Denizli/Kale ash as can be seen in Table 5.38. The phase composition of Denizli/Kale ash could not be quantified according to the Rietveld method but it was certain that the phases determined in XRD analysis were present in the Denizli/Kale ash. It should be always kept in mind that the numeric values presented with XRD results are semi-quantitative. Therefore, the results giving the presence of a phase in an ash sample is more valid than the percentage of the phase in the ash. Cl coming from olive cake could not be detected in the bottom and fly ashes. Si element seen in XRF results was in the form of Quartz (SiO_2) and Muscovite ($KAl_2(Si,Al)_4O_{10}(OH)_2$). While K element was in the form of Arcanite, Fairchildite, Sylvite, Kalicinite, and Muscovite in the ash of olive cake, it seems most of the K was transformed into Muscovite. It was only seen as Potassium Calcium Sulfate in bag filter ash.

Table 5.38 XRD (Rietveld method) results of fuel ashes and ashes formed at the end of the co-combustion test (C2-B1-1)

Phase	Denizli/Kale	Olive Cake	BA	FA-C	FA-BF
		% by wt.			
Quartz, SiO_2	√	15.6	19.2	32.2	24
Calcite, $CaCO_3$	√	17.7			
Anhydrite, $CaSO_4$	√		26.6	12.8	17.6
Hematite, Fe_2O_3	√			1.8	2.9
Arcanite, K_2SO_4		12.1			
Potassium Calcium Sulfate, $K_2Ca_2(SO_4)_3$					3.1
Fairchildite, $K_2Ca(CO_3)_2$		27.8			
Calcium Magnesium Sulfate, $CaMg_3(SO_4)_4$	√				
Sylvite, KCl		1.8			
Kalicinite, $KAl(SO_4)_2 \cdot 11H_2O$		15.6			
Muscovite, $KAl_2(Si,Al)_4O_{10}(OH)_2$	√	9.4	43.5	46.6	50.1
Magnesioferrite, $MgFe_2O_4$			10.7	6.8	2.3

XRD analysis of deposit accumulated on the surface of deposit sampling probe is given in Table 5.39. The main phase in the deposit is Potassium Calcium Sulfate ($K_2Ca_2(SO_4)_3$). Since the surface of the deposit sampling probe is cooled to 550°C, it is likely that the Potassium element in the fuel mixture condenses on the surface of the probe and transforms into the phase of Potassium Calcium Sulfate. Potassium Calcium Sulfate was followed by Quartz. Fe element in fuel ashes was seen as Magnetite, Hematite, and Magnesioferrite on the probe surface.

Table 5.39 XRD (RIR method) results of deposit collected from deposit sampling probe at the end of the co-combustion test (Analyses were done at METU-Central Laboratory) (C2-B1-1)

Phase	Ash Deposit on the Sampling Probe % by wt.
Quartz, SiO_2	27
Potassium Calcium Sulfate, $K_2Ca_2(SO_4)_3$	31
Hematite, Fe_2O_3	15
Magnetite, Fe_3O_4	19
Magnesioferrite, $MgFe_2O_4$	7

5.5.3.1. SEM-EDS Analysis of Bottom Ash (C2-B1-1)

A general view of the sample taken from bottom ash is given in Figure 5.93.

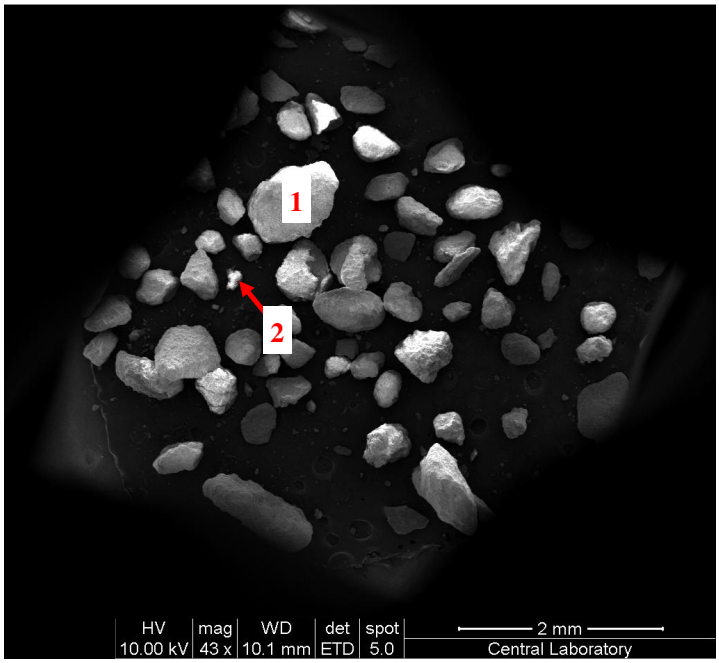

Figure 5.93 General view of sample taken from bottom ash (C2-B1-1)

Two particles in Figure 5.93 were selected and examined by SEM-EDS analysis. The particle shown as "1" in Figure 5.93 was magnified by 250 times and the enlarged view of the particle is given in Figure 5.94.

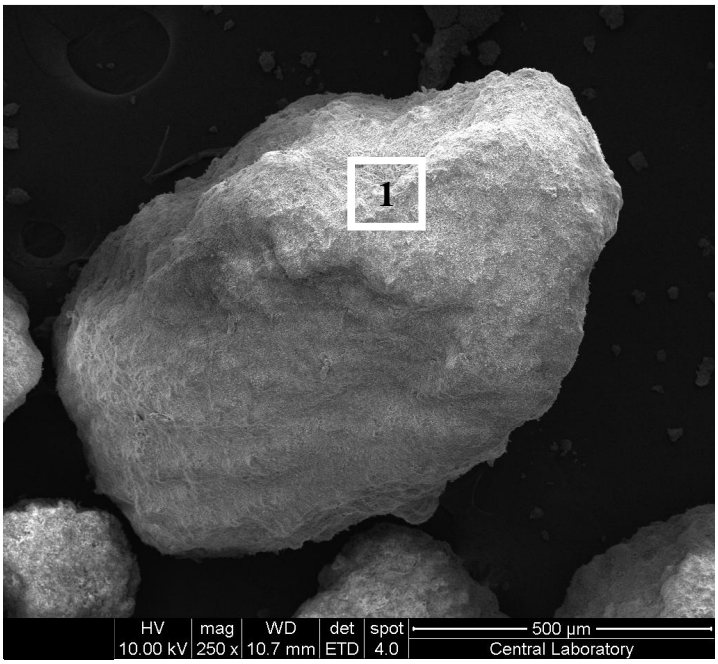

Figure 5.94 Enlarged view of the particle shown as "1" in Figure 5.93

The region of the particle shown as "1" in Figure 5.94 was magnified by 3000 times and the SEM micrograph of it is given in Figure 5.95. Three points, A, B, and C were selected on the particle surface and they were subjected to the SEM-EDS analysis. From the SEM-EDS analysis of these three points in Figure 5.95, Ca, S, Si, K, Al, Fe, and Mg elements were detected in each point. When the XRD results of the bottom ash in Table 5.38 is examined, it may be possible that Ca and S elements are in the form of Anhydrite; Si is in the form of Quartz; and K, are Al in the form of Muscovite. Mg and Fe elements may present in Magnesioferrite.

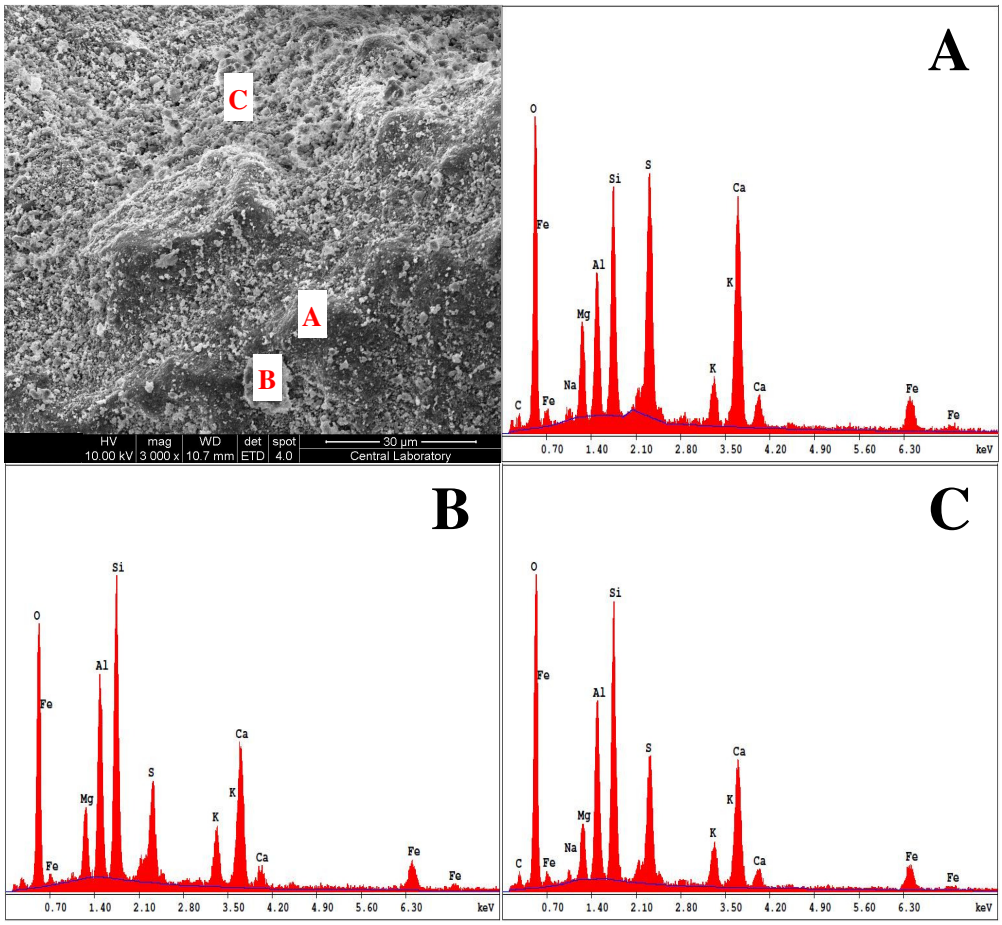

Figure 5.95 SEM micrograph and SEM-EDS results of points A, B and C on the particle shown as "1" in Figure 5.94

The particle shown as "2" in Figure 5.93 was magnified by 1600 times and the SEM micrograph of it is given in Figure 5.96 below. Two points, A and B, on the particle surface were selected and they were subjected to the SEM-EDS analysis. The SEM-EDS results of the two points indicate that the particle was mainly formed by Ca, S and O elements. These elements are in the form of Anhydrite.

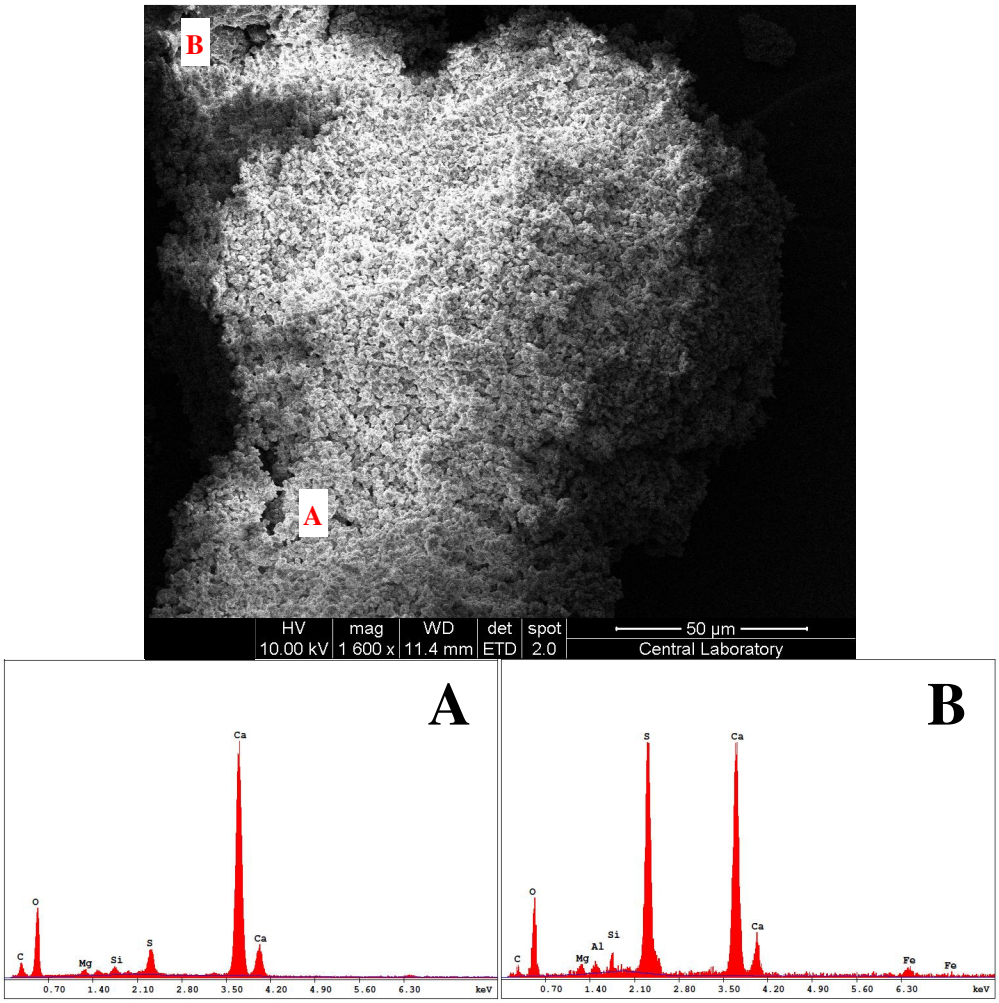

Figure 5.96 Enlarged view of the particle shown as "2" in Figure 5.93 and SEM-EDS results of points A and B

5.5.3.2. SEM-EDS Analysis of Deposit on the Deposit Sampling Probe (C2-B1-1)

After 63 hour and 3 minute-operation, the deposit sampling probe was carefully removed from the combustor. The images of the deposit sampling probe taken from four different sides as described in Section 5.5.1.2 are given in Figure 5.97.

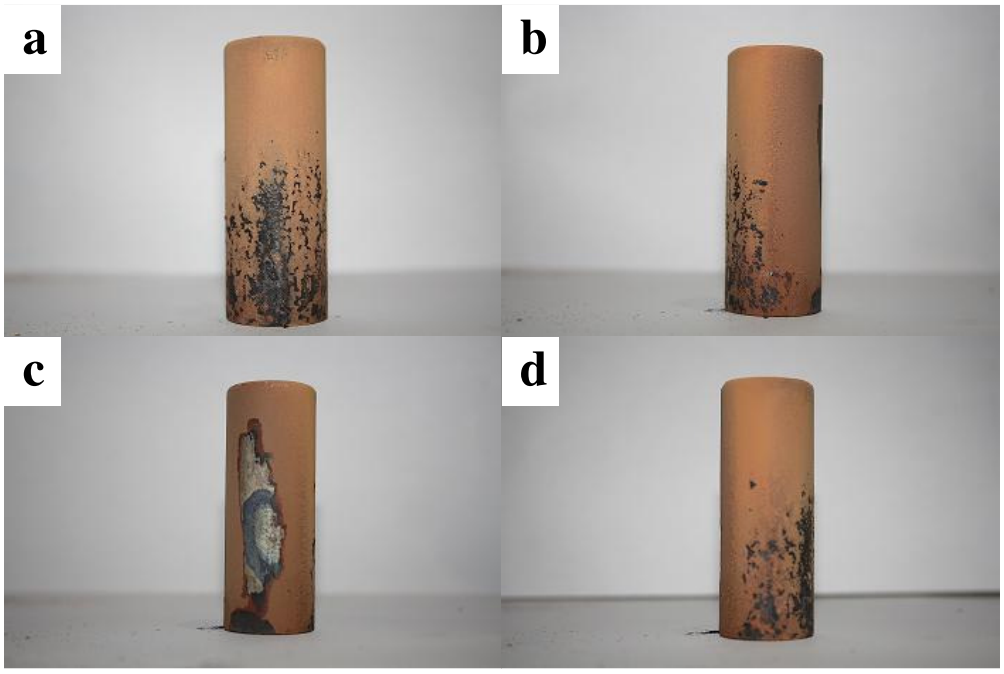

Figure 5.97 Image of the deposit sampling probe a) top b) right-side c) bottom d) left-side (C2-B1-1)

The deposit accumulated on the surface of the probe was collected at the end of the combustion test. The total amount of the deposit accumulated on the probe surface was 1.91 g. The projected surface area where deposit can accumulate was 16.02 cm^2 (OD=26.7 mm; L=60 mm). Total duration for fuel feeding was 49.8 hours. Thus, the deposition rate was calculated as 24 g/m^2-h which is above the index value (20 g/m^2-h in Section 5.5.1.2).

A general view of the sample taken from the deposit sampling probe is given in Figure 5.98. Three different hot points were determined for SEM-EDS analysis. These are shown in Figure 5.98 below.

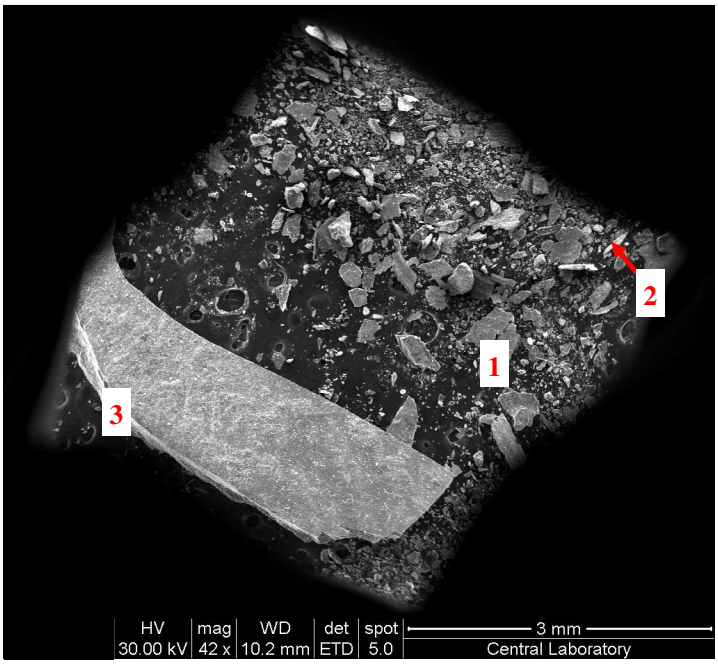

Figure 5.98 General view of sample taken from deposit sampling probe (C2-B1-1)

The particle shown as "1" in Figure 5.98 was magnified by 700 times and the SEM micrograph of it is given in Figure 5.99.

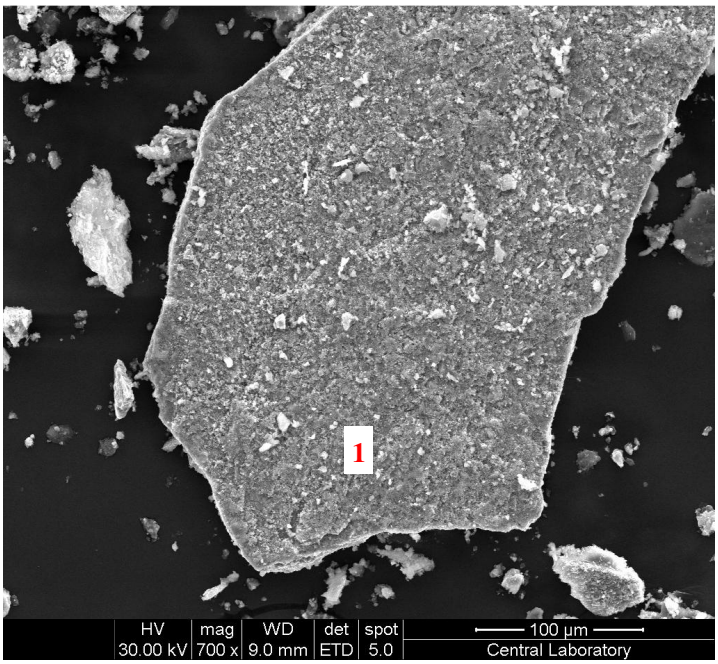

Figure 5.99 Enlarged view of region shown as "1" in Figure 5.98

The point “1” on the particle in Figure 5.99 was then magnified by 6000 times. Its SEM micrograph and SEM-EDS spectrum of two points, A and B, are given in Figure 5.100. When the EDS spectrum of these two points is examined, it can be seen that the point “B” which represents the particle, is composed of Iron (Fe), Chromium (Cr), and Nickel (Ni) elements. It is obvious that this particle was a small part of the probe which was removed with the deposit while the deposit was scraped off the surface of the probe. Several other elements were detected on the point “A”. These elements were O, S, K, Ca, Mg, Fe, and Si according to their atomic weights in the EDS spectrum. In line with the XRD results of deposit in Table 5.39, S, K, and Ca elements were in the phase of Potassium Calcium Sulfate. Mg was in Magnesioferrite. Fe was in Hematite and Magnetite. Si was in Quartz. It seems from the figure that there are many small particles, like the one point “A” indicates. They are stacked on the raptured part of the probe.

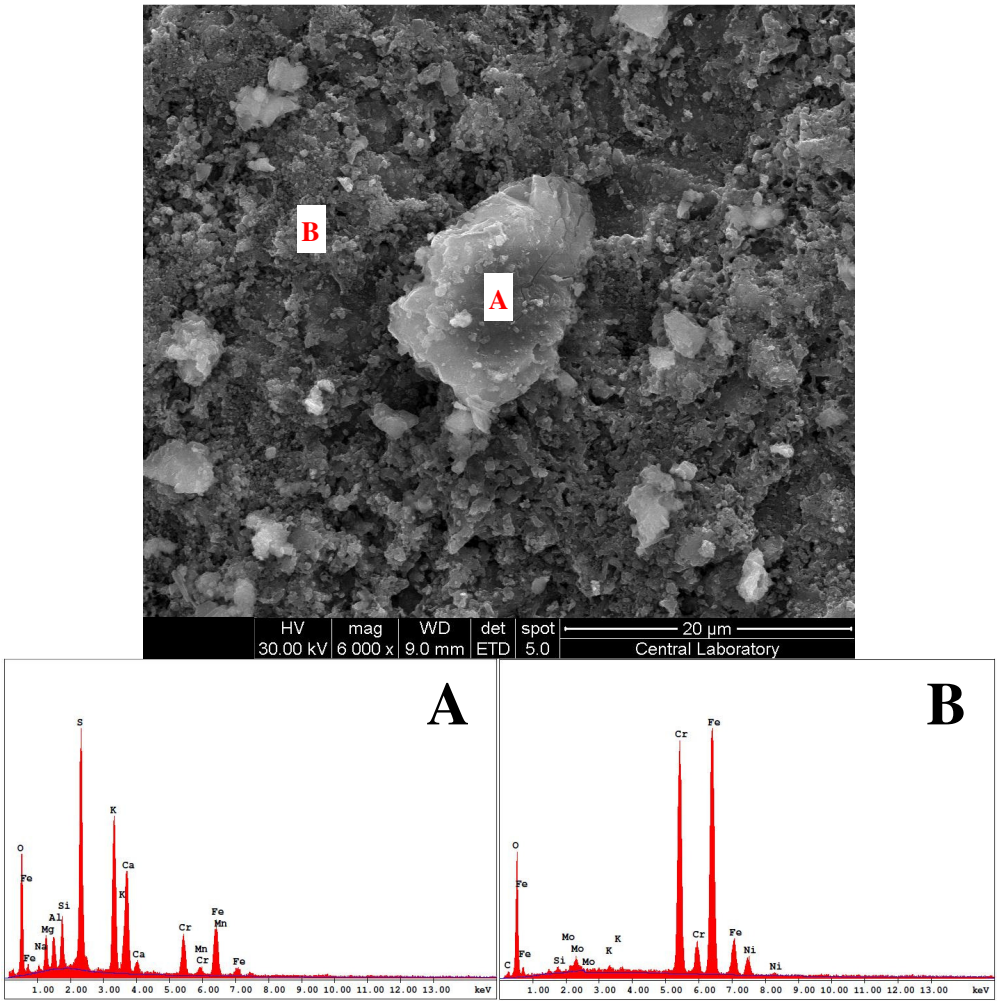

Figure 5.100 SEM micrograph and SEM-EDS results of points A and B on the particle shown as “1” in Figure 5.99

The particle shown as “2” in Figure 5.98 was magnified by 12000 times and its SEM micrograph and SEM-EDS spectrums of three points, A, B and C on the particle are given in Figure 5.101. Because of its high concentration of Fe and Cr, it seems that the particle is another part removed from the metallic surface of the probe.

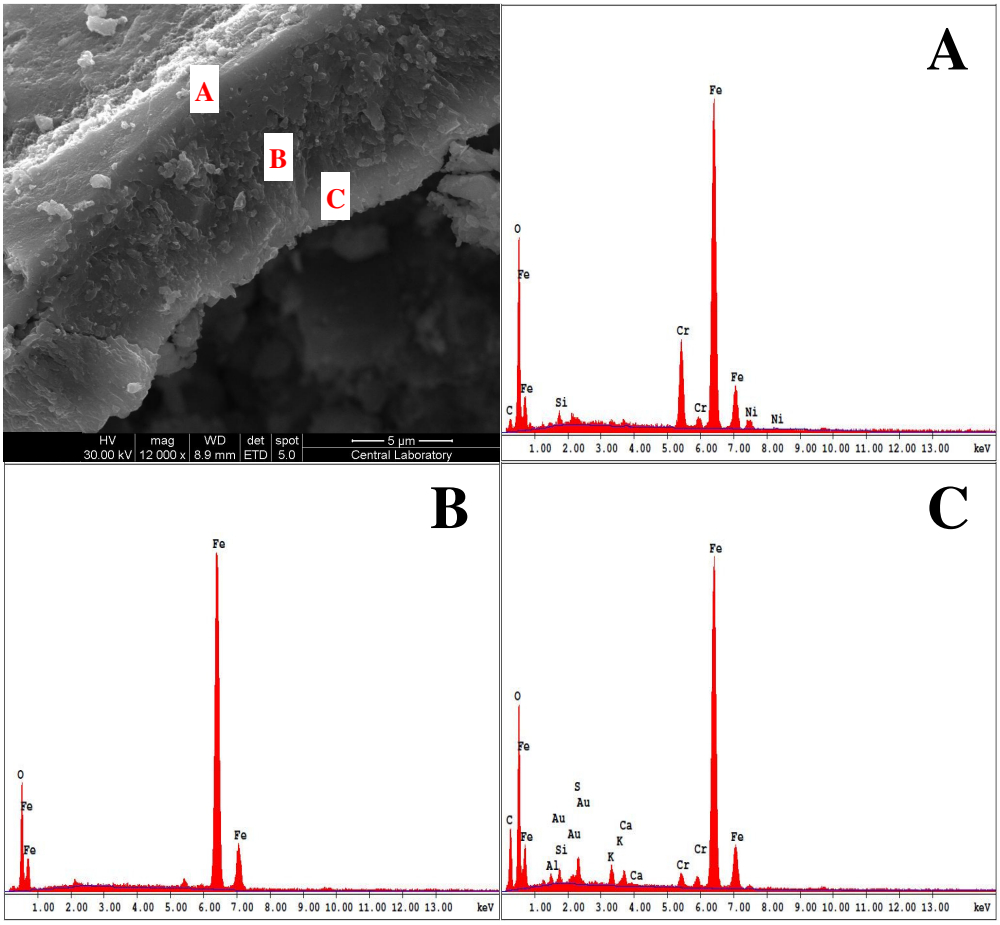

Figure 5.101 Enlarged view of the region shown as “2” in Figure 5.98 and SEM-EDS results of points A, B and C

The particle shown as “3” in Figure 5.98 was magnified by 1600 times and six points on the lateral surface of it was selected. The SEM micrograph of the particle and SEM-EDS spectrum of the six points, A, B, C, D, E and F on the lateral surface of the particle are given in Figure 5.102. Cr, Fe and Ni are the main elements of stainless steel tubing. These three elements seen for the points “A” and “C” is an indication that this layer was from the surface of the probe. In this case, point “A” and “C” represents the layer of the probe surface and the other points along the lateral surface of the particle in the image represent the deposition on the thin layer of the probe surface. When the SEM-EDS spectrums for the other four points, “B”, “D”, “E”, and “F”, are examined, they all contain K, Ca, S, Si,

Fe, Mg and O as well. K, Ca and S seen in SEM-EDS spectrum are most probably in the Potassium Calcium Sulfate phase. Si is present in Quartz; Fe and Mg are presents in Hematite, Magnetite, and Magnesioferrite phases. These findings are also consistent with the XRD results of the deposit in Table 5.39.

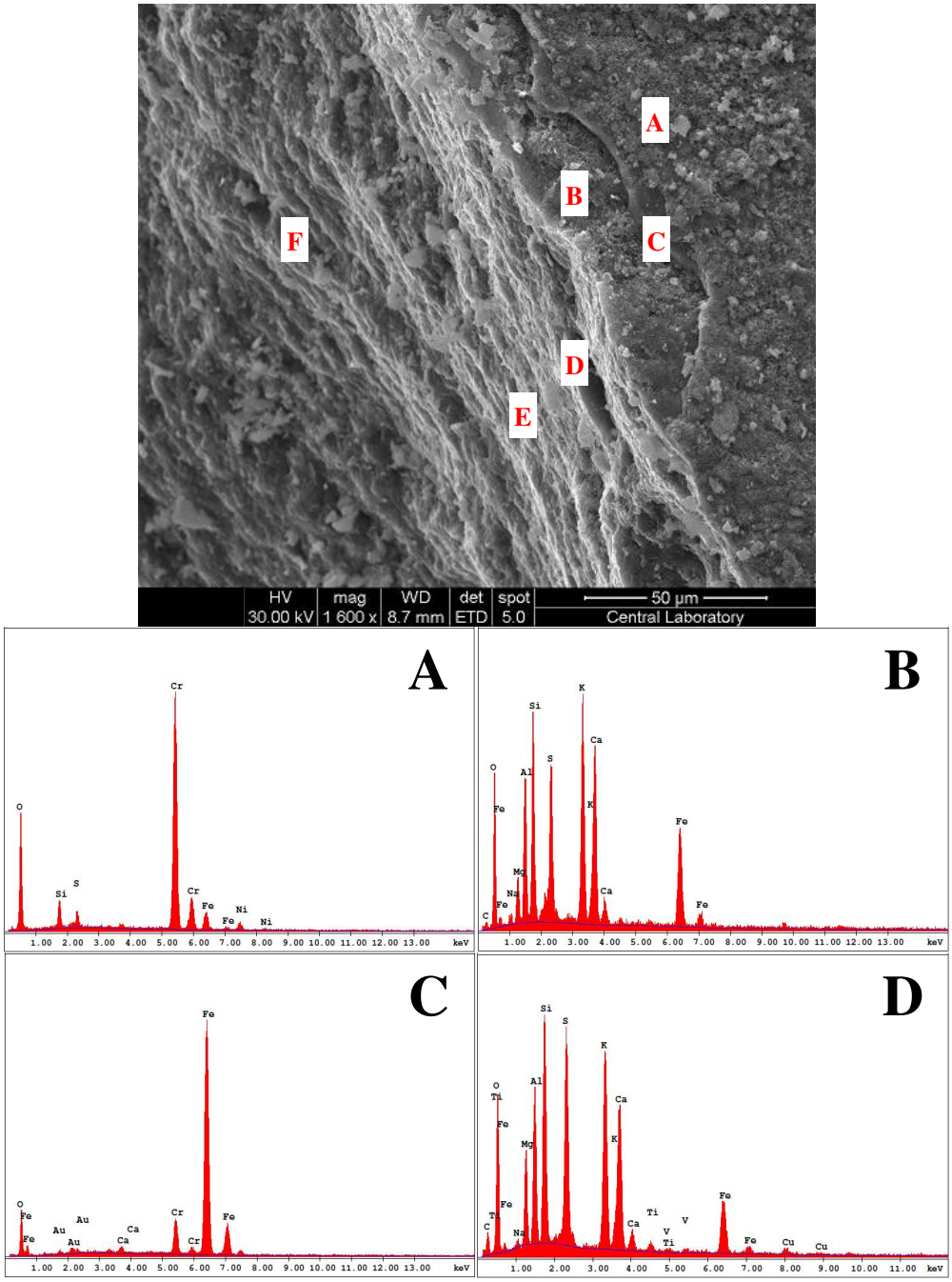

Figure 5.102 Enlarged view of the region shown as "3" in Figure 5.98 and SEM-EDS results of points A, B, C, D, E and F

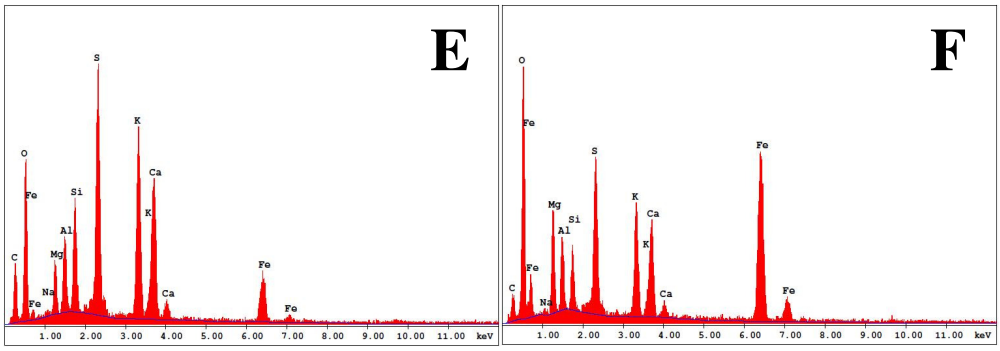

Figure 5.102 (continued)

5.5.4. Co-Combustion of Denizli/Kale Lignite and Olive Cake (50% by wt.) with Çan Limestone (Ca/S_{total} = 2.0) (C2-B1-2)

Denizli/Kale lignite and olive cake was used as coal and biomass materials in the experiment. The weight percent of olive cake in the fuel mixture was 50%. Some of the operational parameters are given in Table 5.40.

Table 5.40 Range of operational parameters for the co-combustion test (C2-B1-2)

Test #	Test Code	Fuel Feeding rate kg/h	λ -	P_{th} [a] kW	U_o [b] m/s
4-4	C2-B1-2	6.3-7.0	1.09-1.42	28-31	3.4-3.6

[a] P_{th}: Thermal power
[b] U_o: Superficial velocity in the combustor (calculated based on the flue gas flow rate, and the average temperature of TT110 and TT111)

The co-combustion test of fuel mixture containing Denizli/Kale lignite and olive cake 50% by weight was performed at dense phase temperature of 806±11°C. XRF and XRD analyses of BA, FA-C, and FA-BF are presented Table 5.41 and Table 5.42, respectively.

Table 5.41 XRF results of fuel ashes and ashes formed at the end of the co-combustion test (C2-B1-2)

Compound	Denizli/Kale	Olive Cake	BA	FA-C	FA-BF
	% by wt.				
Al_2O_3	9.72	3.06	5.51	11.14	10.41
CaO	15.25	18.65	34.60	25.72	23.35
Cl		2.30	0.05	0.15	0.52
Cr_2O_3	0.16	0.03	0.07	0.20	0.10
CuO	0.01	0.07	0.02	0.09	0.08
Fe_2O_3	14.19	5.09	4.50	17.92	16.15
K_2O	0.76	52.10	3.93	6.13	7.79
MgO	12.85	2.93	5.99	7.61	7.41
MnO_2	0.04	0.13	0.05	0.10	0.16
Na_2O	0.71	0.46	0.21	0.38	0.46
P_2O_5	0.20	3.18	0.66	0.68	0.69
SO_3	31.72	3.93	33.01	8.81	14.15
SiO_2	13.71	7.35	10.99	19.97	17.55
Normalized To (%)	100.0	100.0	100.0	100.0	100.0
Sum Before Normaliz. (%)	101.4	87.8	100.7	59.8	60.1

When Table 5.41 is investigated, it can be seen that SiO_2, Al_2O_3, CaO, Fe_2O_3, and MgO are the major oxides in the Denizli/Kale ash. The presence of Al_2O_3 and SiO_2 in the coal ash is an indication of aluminum silicates contamination from soil (Hiltunen et al., 2008). There is also sulfur remained in the Denizli/Kale ash. This result is consistent with the sulfur content of coal ash (S_{ash} (S_{total} − $S_{combustible}$) = 1.85%) according to the ultimate analysis of Denizli/Kale lignite given in Table 5.19. K_2O, CaO, and SiO_2 are the major oxides in the olive cake ash. Because of the limestone usage in this test, CaO is the major oxide in all ash samples. XRD analyses of ash samples and fuel ashes are given in Table 5.42 below. The ash phase composition of Denizli/Kale ash could not be quantified by Rietveld method. With the addition of limestone into the combustor, Lime and Calcite phases were detected in ash samples. While calcite was not seen in the bottom ash, it appears in both fly ash samples. This may be because of some small limestone particles not calcined and escaped to the cyclone and bag filter. Unreacted lime can be seen particularly in the bottom ash. Most of the Ca element was present in the form of Anhydrite. This is due to the sulfation of CaO coming from both limestone and fuel ash. Al_2O_3 seen in XRF analysis in Table 5.41 was present in the form of Kalicinite, Muscovite, and Calcium Magnesium Aluminum Oxide.

Table 5.42 XRD (Rietveld method) results of fuel ashes and ashes formed at the end of the co-combustion test (C2-B1-2)

Phase	Denizli/Kale	Olive Cake	BA[a]	FA-C	FA-BF[a]
	% by wt.				
Quartz, SiO_2	√	15.6	7.9	18.7	19
Calcite, $CaCO_3$	√	17.7		5.4	4.1
Lime, CaO			14	6.9	1.5
Anhydrite, $CaSO_4$	√		72	17.8	34
Hematite, Fe_2O_3	√			2.3	8
Magnetite, Fe_3O_4	√		2.9		7
Arcanite, K_2SO_4		12.1			
Potassium Calcium Sulfate, $K_2Ca_2(SO_4)_3$			0.4		10
Fairchildite, $K_2Ca(CO_3)_2$		27.8			
Calcium Magnesium Sulfate, $CaMg_3(SO_4)_4$	√				
Sylvite, KCl		1.8			
Kalicinite, $KAl(SO_4)_2 \cdot 11H_2O$		15.6			
Muscovite, $KAl_2(Si,Al)_4O_{10}(OH)_2$	√	9.4	√	37.4	6
Magnesioferrite, $MgFe_2O_4$				11.6	11
Calcium Magnesium Aluminum Oxide, $CaMg_2Al_{16}O_{27}$			√		

[a] determined by RIR method

XRD analysis of deposit accumulated on the surface of deposit sampling probe is given in Table 5.43. In addition to the phase encountered in the deposit of the test C2-B1-1, Lime and Anhydrite phases in the deposit of C2-B1-2 were also detected in the XRD analysis. This was due to the limestone usage during the experiment.

Table 5.43 XRD (RIR method) results of deposit collected from deposit sampling probe at the end of the co-combustion test (Analyses were done at METU-Central Laboratory) (C2-B1-2)

Phase	Ash Deposit on the Sampling Probe % by wt.
Quartz, SiO_2	12
Lime, CaO	2.2
Anhydrite, $CaSO_4$	7
Potassium Calcium Sulfate, $K_2Ca_2(SO_4)_3$	25
Hematite, Fe_2O_3	9
Magnetite, Fe_3O_4	33
Magnesioferrite, $MgFe_2O_4$	12

5.5.4.1. SEM-EDS Analysis of Bottom Ash (C2-B1-2)

A general view of the sample taken from bottom ash is given in Figure 5.103.

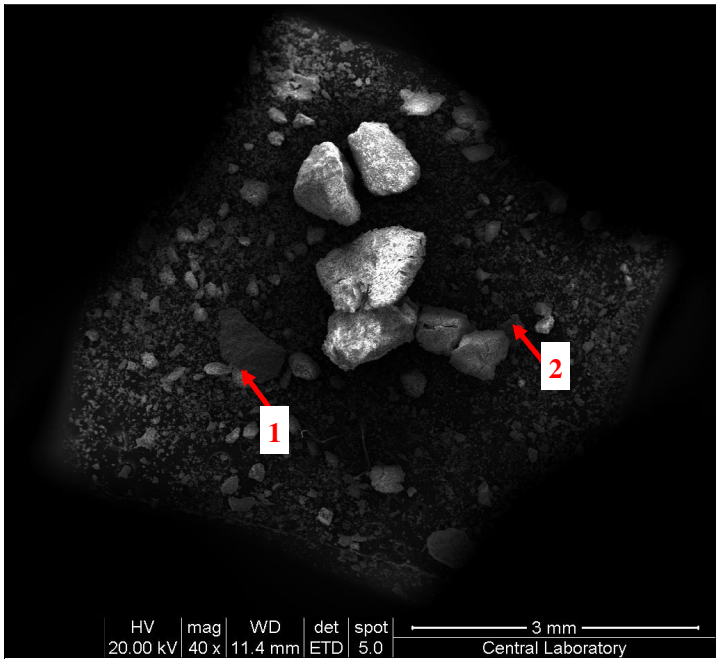

Figure 5.103 General view of sample taken from bottom ash (C2-B1-2)

Two particles in Figure 5.103 were selected for SEM-EDS analysis. The particle shown as "1" in Figure 5.103 was magnified by 1200 times and the SEM micrograph of it is presented in Figure 5.104. Three points were chosen for SEM-EDS analysis. SEM-EDS spectrum of these three points, A, B, and C are given in Figure 5.104. From the atomic weight of the elements according to the EDS spectrum, the particle is most probably made up of $CaSO_4$. This is consistent with the XRD result of the bottom ash in Table 5.42. Lime phase was also observed on the particle which means that full sulfation of CaO could not be done and some CaO remained in the limestone particles.

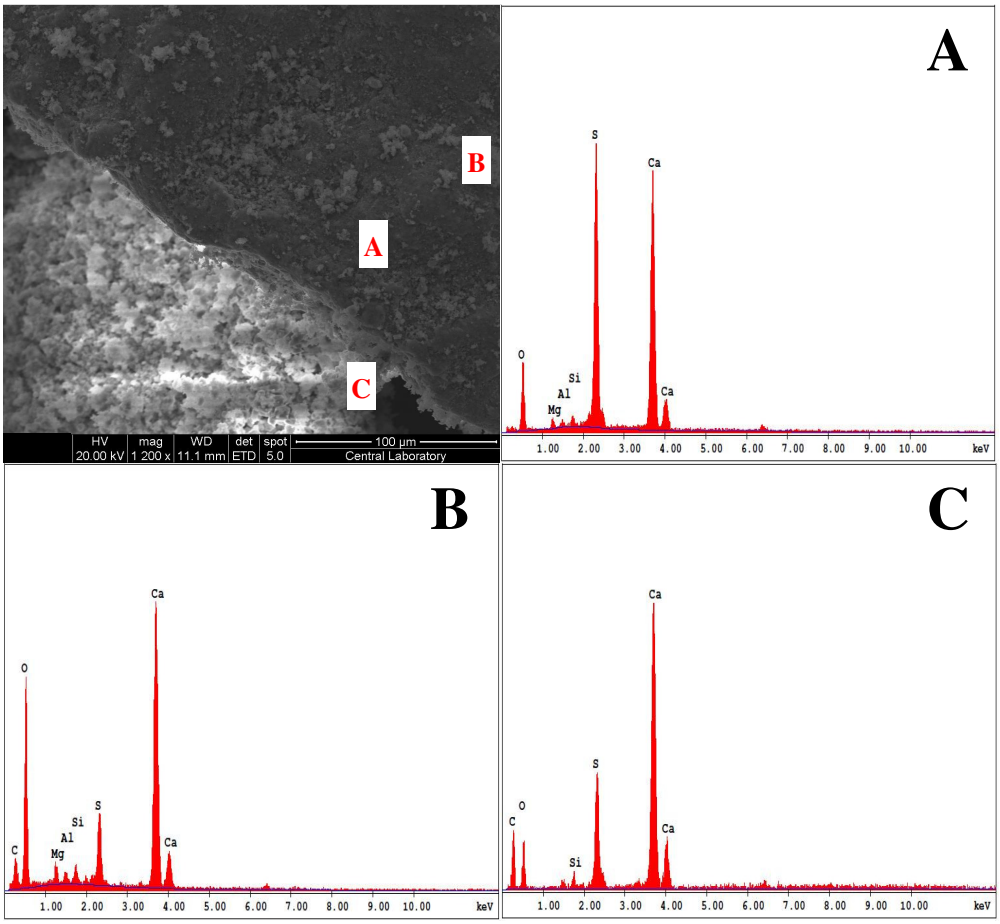

Figure 5.104 Enlarged view of the region shown as "1" in Figure 5.103 and SEM-EDS results of points A, B and C

The particle shown as "2" in Figure 5.103 was magnified by 5000 times. The SEM micrograph of the particle and SEM-EDS spectrum of the two points, A and B, on the particle are given in Figure 5.105. The point "A" consists of Quartz phase because of its high Si and O elements. As can be seen from the point "B", there are some CaO particles on the Quartz.

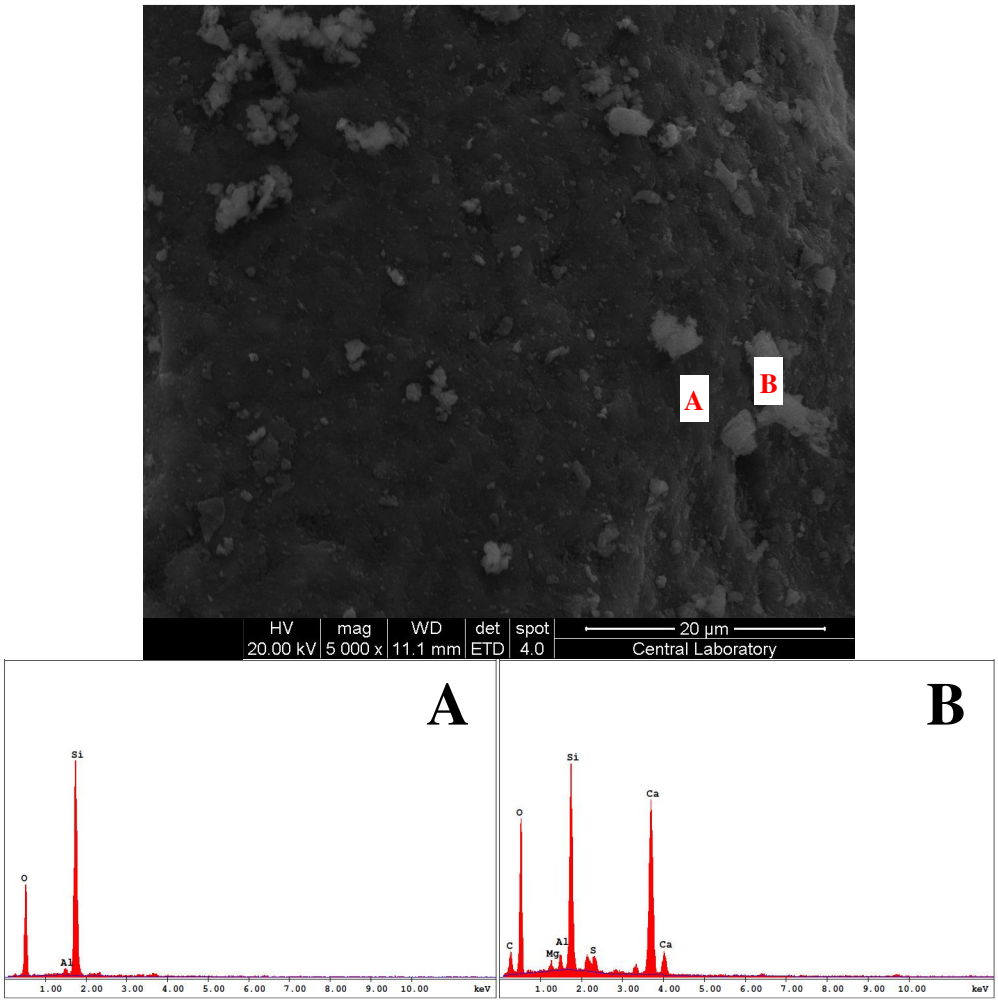

Figure 5.105 Enlarged view of the particle shown as "2" in Figure 5.103 and SEM-EDS results of points A and B

Another view of the sample taken from the bottom ash is given in Figure 5.106.

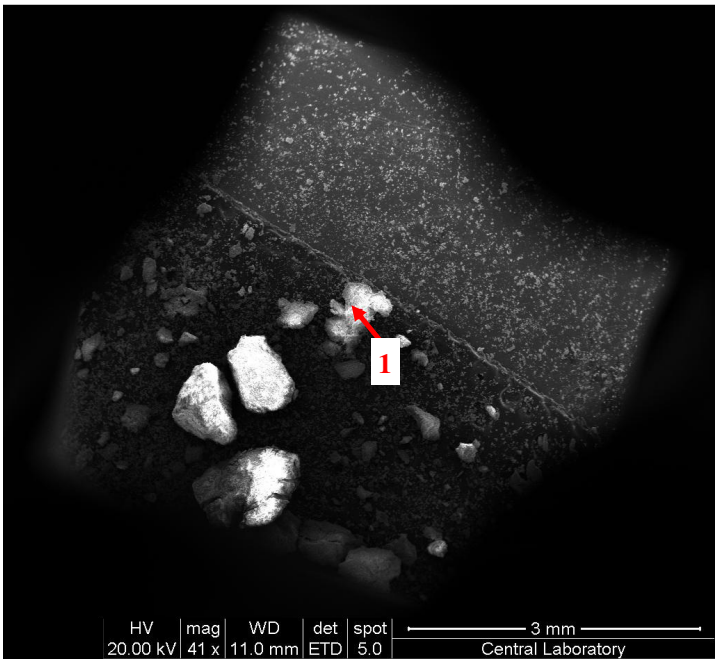

Figure 5.106 Another view of sample taken from bottom ash (C2-B1-2)

The particle shown as "1" in Figure 5.106 was magnified by 1500 times and the SEM micrograph of it is given in Figure 5.107. SEM-EDS spectrum of four points, A, B, C and D shows that this particle is CaO. Due to the presence of sulfur in point "A", it can be said that some part of it underwent to sulfation and formed $CaSO_4$. K which presents in the phase of Potassium Calcium Sulfate and Muscovite according to the XRD results of bottom ash in Table 5.42 could not be detected in SEM-EDS analysis. This is possibly because of the low concentration of K_2O in the bottom ash (3.93% by wt. in Table 5.41).

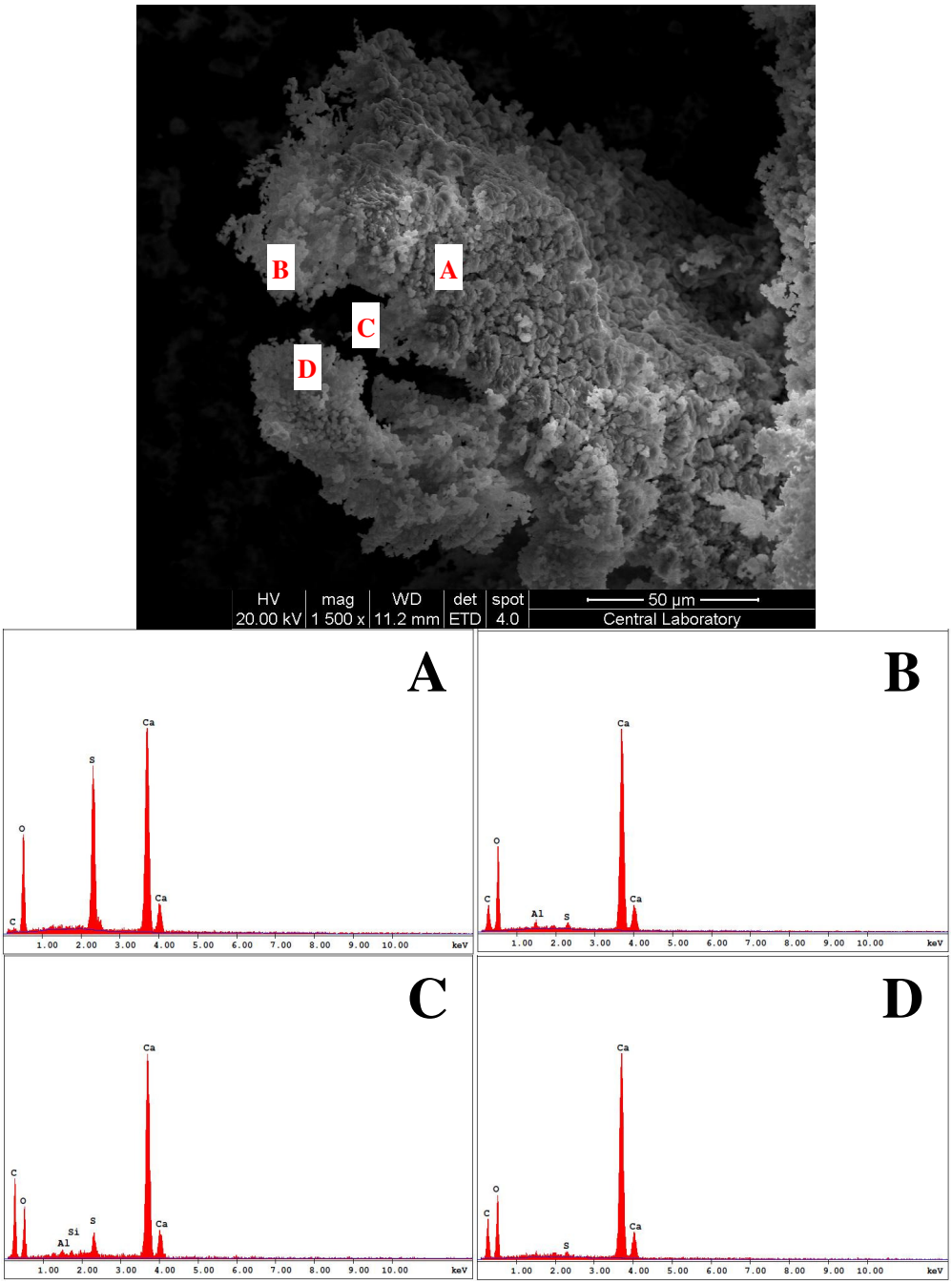

Figure 5.107 Enlarged view of the region shown as "1" in Figure 5.106 and SEM-EDS results of points A, B, C and D

5.5.4.2. SEM-EDS Analysis of Deposit on the Deposit Sampling Probe (C2-B1-2)

The deposit sampling probe was carefully removed from the combustor after 71 hours and 55 minute-operation. The images of the deposit sampling probe taken from four different sides as described in Section 5.5.1.2 are given in Figure 5.108.

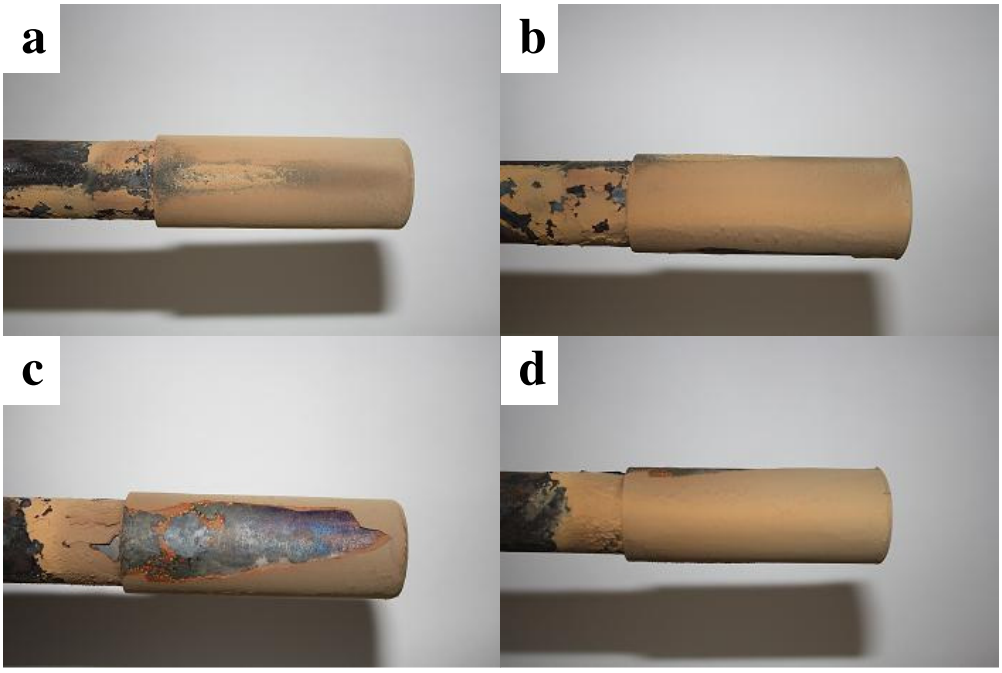

Figure 5.108 Image of the deposit sampling probe a) top b) right-side c) bottom d) left-side (C2-B1-2)

The deposit accumulated on the surface of the probe was collected at the end of the combustion test. The total amount of the deposit accumulated on the probe surface was 2.82 g. The projected surface area where deposit can accumulate was 16.02 cm^2. Total duration for fuel feeding was 51.4 hours. Thus, the deposition rate was calculated as 34 g/m^2-h which is above the index value (20 g/m^2-h in Section 5.5.1.2).

A general view of the sample taken from deposit sampling probe and three particles selected for SEM-EDS analysis are given in Figure 5.109.

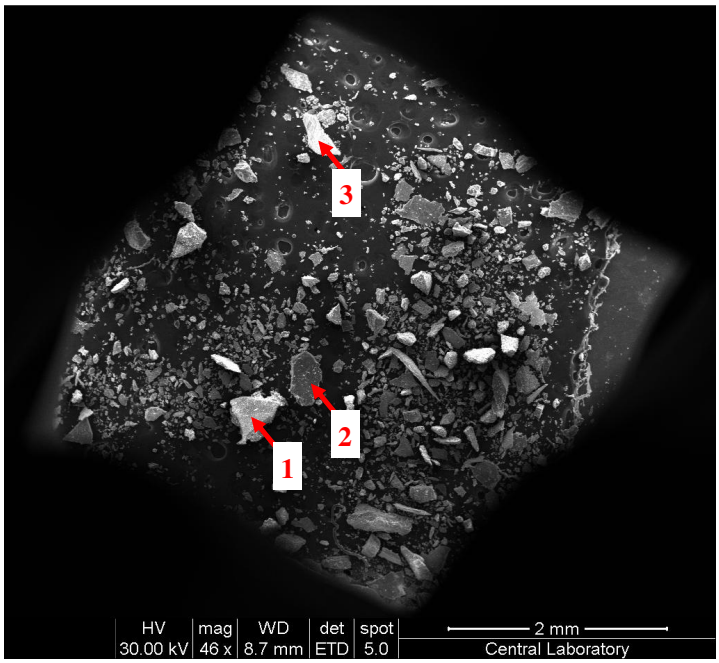

Figure 5.109 General view of sample taken from deposit sampling probe (C2-B1-2)

The image of the particle shown as "1" in Figure 5.109 was magnified by 500 times and the SEM micrograph of it is given in Figure 5.110. Two points, A and B, on the surface of the particle were subjected to SEM-EDS analysis. According to the EDS spectrum of the two points, the point "B" seems to be a part of the probe material due to its high Cr and Fe content. The point "A" is most probably a Potassium Calcium Sulfate particle stuck on the probe material. As can be seem from the figure that there are many small particles like the one in point "A" on the surface of the probe material.

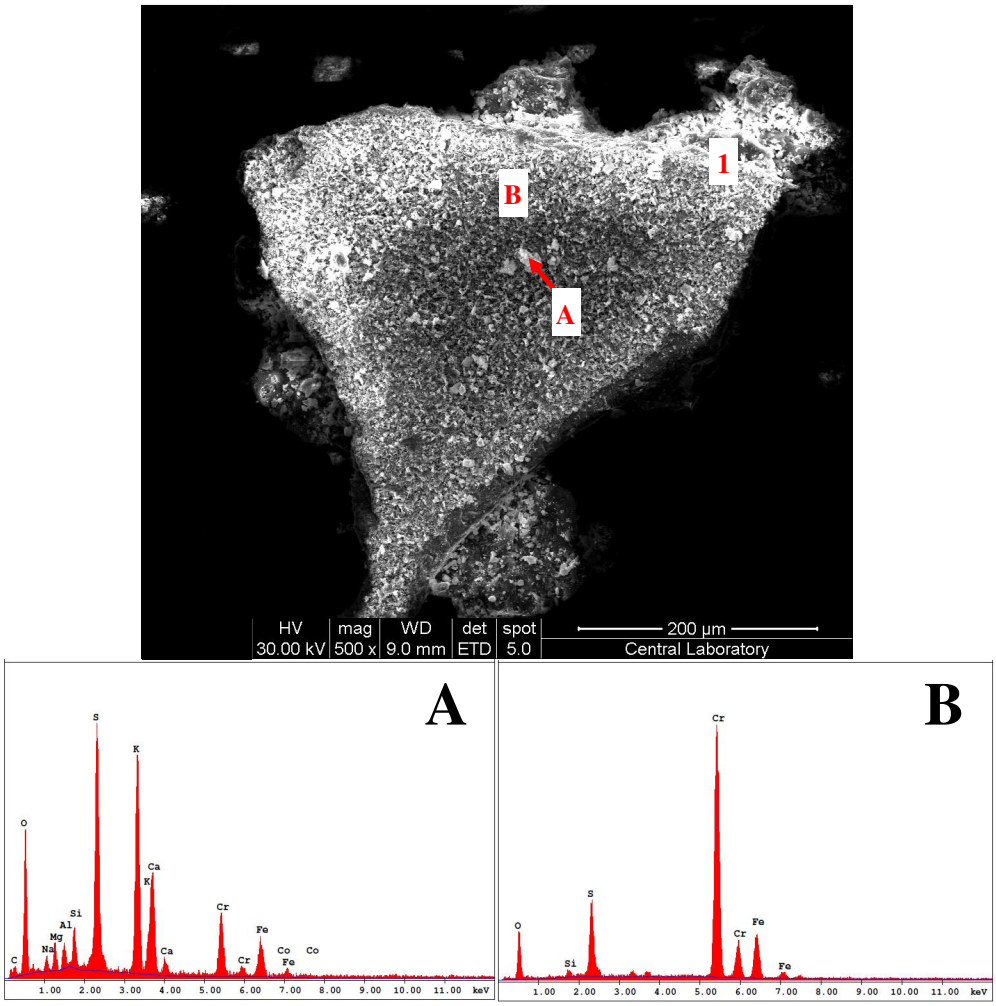

Figure 5.110 Enlarged view of the particle shown as "1" in Figure 5.109 and SEM-EDS results of points A and B

The image of the region shown as "1" on the probe material in Figure 5.110 was magnified by 1000 times and the SEM micrograph of it is given in Figure 5.111. Three points, A, B, and C, on the edge of the material was determined and SEM-EDS analysis of these three points was conducted. In line with the findings in Figure 5.110, Cr and Fe content seen on point "B" indicates that this is the material coming from the probe surface. High Si content for point "A" and "C" shows that there might be sand particles stick on the probe material or an accumulation of SiO_2 on the probe material. Ca, S, and K elements were also detected for points "A" and "C" in small quantities. This may be an indication of Potassium Calcium Sulfate formation on the probe material.

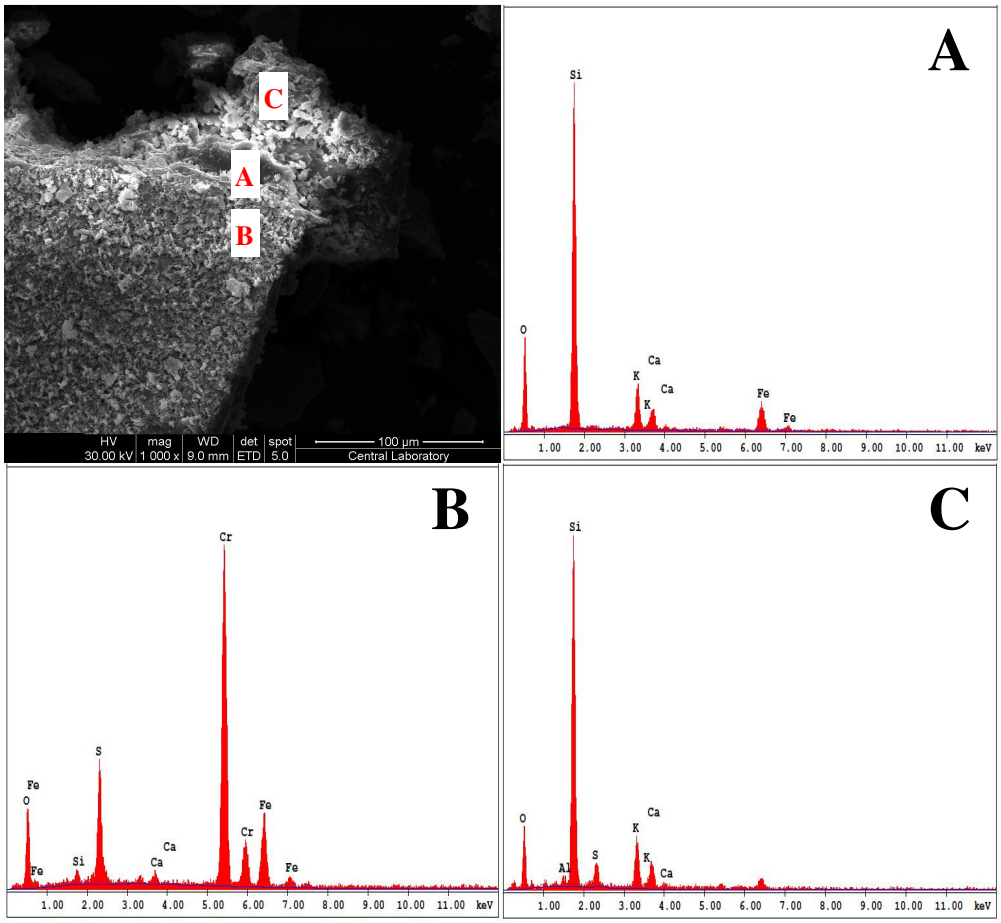

Figure 5.111 Enlarged view of the region shown as "1" in Figure 5.110 and SEM-EDS results of points A, B and C

The enlarged view of the particle shown as "2" in Figure 5.109 and SEM-EDS spectrums of three points, A, B, and C on the particle are given Figure 5.112. From the EDS spectrum of point "A", it is obvious that the particle is SiO_2. There are some small particles accumulated on the SiO_2 particle. These are represented by points "B" and "C". According to the SEM-EDS results, these particles may be Quartz, Potassium Calcium Sulfate or Anhydrite phases.

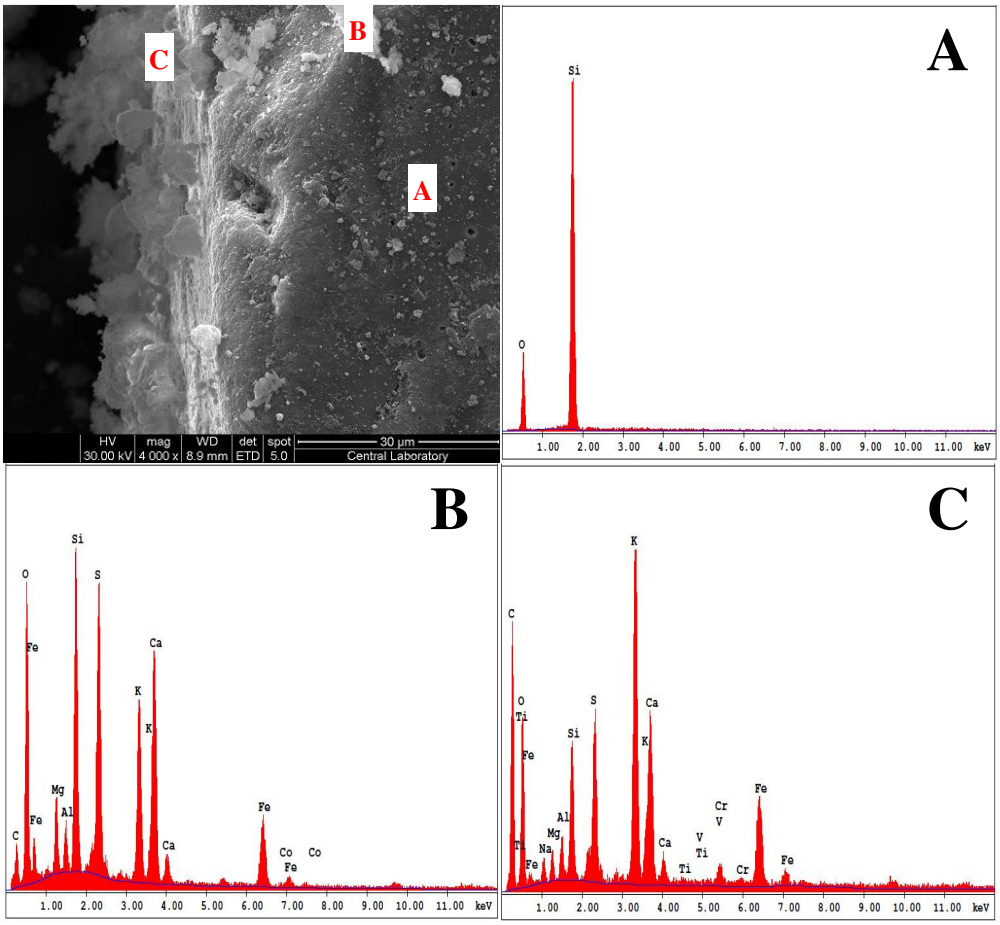

Figure 5.112 Enlarged view of the particle shown as "2" in Figure 5.109 and SEM-EDS results of points A, B and C

Another example of the formation of Quartz and Potassium Calcium Sulfate phases on the probe material can be seen in Figure 5.113. The image of the particle shown as "3" in Figure 5.109 was magnified by 3000 times and SEM micrograph of it is given in Figure 5.113. While the points "A" and "B" shows the particle is from probe material, the point "C" indicates that there is a formation of Quartz, Potassium Calcium Sulfate and Anhydrite phases on the probe material.

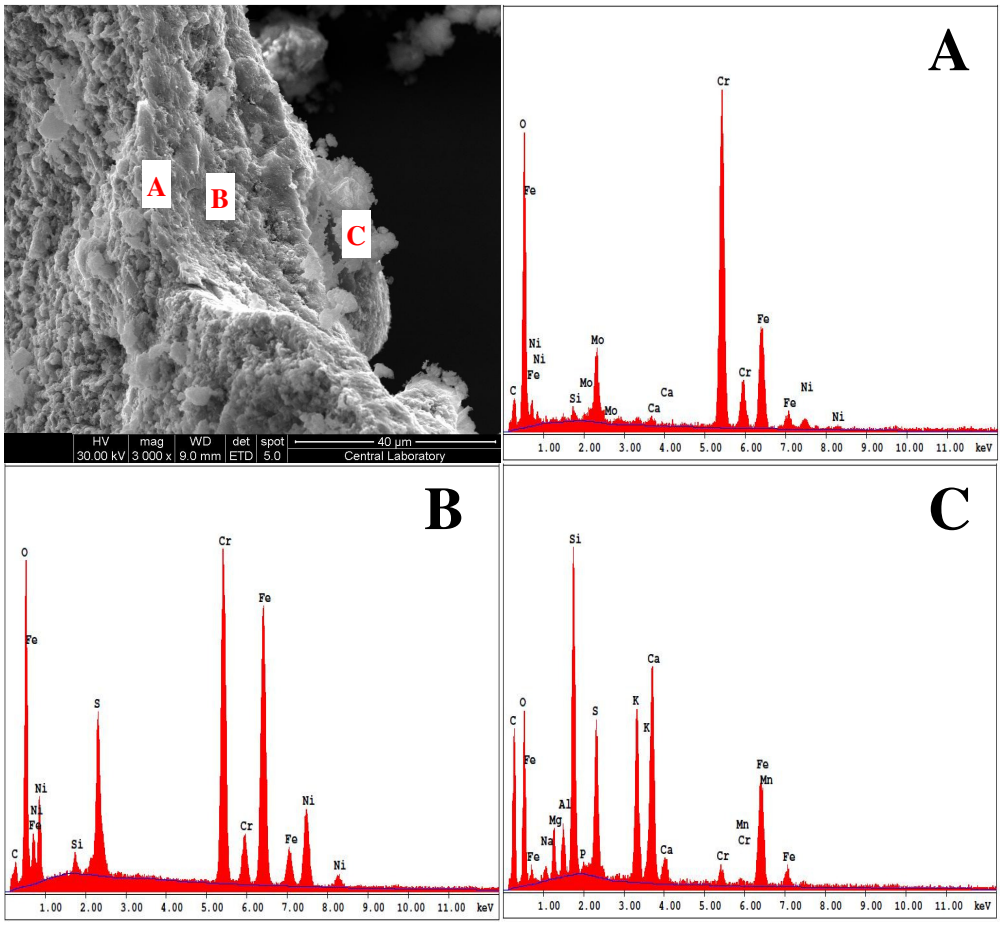

Figure 5.113 Enlarged view of the particle shown as "3" in Figure 5.109 and SEM-EDS results of points A, B and C

Another image of a particle from deposit sample is shown in Figure 5.114 below.

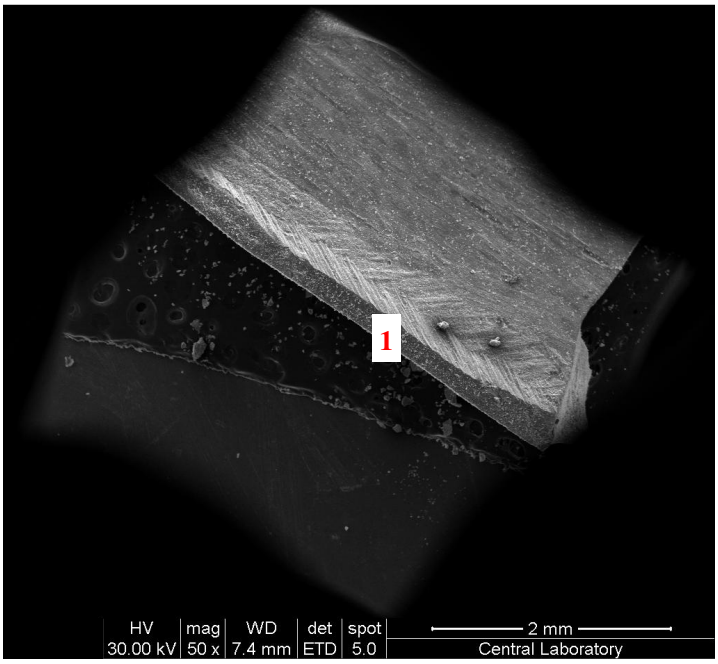

Figure 5.114 Another view of sample taken from deposit sampling probe (C2-B1-2)

The image of the region shown as "1" on the lateral surface of the particle in Figure 5.114 was magnified by 800 times and the SEM micrograph of it is presented in Figure 5.115. The thickness of the particle was measured to be 206.4 µm. Six points were determined for SEM-EDS analysis. SEM-EDS spectrum of the point "A" shows that the upper surface of the particle was a layer coming from the probe material because of its high Cr and Fe content. Other elements such as Ca, K, and S were also detected on point "A". This may be due to the thin layer of the probe material. SEM-EDS analysis can give composition results 3.5 µm below the surface of the sample. Points "B", "C", and "D" show the accumulation of mainly Quartz, Potassium Calcium Sulfate and Anhydrite phases on the probe material. The elements forming these three phases were also seen in points "E" and "F" but the dominant element in these two points is Aluminum. Although a phase containing Aluminum could not be detected by the XRD analysis of the deposit in Table 5.43, it may be in the form of Muscovite phase which was observed in both bottom and fly ashes.

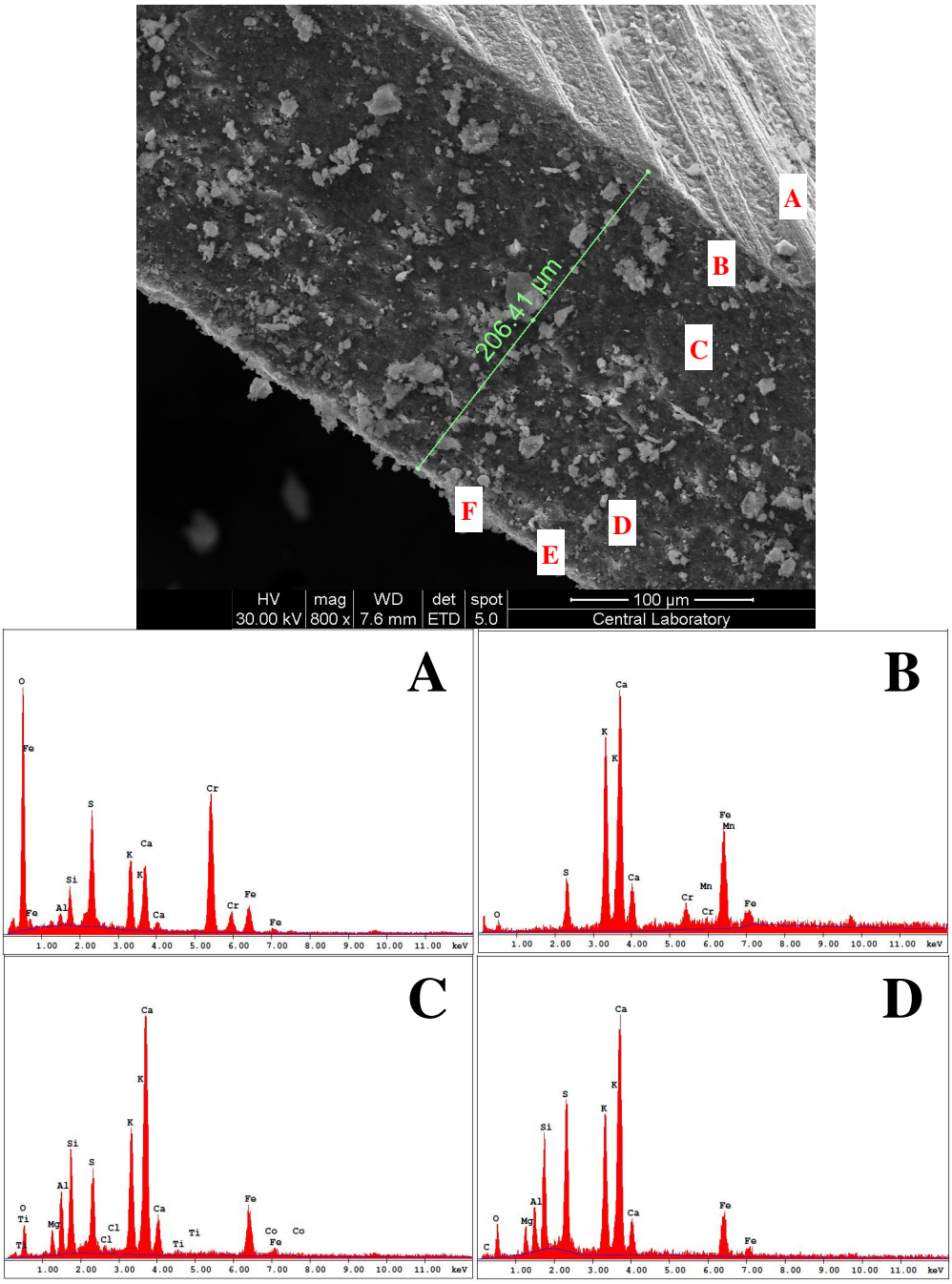

Figure 5.115 Enlarged view of the region shown as "1" in Figure 5.114 and SEM-EDS results of points A, B, C, D, E and F

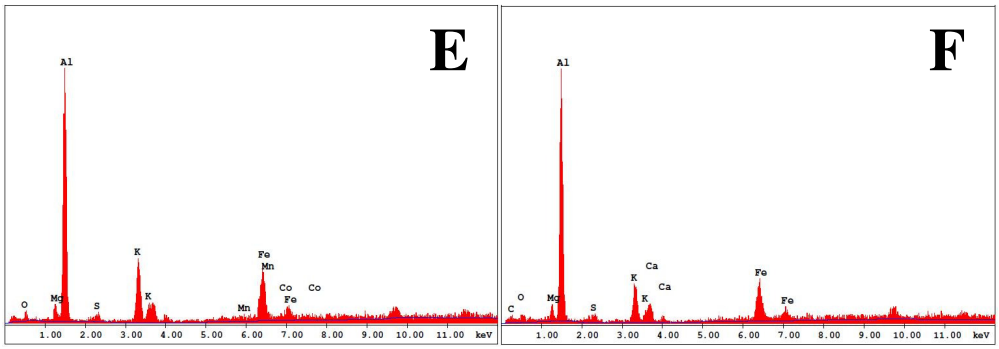

Figure 5.115 (continued)

5.5.5. Discussion on Ash Analyses in SET#4

In the co-combustion tests in SET#4, olive cake was used as biomass fuel for its high K in its ash (K_2O content of olive cake was about 50% by wt. in Table 4.16) and Bursa/Orhaneli and Denizli/Kale lignites were used as coal source to represent low-sulfur (S_{total} < 2.7% in Table 4.1) and high-sulfur coals (S_{total} > 3.6% in Table 4.1), respectively. Before they were used in the experiments, ash fusion temperatures of them were determined according to the ASTM D 1857-04 (See Table 4.17 in Section 4.7.4).

5.5.5.1. Bed Agglomeration

Although agglomeration is a more common problem encountered in BFBCs rather than CFBCs, ash analyses are discussed here in terms of agglomeration problem. The agglomeration is rare for CFBCs due to the high velocities and absence of an apparent bed in the combustor (Khan, 2007). Bed agglomeration in the fluidized bed combustors occurs when some of the fuel ash melts. They stick on the surface of the bed material. Quartz sand is generally used as bed material. It mainly consists of SiO_2 which has a melting point of around 1450°C (Lin et al., 1997). If the system is operated at the same conditions for a long time, at which agglomeration starts, particles of bed material having a sticky surface of sintered ash come together and adhere. When they become too big to be fluidized, the system does not operate well and total shut-down of the system is unavoidable.

There are mainly two important factors on the formation of bed agglomeration. They are: operation temperature and composition of fuel ash. Operation temperature is very important when compounds of the fuel ash have lower melting points than operation temperature. The operational temperature of the combustor was kept at about 850°C which is nearly 270°C less than the initial deformation temperature (IT) of olive cake (1121°C in Table 4.17). Therefore, the risk of agglomeration was at minimum during experiments.

Chemical composition of the fuel ash is also very important with respect to agglomeration. Alkali metals (Na, K) or alkaline earth metals (Ca, Mg) in the ash may form low viscous alkali or alkaline earth salt mixtures such as sulfates, chlorides or carbonates. If there is Si around, highly viscous mixtures may be formed (Skrifvars et al., 1998b). Alkaline content of fuel ash such as K and Na is also very important because these alkali elements in alkali oxides or salts can react with silica in the bed material at temperatures of 700-900°C forming low-melting point eutectics (Valmari et al., 1999; Scala and Chirone, 2006, Scala and Chirone, 2008; Lokare, 2008). Following two reactions (Rxn. 5.3 and Rxn. 5.4) are possible. Alkali carbonates can react with SiO_2 according to the Rxn. 5.3 and Rxn. 5.4 to form eutectic mixtures with melting temperatures of 874°C and 764°C, respectively (Grubor et al., 1995). These melting temperatures are lower than the melting temperatures of alkali carbonates (891°C for K_2CO_3 and 851°C for Na_2CO_3).

$$2SiO_2 + Na_2CO_3 \rightarrow Na_2O \bullet 2SiO_2 + CO_2 \quad \text{Rxn. 5.3}$$

$$4SiO_2 + K_2CO_3 \rightarrow K_2O \bullet 4SiO_2 + CO_2 \quad \text{Rxn. 5.4}$$

Silica sand is the most commonly used bed material in fluidized bed combustors. It is mainly responsible for the formation of silicate compounds. Alkali silicates can form a molten layer on the particle surfaces making the particles sticky in the combustion of biomass having high alkali content (Hupa, 2012). Olive cake, with its high K_2O content, could potentially cause formation of agglomeration in the combustor for long-term tests. However, any agglomeration was not observed during the co-combustion experiment (C1-B1-6) which meant that eutectics given in Rxn. 5.3 and Rxn. 5.4 did not form during the tests. When XRD analyses of bottom ashes for the co-combustion tests of olive cake with both lignites in Table 5.30 (C1-B1-6), in Table 5.34 (C1-B1-7), in Table 5.38 (C2-B1-1), and in Table 5.42 (C2-B1-2) are investigated, it can be seen that these eutectics could not be detected. This may be explained by the high sulfur content of the lignites used in the experiments. Using high-sulfur lignites with olive cake for the co-combustion tests in SET#4 might minimize the risk of agglomeration. Because sulfur in the lignites could react with alkali oxides and form alkali sulfates. Therefore, sulphur being an alternative reactant for alkali metals, generate a competitive reaction to Rxn. 5.3 and Rxn. 5.4. Thus, there was not enough alkali metal left to react with Si in the combustor. As a consequence, alkali silicates which are the main reason for the agglomeration problem could be not formed according to Rxn. 5.3 and Rxn. 5.4. The lowest total sulfur content of the lignites was measured as 2.43% by wt. (on dry basis) for Bursa/Orhaneli lignite in C1-B1-6 test (see Table 5.9). Although Bursa/Orhaneli lignite was selected to represent low-sulfur lignite, its sulfur content may be still considered as high enough to prevent agglomeration. Mixing high-alkali biomass with high-sulfur high-ash coals is also good application to dilute the alkali content of the mixture as stated by Werther et al. (2000).

If there is Fe_2O_3 in the fuel ash, like the case in the co-combustion tests in SET#4, Fe_2O_3 may react with the alkali compounds according to the Rxn. 5.5 and Rxn. 5.6 below. X in the reactions can be K or Na. The Fe_2O_3 in Rxn. 5.5 and Rxn. 5.6 may compete with the

SiO_2 for alkali compounds (Rxn. 5.3 and Rxn. 5.4) forming eutectic mixtures with melting temperatures above 1135°C (Grubor et al., 1995).

$$Fe_2O_3 + X_2O \rightarrow X_2Fe_2O_4 \quad \text{Rxn. 5.5}$$

$$Fe_2O_3 + X_2CO_3 \rightarrow X_2Fe_2O_4 + CO_2 \quad \text{Rxn. 5.6}$$

These two reactions (Rxn. 5.5 and Rxn. 5.6) might be one of the reasons why agglomeration did not occur in the combustor. Fe_2O_3 contents in the ash of Bursa/Orhaneli lignite for C1-B1-6 and C1-B1-7 tests are 9.97% by wt. (see Table 5.29) and 10.11% by wt. (see Table 5.33). Fe_2O_3 contents in the ash of Denizli/Kale lignite for C2-B1-1 and C2-B1-2 tests are 13.01% by wt. (see Table 5.37) and 14.19% by wt. (see Table 5.41). It is 5.16% by wt. (see Table 5.29) in C1-B1-6 and C1-B1-7 tests and 5.09% by wt. (see Table 5.37) in C2-B1-1 and C2-B1-2 tests for the olive cake ash. As can be seen from Table 5.30 for co-combustion of Bursa/Orhaneli lignite and Table 5.34, bottom ash for C1-B1-6 test has 6% Fe_2O_3. Although this amount is enough to react with X_2O or X_2CO_3 according to the reactions (Rxn. 5.5 and Rxn. 5.6), $X_2Fe_2O_4$ could not be determined in the bottom ash by XRD analysis. On the contrary, Fe_2O_3 is the only phase that is detected in the bottom ash. But, it is not the dominant phase.

It is also important to note that while K was kept in the ash as Potassium Calcium Sulfate ($K_2Ca_2(SO_4)_3$), Arcanite (K_2SO_4) and Anhydrite ($CaSO_4$). Si was detected in Forsterite ($Mg_2(SiO_4)$) for the co-combustion tests of Bursa/Orhaneli lignite and olive cake (C1-B1-6 and C1-B1-7) (See Table 5.30 and Table 5.34 for XRD analyses). By this way, it may happen that these two elements, K and Si, could not react to form alkali silicates which are the leading compound for agglomeration. The presence of Mg oxide in the fuel ashes (7.9-9.7% by wt. for Bursa/Orhaneli ash and 2.9% by wt. for olive cake ash (See Table 5.29 and Table 5.33 for XRF analyses)) may have a critical role to prevent the agglomeration. This may be another reason why agglomeration did not happen for the tests C1-B1-6 and C1-B1-7. One of the reasons why there was no agglomeration for the co-combustion tests of Denizli/Kale and olive cake (C2-B1-1 and C2-B1-2) may be the presence of Al in fuel ashes. Al oxide content of fuel ashes (9.7-16.1% by wt. for Denizli/Kale ash and 3.1% by wt. for olive cake ash (See Table 5.37 and Table 5.41 for XRF analyses)) appeared as Muscovite phase in the bottom and fly ashes at high levels. Muscovite contains K and Si elements in its structure preventing them to form alkali silicates. This may be also another supporting argument why agglomeration did not occur for the tests C2-B1-1 and C2-B1-2.

Bed Agglomeration Index (BAI) is a good indication to predict the agglomeration tendency of fuel ash before they are used in a combustor. It is given in Eq. 5.8. If the ratio is less than 0.15, agglomeration is possible (Bapat et al., 1997).

$$BAI = \frac{\%(Fe_2O_3)}{\%(K_2O + Na_2O)} \quad \text{Eq. 5.8}$$

While the BAI for Bursa/Orhaneli lignite was calculated as 11.7 and 24.6 for the tests C1-B1-6 and C1-B1-7, respectively; it was 5.6 and 9.7 for Denizli/Kale lignite used in the

tests C2-B1-1 and C2-B1-2, respectively. Olive cake's BAI was calculated as 0.10 for all co-combustion tests. It is less than 0.15 and this shows that there is a risk of agglomeration for the combustion of olive cake. However, the percentage of olive cake in the fuel mixture was 50% by wt. for the co-combustion tests in SET#4. Taking this into account, BAI was calculated for each test. It was 0.49, 0.38, 0.50, and 0.55 for C1-B1-6, C1-B1-7, C2-B1-1, and C2-B1-2, respectively. Moreover, BAIs for bottom ashes for each test in SET#4 are calculated above 0.8 which is much higher than 0.15. **These can be given as evidence why an agglomeration was not observed in the co-combustion tests in SET#4.**

5.5.5.2. Slagging and Fouling

A deposit sampling probe was used in this study to represent a heat exchanger tube surface in a boiler section for investigating the fouling tendencies of the fuels used in the co-combustion tests. The surface of the deposit sampling probe is cooled internally down to 550°C with air in order to represent the surface temperature of the superheaters. At the end of each combustion test, the deposit accumulated on the surface of the probe was collected and weighted in order to determine the deposition rate. The deposition rate is defined as mass of deposits per square meter of projected surface area of the probe per hour (Theis et al., 2006). If the deposition rate exceeds 20 g/m^2-h, this can be used as a sign of slagging and fouling problems in the measured area of the boiler (Göğebakan, 2007).

The total amount of the deposit accumulated on the probe surface was about 1 g, 1.74 g, 1.91 g, and 2.82 g for the tests C1-B1-6, C1-B1-7, C2-B1-1, and C2-B1-2, respectively. The projected surface area where deposit can accumulate was 16.02 cm^2 (OD=26.7 mm; L=60 mm). Total duration for fuel feeding was 25 hours for the test C1-B1-6. It was 40.5 hours, 49.8 hours, and 51.4 hours for the tests C1-B1-7, C2-B1-1, and C2-B1-2, respectively. Thus, the deposition rate was calculated as 25 g/m^2-h, 27 g/m^2-h, 24 g/m^2-h, and 34 g/m^2-h for the tests C1-B1-6, C1-B1-7, C2-B1-1, and C2-B1-2, respectively. Since the deposition rates calculated for the co-combustion tests are higher than the limit (20 g/m^2-h) value, it is possible to face with a fouling problem in case of co-combustion of olive cake (50% by wt.) with Bursa/Orhaneli and Denizli Kale lignites.

Deposition rate gives an idea about the fouling problem after conducting a real-case application of combustion experiment. In order to predict the fouling and slagging tendency of fuel ashes prior to use them in a combustor, there are several indices in the literature. These indices are overviewed in the Section 2.2.2.3 in detail. Here, only two of them are used to have an idea for fouling and slagging tendencies of fuel ashes before using them in the co-combustion tests. **These indices are the alkali index (AI) for fouling and the ash fusibility index (AFI) for slagging.**

AI is the ratio of alkali metal oxides to silica oxide and given in Eq. 5.9 (Guanyi et al., 1997; Hulkkonen et al., 2003). If it is higher than 1, it is possible to have severe fouling on the heat transfer surfaces (Hulkkonen et al., 2003).

$$AI = \frac{\%(K_2O + Na_2O)}{\%\,(SiO_2)}$$ Eq. 5.9

AI was calculated less than 0.11 for lignite ashes, it was **higher than 6.6 for olive cake.** According to the AI, it was extremely possible to have severe fouling on the heat exchanger surfaces if olive cake was burned alone in the combustor. However, combustion of olive cake was not studied; on the contrary, it was co-combusted with Turkish lignites with 50% by weight. Therefore, AI was re-calculated for the ashes of fuel mixtures. In the case of co-combustion of Bursa/Orhaneli lignite with olive cake, AI was found to be 1.04 and 1.16 for C1-B1-6 and C1-B1-7, respectively. AI values were close to each other which indicate that level of fouling should be close to each other for the two tests. This was also supported by the deposition rates. The deposition rates were also found close to each other; 25 g/m^2-h and 27 g/m^2-h for the tests C1-B1-6 and C1-B1-7, respectively.

In the case of co-combustion of Denizli/Kale lignite with olive cake, AI was found to be 0.95 and 1.75 for C2-B1-1 and C2-B1-2, respectively. In this case, the difference between AI values was bigger than the difference in Bursa/Orhaneli lignite case. This was also consistent with the difference between deposition rates, 24 g/m^2-h and 34 g/m^2-h for the tests C2-B1-1 and C2-B1-2, respectively.

AFI (Eq. 5.10) is used to predict the slagging potential and is different than the other indices given is Section 2.2.2.3 because it is defined according to the ash fusion temperatures (initial deformation temperature (IT) and hemispherical temperature (HT)) rather than ash composition. The slagging potential was reported as low for AFI > 1343^{o}C, medium for 1232^{o}C < AFI ≤ 1343^{o}C, high for 1149^{o}C ≤ AFI ≤ 1232^{o}C, and severe for AFI < 1149^{o}C (Teixeira et al., 2012).

$$AFI = \frac{(4 * IT + HT)}{5}$$ Eq. 5.10

AFI was calculated according to the ash fusion temperature presented in Table 4.17. It was 1285^{o}C, 1254^{o}C, and 1163^{o}C for the ashes of Bursa/Orhaneli lignite, Denizli/Kale lignite, and olive cake, respectively. According to the AFI calculations, it can be said that while the slagging potential is medium for the lignites, there is a high potential for the olive cake.

5.5.5.3. Conclusive Remarks

- SO_3, SiO_2, CaO, Al_2O_3, Fe_2O_3, and MgO are the major oxides in the Bursa/Orhaneli lignite and Denizli/Kale lignite ashes. However, K_2O, CaO, and SiO_2 are the major oxides in the olive cake ash.
- Quartz (SiO_2), Calcite ($CaCO_3$), Anhydrite ($CaSO_4$), and Hematite (Fe_2O_3) are the common phases detected in the ashes of Bursa/Orhaneli and Denizli/Kale lignites. In addition to these phases, Denizli/Kale lignite ash contains Magnetite

(Fe_3O_4), Calcium Magnesium Sulfate ($CaMg_3(SO_4)_4$), and Muscovite ($KAl_2(Si,Al)_4O_{10}(OH)_2$. On the other hand, Fairchildite ($K_2Ca(CO_3)_2$), Potassium Carbonate Hydrate ($K_2CO_3.1,5H_2O$), Calcite ($CaCO_3$), and Arcanite (K_2SO_4) are the main phases in the ash of olive cake. Sylvite (KCl) and Quartz are the other two phases in the ash of olive cake.

- SiO_2 and CaO, SO_3 are the common major oxides in the bottom ash. While MgO is high for the co-combustion cases of Bursa/Orhaneli lignite, it is Al_2O_3 for the Denizli/Kale lignite.
- Quartz, Lime (CaO), Anhydrite, Arcanite and Forsterite ($Mg_2(SiO_4)$) are the phases encountered in the bottom ash for the co-combustion cases of Bursa/Orhaneli lignite.
- Muscovite, Anhydrite, Quartz, and Magnesioferrite ($MgFe_2O_4$) are the phases encountered in the bottom ash for the co-combustion cases of Denizli/Kale lignite. Due to the high Al_2O_3 content, Muscovite is the dominant phase in the bottom ash.
- Quartz and Anhydrite are the common phase observed in the fly ash of the second cyclone. While Hematite and Lime is seen for the cases of Bursa/Orhaneli lignite, Muscovite and Magnesioferrite are present for the cases of Denizli/Kale lignite.
- CaO content in both bottom and fly ashes has increased due to limestone addition.
- Calcite phase is observed in the ash samples for the first time with the addition of limestone.
- Limestone addition to the fuel mixture might transfer K element from Arcanite to Potassium Calcium Sulfate in the bottom ash. While K is in the form of Arcanite in C1-B1-6 test, it mostly appears in the form of Potassium Calcium Sulfate phase in the bottom ash of C1-B1-7 test.
- The main phase determined in deposit from deposit sampling probe is Potassium Calcium Sulfate and Magnetite.
- K is mainly found in the Muscovite phase in the all ash samples for the co-combustion cases of Denizli/Kale lignite. A little amount of K is also observed as Potassium Calcium Sulfate.
- Muscovite is the dominant phase in all ash samples for the co-combustion cases of Denizli/Kale lignite. The presence of K and Si elements in Muscovite phase might one of the reasons why agglomeration did not seen since it prevented the formation of alkali silicates.
- SEM-EDS results are strongly consistent with XRF and XRD results for the bottom ash.
- SEM-EDS results are strongly consistent with XRD results for the deposit from deposit sampling probe.
- Bed Agglomeration Index was calculated as 0.49, 0.38, 0.50, and 0.55 for the co-combustion of Bursa/Orhaneli lignite and olive cake (50% by wt.) mixtures with and without limestone, and Denizli/Kale lignite and olive cake mixtures (50% by wt.) mixtures with and without limestone, respectively. Moreover, BAIs for bottom ashes for each tests are calculated above 0.8 which is much higher than

0.15. These can be given as evidence why an agglomeration was not observed in the co-combustion tests in SET#4.

CHAPTER 6

CONCLUSIONS

The results of this study have shown that the co-combustion of Bursa/Orhaneli lignite with olive cake and woodchips in a circulating fluidized bed combustor can be performed without any operational problems. As the biomass share in the fuel mixture increased, the combustion characteristic of the fuel mixtures changed from char combustion to volatile combustion. Addition of biomass to coal increased the oxygen requirement for the fuel particles to be completely burned out. CO emission increased with the increasing share of biomass due to the escape of some volatile matter unburned from the combustor. Biomass addition to the fuel mixture decreased SO_2 emission but did not change NO emission appreciably.

The **optimum excess air ratio** increased as the biomass share in the fuel mixture increased. While it was in the range of 1.2-1.3 for the Bursa/Orhaneli lignite combustion, it increased to 1.3-1.4, 1.40-1.55, and 1.55-1.60 for the mixtures containing 10, 30, and 50% by wt. olive cake, respectively. For the co-combustion of woodchips, the optimum λ was in the range of 1.2-1.3, 1.25-1.35 and 1.4-1.5 for the mixtures containing 10, 30, and 50% by wt. woodchips, respectively.

CO emissions were below the emission limit value for the case of **Bursa/Orhaneli lignite combustion** at excess air ratio of 1.23. All other measurements exceeded the emission limits for the co-combustion of Bursa/Orhaneli lignite with olive cake. Olive cake addition to Orhaneli lignite did not change NO emissions significantly. NO emissions were below the limit for all cases when the excess air ratio was less than 1.4. SO_2 emissions were only above the limit for the cases of 10% by wt. olive cake and coal combustion.

CO emission resulting from the **co-combustion of Bursa/Orhaneli and woodchips mixture** containing 50% by wt. woodchips was above the emission limit. All other measurements were below the limits in the case of optimum excess air ratio. When the woodchips percentage in fuel mixture was increased, SO_2 emission decreased as it was expected. It was only under the emission limit at the optimum excess air ratio for the fuel mixture containing 50% by wt. woodchips.

NO emissions increased as the excess air ratio increased for all cases. In order to make sure that the NO emission limit was met for each combustion test, the system needed to be operated at an excess air ratio below 1.4. However, when the system was operated

under these conditions, more CO emissions were produced. Therefore, it was necessary to make an optimization on the excess air ratio according to the CO and NO emissions.

Limestone addition was necessary to decrease **SO_2 emission** below the limit values. Ca/S molar ratio was determined as 2 for both lignites to keep the SO_2 emission low. When limestone was added to the combustor for SO_2 capture, CaO content in both bottom and fly ashes increased. This increase in Ca concentration created a synergistic effect between the limestone and biomass.

As a summary for conclusion for emissions without secondary air injection, at Ca/S ratio of 2 the maximum biomass addition is suggested to be below 30% by wt. for Bursa/Orhaneli lignite to be below the emission limits.

Secondary air injection into the combustor increased CO and SO_2 emissions and decreased NO emission slightly. NO emission was under the emission limits for the all cases of secondary air ratios (SAR).

As a summary of **secondary air injection**, for the case of Bursa/Orhaneli and woodchips co-combustion tests, secondary air should be given at 142 cm above the distributor plate and SAR should be less than 15% for the fuel mixture containing 30% by wt. woodchips to keep CO emissions below the emission limit. For the fuel mixture containing 50% by wt. woodchips, secondary air should be given at 324 cm or 415 cm above the distributor plate and SAR should be higher than 20%. For Bursa/Orhaneli and olive cake co-combustion tests, secondary air should be given at 142 cm above the distributor plate and SAR should be less than 10% for the fuel mixture containing 30% by wt. olive cake to keep CO emissions below the emission limit. For the fuel mixture containing 50% by wt. olive cake, secondary air should be given at 324 cm or 415 cm above the distributor plate and SAR should be between 10-15%.

The study on **ash composition** showed that SiO_2 and CaO, SO_3 were the common major oxides in the bottom ash. While MgO was high in the ash for the co-combustion cases of Bursa/Orhaneli lignite and olive cake, it was Al_2O_3 which was found to be high for the co-combustion cases of Denizli/Kale lignite. Due to the high Al_2O_3 content, Muscovite was the dominant phase in the bottom ash.

Limestone addition to the fuel mixture might transfer Potassium (K) element from Arcanite to Potassium Calcium Sulfate in the bottom ash. While K was in the form of Arcanite in the co-combustion test of Bursa/Orhaneli lignite and olive cake, it mostly appeared in the form of Potassium Calcium Sulfate phase in the bottom ash with limestone addition to the fuel mixture.

The main phase determined in the deposit on the deposit sampling probe was Potassium Calcium Sulfate and Magnetite. K was mainly found in the Muscovite phase which was the dominant phase in all ash samples for the co-combustion tests of Denizli/Kale lignite with olive cake. The presence of K and Si elements in Muscovite phase was believed to

be the reason why agglomeration did not happen in the combustor since it prevented the formation of alkali silicates.

In conclusion, **presence of Sulfur in the combustion medium is very advantageous** while burning high-K content olive cake to minimize the risk of agglomeration. K was detected in Arcanite or Potassium Calcium Sulfate phases and in Muscovite phase in the bottom ashes for the co-combustion tests of olive cake with Bursa/Orhaneli and Denizli/Kale lignites, respectively. Moreover, potassium silicates which are the main reason for the agglomeration problem could not be found in the bottom ashes. Therefore, according to the results of this study it is advantageous to add high sulfur coals to the combustor during the combustion of high-alkali content olive cake.

Bed agglomeration was not seen during the tests. Bed Agglomeration Index (BAI) was all higher than 0.15 for the co-combustion of Bursa/Orhaneli lignite and olive cake (50% by wt.) mixtures with and without limestone, and Denizli/Kale lignite and olive cake (50% by wt.) mixtures with and without limestone. If the BAI is lower than 0.15, there is a danger of bed agglomeration. Moreover, BAIs for bottom ashes for each test were calculated above 0.8 which is much higher than 0.15.

As an overall conclusion it can be said that:

- Increasing share of biomass in the fuel mixture shifted combustion characteristics from char combustion to volatile combustion.
- Addition of biomass increased CO emission, reduced char formation and NO emission.
- It was proved that sulfur in coal helped to prevent agglomeration, slagging and fouling in the combustor. Bed agglomeration was not seen in the tests. Bed Agglomeration Index values were much higher than the limit value of 0.15.
- Optimum excess air ratio increased with addition of biomass to fuel mixture.

CHAPTER 7

RECOMMENDATIONS FOR FURTHER STUDIES

Some recommendations can be done for further studies. These recommendations can be listed as follows:

- Due to the plugging of the return leg during the long term experiments (more than 24 hours) of olive cake, olive cake combustion could not be sustained for a long time. In order to provide continuous flow of solids throughout the return leg, it is suggested to make a modification on the system and to increase the diameter of the return leg.
- For the co-combustion experiments of woodchips and Bursa/Orhaneli lignite, it was first tried to feed the fuels into the combustor from separate fuel hoppers. However, some feeding problems occurred because the screw feeder was not suitable to feed the woodchips particles into the combustor. This was mainly due to the fiber structure of woodchips particles. Therefore, the co-combustion experiments of woodchips and Bursa/Orhaneli lignite was done by mixing these two fuels and feeding them into the combustor from the same fuel hopper. It is suggested to design a special screw feeder for feeding biomass taking into account the characteristics of biomass fuels, particularly woody biomass.
- When the secondary air is introduced into the combustor, CO emissions generally got worse and CO concentration increased in the flue gas. In order to explain why this happened, it was thought that the secondary air where it was given into the combustor might divide the combustor into two different parts in terms of hydrodynamics, namely, dense and hot lower part and dilute and cold upper part. It caused to lower the recirculation rate and to cool the upper part of the combustor. That might be the reason why CO emissions increased with secondary air injection. It is recommended to modify the secondary air injection ports to supply the secondary air into the combustor tangentially. By this way, it will be possible for the secondary air to follow a spiral path along the combustor.
- Among the carbon capture technologies, **"oxy-firing"** is a promising one used to increase the CO_2 concentration in the flue gas in order to capture it more efficiently. It is possible to enrich the flue gas in terms of CO_2 more than 95% by volume. It is a new technology in the world. There is no example and application of the oxy-firing technology in Turkey. Therefore, it is strongly recommended to modify the circulating fluidized bed combustor in order to be able to conduct oxy-firing studies.

REFERENCES

2010-2014 Strategic Plan (in Turkish). (2009). *Republic of Turkey, Ministry of Energy and Natural Resources*.

Abu-Qudais, M. (1996). Fluidized-bed combustion for energy production from olive cake. *Energy, 21*, 173–178.

Acar, H. H., Kalaycıoglu, H., Topalak, O. (2001). Harvesting of Rhododendron wood by chippers. *Third Balkan Scientific Conference*. Sofia.

Acar, H. H., Eker, M., Özkaya, M. S. (2011). An Assessment on the Procurement Possibilities of Rhododendron spp. Biomass in Turkey. *Tree-Stumps for Bioenergy, International Symposium Poster Session*. Uppsala-Sweden.

Adanez, J., Gayan, P., Grasa, G., Diego, L. F., Armesto, L., Cabanillas, A. (2001). Circulating fluidized bed combustion in the turbulent regime: modelling of carbon combustion efficiency and sulphur retention. *Fuel*, *80*, 1405–1414.

Afacan, O. (2005). *Mathematical modeling of NO_x Emissions in Bubbling Fluidized Bed Combustors*. M.Sc. Thesis. Middle East Technical University, Ankara, Turkey.

Afacan, O., Gogebakan, Y., Selçuk, N. (2007). Modeling of NO_x Emissions from Fluidized Bed Combustion of High Volatile Lignites. *Combustion Science and Technology*, *179*, 227–247.

Agricultural Biomass Potential of Turkey. (2013). *Republic of Turkey, Ministry of Energy and Natural Resources-General Directorate of Renewable Energy*. Retrieved July 1, 2013, from http://www.eie.gov.tr/yenilenebilir/tur_tar_biyo_pot.aspx.

Akdeniz, F., Çağlar, A., Güllü, D. (2002). Recent energy investigations on fossil and alternative nonfossil resources in Turkey. *Energy Conversion and Management*, *43*, 575–589.

Akışkan Yataklı Kazanlar (in Turkish). (2013). *Mimag Energy*. Retrieved July 19, 2013, from http://www.mimagenerji.com/index.php/tr/teknik-bilgi/akiskan-yatakli-kazanlar?id=91.

Alkhamis, T.M., Kablan, M.M. (1999). Olive cake as an energy source and catalyst for oil shale production of energy and its impact on the environment. *Energy Conversion and Management, 40*, 1863–1870.

Al-Mansour, F., Zuwala, J. (2010). An evaluation of biomass co-firing in Europe. *Biomass and Bioenergy*, *34*, 620–629.

Anthony, E. J., Jia, L. (2000). Agglomeration and strength development of deposits in CFBC boilers firing high-sulfur fuels. *Fuel, 79*, 1933–1942.

Anthony, E. J., Granatstein, D. L. (2001). Sulfation phenomena in fluidized bed combustion systems. *Progress in Energy and Combustion Science*, *27*, 215–236.

Armesto, L., Bahillo, A., Cabanillas, A., Veijonen, K., Otero, J., Plumed, A., Salvador, L. (2003a). Co-combustion of Coal and Olive Oil Industry Residues in Fluidised Bed. *Fuel, 82*, 993–1000.

Armesto, L., Boerrigter, H., Bahillo, A., Otero, J. (2003b). N_2O Emissions from Fluidised Bed Combustion. The Effect of Fuel Characteristics and Operating Conditions. *Fuel, 82*, 1845–1850.

Arvelakis, S., Vourliotis, P., Kakaras, E., & Koukios, E. G. (2001). Effect of leaching on the ash behavior of wheat straw and olive residue during fluidized bed combustion. *Biomass and Bioenergy*, *20*, 459–470.

Arvelakis, S., Gehrmann, H., Beckmann, M., Koukios, E. G. (2003). Agglomeration problems during fluidized bed gasification of olive-oil residue: evaluation of fractionation and leaching as pre-treatments. *Fuel*, *82*, 1261–1270.

ASTM Standard D1857 Standard Test Method for Fusibility of Coal and Coke Ash. (2004). ASTM International West Conshohocken, PA.

Atimtay, A. T., Topal, H. (2004). Co-combustion of olive cake with lignite coal in a circulating fluidized bed. *Fuel*, *83*, 859–867.

Atimtay, A. T., Varol, M. (2009). Investigation of co-combustion of coal and olive cake in a bubbling fluidized bed with secondary air injection. *Fuel*, *88*, 1000–1008.

Balat, M. (2005). Use of biomass sources for energy in Turkey and a view to biomass potential. *Biomass and Bioenergy*, *29*, 32–41.

Bapat, D. W., Kulkarni, S. V., Bhandarkar, V. P. (1997). Design and operating experience on fluidised bed boiler burning biomass fuels with high alkali ash. In F. D. S. Preto (Ed.), *Proceedings of 14th International Conference on Fluidized Bed Combustion* (pp. 165–174). Vancouver: ASME.

Bartels, M. (2008). *Agglomeration in Fluidized Beds: Detection and Counteraction*. Ph.D. Thesis, Delft University of Technology, Delft, Netherlands.

Basu, P., Fraser, S. A. (1991). *Circulating Fluidized Bed Boilers Design and Operations*. Stoneham, MA: Butterworth-Heinemann.

Basu, P. (2006). *Combustion and gasification in fluidized beds*. Boca Raton: Taylor & Francis Group, LLC.

Batu, A. (2008). *Investigation of Combustion Characteristics of Indigenous Lignite in a 150 kWt Circulating Fluidized Bed Combustor*. Ph.D. Thesis, Middle East Technical University, Ankara, Turkey.

Baumbach, G. (1996). *Air Quality Control*. Springer. ISBN: 3-540-57992-3.

Baxter, L. (2005). Biomass-coal co-combustion: opportunity for affordable renewable energy. *Fuel*, *84*, 1295–1302.

Baxter, L. L., Miles, T. R., Miles Jr., T. R., Jenkins, B. M., Milne, T., Dayton, D., Bryers, R. W., Oden, L.L. (1998). The behavior of inorganic material in biomass-fired power boilers: field and laboratory experiences. *Fuel Processing Technology*, *54*, 47–78.

Belen, İ., Kaplan, E., Cilan, S., Örs, B., Tüfekçioğlu, U., Kip, S., Taşkıran, I., Doğan, R. (2009). *Yenilenebilir Enerjide Orman Biyokütlesinin Durumu (in Turkish)*. Ankara: Republic of Turkey, Ministry of Environment and Forestry-General Directorate of Forestry.

Bloem, H., Monforti-Ferrario, F., Szabo, M., Jäger-Waldau, A. (2010). *Renewable Energy Snapshots 2010*. Italy: European Commission Joint Research Centre Institute for Energy.

Borman, G. L., Ragland, K. W. (1998). *Combustion Engineering* (1st Edition). Singapore: McGraw-Hill.

Boubel, R. W., Fox, D. L., Turner, D. B., Stern, A. C. (1994). *Fundamentals of Air Pollution* (3rd Edition). San Diego: Academic Press.

Brus, E., Öhman, M., Nordin, A., Boström, D., Hedman, H., Eklund, A. (2004). Bed Agglomeration Characteristics of Biomass Fuels Using Blast-Furnace Slag as Bed Material, *Energy & Fuels* 18, 1187–1193.

Brus, E., Öhman, M., Nordin, A. (2005). Mechanisms of Bed Agglomeration during Fluidized-Bed Combustion of Biomass Fuels. *Energy & Fuels*, 19, 825–832.

Caneghem, J. V., Brems, A., Lievens, P., Block, C., Billen, P., Vermeulen, I., Dewil, R., Baeyens, J., Vandecasteele, C. (2001). Fluidized bed waste incinerators: Design, operational and environmental issues. *Progress in Energy and Combustion Science*, *38*, 551–582.

Cliffe, K. R., Patumsawad, S. (2001). Co-combustion of waste from olive oil production with coal in a fluidised bed. *Waste Management*, *21*, 49–53.

Coal, Country Profiles, Turkey. (2011). *European Association for Coal and Lignite*. Retrieved June 24, 2013, from http://www.euracoal.be/pages/layout1sp.php?idpage=475.

Couch, G. R. (1994). *Understanding slagging and fouling in pf combustion. London: IEA Coal Research; 1994.* (p. 118). London: IEA Coal Research.

Davidsson, K. O., Åmand, L.-E., Steenari, B.-M., Elled, A.-L., Eskilsson, D., Leckner, B. (2008). Countermeasures against alkali-related problems during combustion of biomass in a circulating fluidized bed boiler. *Chemical Engineering Science*, *63*, 5314–5329.

Desroches-Ducarne, E., Marty, E., Martin, G., Delfosse, L. (1998). Co-combustion of coal and municipal solid waste in a circulating fluidized bed. *Fuel*, *77*, 1311–1315.

Directive 2001/08/EC of the European Parliament and of the Council of 23 October 2001 on the limitation of emission of certain pollutants into air from large combustion plants. (2001).*Official Journal of the European Communities*, L 309/1–21.

Energy Balances of Turkey. (2013). *Republic of Turkey, Ministry of Energy and Natural Resources*. Retrieved June 21, 2013, from http://www.enerji.gov.tr/index.php?dil=tr&sf=webpages&b=y_istatistik&bn=244&hn=244&id=398.

Enerji ve Tabii Kaynaklar Bakanlığı ile Bağlı ve İlgili Kuruluşlarının Amaç ve Faaliyetleri (in Turkish). (2012). Ankara: *Republic of Turkey, Ministry of Energy and Natural Resources*.

Ersoy, L. E., Golriz, M. R., Koksal, M., Hamdullahpur, F. (2004). Circulating fluidized bed hydrodynamics with air staging: an experimental study. *Powder Technology*, *145*, 25–33.

Evrendilek, F., Ertekin, C. (2003). Assessing the potential of renewable energy sources in Turkey. *Renewable Energy*, *28*, 2303–2315.

FAOSTAT Crop Productions. (2013). *Food and Agriculture Organization of the United Nations*. Retrieved July 2, 2013, from http://faostat3.fao.org/home/index.html#DOWNLOAD.

Fernández Llorente, M. J., Carrasco García, J. E. (2005). Comparing methods for predicting the sintering of biomass ash in combustion. *Fuel*, *84*, 1893–1900.

Fifth Ministerial Conference on the Protection of Forest in Europe Warsaw Resolution 1 Forests, Wood and Energy. (2007). Warsaw. Retrieved July 19, 2013, from http://www.foresteurope.org/ministerial_conferences/warsaw2007.

Forestry-based Biomass Potential of Turkey. (2013). *Republic of Turkey, Ministry of Energy and Natural Resources-General Directorate of Renewable Energy*. Retrieved July 1, 2013, from http://www.eie.gov.tr/yenilenebilir/tur_or_kay_biyo_pot.aspx.

Gayan, P., Adanez, J., Diego, L. F., García-Labiano, F., Cabanillas, A., Bahillo, A., Aho, M., Veijonen, K. (2004). Circulating fluidised bed co-combustion of coal and biomass. *Fuel, 83*, 277–286.

Glarborg, P., Jensen, A. D., Johnsson, J. E. (2003). Fuel nitrogen conversion in solid fuel fired systems. *Progress in Energy and Combustion Science*, *29*, 89–113.

Global Warming Potentials. (2013). *United Nations Framework Convention on Climate Change*. Retrieved July 11, 2013, from http://unfccc.int/ghg_data/items/3825.php.

Göğebakan, Z. (2007). *Co-Firing Biomass with Coal in Bubbling Fluidized Bed Combustors*. Ph.D. Thesis, Middle East Technical University, Ankara, Turkey.

Grace, J. R., Avidan, A. A., Knowlton, T. M. (Eds.). (1997). *Circulating Fluidized Beds*. London: Blackie Academic&Professional.

Grubor, B. D., Oka, S. N., Ilic, M. S., Dakic, D. V., Arsic, B. T. (1995). Biomass FBC combustion-bed agglomeration problems. In K. J. Heinschel (Ed.), *Proceedings of the 13th International Conference on Fluidized Bed Combustion* (pp. 515–22). Orlando, FL: ASME.

Guanyi, C., Mengxiang, F., Zhongyang, L., Xuantian, L., Zhenglun, S., Kefa, C. (1997). Experimental research on rice husk combustion in CFB boiler and the design of a 35 t/h rice husk fired CFB boiler. In F. D. S. Preto (Ed.), *Proceedings of 14th International Conference on Fluidized Bed Combustion* (pp. 175–181). Vancouver: ASME.

Gungor, A. (2008). Analysis of combustion efficiency in CFB coal combustors." *Fuel, 87*, 1083–1095.

Gungor, A. (2010). Simulation of emission performance and combustion efficiency in biomass fired circulating fluidized bed combustors. *Biomass and Bioenergy*, *34*, 506–514.

Gündüz, G. (1996). *Ormangülü (Rhododendron ponticum L.) Çiçeklerinin Ekstraksiyonu ve Boya Maddesi Özelliğinin İncelenmesi (in Turkish)*. M.Sc. Thesis, Zonguldak Karaelmas University, Zonguldak, Turkey.

Hayashi, J.-i., Hirama, T., Okawa, R., Taniguchi, M., Hosoda, H., Morishita, K., Li, C.-Z., Chiba, T. (2002). Kinetic Relationship Between NO/N_2O Reduction and O_2 Consumption During Flue-gas Recycling Coal Combustion in a Bubbling Fluidized-bed. *Fuel, 81*, 1179–1188.

Hiltunen, M., Barišić, V., Zabetta, E. C. (2008). Combustion of Different Types of Biomass in CFB Boilers-Foster Wheeler. *presented at 16th European Biomass Conference*. Valencia, Spain.

Hulkkonen, S., Fabritius, M., Enestam, S. (2003). Application of BFB Technology for Biomass Fuels: Technical Discussion and Experiences from Recent Projects. In S. Pisupati (Ed.), *Proceedings of 17th International Conference on Fluidized Bed Combustion*. Jacksonville, Florida: ASME.

Hupa, M. (2005). Interaction of fuels in co-firing in FBC. *Fuel*, *84*, 1312–1319.

Hupa, M. (2008). Ash Behavior in Fluidized Bed Combustion - Recent Research Highlights. *9th International Conference on Circulating Fluidized Bed* (Vol. 3). Hamburg.

Hupa, M. (2012). Ash-Related Issues in Fluidized-Bed Combustion of Biomasses: Recent Research Highlights. *Energy & Fuels*, *26*, 4–14.

Iancu, I., Clarke, A. W., Trinnaman, J. A. (Eds.). (2010). *WEC 2010 Survey of Energy Resources*. London: World Energy Council.

IEA Bioenergy Task 32 Biomass Combustion and Co-firing: An Overview. (2002).

IEA Bioenergy Task 32: Biomass Combustion and Co-firing, Database of Biomass Co-firing initiatives. (2013). Retrieved July 26, 2013, from http://www.ieabcc.nl/.

IEA Key World Energy Statistics. (2012). Paris: OECD/IEA.

IEA Statistics CO_2 Emissions from Fuel Combustion. (2012). Paris: OECD/IEA.

IEA Statistics Coal Information. (2012). Paris: OECD/IEA.

IEA Statistics Renewables Information. (2012). Paris: OECD/IEA.

IEA World Energy Outlook. (2012). Paris: OECD/IEA.

Jenkins, B. M., Baxter, L. L., Miles Jr., T. R., Miles, T. R. (1998). Combustion properties of biomass. *Fuel Processing Technology*, *54*, 17–46.

Johnsson, J. E., Dam-Johansen, K. (1991). Formation and reduction of NO_x in a fluidized bed combustor. In E. J. Anthony (Ed.), *Proceedings of the 11th International Conference on Fluidized Bed Combustion* (pp. 1389–96). Montreal: ASME.

Johnsson, J. E. (1994). Formation and reduction of nitrogen oxides in fluidized bed combustion. *Fuel*, *73*, 1398–415.

Kaygusuz, K., Türker, M. (2002). Biomass energy potential in Turkey. *Renewable Energy*, *26*, 661–678.

Kaynak, B., Topal, H., Atimtay, A. T. (2005). Peach and apricot stone combustion in a bubbling fluidized bed. *Fuel Processing Technology*, *86*, 1175–1193.

Khan, A. A., De Jong, W., Jansens, P. J., Spliethoff, H. (2009). Biomass combustion in fluidized bed boilers: Potential problems and remedies. *Fuel Processing Technology*, *90*, 21–50.

Khan, A. A. (2007). *Combustion and co-combustion of biomass in a bubbling fluidized bed boiler*. Ph.D. Thesis, Delft University of Technology, Delft, Netherlands.

Kiliç, F. Ç., Kaya, D. (2007). Energy production, consumption, policies, and recent developments in Turkey. *Renewable and Sustainable Energy Reviews*, *11*, 1312–1320.

Kunii, D., Levenspiel, O. (1991). *Fluidization Engineering* (2nd Edition). USA: Butterworth-Heinemann.

Kuprianov, V. I., Kaewklum, R. Chakritthakul, S. (2011). Effects of operating conditions and fuel properties on emission performance and combustion efficiency of a swirling fluidized-bed combustor fired with a biomass fuel. *Energy 36*, 2038–2048.

Laursen, K., Grace, J. R. (2002). Some implications of co-combustion of biomass and coal in a fluidized bed boiler. *Fuel Processing Technology, 76*, 77–89.

Leckner, B., Åmand, L.-E., Lücke, K., Werther, J. (2004). Gaseous emissions from co-combustion of sewage sludge and coal/wood in a fluidized bed. *Fuel*, *83*, 477–486.

Li, Y. H., Lu, G. Q., Rudolph, V. (1998). The kinetics of NO and N_2O reduction over coal chars in fluidised-bed combustion. *Chemical Engineering Science*, *53*, 1–26.

Li, Z., Ren, F., Chen, Z., Chen, Z., Wang, J. (2010). Influence of declivitous secondary air on combustion characteristics of a down-fired 300-MW_e utility boiler. *Fuel, 89*, 410–416.

Lin, W., Krusholm, G., Dam-Johansen, K., Musahl, E., Bank, L. (1997). Agglomeration phenomena in fluidized bed combustion of straw. In F.D.S. Preto (Ed.), *Proceedings of the 14th International Conference on Fluidized Bed Combustion V1* (pp. 831–837). Vancouver: ASME.

Lin, W., Dam-Johansen, K., Frandsen, F. (2003). Agglomeration in bio-fuel fired fluidized bed combustors. *Chemical Engineering Journal*, *96*, 171–185.

Liu, R., Jin, B., Zhong, Z., Zhao, J. (2007). Reduction of bed agglomeration in CFB combustion biomass with aluminium-contain bed material. *Process Safety and Environmental Protection, 85*, 441–445.

Lokare, S. S. (2008). *A Mechanistic Investigation of Ash Deposition in Pulverized-Coal and Biomass Combustion*. Brigham Young University.

Loo, S. V., Koppejan, J. (Eds.). (2008). *The Handbook of Biomass Combustion and Co-firing* (2nd Edition). London: Earthscan.

Löffler, G., Wargadalam, V. J., Winter, F. (2002). Catalytic effect of biomass ash on CO, CH_4 and HCN oxidation under fluidised bed combustor conditions. *Fuel*, *81*, 711–717.

Lyngfelt, A., Leckner, B. (1993). SO_2 Capture and N_2O Reduction in a Circulating Fluidized-Bed Boiler: Influence of Temperature and Air Staging. *Fuel*, *72*, 1553–1561.

Lyngfelt, A., Leckner, B. (1999). Combustion of wood-chips in circulating fluidized bed boilers — NO and CO emissions as functions of temperature and air-staging. *Fuel*, *78*, 1065–1072.

Maciejewska, A., Veringa, H., Sanders, J., Peteves, S. D. (2006). *Co-firing of biomass with coal: constraints and role of biomass pre-treatment*. Luxembourg: European Communities.

Madhiyanon, T., Sathitruangsak, P., Soponronnarit, S. (2010). Combustion characteristics of rice-husk in a short-combustion-chamber fluidized-bed combustor (SFBC). *Applied Thermal Engineering*, *30*, 347–353.

Mahmoudi, S., Baeyens, J., Seville, J. P. K. (2010). NO_x formation and selective non-catalytic reduction (SNCR) in a fluidized bed combustor of biomass. *Biomass and Bioenergy*, *34*, 1393–1409.

McIlveen-Wright, D. R., Huang, Y., Rezvani, S., Mondol, J. D., Redpath, D., Anderson, M., Hewitt, N. J., Williams, B. C. (2011). A Techno-economic assessment of the reduction of carbon dioxide emissions through the use of biomass co-combustion. *Fuel*, *90*, 11–18.

Melikoglu, M. (2013). Vision 2023: Feasibility analysis of Turkey's renewable energy projection. *Renewable Energy*, *50*, 570–575.

Miles, T. R., Miles, Jr., T. R., Baxter, L. L., Bryers, R. W., Jenkins, B. M., Oden, L. L. (1995). *Alkali deposits found in biomass power plants: a preliminary investigation of their extent and nature* (Vol. II). Golden, CO: National Renewable Energy Laboratory.

Miller, J. A., Bowman, C. T. (1989). Mechanism and modelling of nitrogen chemistry in combustion. *Progress in Energy and Combustion Science*, *15*, 287–338.

Mineral and energy resources in Bursa (in Turkish). (2010). Ankara. Retrieved July 20, 2013, from http://www.mta.gov.tr/v2.0/default.php?id=il_maden_potansiyelleri

Mineral and energy resources in Denizli (in Turkish). (2010). Ankara. Retrieved July 20, 2013, from http://www.mta.gov.tr/v2.0/default.php?id=il_maden_potansiyelleri

Munir, S., Nimmo, W., Gibbs, B. M. (2011). The effect of air staged, co-combustion of pulverised coal and biomass blends on NO_x emissions and combustion efficiency. *Fuel*, *90*, 126–135.

Namkung, H., Xu, L.-H., Kang, T.-J., Kim, D. S., Kwon, H.-B., Kim, H.-T. (2013). Prediction of coal fouling using an alternative index under the gasification condition. *Applied Energy*, *102*, 1246–1255.

Nevers, N. D. (1995). *Air Pollution Control Engineering*. Singapore: McGraw-Hill.

Nussbaumer, T. (2003). Combustion and co-combustion of biomass: fundamentals, technologies, and primary measures for emission reduction. *Energy & Fuels*, *17*, 1510–1521.

OECD "Turkey", in Inventory of Estimated Budgetary Support and Tax Expenditures for Fossil Fuels 2013. (2013).

Olive Black Water and Olive Cake (in Turkish). (2013). *Republic of Turkey, Ministry of Food, Agriculture and Livestock Olive Research Institute*. Retrieved July 2, 2013, from http://www.zae.gov.tr/index.php/bolumler/gida-teknolojileri/karasu-ve-prina.html.

Ozdamar, A., Gursel, K. T., Orer, G., Pekbey, Y. (2004). Investigation of the potential of wind–waves as a renewable energy resource: by the example of Cesme—Turkey. *Renewable and Sustainable Energy Reviews*, *8*(6), 581–592.

Ozgur, M. A. (2008). Review of Turkey's renewable energy potential. *Renewable Energy*, *33*, 2345–2356.

Pai, D., Engström, F. (1999). Fluidised bed combustion technology—the past, the present, the future. *Modern Power Systems.* Retrieved July 20, 2013, from http://www.modernpowersystems.com/features/featurefluidised-bed-combustion-technology-the-past-present-and-future/.

Permchart, W., Kouprianov, V. I. (2004). Emission performance and combustion efficiency of a conical fluidized-bed combustor firing various biomass fuels. *Bioresource Technology*, *92*, 83–91.

Perry, R. H., Chilton, H. C. (1973). Chemical Engineers' Handbook (5th Edition). McGraw Hill Chemical Engineering Series. p3-145,146.

Petersen, B., Nielsen, C., Jansen, P. (1991). Corrosion in straw fired district heating boilers. In G. Grassi, A. Collina, & H. Zibetta (Eds.), *Biomass for energy, industry and environment: 6th E.C. Conference* (pp. 1177–81). London: Elsevier Applied Science.

Piao, G., Aono, S., Kondoh, M., Yamazaki, R., Mori, S. (2000). Combustion test of refuse derived fuel in a fluidized bed. *Waste Management, 20*, 443–447.

Pronobis, M. (2005). Evaluation of the influence of biomass co-combustion on boiler furnace slagging by means of fusibility correlations. *Biomass and Bioenergy*, *28*, 375–383.

Reddy, G. V., Mahapatra, S. K. (1999). Effect of coal particle size distribution on agglomerate formation in a fluidized bed combustor (FBC). *Energy Conversion and Management*, *40*, 447–458.

REN21 Renewables 2012 Global Status Report 2012. (2012). Paris: (REN21 Secretariat).

Risnes, H., Fjellerup, J., Henriksen, U., Moilanen, A., Norby, P., Papadakis, K., Posselt, D., Sørensen, L.H. (2003). Calcium addition in straw gasification. *Fuel*, *82*, 641–651.

Robinson, A. L., Junker, H., Baxter, L. L. (2002). Pilot-Scale Investigation of the Influence of Coal–Biomass Cofiring on Ash Deposition. *Energy & Fuels*, *16*, 343–355.

Saikaew, T., Supudommak, P., Mekasut, L. Piumsomboon, P., Kuchonthara, P. (2012). Emission of NO_x and N_2O from co-combustion of coal and biomasses in CFB combustor. *International Journal of Greenhouse Gas Control, 10*, 26–32.

Salmenoja, K., Mäkelä, K. (2000). Chlorine-induced superheater corrosion in boilers fired with biomass. *Proceedings to the 5th European Conference on Industrial Furnaces and Boilers*. Espinho, Portugal.

Scala, F., Chirone, R. (2006). Characterization and early detection of bed agglomeration during the fluidized bed combustion of olive husk. *Energy & Fuels*, *20*, 120–132.

Scala, F., Chirone, R. (2008). An SEM/EDX study of bed agglomerates formed during fluidized bed combustion of three biomass fuels. *Biomass and Bioenergy*, *32*, 252–266.

Shimizu, T., Han, J., Choi, S., Kim, L., Kim, H. (2006). Fluidized-Bed Combustion Characteristics of Cedar Pellets by Using an Alternative Bed Material. *Energy & Fuels*, *20*, 2737–2742.

Silvennoinen, J., Hedman, M. (2013). Co-firing of agricultural fuels in a full-scale fluidized bed boiler. *Fuel Processing Technology*, *105*, 11–19.

Skrifvars, B.-J., Backmann, R., Hupa, M. (1998a). *Ash chemistry and behaviour in fluidized bed combustion—an overview. In: Hupa M., Matinlinna J., editors. LIEKKI 2, Combustion and Gasification Research Program, Technical Review 1993–98, vol. 1* (pp. 609–38). Finland.

Skrifvars, B.-J., Backman, R., Hupa, M. (1998b). Characterization of the sintering tendency of ten biomass ashes in FBC conditions by a laboratory test and by phase equilibrium calculations. *Fuel Processing Technology*, *56*, 55–67.

Su, S., Pohl, J. H., Holcombe, D. (2003). Fouling propensities of blended coals in pulverized coal-fired power station boilers. *Fuel*, *82*, 1653–1667.

Suksankraisorn, K., Patumsawad, S., Vallikul, P., Fungtammasan, B., Accary, A. (2004). Co-combustion of municipal solid waste and Thai lignite in a fluidized bed. *Energy Conversion and Management*, *45*, 947–962.

Sun, Z.-A., Jin, B.-S., Zhang, M.-Y., Liu, R.-P., Zhang, Y. (2008). Experimental Study on Cotton Stalk Combustion in a Circulating Fluidized Bed. *Applied Energy, 85*, 1027–1040.

Szemmelveisz, K., Szűcs, I., Palotás, Á. B., Winkler, L., Eddings, E. G. (2009). Examination of the combustion conditions of herbaceous biomass. *Fuel Processing Technology*, *90*, 839–847.

Tamzok, N., Özcan, M., Gülsen, Ö., Demirkol, Ö., Demir, E., Babayiğit, S. S. (2012). *Coal Sector Report (Lignite) 2011 (in Turkish)*.

Tangsathitkulchai, C., Tangsathitkulchai, M. (2001). Effect of bed materials and additives on the sintering of coal ashes relevant to agglomeration in fluidized bed combustion. *Fuel Processing Technology*, *72*, 163–183.

Taşkıran, I. (2009). Orman artiklarinin enerji dönüşümünde kullanilmasi ve gazlaştiricilar (in Turkish). *Presented at International Waste to Energy Symposium*. Istanbul.

Teixeira, P., Lopes, H., Gulyurtlu, I., Lapa, N., Abelha, P. (2012). Evaluation of slagging and fouling tendency during biomass co-firing with coal in a fluidized bed. *Biomass and Bioenergy*, *39*, 192–203.

The Master Planning of Forestry Research of Ministry of Forestry for 1995-1998 (in Turkish). (1995). Ankara.

Theis, M., Skrifvars, B.-J., Hupa, M., Tran, H. (2006). Fouling tendency of ash resulting from burning mixtures of biofuels. Part 1: Deposition rates. *Fuel*, *85*, 1125–1130.

Thrän, D., Bunzel, K., Seyfert, U., Zeller, V., Buchhorn, M., Müller, K., Matzdorf, B., et al. (2011). *DBFZ Report Nr. 7 Final Report Global and Regional Spatial Distribution of Biomass Potentials – Status quo and options for specification –*. Leipzig: Deutsches BiomasseForschungsZentrum gemeinnützige GmbH (DBFZ).

Toklu, E. (2013). Overview of potential and utilization of renewable energy sources in Turkey. *Renewable Energy*, *50*, 456–463.

Topal, H., Atimtay, A. T., Durmaz, A. (2003). Olive cake combustion in a circulating fluidized bed. *Fuel*, *82*, 1049–1056.

Toscano, G., Corinaldesi, F. (2010). Ash Fusibility Characteristics of Some Biomass Feedstocks and Examination of the Effects of Inorganic Additives. *Journal of Agricultural Engineering*, *41*, 13–19.

Turkish Regulation for Industrial Air Pollution Control. (2009). *Official Gazette no. 27277*. Ankara: Republic of Turkey, Ministry of Environment and Urbanism.

TurkStat National Greenhouse Gas Inventory Report 1990-2010. (2012). Ankara: Turkish Statistical Institute.

U.S. Energy Information Administration, Country Briefs, Turkey. (2013). Retrieved July 20, 2013, from http://www.eia.gov/countries/cab.cfm?fips=TU.

Ültanır, M. (1998). *21. Yüzyıla Girerken Türkiye'nin Enerji Stratejisinin Değerlendirilmesi (in Turkish). TÜSİAD Yayınları, Yayın No: TÜSİAD-T/98-12/239* (p. 316). İstanbul: Türk Sanayicileri ve İşadamları Derneği. Retrieved July 20, 2013, from http://www.tusiad.org.tr/__rsc/shared/file/21yy.pdf.

Üretim Lisansı Verilen Tüzel Kişiler (in Turkish). (2013). *EPDK*. Retrieved July 19, 2013, from http://www2.epdk.org.tr/lisans/elektrik/lisansdatabase/verilenuretim.asp.

Valmari, T., Lind, T. M., Kauppinen, E. I., Sfiris, G., Nilsson, K., Maenhaut, W. (1999). Field Study on Ash Behavior during Circulating Fluidized-Bed Combustion of Biomass. 1. Ash Formation. *Energy & Fuels*, *13*, 379–389.

Vamvuka, D., Zografos, D., Alevizos, G. (2008). Control methods for mitigating biomass ash-related problems in fluidized beds. *Bioresource Technology*, *99*, 3534–3544.

Vamvuka, D., Sfakiotakis, S., Kotronakis, M. (2012). Fluidized bed combustion of residues from oranges' plantations and processing. *Renewable Energy*, *44*, 231–237.

Varol, M., Atimtay, A. T. (2007). Combustion of olive cake and coal in a bubbling fluidized bed with secondary air injection. *Fuel*, *86*, 1430–1438.

Vuthaluru, H. B., Linjewile, T. M., Zhang, D., Manzoori, A. R. (1999). Investigations into the control of agglomeration and defluidisation during fluidised-bed combustion of low-rank coals. *Fuel, 78*, 419–425.

Vuthaluru, H. B, Zhang, D. (1999). Control methods for remediation of ash-related problems in fluidised-bed combustors. *Fuel Processing Technology, 60,* 145–156.

Vuthaluru, H. B, Zhang, D., Linjewile, T. M. (2000). Behaviour of inorganic constituents and ash characteristics during fluidised-bed combustion of several Australian low-rank coals. *Fuel Processing Technology*, *67*, 165–176.

WEC-TNC Energy Report (in Turkish). (2012). Ankara: World Energy Council-Turkish National Committee.

Werther, J., Ogada, T. (1999). Sewage sludge combustion. *Progress in Energy and Combustion Science*, *25*, 55–116.

Werther, J., Saenger, M., Hartge, E.-U., Ogada, T., Siagi, Z. (2000). Combustion of agricultural residues. *Progress in Energy and Combustion Science*, *26*, 1–27.

Werther, J. (2007). *Fluidized-Bed Reactors In: Ullmann's Encyclopedia of Industrial Chemistry Vol. 15* (pp. 320–366).

Williams, A., Jones, J. M., Ma, L., Pourkashanian, M. (2012). Pollutants from the combustion of solid biomass fuels. *Progress in Energy and Combustion Science, 38*, 113–137.

Winter, F., Szentannai, P. (2010). *IEA Fluidized Bed Conversion Programme Status Report 2010*.

Xie, J., Yang, X., Zhang, L., Ding, T., Song, W., Lin, W. (2007). Emissions of SO_2, NO and N_2O in a circulating fluidized bed combustor during co-firing coal and biomass. *Journal of Environmental Sciences*, *19*, 109–117.

Yang, T., Kai, X., Sun, Y., He, Y., Li, R. (2011). The effect of coal sulfur on the behavior of alkali metals during co-firing biomass and coal. *Fuel*, *90*, 2454–2460.

Youssef, M. A., Wahid, S. S., Mohamed, M. A., Askalany, A. A. (2009). Experimental study on Egyptian biomass combustion in circulating fluidized bed. *Applied Energy, 86*, 2644–2650.

Zevenhoven-Onderwater, M., Blomquist, J.-P., Skrifvars, B.-J., Backman, R., Hupa, M. (2000). The prediction of behaviour of ashes from five different solid fuels in fluidised bed combustion. *Fuel*, *79*, 1353–1361.

Zevenhoven-Onderwater, M, Öhman, M., Skrifvars, B.-J., Backman, R., Nordin, A., Hupa, M. (2006). Bed Agglomeration Characteristics of Wood-Derived Fuels in FBC. *Energy & Fuels,* 20, 818–824.

Zhao, J., Brereton, C., Grace, J. R., Lim, C J. Legros, R. (1997). Gas Concentration Profiles and NO_x Formation in Circulating Fluidized Bed Combustion. *Fuel, 76*, 853–860.

Zheng, Y., Jensen, P. A., Jensen, A. D., Sander, B., Junker, H. (2007). Ash transformation during co-firing coal and straw. *Fuel*, *86*, 1008–1020.

Zhu, J., Lu, Q., Niu, T., Song, G., Na, Y. (2009). NO emission on pulverized coal combustion in high temperature air from circulating fluidized bed – An experimental study. *Fuel Processing Technology, 90*, 664–670.

APPENDIX A

STANDARD PIPE SIZES FOR SELECTED PIPES

The following table gives standard pipe sizes for the pipes used in the combustion system.

Table A.1 Standard Pipe Sizes for Selected Pipes

NPS	DN	OD	Wall Thickness (SCH 10)
	mm	inches (millimeters)	inches (millimeters)
¼	**8**	0.540 in (13.72 mm)	0.065 in (1.651 mm)
½	**15**	0.840 in (21.34 mm)	0.083 in (2.108 mm)
¾	**20**	1.050 in (26.67 mm)	0.083 in (2.108 mm)
1	**25**	1.315 in (33.40 mm)	0.109 in (2.769 mm)
1¼	**32**	1.660 in (42.16 mm)	0.109 in (2.769 mm)
1½	**40**	1.900 in (48.26 mm)	0.109 in (2.769 mm)
2	**50**	2.375 in (60.33 mm)	0.109 in (2.769 mm)
3	**80**	3.500 in (88.90 mm)	0.120 in (3.048 mm)
4	**100**	4.500 in (114.30 mm)	0.120 in (3.048 mm)
5	**125**	5.563 in (141.30 mm)	0.134 in (3.404 mm)

NPS: Nominal Pipe Size
DN: Diameter Nominal
OD: Outer Diameter

APPENDIX B

TECHNICAL DRAWINGS

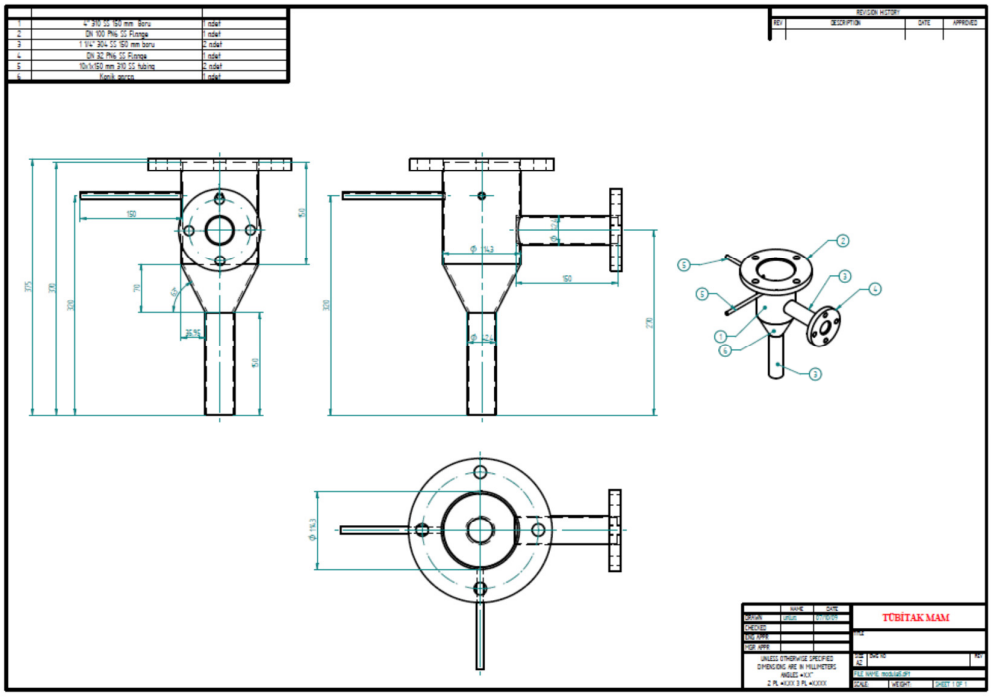

Figure B.1 Technical drawings of Windbox

Table B.1 Specifications of Windbox

#	Specifications	Quantity
1	DN 100 SCH 10, 310 SS 150 mm	1
2	DN 100 PN6, SS flange	1
3	DN 32 SCH 10, 304 SS 150 mm	2
4	DN 32 PN6, SS flange	1
5	10x1x150 mm, 310 SS tubing	2
6	conical item	1

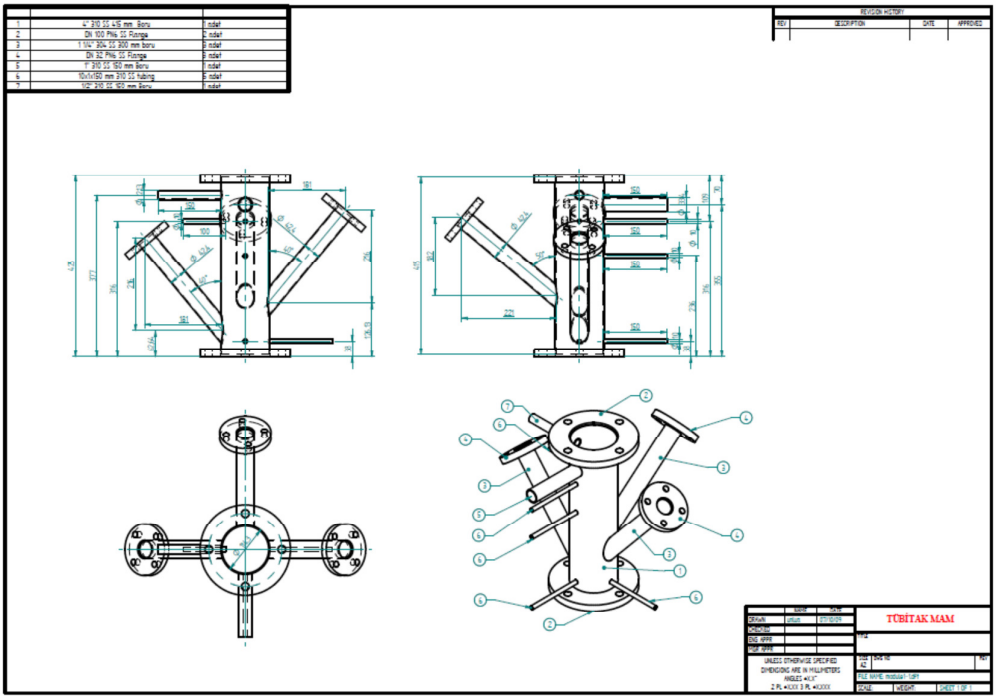

Figure B.2 Technical drawings of Module-101

Table B.2 Specifications of Moduel-101

#	Specifications	Quantity
1	DN 100 SCH 10, 310 SS 415 mm	1
2	DN 100 PN6, SS flange	2
3	DN 32 SCH 10, 304 SS 300 mm	3
4	DN 32 PN6, SS flange	3
5	DN 25 SCH 10, 310 SS 150 mm	1
6	10x1x150 mm, 310 SS tubing	5
7	DN 15 SCH 10, 310 SS 150 mm	1

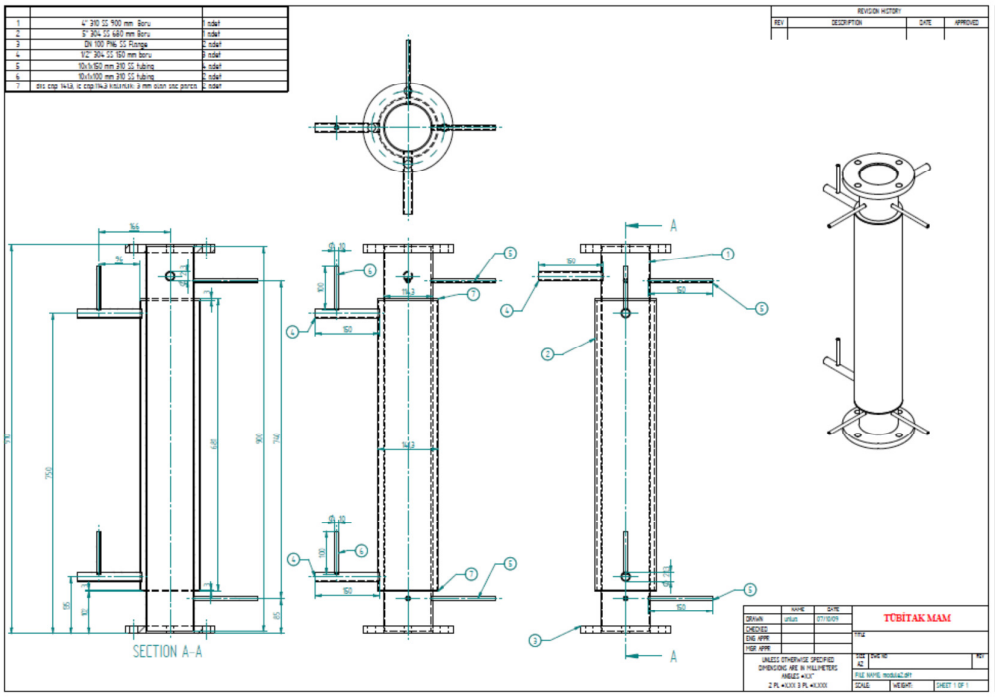

Figure B.3 Technical drawings of Module-102 and Module-107

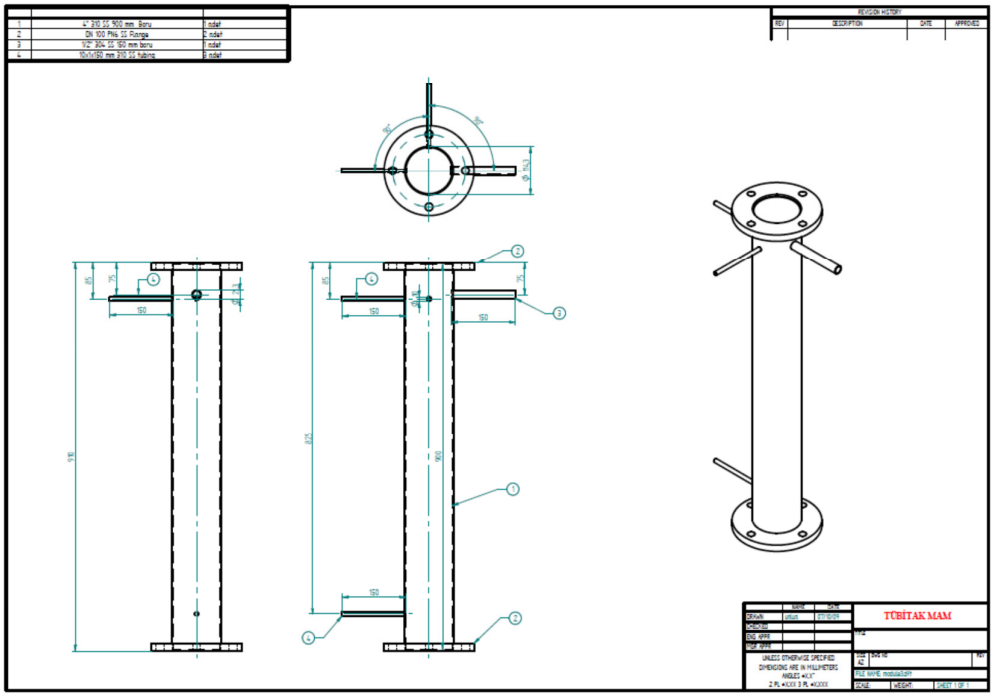

Figure B.4 Technical drawings of Module-103, Module-104, Module-105 and Module-106

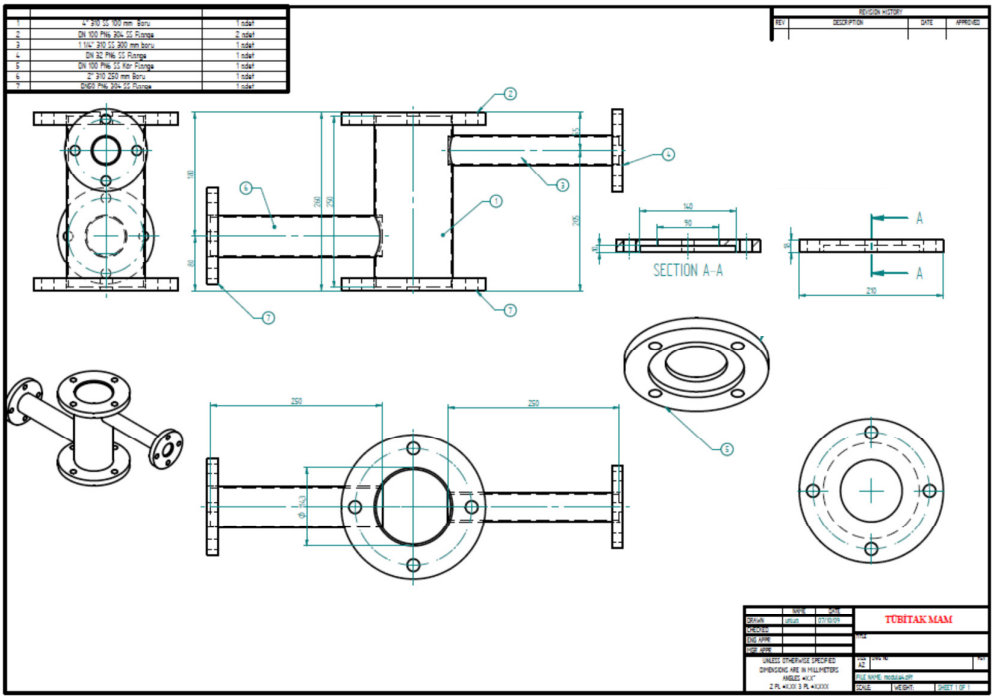

Figure B.5 Technical drawings of Module-108

Table B.3 Temperature Transmitters

Code	Description	On
TT-101	Temperature Transmitter (Primary Air)-01	P-101
TT-102	Temperature Transmitter (Primary Air)-02	HT-101
TT-103	Temperature Transmitter (Primary Air)-03	HT-102
TT-104	Temperature Transmitter (Primary Air)-04	HT-103
TT-105	Temperature Transmitter (Primary Air)-05	HT-104
TT-106	Temperature Transmitter (Primary Air)-06	HT-105
TT-107	Temperature Transmitter (Primary Air)-07	HT-106
TT-108	Temperature Transmitter (Combustor/Windbox)-08	Windbox
TT-109	Temperature Transmitter (Combustor/Module-101)-09	Module-101
TT-110	Temperature Transmitter (Combustor/Module-101)-10	Module-101
TT-111	Temperature Transmitter (Combustor/Module-101)-11	Module-101
TT-112	Temperature Transmitter (Combustor/Module-102)-12	Module-102
TT-113	Temperature Transmitter (Combustor/Module-103)-13	Module-103
TT-114	Temperature Transmitter (Combustor/Module-103)-14	Module-103
TT-115	Temperature Transmitter (Combustor/Module-104)-15	Module-104
TT-116	Temperature Transmitter (Combustor/Module-104)-16	Module-104
TT-117	Temperature Transmitter (Combustor/Module-105)-17	Module-105
TT-118	Temperature Transmitter (Combustor/Module-105)-18	Module-105

The connection size of the temperature transmitter is DN 8 (SCH 10).
They are all K-type 3 mm (NiCr-Ni) Inconel 600 DIN.

Table B.3 (Continued)

Code	Description	On
TT-119	Temperature Transmitter (Combustor/Module-106)-19	Module-106
TT-120	Temperature Transmitter (Combustor/Module-106)-20	Module-106
TT-121	Temperature Transmitter (Combustor/Module-107)-21	Module-107
TT-122	Temperature Transmitter (Combustor/Cyclone-01)-22	Module-107
TT-201	Temperature Transmitter (Return Leg)-23	Module-201
TT-202	Temperature Transmitter (Return Leg)-24	Module-202
TT-203	Temperature Transmitter (Return Leg)-25	Module-203
TT-204	Temperature Transmitter (Return Leg)-26	Module-204
TT-301	Temperature Transmitter (Flue Gas Pipeline)-27	P-301
TT-302	Temperature Transmitter (Flue Gas Pipeline)-28	P-302
TT-303	Temperature Transmitter (Flue Gas Pipeline)-29	P-303
TT-304	Temperature Transmitter (Flue Gas Pipeline)-30	P-304
TT-305	Temperature Transmitter (Flue Gas Pipeline)-31	P-305
TT-401	Temperature Transmitter (Secondary Air)-32	P-401
TT-402	Temperature Transmitter (Secondary Air)-33	P-402
TT-403	Temperature Transmitter (Secondary Air)-34	P-403
TT-404	Temperature Transmitter (Secondary Air)-35	P-404
TT-405	Temperature Transmitter (Secondary Air)-36	P-405
TT-406	Temperature Transmitter (Secondary Air)-37	P-406
TT-407	Temperature Transmitter (Secondary Air)-38	P-407
TT-501	Temperature Transmitter (Cooling Air)-39	P-505
TT-502	Temperature Transmitter (Inlet Coolant Temp.@Module-102)-40	P-511
TT-503	Temperature Transmitter (Outlet Coolant Temp.@Module-102)-41	P-518
TT-504	Temperature Transmitter (Inlet Coolant Temp.@Module-107)-42	P-512
TT-505	Temperature Transmitter (Outlet Coolant Temp.@Module-107)-43	P-519
TT-506	Temperature Transmitter (Inlet Coolant Temp.@Module-301)-44	P-513
TT-507	Temperature Transmitter (Outlet Coolant Temp.@Module-301 & Inlet Coolant Temp.@Module-302)-45	P-514
TT-508	Temperature Transmitter (Outlet Coolant Temp.@Module-302 & Inlet Coolant Temp.@Module-303)-46	P-515
TT-509	Temperature Transmitter (Outlet Coolant Temp.@Module-303 & Inlet Coolant Temp.@Module-304)-47	P-516
TT-510	Temperature Transmitter (Outlet Coolant Temp.@Module-304 & Inlet Coolant Temp.@Module-305)-48	P-517
TT-511	Temperature Transmitter (Outlet Coolant Temp.@Module-305)-49	P-521

The connection size of the temperature transmitter is DN 8 (SCH 10).
They are all K-type 3 mm (NiCr-Ni) Inconel 600 DIN.

Table B.4 Pressure Transmitters

Code	Description	Type	On
PT-101	Pressure Transmitter (Primary Air)-01	0...0.4 bar	P-101
PT-102	Pressure Transmitter (Combustor/Windbox)-02	0...0.3 bar	Windbox
PT-103	Pressure Transmitter (Combustor/Module-101)-03	0...0.3 bar	Module-101
PT-104	Pressure Transmitter (Combustor/Module-101)-04	-1...1 bar	Module-101
PT-105	Pressure Transmitter (Combustor/Module-102)-05	-1...1 bar	Module-102
PT-106	Pressure Transmitter (Combustor/Module-103)-06	-1...1 bar	Module-103
PT-107	Pressure Transmitter (Combustor/Module-104)-07	-1...1 bar	Module-104
PT-108	Pressure Transmitter (Combustor/Module-105)-08	-1...1 bar	Module-105
PT-109	Pressure Transmitter (Combustor/Module-106)-09	-1...1 bar	Module-106
PT-110	Pressure Transmitter (Combustor/Module-107)-10	-1...1 bar	Module-107
PT-201	Pressure Transmitter (Return Leg)-11	-1...1 bar	Module-201
PT-202	Pressure Transmitter (Return Leg)-12	-1...1 bar	Module-202
PT-203	Pressure Transmitter (Return Leg)-13	-1...1 bar	Module-203
PT-204	Pressure Transmitter (Return Leg)-14	0...0.4 bar	Module-204
PT-301	Pressure Transmitter (Flue Gas Pipeline)-15	-1...1 bar	P-301
PT-302	Pressure Transmitter (Flue Gas Pipeline)-16	-1...1 bar	P-302
PT-303	Pressure Transmitter (Flue Gas Pipeline)-17	-1...1 bar	P-303
PT-304	Pressure Transmitter (Flue Gas Pipeline)-18	0...0.3 bar	P-304
PT-305	Pressure Transmitter (Flue Gas Pipeline)-19	0...0.3 bar	P-305
PT-401	Pressure Transmitter (Secondary Air)-20	0...0.3 bar	P-401
PT-501	Pressure Transmitter-21 (Cooling Air)	0...0.3 bar	P-505

The connection size of the pressure transmitter is DN 8 (SCH 10).

Table B.5 Critical measurement points on the combustion system

Critical Measurement Points	Reference	Vertical Distance, cm
PT-101, TT-101	Ground Level	48.0
PT-102, TT-108	Ground Level	110.5
PT-103, TT-109	Distributor Plate	4.0
TT-110	Distributor Plate	24.0
PT-104, TT-111	Distributor Plate	32.0
PT-105, TT-112, SP-101	Distributor Plate	125.0
TT-113	Distributor Plate	170.5
PT-106, TT-114, SP-102	Distributor Plate	216.0
TT-115	Distributor Plate	261.5
PT-107, TT-116, SP-103	Distributor Plate	307.0
TT-117	Distributor Plate	355.0
PT-108, TT-118, SP-104	Distributor Plate	398.0
TT-119	Distributor Plate	443.5
PT-109, TT-120, SP-105	Distributor Plate	489.0
PT-110, TT-121, SP-106	Distributor Plate	580.0
TT-122	Distributor Plate	605.0

Table B.5 (Continued)

Critical Measurement Points	Reference	Vertical Distance, cm
PT-201, TT-201	Distributor Plate	470.7
PT-202, TT-202	Distributor Plate	319.7
PT-203, TT-203	Distributor Plate	187.2
PT-204, TT-204	Distributor Plate	95.7
PT-205, TT-205	Distributor Plate	34.7
PT-301, TT-301, SP-301	Distributor Plate	637.6
PT-302, TT-302, SP-302	Distributor Plate	664.7
PT-303, TT-303, SP-303	Ground Level	47.0
PT-304, TT-304, SP-304	Ground Level	49.5
PT-305, TT-305	Ground Level	103.8
TT 200	Ground Level	677.4
TT 201	Ground Level	590.4
TT 202	Ground Level	438.4
TT 203	Ground Level	306.8
TT 204	Ground Level	217.5
Distributor Plate	Ground Level	121.8
Entrance of Combustor	Ground Level	109.0
FH-01 Entrance of Combustor	Distributor Plate	10.7
FH-02 Entrance of Combustor	Distributor Plate	16.3
TT-101, Primary Air Line	Ground Level	48.0
Third Floor Level	Ground Level	606.0
TT-402, Secondary Air Line - 1	Distributor Plate	51.0
TT-403, Secondary Air Line - 2	Distributor Plate	142.0
TT-404, Secondary Air Line - 3	Distributor Plate	233.0
TT-405, Secondary Air Line - 4	Distributor Plate	324.0
TT-406, Secondary Air Line - 5	Distributor Plate	415.0
TT-407, Secondary Air Line - 6	Distributor Plate	506.0

APPENDIX C

CALIBRATION OF THE FUEL FEEDING SYSTEM

The electrical motors, M-01 and M-02, of the feeding system was calibrated for the olive cake, the woodchips, the Bursa/Orhaneli lignite, and the Denizli/Kale lignite. The feeding rates are given in Table C.1. The calibration curves of M-01 for olive cake and woodchips are shown in Figure C.1 and Figure C.2, respectively. The calibration curves of M-02 for Bursa/Orhaneli lignite and Denizli/Kale lignite are given in Figure C.3 and Figure C.4, respectively. The electrical motor of the screw feeder can operate at different percentages between 0 and 100 with an increment of 1. Fuel feeding calibration for each fuel was done at six different operational percentage of the electrical motor. At each one, at least two measurements were done. The collected fuel amount in a period of one minute was weighted. Average of all measurements for that operational percentage gave the feeding rate in units of kg/h at that operational percentage for the fuel. For each operational percentage, this procedure was repeated and calibration curve of the system for the fuel was obtained. With the formula of the calibration line, desired feeding rate was supplied by setting corresponding percentage value on the control screen of the computer shown in Figure 4.2.

Table C.1 Fuel feeding rates of M-01 and M-02 for biomass and Coal feedstocks

Fuel Feeding Rates for Biomass and Coal Feedstocks, kg/h					
M-01 [%]	**Olive Cake 1-2 mm**	**Woodchips 1-2 mm**	**M-02 [%]**	**Bursa/Orhaneli 1-2 mm**	**Denizli/Kale 1-2 mm**
20	3.91	0.80	20	2.72	3.51
40	8.12	1.58	40	5.50	7.03
60	12.33	2.36	60	8.28	10.54
80	16.54	3.14	80	11.06	14.06
100	20.75	3.91	100	13.83	17.58

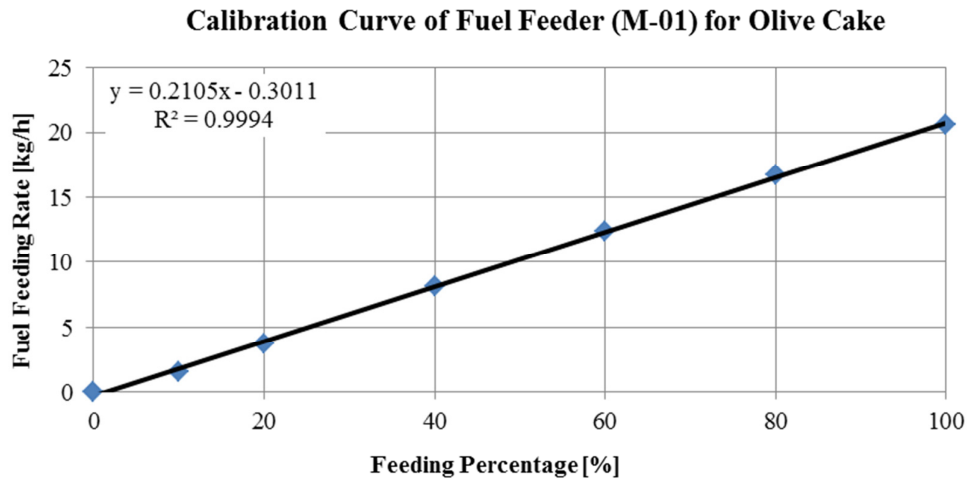

Figure C.1 Feeding rate calibration curve of M-01 for Olive Cake

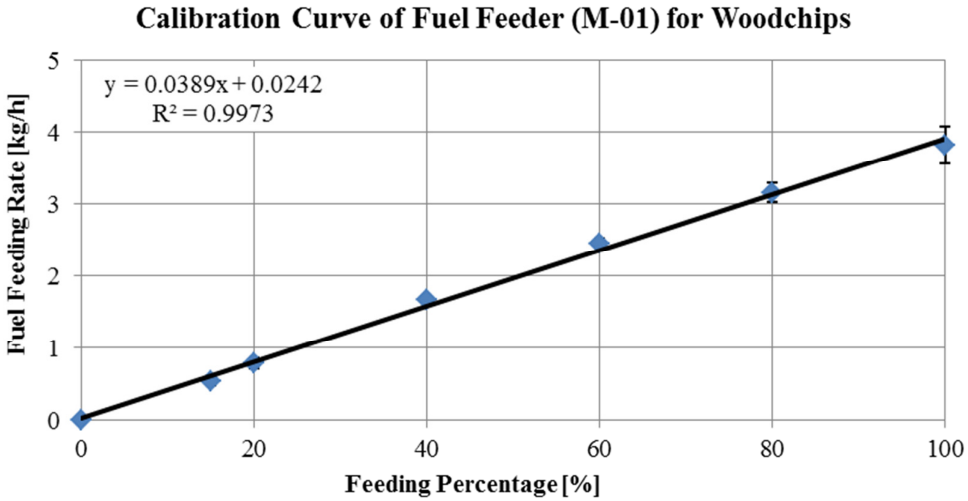

Figure C.2 Feeding rate calibration curve of M-01 for Woodchips

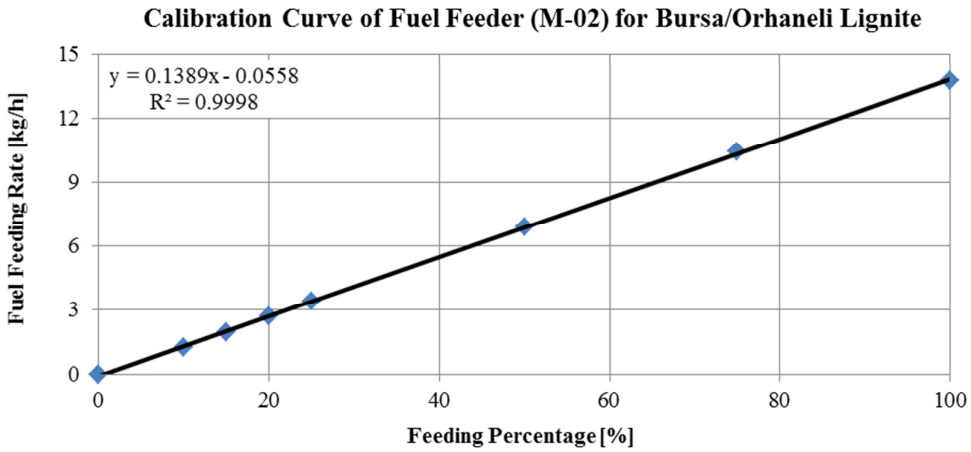

Figure C.3 Feeding rate calibration curve of M-02 for Bursa/Orhaneli lignite

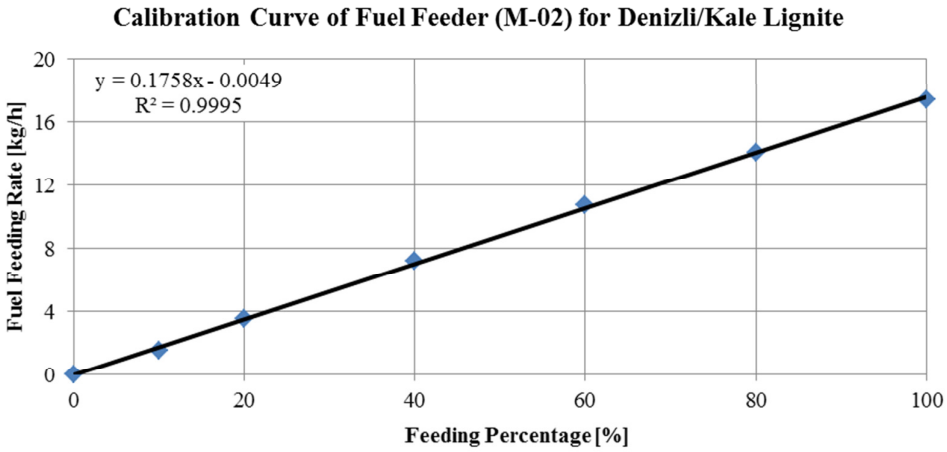

Figure C.4 Feeding rate calibration curve of M-02 for Denizli/Kale lignite

CURRICULUM VITAE

PERSONAL INFORMATION

Surname, Name: Varol, Murat
Nationality: Turkish (TC)
Date and Place of Birth: 06 January 1980, Sakarya
Marital Status: Single
Phone: +90 312 210 58 62
Fax: + 90 312 210 26 46
e-mail: murat_varol@hotmail.com

EDUCATION

Degree	Institution	Year of Graduation
MS	METU Environmental Engineering	2006
BS	Marmara University Environmental Engineering	2002
High School	Adapazarı Atatürk Super High School	1997

ACADEMIC/PROFESSIONAL EXPERIENCE

Year	Place	Enrollment
2002-present	METU Environmental Engineering	Teaching Assistant

FOREIGN LANGUAGES

English

AWARDS

2002 The best M.S. Thesis award of the Department of Environmental Engineering in 2005-2006 given by Graduate School of Natural and Applied Sciences, Middle East Technical University (advisor: Prof. Dr. Aysel Atımtay)

PUBLICATIONS

Peer-Reviewed Journals Articles

1) Varol, M., Atimtay, A.T., Olgun, H., Atakul, H. Emission characteristics of co-combustion of a low calorie and high sulfur-lignite coal and woodchips in a circulating fluidized bed combustor: Part 1. Effect of excess air ratio. *Fuel,* **(accepted)**.
2) Varol, M., Atimtay, A.T., Bay, B., Olgun, H. (2010). Investigation of co-combustion characteristics of low quality lignite coals and biomass with thermogravimetric analysis. *Thermochimica Acta, 510*, 195-201.
3) Akpulat, O., Varol, M., Atimtay, A.T. (2010). Effect of freeboard extension on co-combustion of coal and olive cake in a fluidized bed combustor. *Bioresource Technology, 101*, 6177-6184.
4) Atimtay, A.T., Varol, M. (2009). Investigation of co-combustion of coal and olive cake in a bubbling fluidized bed with secondary air injection. *Fuel, 88*, 1000-1008.
5) Varol, M., Atimtay, A.T. (2007). Combustion of olive cake and coal in a bubbling fluidized bed with secondary air injection. *Fuel, 86*, 1430-1438.

Conference Proceeding Publications
International

1) Varol, M., Atimtay, A., Olgun, H. (2012). Effect of Secondary Air and Its Location on Emissions for Co-combustion of Lignite Coal and Woodchips in a Circulating Fluidized Bed Combustor. *21st European Biomass Conference and Exhibition*, 2DV.3.50, October 15-18, Pittsburgh-PA-USA. ISBN: 978-88-89407-53-0.
2) Varol, M., Atimtay, A.T., Olgun, H., Atakul, H. (2012). Effect of Excess Air Ratio on Flue Gas Emissions for Co-combustion of a Lignite Coal and Woodchips in a Circulating Fluidized Bed Combustor. *29th Annual International Pittsburgh Coal Conference*, Volume 2, p. 1213-1228, October 15-18, Pittsburgh-PA-USA.
3) Varol, M., Atimtay, A.T. (2012). Investigation of the Effect of Biomass-Limestone Interaction on the Ash Composition for Co-combustion of a Lignite Coal and Olive Cake in a Circulating Fluidized Bed Combustor. *29th Annual International Pittsburgh Coal Conference*, Volume 2, p. 1412-1438, October 15-18, Pittsburgh-PA-USA.
4) Varol, M., Atimtay, A.T., Olgun, H., Atakul, H. (2012). Effect of Secondary Air and Its Location on Emissions for Co-combustion of Lignite Coal and Olive Cake in a Circulating Fluidized Bed Combustor. *Proceedings CD of 6th International Ege Energy Symposium and Exhibition*, June 28-30, Izmir-Turkey.
5) Atimtay, A.T., Varol, M., Olgun, H., Kayahan, U., Unlu, A., Atakul, H. (2012). Effect of Various Biowastes on Emissions in Combustion of Lignite Coal in a Circulating Fluidized Bed Combustor. *Environmental Science and Technology*, Volume 1. George Sorial and Jihua Hong, Eds. American Science Press, Houston, USA, PP478. ISBN: 9780976885351.

6) Varol, M., Atimtay, A.T., Celebi, M.C., Olgun, H., Atakul, H., Kayahan, U., Bay, B., Unlu, A. (2011). Co-combustion of Hazelnut Shells with a High-Sulfur Turkish Lignite in a Circulating Fluidized Bed Combustor with Air Staging. *Proceedings CD of II. International Conference on Air Pollution and Control*, September 19-23, Antalya-Turkey.
7) Celebi, M.C., Atimtay, A.T., Varol, M., Olgun, H., Atakul, H., Bay, B., Kayahan, U., Unlu, A., Bardakcioglu, G., Ozcan, M. (2011). Co-combustion of Various Agrowastes with a High-Sulfur Turkish Lignite in a Circulating Fluidized Bed Combustor: Effect of Air Staging on Pollutants along the Combustor. *Proceedings CD of 5th International Conference on Clean Coal Technologies*, May 08-12, Zaragoza-Spain.
8) Varol, M., Celebi, M.C., Olgun, H., Atimtay, A.T., Atakul, H., Unlu, A., Bay, B., Kayahan, U. (2010). Co-combustion of Various Biowastes with a High-Sulfur Turkish Lignite in a Circulating Fluidized Bed Combustor. *Proceedings CD of 27th Annual International Pittsburgh Coal Conference*, October 11-14, Istanbul-Turkey.
9) Varol, M., Akpulat, O., Atimtay, A.T., Olgun, H. (2010). SO_2 Capture in a Fluidized Bed Combustor with Limestone and the Effect of Olive Cake Addition on the SO_2 Capture Efficiency. *Proceedings CD of Fifth International Ege Energy Symposium and Exhibition (IEESE-5)*, June 27-30, Pamukkale University, Denizli-Turkey.
10) Varol, M., Atimtay, A.T., Bay, B., Olgun, H. (2010). A Study of Co-combustion Characteristics of Biomass Fuels and a Lignite Coal with Thermo Gravimetric Analysis. *Proceedings of the Tenth International Conference on Combustion and Energy Utilization*, p. 306-313, May 04-08, Mugla University, Mugla-Turkey.
11) Akpulat, O., Varol, M., Atimtay, A.T. (2010). Investigation of Emissions and Combustion Efficiency During Combustion and Co-combustion of Coal and Olive Cake in a Bubbling Fluidized Bed. *Proceedings of the Tenth International Conference on Combustion and Energy Utilization*, p. 60-66, May 04-08, Mugla University, Mugla-Turkey.
12) Olgun, H., Atimtay, A.T., Varol, M., Gul, S., Bay, B., Kayahan, U., Atakul, H., Celebi, M.C., Cetinkaya, E. (2010). Combustion of Lignite Coal in a Circulating Fluidized Bed Combustor. *Proceedings of the Tenth International Conference on Combustion and Energy Utilization*, p. 36-41, May 04-08, Mugla University, Mugla-Turkey.
13) Varol, M., Atimtay, A.T. (2007). Effect of Secondary Air Injection on the Co-combustion of Olive Cake and Coal Mixtures in a Bubbling Fluidized Bed. *Abstracts: of the International Conference on Environment: Survival and Sustainability-ESS2007*, p. 249, February 19-24, Nicosia (Lefkoşa)-K.K.T.C.

National

14) Varol, M., Celebi, M.C., Atimtay, A.T., Olgun, H., Atakul, H., Unlu, A., Bay, B., Kayahan, U., Bardakcıoglu, G. (2010). Ormangülünün Orhaneli (Bursa) Kömürü ile Birlikte Dolaşımlı Akışkan Yatakta Yakılması (in Turkish). *IV. Ulusal Hava Kirliliği ve Kontrolü Sempozyumu*, p.606-618, October 25-27, Ankara-Turkey.
15) Varol, M., Atımtay, A.T. (2006). Prina ve kömürün ikincil hava ilavesiyle kabarcıklı akışkan yatakta yakılması (in Turkish). *Uluslararası 9. Yanma Sempozyumu-Bildiriler Kitabı*, p. 31-39, November 16-17, Kırıkkale University, Kırıkkale-Turkey.
16) Varol, M., Atımtay, A.T. (2006). Akışkan yatakta prinanın ikincil hava ilavesi ile yakılması ve emisyon karakteristiklerinin belirlenmesi (in Turkish). *6. Ulusal Temiz Enerji Sempozyumu-Bildiriler Kitabı,* p. 869-879, May 25-27, Süleyman Demirel University, Isparta-Turkey.

Books and Journals Edited

National

1) Yorulmaz, S., Doğan, G., Varol, M., Tokgöz, D., Yılmaz, M., Atımtay, A., Tuncel, G. (2010). *IV. Ulusal Hava Kirliliği ve Kontrolü Sempozyumu-HKK2010-Bildiriler Kitabı*, October 25-27, METU, Ankara-Turkey.

Research Projects

1) Atimtay, A.T., Olgun, H., Bardakcioglu, G., "Development of Circulating Fluidized Bed Combustion (CFBC) Technology and Investigation of Biomass/Lignite Coal Combustion", (Project Code: TUBITAK- KAMAG 105G023), **Researcher**, 2007-2012.

Conferences Organized

As a Member of Organization Committee

1) IV. Ulusal Hava Kirliliği ve Kontrolü Sempozyumu-HKK2010, October 25-27, METU, Ankara-Turkey, 2010.

As a Member of Technical Committee

2) 3rd INTERNATIONAL SYMPOSIUM on AIR QUALITY MANAGEMENT at Urban, Regional and Global Scales, September 26-30, Mövenpick Hotel, Istanbul-Turkey, 2005.